UNIVERSITÉ DE STRASBOURG

ÉCOLE DOCTORALE DES SCIENCES CHIMIQUES (ED 222)

Systèmes complexes en synthèse et catalyse
Institut de science et d'ingénierie supramoléculaires (UMR 7006)

THÈSE présentée par :

Sebastián Martínez

Soutenue le 24 Juin 2022

pour obtenir le grade de : **Docteur de l'université de Strasbourg**

Discipline/ Spécialité : Chimie Moleculaire

TITRE de la thèse

Développement de procédés chimiques exploitant des réactions catalytiques réversibles, à partir d'une approche mécanistique.

THÈSE dirigée par :
  Prof. EBBESEN Thomas   Université de Strasbourg
  Dr. DYDIO Paweł   Université de Strasbourg

RAPPORTEURS :
  Prof. MORANDI Bill   Eidgenössische Technische Hochschule (ETH) Zürich
  Prof. DAUBAN Philippe   Université de Paris-Saclay

AUTRES MEMBRES DU JURY :
  Dr. WENCEL-DELORD Joanna   Université de Strasbourg
  Prof. DE BRUIN Bas   Universiteit van Amsterdam

Table of Contents

Chapter 5. Mechanism of the Isoselective Hydroformylation of Propylene
by Iodide-Assisted Palladium Catalysis **127**

Aknowledgements

First and foremost, I would like to thank my supervisor Dr. Paweł Dydio for giving me the opportunity to join his group and work on exciting and challenging research projects. I specially thank him for being always enthusiastic and available for discussion, for encouraging me to do my best at every experiment and for sharing valuable advice during challenging times of this thesis.

I would like to thank Prof. Thomas Ebbesen for his support and valuable advice on my future career. I thank the Frontier Research in Chemistry Foundation for providing me with the Excellence Solvay PhD fellowship. I thank in this context Dr. Robert Gresser (Vice-president of Solvay) and Dr. Patrick Maestro (Scientific Director of the Solvay group) for their interest on my PhD project and for opening further opportunities in industry for my future career.

I thank the members of the jury Prof. Bill Morandi, Prof. Philippe Dauban, Prof. Bas de Bruin and Dr. Joanna Wencel-Delord for accepting the invitation to participate in it.

I thank Dr. David Leboeuf for his support on the mid thesis defense and preparation of the documents for the defense and Claire Menouna-Ekani, the group secretary, for helping me get the paper work done upon my arrival in France and later on.

At his point I would like to thank my colleagues at the lab of both Dr. Paweł Dydio, Prof. Moran and Prof. Hoveyda for their support and shared knowledge during this years. I thank Dr. Alessandra Casnati for being an amazing partner and fumehood neighbor who helped me the most in the lab after my hand operation and for sharing the best of Italian cuisine and more, Dr. Hanusch Grab for sharing his skills in synthetic organic chemistry and for taking care countless hours of music entertainment during work (and non working) hours, Lukas Veth for sharing and working hard on the hardest part of my thesis and for bringing to the group the best sense of discipline, Dr. Yang Zhang for sharing his amazing skills when working with sensitive compounds and most importantly for showing the best of his football technique at every match, Michel Sigrist for being always available for discussion and for sharing the best of Alsatian cuisine and French language, Bruno Lainer for spreading the best humor in the lab and beyond. I thank Dr. Filippo Romiti, for his advice and help in the organic synthesis done in this thesis. I thank Dr. Sebastian Torker for useful advice regarding DFT studies. Lastly, I would like to thanks a large number of people with who I shared very good times and experiences, among which are Sergiu Bicic, Debora Schirol, Ankita Malik, Paul Chatelain, Harprett Kaur, Shaofei Zhang, Sophia Rauscher, Jing Yi and many others.

Desde este página, cambio a español para dar mi más sincero agradecimiento a quienes más estimo.

Primero que nada, agradecer al Hno. Rogelio Dewaele, quien me abrió las puertas al mundo de la química y supo inspirarme profundamente en mis primeros inicios.

Quisiera agradecer muchísimo al Prof. Nicolás Veiga por motivarme y apoyarme a seguir adelante con mis estudios de doctorado en el exterior, y por enseñarme el mundo de la química computacional, que ha sido un pilar fundamental para la realización de esta tesis.

Segundo, agradecer a mi amigos, Marcos, Santiago, Gonzalo y Carlos, a quienes poco pude ver durante la realización de esta tesis, pero han sabido cumplir.

Por último, agradecer enormemente a mi familia, a mi hermano, a mis padres, a quienes he extrañado muchísimo y sin quienes la realización de esta tesis hubiera sido imposible. Gracias.

Résumé de la thèse

1. Introduction

L'émergence de la catalyse des métaux de transition a eu un impact transformateur sur la synthèse organique.[1] Ces dernières années, l'utilisation de catalyseurs uniques ou multiples, effectuant une seule ou plusieurs réactions simultanément s'est avérée être une stratégie précieuse pour améliorer l'efficacité, la sélectivité et l'économie d'atomes du processus de synthèse de manière globale.[2–4] La compréhension de la séquence des événements se produisant au niveau moléculaire dans de tels processus est de la plus haute importance pour concevoir, développer et améliorer avec succès de nouveaux systèmes catalytiques précieux capables de surpasser les protocoles actuels. Cette approche mécanistique du développement de nouvelles méthodologies catalytiques permet non seulement de contourner le processus classique d'optimisation par essais et erreurs, mais surtout d'approfondir la compréhension mécanistique afin d'exploiter tout le potentiel de ces systèmes catalytiques. La portée de cette thèse de doctorat diverge en quatre axes principaux, qui sont brièvement résumés ci-dessous. Dans un premier temps, je présente une perspective générale des défis et des opportunités dans le domaine émergent de la multi-catalyse (Chapitre 1), en guise d'introduction aux études expérimentales et computationnelles des systèmes catalytiques décrites dans les chapitres suivants de cette thèse.[5] Ensuite, je décris la conception et le développement d'un nouvel exemple de ces systèmes multi-catalytiques complexes, qui combinent la puissance des réactions catalytiques réversibles avec les réactions de fonctionnalisation catalytique orthogonale. Le système développé permet d'accéder à la réactivité de type diénique non inhérente de molécules fonctionnalisées, telles que des nitriles alcényles, des aldéhydes ou des cétones, dans le processus orthogonal de Diels-Alder, élargissant pour la première fois la " chimie d'emprunt " au-delà de la catalyse classique d'emprunt d'hydrogène (Chapitre 2). Ensuite, je présente nos études concernant le développement mécanistique d'une nouvelle réaction catalytique réversible, qui pourrait être intéressante pour la synthèse en chimie fine. En particulier, nous avons poursuivi le développement d'un protocole de borylation C–H synthétiquement attrayant par le biais d'une méthodologie du transfert de groupes boryles générale, en exploitant l'étape « Rh-β-boryle elimination », qui est jusqu'à présent, inconnu pour le rhodium. De plus, nous avons fourni une étude mécanistique expérimentale et théorique complète du mécanisme de réaction et nous avons mieux compris comment les modifications de la structure du ligand et du catalyseur influencent le profil de réaction et la sélectivité du produit (Chapitre 3 et Chapitre 4). Enfin, je présente nos études visant à fournir des informations mécanistiques détaillées sur les processus établis, en particulier ceux qui présentent un intérêt industriel, afin de faciliter l'amélioration rationnelle de leurs performances. Plus précisément, j'ai étudié le mécanisme de l'hydroformylation isosélective du propylène catalysée par le palladium, qui a été récemment développée par notre groupe, dans le but principal de démêler le cycle catalytique réel parmi les multiples voies possibles, ainsi que les origines de l'isosélectivité inhabituelle (Chapitre 5).

Les challenges et les opportunités de la multi-catalyse (Chapitre 1)

La multi-catalyse est un domaine émergent qui vise le développement de transformations catalytiques efficaces pour convertir rapidement des matières premières relativement simples, en produits plus complexes à valeur ajoutée.[2–4] Dans le cadre des procédés multi-catalytiques, soit plusieurs catalyseurs exécutent des réactions uniques, soit des séquences précises de réactions catalytiques multiples se déroulent en "one-pot". Il est intéressant de noter que les protocoles multi-catalytiques permettent non seulement de réaliser des transformations inaccessibles par les approches classiques, mais aussi de réduire considérablement le temps, les déchets et le coût des processus de synthèse, ce qui rend la synthèse organique plus efficace en termes de ressources. Dans ce chapitre, je passe en revue les différentes stratégies de la multi-catalyse qui présentent des défis et des

opportunités distincts. Ce domaine global est divisé en trois catégories principales : la catalyse coopérative, la catalyse domino et la catalyse relais. Chaque catégorie est décrite avec des exemples représentatifs pour mettre en évidence ses caractéristiques. Une attention particulière est accordée à la catalyse à relais, qui est examinée plus en détail dans ses sous-catégories. Enfin, une analyse des systèmes qui intègrent des niveaux de complexité plus élevés et soulignent davantage le potentiel des systèmes multi-catalytiques est fournie. Ce travail de perspective a été achevé et publié.[5]

2. Résultats et discussion

Comme indiqué ci-dessus, les investigations expérimentales et théoriques réalisées au cours de mes études de doctorat sont axées sur des problèmes de recherche entrelacés centrés sur le développement mécanistique de quatre réactions chimiques qui engagent des processus réversibles. Les résultats obtenus pour chaque transformation chimique sont brièvement résumés ci-dessous.

2.1 La catalyse coopérative engageant l'emprunt de groupes hydro-fonctionnels débloque la réactivité non-inhérente (Chapitre 2)

L'exploitation de la réactivité non inhérente des molécules organiques dans un réseau de réactions est une approche puissante pour améliorer l'efficacité globale de la synthèse organique.[6] Cette réactivité non inhérente peut être débloquée par des réactions catalytiques réversibles, qui peuvent modifier de façon transitoire la réactivité du matériau de départ en réagissant avec un groupe fonctionnel cible. Lorsqu'elles coopèrent avec d'autres réactions, de nouvelles transformations stimulantes peuvent être exécutées à des positions initialement non réactives, offrant ainsi de précieux raccourcis au praticien de la synthèse. Bien que de nombreux réseaux de réactions catalytiques réversibles et de réactions de transformation aient été signalés, seule la déshydrogénation réversible - appelée "emprunt d'hydrogène" - a été exploitée pour accéder à la réactivité non inhérente des matières premières.[6,7] Je présente ici une série de transformations qui exploitent les réactions d'hydrofonctionnalisation catalytique réversible comme élément clé des réseaux pour débloquer une réactivité diénique temporelle sans précédent, montrant pour la première fois que la "borrowing strategy" est une approche plus générale que nous nommons ici "catalyse de type boomerang". Plus précisément, nous avons développé une série de systèmes catalytiques basés sur des catalyseurs Ni- ou Rh-, qui engagent des produits de départ nitrile, aldéhyde ou cétone (homo)allyliques dans une séquence de i) *rétro-hydrofonctionnalisation* pour former un diène hautement réactif, ii) *cycloaddition de Diels*-Alder de l'intermédiaire diénique et d'un diénophile, suivie par iii) *(re)-hydrofonctionnalisation* de l'adduit de Diels-Alder généré in situ pour former un produit (poly)cyclique fonctionnalisé en une seule étape avec une économie d'atomes de 100% (Figure 1A). Une réaction intermoléculaire modèle a montré que le nitrile **1a** ou **1b** et *n*-butyle crotonate réagissent pour former le nitrile bicyclique ponté cible **2** avec un rendement de 99 %, en présence de 5 % en moles de Ni(cod)$_2$, 5 % en moles de DPEPhos et 40 % en moles d'AlMe$_2$Cl, après 72 h, à 50 ^{o}C (Figure 1B). D'autres classes de diénophiles comme le méthacrylate, le carboxiamide ou le maléimide se sont également engagés avec succès dans le réseau envisagé pour former les composés **3** et **4** (un dérivé de crotamiton), entre autres, avec des rendements modérés à élevés. De plus, en utilisant les conditions développées pour une hydroformylation réversible basée sur un catalyseur de Rh, un réseau de réactions similaire fournit des composés polycycliques **5**, **6** et **7** avec des rendements modérés à élevés. La stratégie développée a été appliquée à la construction facile d'une série de cadres polycycliques trouvés dans les produits naturels en exploitant les réactions intramoléculaires (Figure 1C). Par exemple, de telles réactions ont permis d'obtenir le noyau de l'*isosativene* et du *cedranediol* avec des rendements élevés (composés **8-11**). Un manuscrit incluant les résultats obtenus dans ce travail est actuellement en préparation.
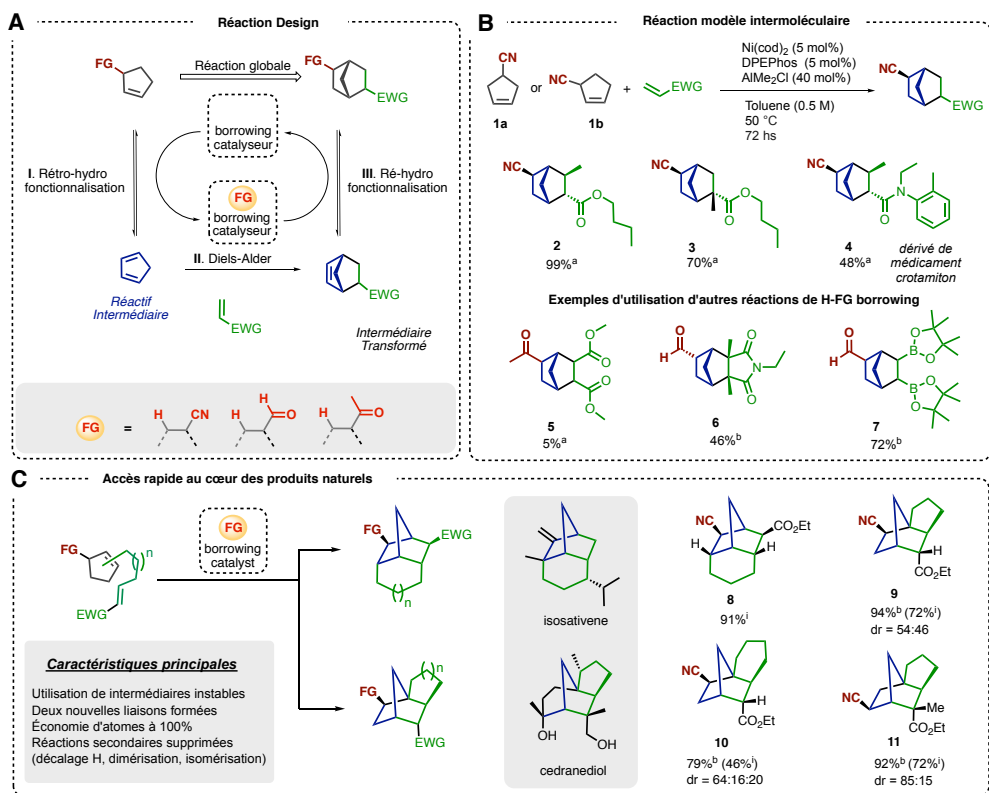
Figure 1. A) Notre conception de la réaction pour les systèmes catalytiques coopératifs engageant l'emprunt hydrofonctionnel et la réaction de Diels-Alder. B) Réaction modèle et exemples sélectionnés pour l'emprunt H-CN. Exemples supplémentaires impliquant l'emprunt H-CHO. C) Réactions intramoléculaires comme voies de synthèse rapides vers la préparation du cœur des produits naturels.. [a]GC-rendement. [b]RMN rendement. dr = diastéréoisomère ratio. [i] rendement isolé du composé.

2. 2 Borylation C-H de transfert d'alcènes sous catalyse Rh(I) : Aperçu de la capacité de synthèse, du mécanisme et du contrôle de la sélectivité (Chapitre 3)

La borylation C–H par transfert d'alcènes offre la possibilité de débloquer une série de transformations intéressantes pour la synthèse modulaire et la dérivation tardive de molécules complexes.[8] Cependant, son faible nombre de précédents et sa compréhension limitée de la mécanique entravent le développement de protocoles de synthèse pratiques. Je présente ici nos études sur une borylation C–H de transfert catalysée par Rh(I)/Xantphos (Figure 2A), qui est applicable à divers alcènes terminaux et internes et compatible avec une pléthore de groupes fonctionnels (**14a-e**), y compris des groupes hétéroaromatiques (**15**), des alcènes électroniquement variés (**16**) entre autres, et notamment, permet également le transfert de différents esters boroniques (**17**). La borylation late-stage de molécules bioactives, y compris des dérivés du zéaralénol macrocyclique et du médicament Bromphéniramine, souligne sa capacité de synthèse. Une étude mécanistique approfondie comprenant une série d'expériences catalytiques et stœchiométriques ainsi que des études computationnelles ont permis de comprendre le cycle catalytique complet employant une élimination β-boryle, ce qui est sans précédent pour la catalyse Rh, et d'élucider les caractéristiques contrôlant l'activité et la sélectivité (Figure 2, B et C). Ces travaux ouvrent la voie au développement d'autres réactions d'échange d'hydrogène contre des groupes fonctionnels empruntant des voies similaires. Ce travail réalisé en collaboration a été terminé et accepté pour publication. (Lukas Veth,# Hanusch Grab,# **Sebastián Martínez,#** Cyril Antheaume and Paweł Dydio, *Transfer C-H Borylation of Alkenes under Rh(I)-Catalysis: Insight into the Synthetic Capacity, Mechanism & Selectivity-Control*, *Chem Catalysis* **2022**, 2, 762–788; # - equal contribution).
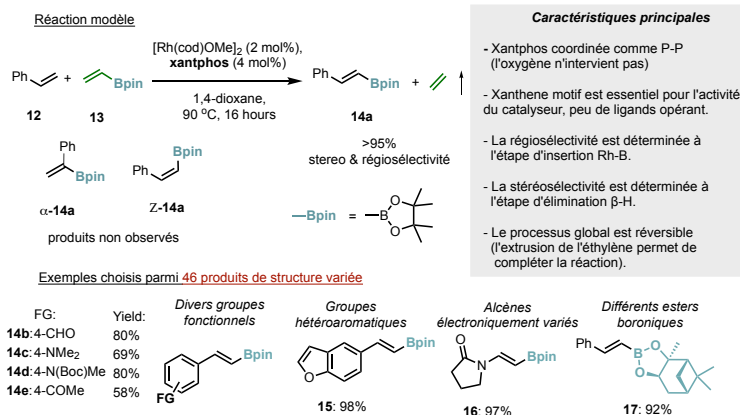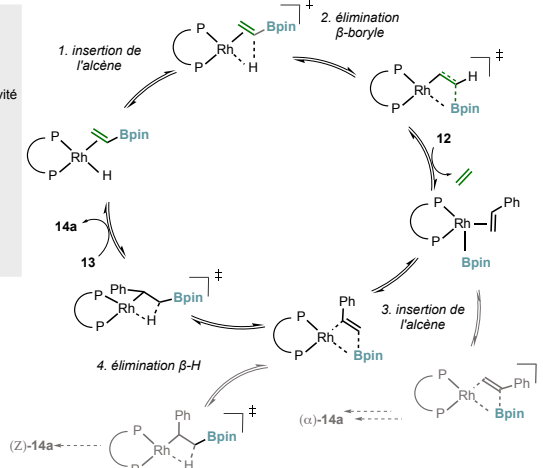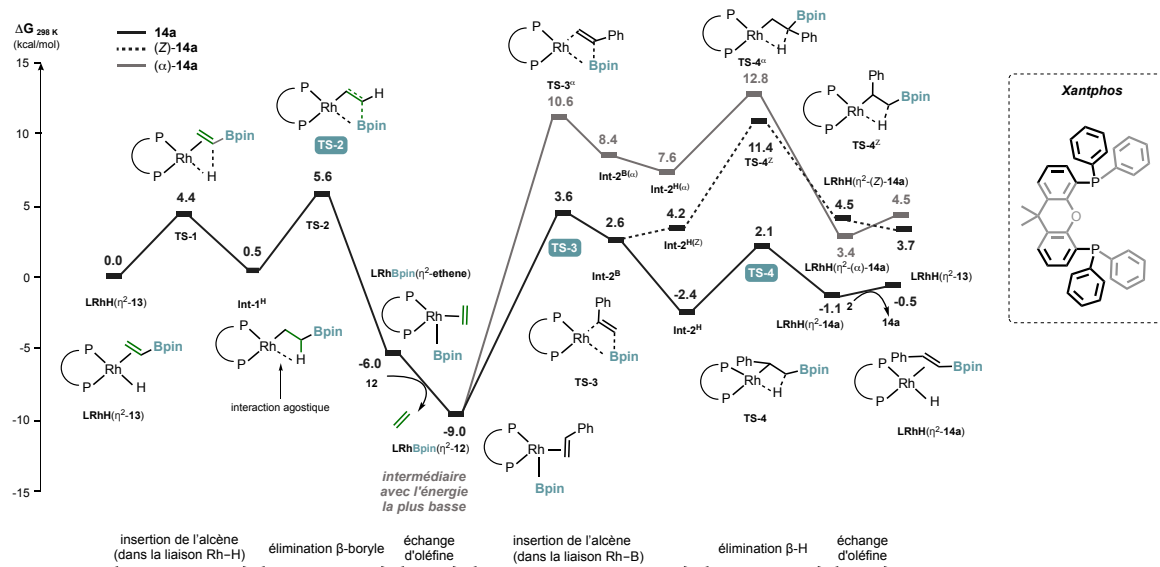
Figure 2. A) Borylation C-H par transfert développé pour les alkènes sous catalyse Rh(I), réaction modèle et exemples représentatifs. Rendement RMN. B) Mécanisme de réaction élucidé par le travail expérimental et théorique. C) Étude DFT sur les surfaces d'énergie libre pour les voies de réaction menant aux produits **14a**, (*Z*)-**14a**, or (α)-**14a**. D) Aperçu de la relation structure du catalyseur - activité et sélectivité. E) Barrières d'énergie libre globales pour la formation des produits avec différents catalyseurs portant des ligands avec une demande électronique et stérique diverse.

X

2. 3 Aperçu de la relation structure-activité du catalyseur dans la borylation C−H par transfert catalysée par Rh(I): Une étude DFT (Chapitre 4)

La compréhension des relations structure-activité des catalyseurs est essentielle pour l'amélioration des performances d'un catalyseur. En utilisant les études DFT comme outil, l'effet que certaines modifications de la structure du catalyseur ont sur le profil de réaction, peut être facilement exploré et compris.[9] De telles études sont particulièrement intéressantes avant l'expérimentation, car elles permettent une conception rationnelle et une présélection de nouveaux candidats catalyseurs, ce qui permet d'économiser d'importantes ressources et du temps. Dans ce chapitre, je présente nos études visant à comprendre comment les caractéristiques électroniques et stériques du ligand phosphine du catalyseur affectent l'activité et la sélectivité de notre réaction de borylation par transfert catalysée par Rh(I)-Xantphos récemment rapportée (chapitre 3). Plus précisément, la discussion comprend les résultats d'une étude computationnelle de quatre variations du catalyseur avec un ligand bisphosphine introduisant soit des motifs donneurs d'électrons, soit des motifs attracteurs d'électrons, soit des motifs stériquement exigeants, dans le but général d'évaluer les effets que ces modifications ont sur les surfaces d'énergie libre de la réaction (Figure 2D).

L'étude révèle que les modifications des propriétés électroniques ou stériques conduisent à un profil de réaction qualitativement similaire, dans lequel la plus grande surface d'énergie se produit à l'étape d'insertion de l'alcène dans la liaison Rh−B, tout en conservant les étapes originales de la réaction déterminant la régio- et la stéréosélectivité. J'ai observé que les effets électroniques ont une influence assez limitée sur les surfaces d'énergie libre, alors que les effets stériques ont un effet plus prononcé. Par exemple, des profils similaires sont obtenus lorsque les cycles phényles sont substitués par des groupes 4-méthoxyphényles riches en électrons ou par des groupes 4-(trifluorométhyl)phényles déficients en électrons. De même, l'installation de Cy, riche en électrons, à la place de Ph, a une influence limitée sur les surfaces d'énergie libre. Bien que les effets soient limités, les études suggèrent que les complexes portant des phosphines riches en électrons forment un catalyseur plus actif. En revanche, les modifications avec le *t*-butyl comme groupe stériquement exigeant, conduisent à une augmentation significative des barrières d'énergie libre globales (Figure 2E). En résumé, nous concluons que de nouveaux catalyseurs comprenant des modifications du noyau du squelette du ligand Xantphos avec un grou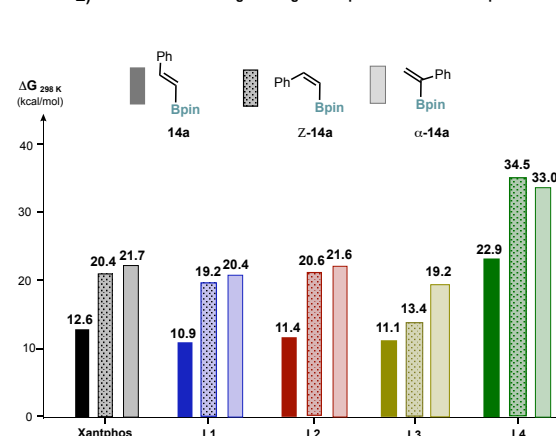pe donneur d'électrons pourraient améliorer les performances du système catalytique. Dans l'ensemble, ce travail a ouvert la voie à la conception rationnelle de nouveaux catalyseurs pour la réaction de borylation par transfert. Un manuscrit incluant les résultats obtenus dans ce travail est actuellement en préparation.

2. 4 Mécanisme d'hydroformylation isosélective du propylène par catalyse au palladium assistée par iodure (Chapitre 5)

La synthèse du *n*-butanal et de l'*iso*-butanal par réaction d'hydroformylation du propylène et du gaz de synthèse est un procédé industriel important, avec une production mondiale de plus de 7 millions de tonnes par an.[10] Cependant, l'un des challenges de ce procédé représente la formation sélective de l'*iso*-butanal, qui est un matériau de plus en plus demandé, par rapport au *n*-butanal. Récemment, notre groupe a rapporté un nouveau protocole pour la réaction titre qui donne une sélectivité exceptionnelle pour l'*iso* par rapport au *n*-butanal, en utilisant un système catalytique basé sur un système catalytique PdI_2–PCy_3.[11] Cependant, le mécanisme de la réaction et les origines de la sélectivité sans précédent, qui sont tous deux cruciaux pour la compréhension et l'amélioration rationnelle du système, restent obscurs. Je présente ici mon enquête mécanistique basée sur les calculs DFT pour démêler la voie de réaction réelle, en étudiant une variété de voies différentes, y compris les propositions communément invoquées. Une série d'études computationnelles a montré que la voie la plus basse en énergie menant à la formation du produit aldéhyde implique une étape

d'élimination réductrice binucléaire isosélective à partir d'espèces neutres (Figure 3). L'anion iodure présent dans le système s'est avéré être un facteur clé pour assurer des énergies libres plus faibles sur la formation des espèces neutres en réaction par rapport aux espèces cationiques, dont la formation représente des pénalités et des barrières d'énergie libre plus élevées. D'autres voies communément proposées, comme l'hydrogénolyse des complexes Pd-acyle, présentent des barrières d'énergie libre plus élevées et sont donc écartées comme voies concurrentes possibles. De plus, l'effet du HI généré pendant la réaction est censé favoriser la réaction, en promouvant la décoordination du ligand PCy3 pendant les étapes élémentaires critiques du cycle catalytique. Dans l'ensemble, ce travail contribue à mieux comprendre la séquence d'événements catalytiques qui est la plus susceptible de se produire, fournissant des connaissances précieuses pour l'amélioration des performances du catalyseur. Un manuscrit incluant les résultats obtenus dans ce travail est actuellement en préparation.
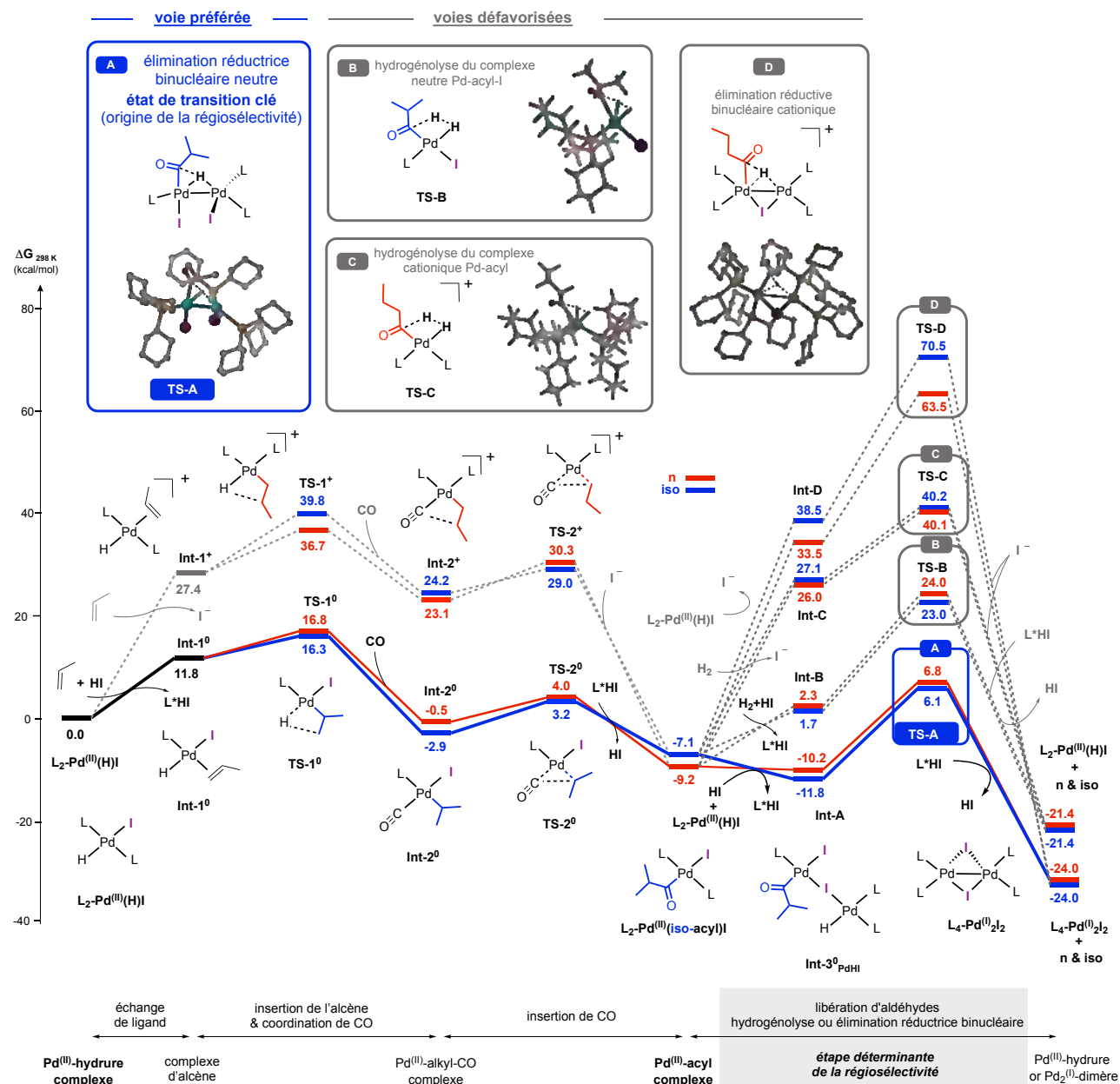

Figure 3. Études mécanistiques computationnelles sur l'hydroformylation isosélective du propylène catalysée par Pd et assistée par un iodure. Les calculs ont été effectués au niveau de théorie M06-L-GD3/def2-TZVP(SMD)//M06-L/def2-SVP dans l'anisole comme solvant ; Int, intermédiaire, TS, état de transition.

3. Conclusion générale

Dans ma thèse de doctorat, j'ai cherché à souligner l'importance de la multicatalyse en tant que domaine émergent pour renforcer la synthèse organique, en passant en revue les avancées les plus pertinentes dans ce domaine, ce qui sert d'introduction à la partie de cette thèse dans laquelle des catalyseurs multiples sont employés (Chapitre 1). Ensuite, j'ai décrit les explorations expérimentales et computationnelles de la puissance des systèmes multicatalytiques. J'ai développé un système bi-catalytique qui exploite des réactions d'hydrofonctionnalisation catalytique réversible orthogonale à la réaction de Diels-Alder pour accéder à une réactivité non-inhérente sans précédent des matériaux de départ, montrant que l'augmentation de la coopérativité et de la complexité en catalyse ouvre l'accès à des raccourcis précieux en synthèse organique (Chapitre 2). Par la suite, je me suis concentré sur le développement de nouvelles réactions catalytiques réversibles, inspirées par la mise en œuvre réussie de celles-ci dans le système multicatalytique mentionné précédemment. Dans le cadre d'un projet collaboratif, nous avons conçu et développé avec succès une nouvelle réaction de borylation par transfert qui fournit, pour la première fois, une méthode générale de transfert de groupes boryles avec une très bonne tolérance aux groupes fonctionnels. Nous avons acquis des connaissances sur la séquence réelle des événements catalytiques d'un point de vue expérimental et théorique, ce qui nous a permis d'identifier les caractéristiques clés contrôlant l'activité du catalyseur et les étapes déterminant la vitesse et la régiosélectivité de la réaction (Chapitre 3). En outre, une étude informatique complémentaire nous a permis de comprendre l'importance des propriétés électroniques et stériques du ligand du catalyseur sur le profil réactionnel, et de conclure que les modifications électroniques (donneuses ou attractrices d'électrons) ont un impact modéré, tandis que l'augmentation de la demande stérique a un effet plus prononcé sur le profil réactionnel (Chapitre 4). Dans l'ensemble, l'installation de petits groupes donneurs d'électrons s'est avérée être un bon point de départ pour la conception et la préparation de catalyseurs plus actifs. Enfin, j'ai décrit nos efforts pour étudier, comprendre et décomposer le mécanisme d'un nouveau protocole pour l'hydroformylation isosélective du propylène, qui est un processus industriel de grande valeur (Chapitre 5). Une série d'études computationnelles montre que la voie la moins énergétique menant à la formation du produit aldéhyde, parmi plusieurs propositions étudiées, implique une voie inhabituelle opérant à travers des intermédiaires neutres, et engage une étape d'élimination réductrice binucléaire isosélective pour libérer le produit aldéhyde. Les connaissances acquises sur la voie de réaction la plus probable constituent la base de la conception et de l'amélioration des performances des catalyseurs. Le travail effectué au cours de cette thèse a conduit à trois manuscrits en préparation et deux articles publiés dans des revues internationales réputées.

4. Références

(1)   Bartholomew, C. H.; Farrauto, R. J. *Fundamentals of Industrial Catalytic Processes*; John Wiley & Sons, Inc.: Hoboken, NJ, USA, 2005.

(2)   Galván, A.; Fañanás, F. J.; Rodríguez, F. Multicomponent and Multicatalytic Reactions - A Synthetic Strategy Inspired by Nature. *Eur. J. Inorg. Chem.* **2016**.

(3)   Fogg, D. E.; dos Santos, E. N. Tandem Catalysis: A Taxonomy and Illustrative Review. *Coord. Chem. Rev.* **2004**, *248* (21–24), 2365–2379.

(4)   Patil, N. T.; Shinde, V. S.; Gajula, B. A One-Pot Catalysis: The Strategic Classification with Some Recent Examples. *Org. Biomol. Chem.* **2012**, *10* (2), 211–224.

(5)   Martínez, S.; Veth, L.; Lainer, B.; Dydio, P. Challenges and Opportunities in Multicatalysis. *ACS Catal.* **2021**, *11* (7), 3891–3915.

(6)   Reed-Berendt, B. G.; Latham, D. E.; Dambatta, M. B.; Morrill, L. C. Borrowing Hydrogen for Organic Synthesis. *ACS Cent. Sci.* **2021**, *7* (4), 570–585.

(7)   Lichosyt, D.; Zhang, Y.; Hurej, K.; Dydio, P. Dual-Catalytic Transition Metal Systems for Functionalization of Unreactive Sites of Molecules. *Nat. Catal.* **2019**, *2* (2), 114–122.

(8)   Hartwig, J. F.; Larsen, M. A. Undirected, Homogeneous C–H Bond Functionalization: Challenges and Opportunities. *ACS Cent. Sci.* **2016**, *2* (5), 281–292.

(9)   Funes-Ardoiz, I.; Schoenebeck, F. Established and Emerging Computational Tools to Study Homogeneous Catalysis—From Quantum Mechanics to Machine Learning. *Chem* **2020**, *6* (8), 1904–1913.

(10) Cornils, B.; Börner, A.; Franke, R.; Zhang, B.; Wiebus, E.; Schmid, K. Hydroformylation. In *Applied Homogeneous Catalysis with Organometallic Compounds*; Wiley Online Books; Wiley, 2017; pp 23–90.

(11) Sigrist, M.; Zhang, Y.; Antheaume, C.; Dydio, P. Isoselective Hydroformylation of Propylene by Iodide-Assisted Palladium Catalysis. *Angew. Chemie Int. Ed.* **2022**, *n/a* (n/a).

Summary of the thesis

1. Introduction

The emergence of transition metal catalysis has had a transformative impact on organic synthesis.[1] In recent years, the use of multiple or single catalysts performing several or single complex reactions in concert proved to be a valuable strategy toward the improvement of the efficiency, selectivity, and atom economy of the overall synthetic process.[2–4] Understanding the sequence of events occurring at a molecular level in such processes is of utmost importance to successfully design, develop, and improve new valuable catalytic systems able to outcompete the current protocols. This mechanistically driven approach for the development of new catalytic methodologies, not only bypass the classical tedious trial and error optimization process but most importantly, provides deeper mechanistic understanding to exploit the full potential of such catalytic systems.

The scope of this PhD thesis diverges into four main axes, which are briefly summarized below. Initially, I provide a broad perspective of the challenges and opportunities in the emerging field of multicatalysis (Chapter 1), as an introduction for the experimental and computational studies of catalytic systems described in the subsequent chapters of this thesis.[5] Subsequently, I describe the design and development of one novel example of such complex multicatalytic systems, which merge the power of reversible catalytic reactions with orthogonal catalytic functionalization reactions. The developed system enables access to non-inherent diene-like reactivity of functionalized molecules, such as alkenyl nitriles, aldehydes, or ketones, in the orthogonal Diels-Alder process, expanding for the first time the 'borrowing chemistry' beyond classical hydrogen borrowing catalysis (Chapter 2). Next, I present our studies regarding a mechanistically driven development of a novel reversible catalytic reaction, which could be attractive for fine chemical synthesis. In particular, we pursued the development of synthetically appealing C–H borylation protocol through a general transfer borylation methodology, exploiting the unprecedented Rh-β–boryl elimination step. Additionally, we provided a comprehensive experimental and theoretical mechanistic study of the reaction mechanism and we gained further understanding on how the modifications on the catalyst's ligand structure influence the reaction profile and product selectivity (Chapter 3 and Chapter 4). Finally, I present our studies focused on providing detailed mechanistic insights into established processes, especially those of industrial relevance, facilitating the rational improvement of their performance. Specifically, I studied the mechanism of the isoselective Pd-catalyzed hydroformylation of propylene, which has been recently developed by our group, with the main goal of unravelling the actual catalytic cycle among the multiple possible pathways, as well as the origins of the unusual isoselectivity (Chapter 5).

Challenges and opportunities in multicatalysis (Chapter 1)

Multicatalysis is an emerging field targeting the development of efficient catalytic transformations to quickly convert relatively simple starting materials into more complex value-added products.[2–4] Within multicatalytic processes either multiple catalysts execute single reactions or precise sequences of multiple catalytic reactions occur in a "one-pot" fashion. Attractively, multicatalytic protocols not only enable transformations that are inaccessible through classic approaches but also are able to significantly reduce time, waste, and cost of the synthetic processes, making organic synthesis more resources efficient. In this chapter, I provide a review of different strategies in multicatalysis that bring distinct challenges and opportunities. This overarching field is divided into three main categories: cooperative, domino, and relay catalysis. Each category is described along with representative examples to highlight its features. Special emphasis is dedicated to relay catalysis, which is further discussed in its subcategories. Lastly, an analysis of systems that incorporate higher levels of complexity and further underscore the potential of multicatalytic systems is provided. This perspective work was finished and published.[5]

2. Results and discussion

As indicated above, the experimental and computation investigations performed during my PhD studies are focused on intertwined research problems centered around mechanistically driven development of four chemical reactions that engage reversible processes. The results obtained for each chemical transformation are briefly summarized below.

2.1 Cooperative catalysis engaging hydro-functional group borrowing unlocks non-inherent reactivity (Chapter 2)

Exploiting non-inherent reactivity of organic molecules within a network of reactions is a powerful approach to improve the overall efficiency of organic synthesis.[6] Such non-inherent reactivity can be unlocked by reversible catalytic reactions, which can transiently change the reactivity of the starting material by reacting with a target functional group. When cooperating with other reactions, challenging new transformations can be executed at initially non-reactive positions, providing valuable shortcuts to the synthetic practitioner. Although many networks of reversible catalytic reactions and transformation reactions have been reported, only reversible dehydrogenation – coined as 'hydrogen borrowing' – has been exploited to access non-inherent reactivity of the starting materials.[6,7] Here I present a series of transformations that exploit reversible catalytic hydrofunctionalization reactions as a key component in the networks to unlock unprecedented temporal diene reactivity, showing for the first time that the 'borrowing strategy' is a more general approach that we name here as 'boomerang-like catalysis'. Specifically, we developed a series of catalytic systems based on Ni- or Rh-catalysts, that engage (homo)allylic nitrile, aldehyde, or ketone starting materials in a sequence of i) *retro-hydrofunctionalization* to form a highly reactive diene, ii) *Diels-Alder cycloaddition* of the diene intermediate and a dienophile, followed by iii) *(re)-hydrofunctionalization* of the in situ generated Diels-Alder adduct to form a functionalized (poly)cyclic product in one step with 100% atom economy (Figure 1A). A model intermolecular reaction showed that nitrile **1a** or **1b** and *n*-butyl crotonate react to form the target bridged bicyclic nitrile **2** in 99 % yield, in the presence of 5 mol % Ni(cod)$_2$, 5 mol % DPEPhos, and 40 mol % AlMe$_2$Cl, after 72 h, at 50 °C (Figure 1B). Other classes of dienophiles such as methacrylate or carboxiamide or maleimide also engaged successfully in the envisioned network to form compounds **3** and **4** (a crotamiton drug derivative) among others, with moderate to high yields. Additionally, employing developed conditions for reversible hydroformylation based on a Rh catalyst, a similar network of reactions furnishes polycyclic compounds **5**, **6** and **7** with moderate to high yields. The developed strategy was applied to the facile construction of a series of polycyclic frameworks found in natural products by exploiting intramolecular reactions (Figure 1C). For instance, such reactions delivered the core of *isosativene* and *cedranediol* in high yields (compounds **8-11**). A manuscript including the results obtained in this work is currently in preparation.
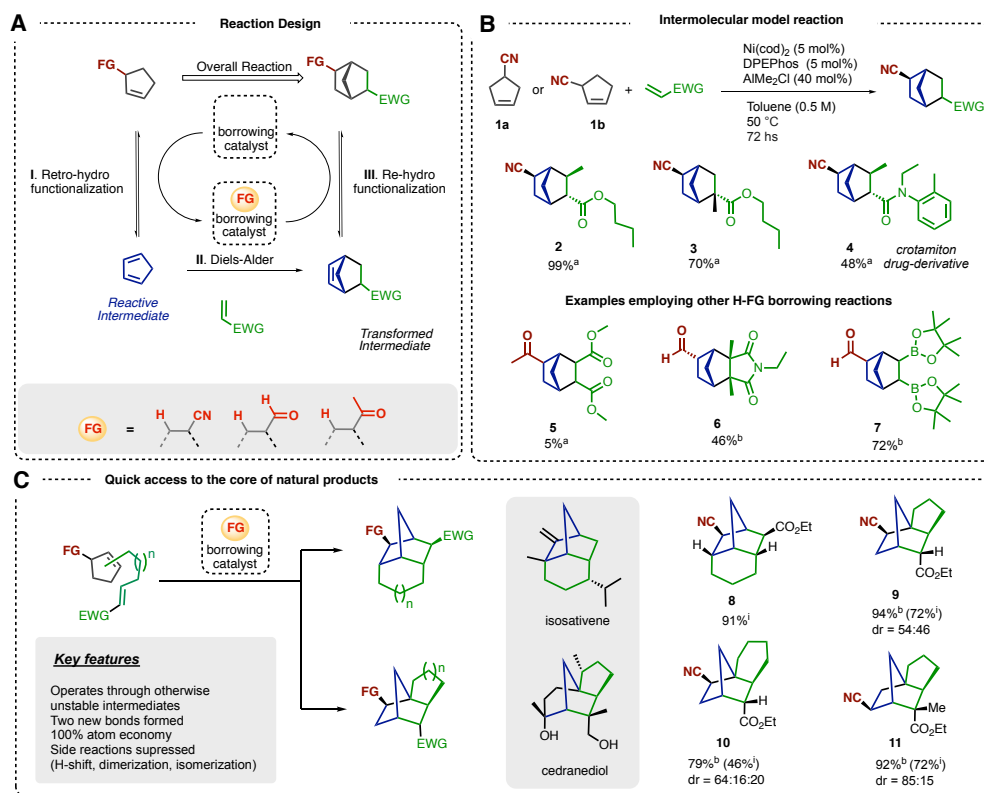
Figure 1. A) Our reaction design for cooperative catalytic systems engaging hydro-functional borrowing and the Diels-Alder reaction. B) Model reaction and selected examples for H-CN borrowing. Additional examples involving H-CHO borrowing. C) Intramolecular reactions as quick synthetic pathways toward the preparation of the core of natural products. [a]GC-yield. [b]NMR yield. dr = diastereomeric ratio. [i] isolated yield.

2. 2 Transfer C-H Borylation of Alkenes under Rh(I)-Catalysis: Insight into the Synthetic Capacity, Mechanism & Selectivity-Control (Chapter 3)

Transfer C−H borylation of alkenes bears the potential to unlock a range of attractive transformations for modular synthesis and late-stage derivatization of complex molecules.[8] However, its scarce precedence and limited mechanistic understanding hinders the development of practical synthetic protocols. Here I present our studies on a Rh(I)/Xantphos-catalyzed transfer C−H borylation (Figure 2A), that is applicable to various terminal and internal alkenes and compatible with a plethora of functional groups (14a-e), including heteroaromatic groups (15), electronically varied alkenes (16) among others, and notably, enables also the transfer of different boronic esters (17). The successful late-stage borylation of bioactive molecules, including derivatives of macrocyclic Zearalenol and the drug Brompheniramine, underscores its synthetic capacity. A thorough mechanistic investigation involving a series of catalytic and stoichiometric experiments as well as computational studies gave insight into the full catalytic cycle employing a β-boryl elimination, which is unprecedented for Rh-catalysis, and elucidated the features controlling the activity and the selectivity (Figure 2, B and C). This work sets the stage for the development of other hydrogen-for-functional group exchange reactions undergoing similar pathways. This work conducted in collaboration was finished and accepted for publication (Lukas Veth,# Hanusch Grab,# **Sebastián Martínez,#** Cyril Antheaume and Paweł Dydio, *Transfer C-H Borylation of Alkenes under Rh(I)-Catalysis: Insight into the Synthetic Capacity, Mechanism & Selectivity-Control, Chem Catalysis* **2022**, 2, 762–778; # - equal contribution).
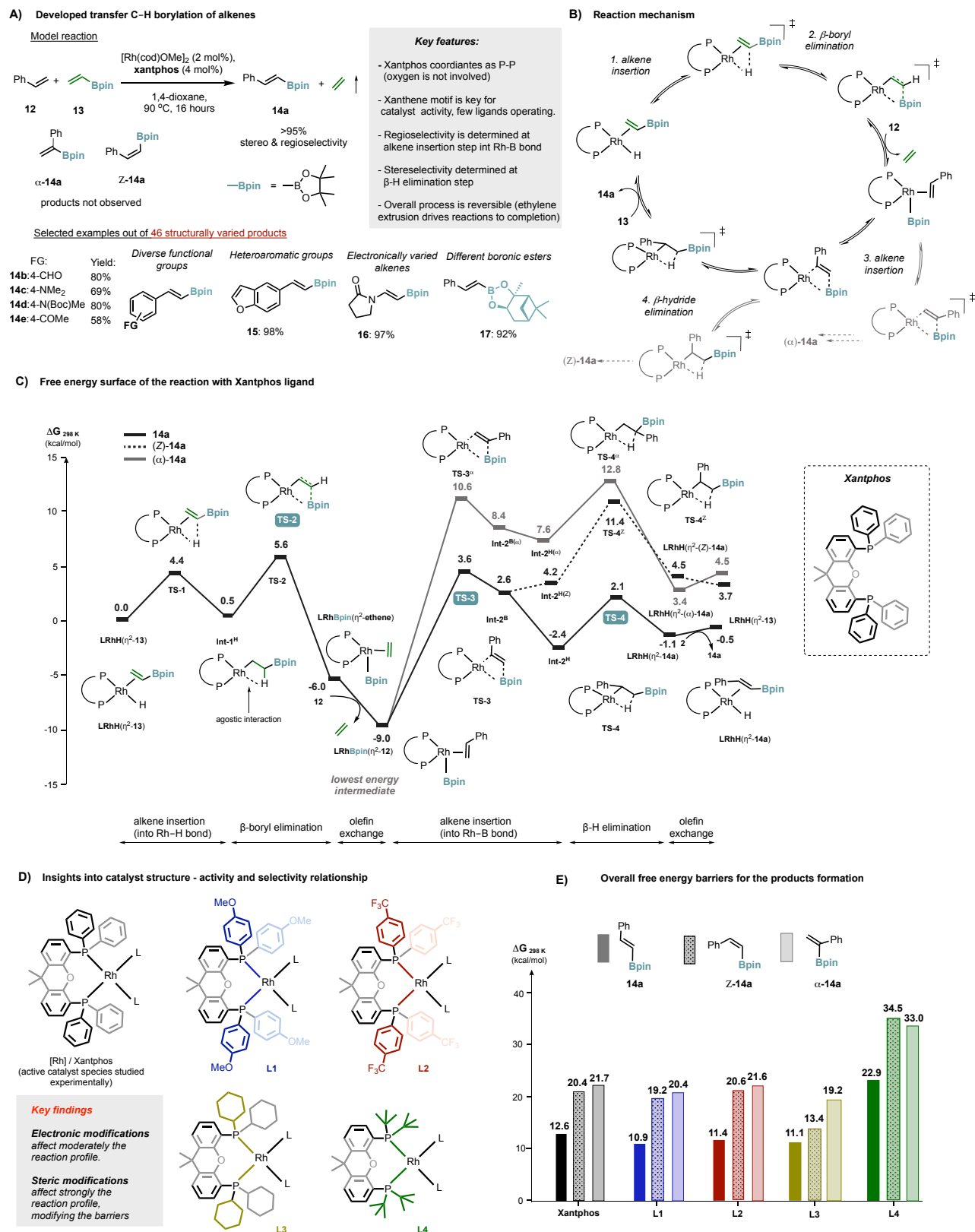
Figure 2. A) Developed transfer C–H borylation of alkenes under Rh(I)-catalysis, model reaction and representative examples. NMR yields. B) Reaction mechanism elucidated by experimental and theoretical work. C) DFT investigation on the free energy surfaces for the reaction pathways leading to products **14a**, (*Z*)-**14a**, or (α)-**14a**. D) Insights into catalyst structure – activity and selectivity relationship. E) Overall free energy barriers for the products formation with different catalysts bearing ligands with diverse electronic and steric demand.

2. 3 Insights into catalyst structure - activity relationship in Rh(I)-catalyzed transfer C-H borylation: A DFT study (Chapter 4)

Understanding the catalyst structure – activity relationships is essential for the enhancement of a catalyst's performance. Using DFT studies as a tool, the effect that certain modifications to catalyst structure have on the reaction profile, can be easily explore and understood.[9] Such studies are particularly attractive prior to experimentation, as they enable a rational design and pre-selection of new catalyst candidates, saving significant resources and time. In this chapter, I present our studies aiming to unravel how the electronic and steric features of the catalyst's phosphine ligand affect the activity and selectivity of our recently reported Rh(I)-Xantphos catalyzed transfer borylation reaction (cf. Chapter 3). Specifically, the discussion includes the results of a computational investigation of four variations to the catalyst with a bisphosphine ligand introducing either electron donating, electron withdrawing, or sterically demanding motifs, with the overall aim to evaluate the effects that these modifications have on the free energy surfaces of the reaction (Figure 2D).

The study uncovers that modifications to either electronic or steric properties, lead to a qualitatively similar reaction profile, in which the highest energetic span occurs at the alkene insertion into Rh–B bond step, while maintaining the original regio- and stereoselectivity-determining steps of the reaction. I observed that electronic effects have a rather limited influence on the free energy surfaces, whereas steric effects have a more pronounced effect. For instance, similar profiles are obtain when phenyl rings were substituted with either electron-rich 4-methoxyphenyl or electron-deficient 4-(trifluoromethyl)phenyl groups. Similarly, the installation of electron-rich Cy in place of Ph has a limited influence on the free energy surfaces. Although the effects are limited, the studies suggest that complexes bearing electron-rich phosphines form a more active catalyst. In contrast, modifications with *t*-butyl as a sterically demanding group, lead to a significant increase in the overall free energy barriers (Figure 2E). In summary, we conclude that new catalysts including modifications to the backbone core of the Xantphos ligand with electron donating group could improve the catalytic system performance. Overall, this work set the stage for the rational design of new catalysts for the transfer borylation reaction. A manuscript including the results obtained in this work is currently in preparation.

2. 4 Mechanism of isoselective hydroformylation of propylene by iodide-assisted palladium catalysis (Chapter 5)

The synthesis of *n*-butanal and *iso*-butanal via hydroformylation reaction of propylene and syngas is an industrially important process, with a global production of over 7 million tons per year.[10] However, one of the challenges of this process represents the selective formation of *iso*-butanal, which is a material of increasing demand, over *n*-butanal. Recently, our group reported a novel protocol for the title reaction that yields outstanding selectivity for *iso* over *n*-prodcut, by using a catalytic system based on a PdI_2–PCy_3 catalytic system.[11] However, the mechanism of the reaction and origins of the unprecedented selectivity, both of which are crucial for understanding and further rational improvement of the system, remain unclear. Here, I present my mechanistic investigation based on the DFT calculations to unravel the actual reaction pathway, by studying a variety of different pathways including commonly invoked proposals. A series of computational studies showed that the lowest energy pathway leading to the formation of the aldehyde product involves an isoselective binuclear reductive elimination step from neutral species (Figure 3). The iodide anion present in the system was found to be a key factor to ensure lower free energies on the formation of the reacting neutral species respect to the cationic ones, of which its formation account for higher free energy penalties and barriers. Other pathways commonly proposed, such as hydrogenolysis of

the Pd-acyl complexes, have higher free energy barriers and therefore are discarded as possible competing pathways. Moreover, the effect of HI generated during the reaction is predicted to favor the reaction, by promoting decoordination of the PCy$_3$ ligand during critical elementary steps of the catalytic cycle. Overall, this work contributes to gain insights into the sequence of catalytic events that is most likely to occur, providing valuable knowledge for further improvement on the catalyst's performance. A manuscript including the results obtained in this work is currently in preparation.
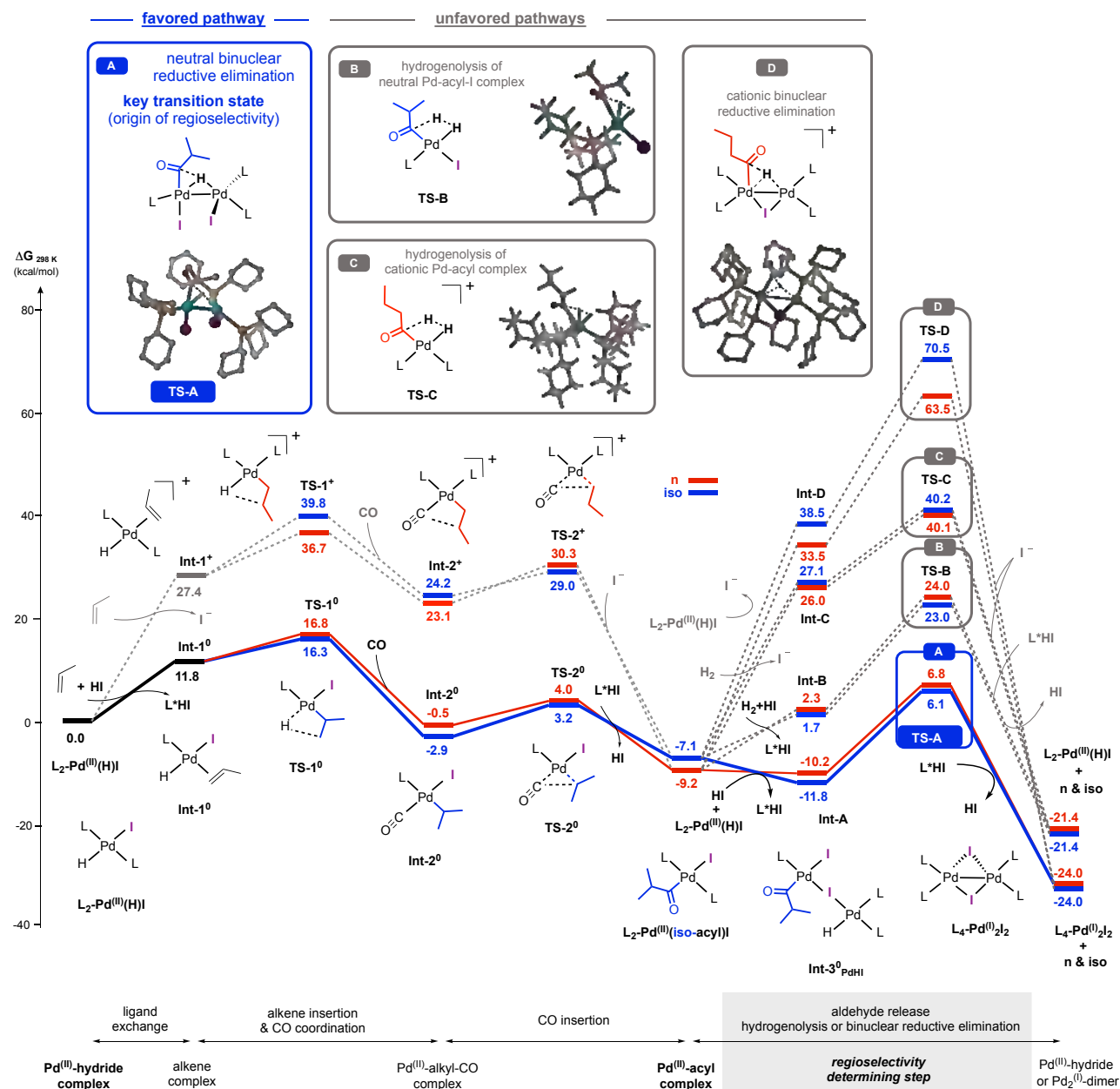

Figure 3. Mechanistic computational studies on isoselective Pd-catalyzed hydroformylation of propylene assisted by iodide. Calculations have been performed at M06-L-GD3/def2-TZVP(SMD)//M06-L/def2-SVP level of theory in anisole as solvent; Int, intermediate, TS, transition state.

3. General conclusion

In my PhD thesis, I aimed to highlight the importance of multicatalysis as an emerging field to empower organic synthesis, providing a review in a perspective fashion of the most relevant advances in the field, which serves as an introduction for the part of this thesis in which multiple catalysts are employed (Chapter 1). Next, I described the experimental and computational explorations of the power of multicatalytic systems. I developed a dual-catalytic system that that exploits reversible catalytic hydrofunctionalization reactions orthogonal to the Diels-Alder reaction to access unprecedented non-inherent reactivity of starting materials, showing that increasing cooperativity and complexity in catalysis open the access to valuable shortcuts in organic synthesis (Chapter 2). Subsequently, I focused on developing new catalytic reversible reactions, inspired by the successful implementation of this ones in the previously mentioned multicatalytic system. In a collaborative project, we successfully designed and developed a novel transfer borylation reaction that provides, for the first time, a general method for boryl group transfer with very good functional group tolerance. We gained insights into the actual sequence of catalytic events from both experimental and theoretical viewpoints that led us to identify the key features controlling the catalyst activity and the rate- and regioselectivity determining steps of the reaction (Chapter 3). Furthermore, a follow up computational investigation allowed us to understand the relevance that electronic and steric properties of the catalysts' ligand have on the reaction profile, concluding that electronic modifications (either electron donating or withdrawing) have a moderate impact, while increasing the steric demand leads to a more pronounce effect on the reaction profile. Overall, the installation of small electron donating groups was found to be a good starting point toward the design and preparation of more active catalysts. Finally, I described our efforts to study, understand, and breakdown the mechanism of a novel protocol for isoselective hydroformylation of propylene, which is a highly valuable industrial process. A series of computational studies show that the lowest energy pathway leading to the formation of the aldehyde product, among several proposals studied, involves an unusual pathway operating through neutral intermediates, and engages an iso-selective binuclear reductive elimination step to release the aldehyde product. The insights gained into the actual reaction pathway that is most likely to occur, set the basis for further design and improvement of the catalysts' performance. The work done during this thesis lead to three manuscripts in preparation and two articles published in reputable international journals.

4. References

(1)   Bartholomew, C. H.; Farrauto, R. J. *Fundamentals of Industrial Catalytic Processes*; John Wiley & Sons, Inc.: Hoboken, NJ, USA, 2005.

(2)   Galván, A.; Fañanás, F. J.; Rodríguez, F. Multicomponent and Multicatalytic Reactions - A Synthetic Strategy Inspired by Nature. *Eur. J. Inorg. Chem.* **2016**.

(3)   Fogg, D. E.; dos Santos, E. N. Tandem Catalysis: A Taxonomy and Illustrative Review. *Coord. Chem. Rev.* **2004**, *248* (21–24), 2365–2379.

(4)   Patil, N. T.; Shinde, V. S.; Gajula, B. A One-Pot Catalysis: The Strategic Classification with Some Recent Examples. *Org. Biomol. Chem.* **2012**, *10* (2), 211–224.

(5)   Martínez, S.; Veth, L.; Lainer, B.; Dydio, P. Challenges and Opportunities in Multicatalysis. *ACS Catal.* **2021**, *11* (7), 3891–3915.

(6)   Reed-Berendt, B. G.; Latham, D. E.; Dambatta, M. B.; Morrill, L. C. Borrowing Hydrogen for Organic Synthesis. *ACS Cent. Sci.* **2021**, *7* (4), 570–585.

(7)   Lichosyt, D.; Zhang, Y.; Hurej, K.; Dydio, P. Dual-Catalytic Transition Metal Systems for Functionalization of Unreactive Sites of Molecules. *Nat. Catal.* **2019**, *2* (2), 114–122.

(8)   Hartwig, J. F.; Larsen, M. A. Undirected, Homogeneous C–H Bond Functionalization: Challenges and Opportunities. *ACS Cent. Sci.* **2016**, *2* (5), 281–292.

(9)   Funes-Ardoiz, I.; Schoenebeck, F. Established and Emerging Computational Tools to Study Homogeneous Catalysis—From Quantum Mechanics to Machine Learning. *Chem* **2020**, *6* (8), 1904–1913.

(10)   Cornils, B.; Börner, A.; Franke, R.; Zhang, B.; Wiebus, E.; Schmid, K. Hydroformylation. In *Applied Homogeneous Catalysis with Organometallic Compounds*; Wiley Online Books; Wiley, 2017; pp 23–90.

(11)   Sigrist, M.; Zhang, Y.; Antheaume, C.; Dydio, P. Isoselective Hydroformylation of Propylene by Iodide-Assisted Palladium Catalysis. *Angew. Chemie Int. Ed.* **2022**, *n/a* (n/a).

CHAPTER 1

Challenges and opportunities in multicatalysis
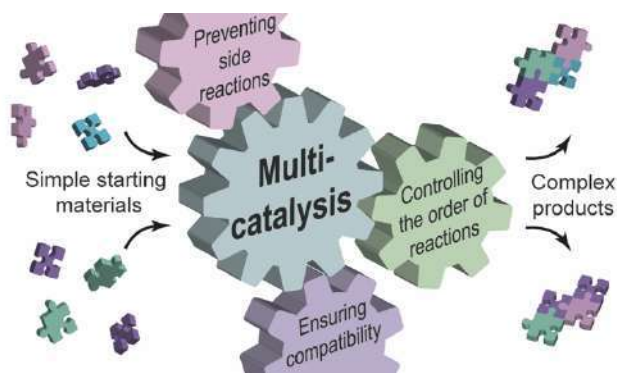
1.1 Introduction

The emergence of catalysis has had a transformative impact on various areas, including the production of chemicals, materials, and fuels, but also healthcare, agriculture, and the environment.[1] From a historical standpoint, first catalysts were developed to enhance the performance of known reactions, but later catalysis started enabling new transformations to address new challenges of the time. Catalytic transformations are typically constrained to one catalyst enabling a single reaction. However, the field continues evolving in complexity to further increase its potential.[2-19] Recently, there has been growing interest in developing multi-catalytic systems, which are inspired by the complexity of catalytic reactions occurring in nature.[2,3] Such efforts are further driven by remarkable characteristics of biosynthesis, that is, excellent selectivity, high yields, and material efficiency when producing complex molecules directly without any isolation of intermediates. However, to develop such multi-catalytic systems, major challenges need to be addressed, including incompatibility between multiple catalysts or reagents, precise ordering of all individual processes, and operation of all reactions under a single set of conditions.

To shed light on different approaches that address the challenges and take advantage of the opportunities of multi-catalysis, i analyze the field and provide insights into its three main categories: cooperative, domino, and relay catalysis. Each type of multi-catalysis is illustrated with a selection of representative reports that highlight their different features. Special emphasis is paid to relay catalysis, sub-categories of which are discussed and further portrayed with corresponding examples. Lastly, more complex systems, consisting of combinations of main multi-catalytic categories, are reviewed. The overall goal of this chapter is to emphasize the vast potential of multi-catalytic 'one-pot' processes to further inspire development and promote applications of such processes across molecular sciences.

Noteworthy, domino catalysis that uses a single catalyst to execute a series of reactions within one catalytic cycle lays at the edge of multi-catalysis, and as such, it might be considered to be outside of the field. However, we included domino catalysis into the scope of this chapter purposefully, in the efforts of portraying the full picture of synthetic systems that execute multiple catalytic events in one-pot.

Because multi-catalytic systems based solely on enzymatic catalysis encounter distinct challenges than the multi-catalytic systems incorporating 'small-molecule' catalysts, they stay beyond the scope of this chapter. I refer the readers to the corresponding reviews.[4–7]

1.2 Definitions and classification

The classification of different types of the multi-catalytic one-pot processes is somewhat inconsistent in the chemical literature. The herein proposed classification is inspired by the efforts of Fogg and Santos,[8] and Patil[9] and aims to provide a systematic analysis that includes all current approaches in this field. All systems with either multiple catalysts or multiple catalytic reactions taking place in the same reaction vessel are accounted for, irrespectively if all reagents or catalysts are present from the start or are added during the reaction along with the possible change of reaction conditions.

Our primary classification of multi-catalytic systems takes into account (i) how the catalysts operate, i.e., the number of catalytic cycles that are involved and if the catalytic cycles are intertwined, and (ii) the number of independent catalytic reactions, i.e., number of bonds being formed, modified, or broken in the overall process, leading to the three categories of "cooperative catalysis", "domino catalysis", and "relay catalysis". Because relay catalysis encompasses a range of

distinct systems bearing different challenges and opportunities, the further division into sub-categories is proposed. Here, the distinction is based on whether one or multiple pre-catalysts are used, i.e., whether each pre-catalyst operates in single or multiple independent catalytic cycles, and whether a change in reaction conditions or an addition of components throughout the process takes place. The general features for each category and sub-category are summarized in Figure 1.
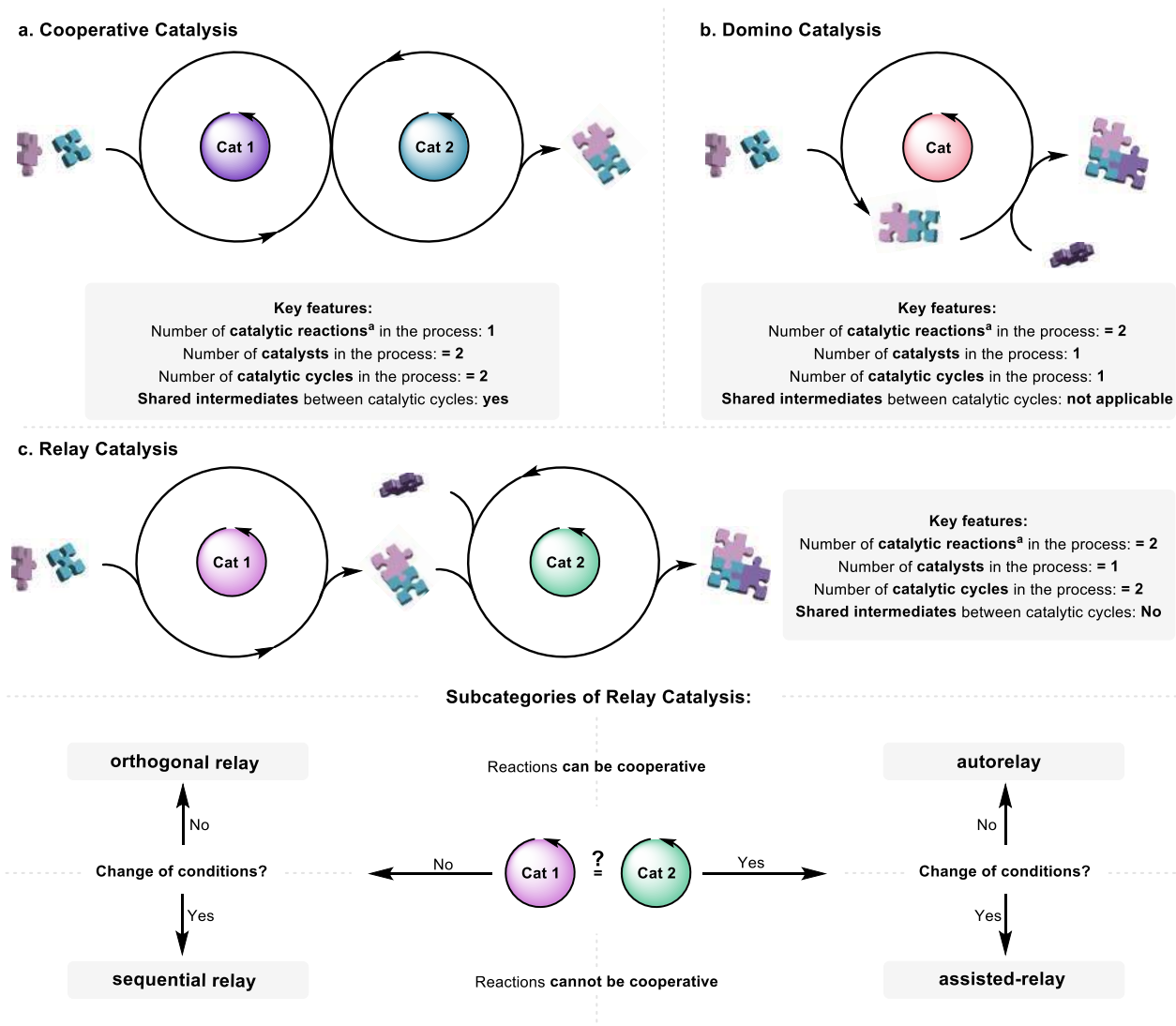
Figure 1. General characteristics of different categories and subcategories of multi-catalytic one-pot processes discussed in the chapter. [a] A single catalytic reaction is understood as a distinct event of making, modifying, or breaking a bond occurring without any noncatalytic reaction intermediates

It is noteworthy that the literature often refers to some multi-catalytic processes as "cascade catalysis". Because of its wide-spread use in different independent contexts, we propose the term "cascade catalysis" to be avoided in the future, as previously also suggested by Tietze.[10]

We also need to note that for the sake of simplicity in this chapter, we use the term 'catalyst' rather liberally to indicate a molecule that is either catalytically active or itself forms a catalytically active species under reaction conditions. When necessary for clarity, we differentiate between a 'pre-catalyst' and an actual 'catalyst' or 'catalytic species'.

4

1.3 Cooperative catalysis

Cooperative catalysis, often referred to as *synergistic catalysis,*[11] refers to catalytic systems in which multiple catalysts operate in concert by sharing their individual catalytic cycles in a single reaction to create, modify, or break a single bond. Consequently, the accumulation of reaction intermediates is not possible. The field of research has been extensively reviewed recently.[12–15] Therefore, below we only discuss representative examples that indicate the key features enabled by cooperative catalysis, noting all possible combinations regarding the different types of catalysts, such as organo/organo, organo/metal, and metal/metal, found in dual-catalytic systems. It is worth noting that in a recent perspective article on enantioselective synthesis with the aid of cooperative dual-catalytic systems,[16] Hoveyda and co-workers pointed out that the two catalysts are not necessarily acting cooperatively in such reactions. Therefore, the term *cooperative catalysis* might be somewhat misleading.

Enabling precise stereocontrol

In stereoselective synthesis, the synergistic action of two catalysts enables the enhancement of stereoselectivity control through the formation of highly organized transition states. For instance, Carreira[17] and co-workers developed a metal/organo dual-catalytic system for the enantio- and diastereodivergent α-allylation of branched aldehydes **1.1** to form γ,δ-unsaturated aldehydes **1.3** from a pair of racemic starting materials (Scheme 1).
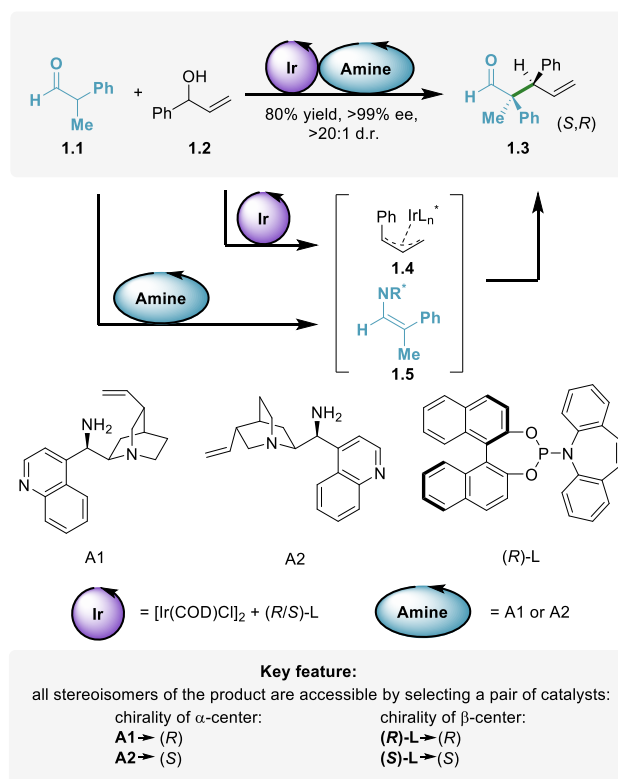
Scheme 1. Ir-/chiral amine-catalyzed cooperative enantio- and diastereodivergent α-allylation of α-branched aldehydes

The reaction occurs in the presence of a chiral Ir-phosphoramidite complex that activates allylic alcohol **1.2** to form allyliridium intermediate **1.4** and chiral cinchona alkaloid A1 or A2 that activates aldehyde **1.1** through the formation of an iminium intermediate **1.5**. Because each catalyst controls the selectivity of each new stereogenic center independently, each of all four possible stereoisomers of **1.3** can be prepared selectively by selecting a pair of suitable enantiomers of both catalysts. By adapting the strategy, the same group subsequently reported two similar systems for the α-allylation of linear aldehydes,[18] and protected α-amino or α-hydroxyacetaldehydes.[19] The strategy was also utilized in a number of other studies with metal/metal[20–26], metal/organo,[27–29] and organo/organo[30] dual-catalytic systems, which demonstrated that multi-catalysis provides powerful tools for stereodivergent asymmetric synthesis.
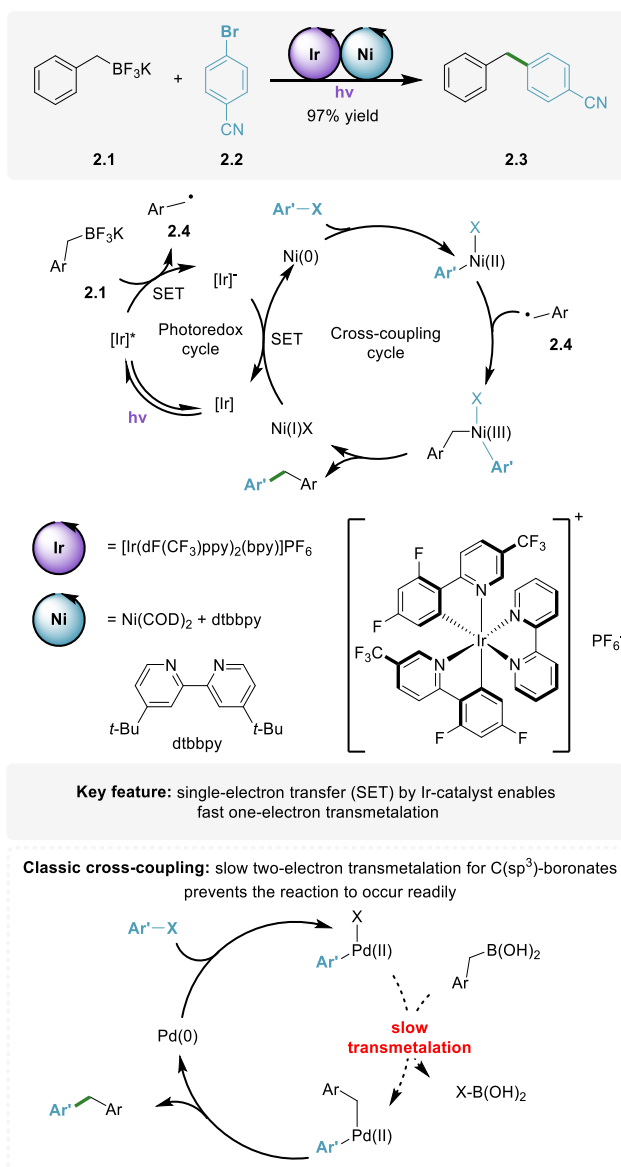
Scheme 2. Ir-/Ni-catalyzed cooperative cross-coupling of sp³-nucleophiles with aryl bromides assisted by a single-electron transmetalation step

Enabling new reaction pathways

        Thanks to the interactions between multiple catalytic cycles, multi-catalysis can create new reaction pathways, enabling transformations that are otherwise either kinetically or thermodynamically unfeasible. For instance, cross-coupling reactions involving alkyl boronic acids occurring in the presence of a single catalyst are typically sluggish, because transmetalation involving sp^3-hybridized organoboronic acid **2.1** is rather slow and requires harsh reaction conditions, limiting the overall applicability.

  To address these issues, Molander[31] and co-workers developed a metal/metal dual-catalytic system that combines a classical Ni-catalyst with an Ir-photoredox catalyst (Scheme 2).[32] The latter mediates a single-electron transfer (SET) to readily form benzyl radicals **2.4** from **2.1**, which undergo fast single electron transmetalation with the Ni-catalyst. Overall, incorporation of a SET enables efficient cross-coupling between sp^3-centered potassium alkoxyalkyl- or benzyltrifluoroborates **2.1** and aryl bromides **2.2** under mild conditions and consequently for a broad range of substrates. In turn, the merger of photoredox catalysis and transition metal catalysis was examined by MacMillan and Doyle to execute cross-coupling reactions with alkyl carboxylic acids as coupling partners.[33] The versatility of the approach was further indicated in other studies, including the report of Molander[34] on using alkyl silicon derivatives as coupling partners and the work of Nishibayashi[35] on using alkyl dihydropyridines as coupling partners. The field of cross-coupling reactions exploiting the combination of photo- and transition metal-catalysts was recently reviewed.[36]

The latter undergoes sequential oxidative addition of aryl halide **3.2** to furnish a Ni^{III}(aryl)(alkyl) species followed by subsequent reductive elimination affording the cross-coupled product **3.3**. Lastly, a series of electron transfer events regenerates catalytic species, closing both catalytic cycles. Other reports on functionalization of unactivated C-H bonds occurring in the presence of analogous metal/metal dual-catalytic systems further underscored the efficacy of the strategy.[43–45]
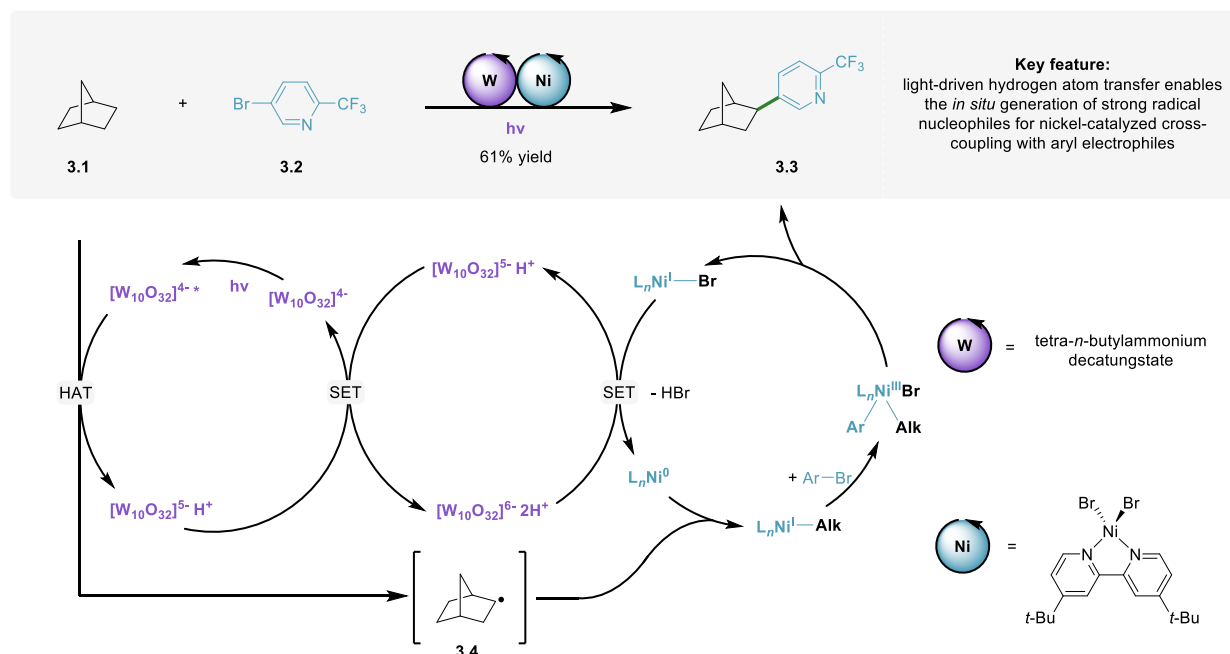
Scheme 3. W-/Ni-catalyzed arylation of strong sp^3-C-H bonds with aryl bromides enabled by light-driven hydrogen atom transfer (HAT)

Cooperation between a photocatalyst (PC) and a hydrogen atom transfer (HAT) catalyst provided new opportunities for free radical organic chemistry.[46] In general, open-shell radical intermediates can be readily generated by an electron transfer process between PCs and organic starting materials. Such radicals can be engaged in transformations that are inaccessible for the closed-shell starting materials. Upon completing the target reactions, the radical intermediates are converted back to the closed-shell products by reacting with the HAT catalysts.[47] For instance, Nicewicz and coworkers[48] recently established anti-Markovnikov hydrohalogenation of styrenyl alkenes occurring selectively in the presence of a organo/organo dual-catalytic system built of an acridinium salt acting as a PC and a thiophenol derivative acting as a HAT catalyst (Scheme 4). Initially, the visible light-excited photoredox catalyst reacts with alkene **4.1** through photoinduced electron-transfer (PET) to form alkene radical cation **4.4**. The latter reacts with a chloride anion through the nucleophilic addition to produce benzylic carbon-centered radical **4.5**. Upon a HAT from the redox-active thiol, the anti-Markovnikov hydrohalogenation product **4.3** is formed. Lastly, a source of acidic protons converts thiolate to the active hydrogen atom donor, allowing turnover of the HAT catalyst. Notably, several halogen, phosphate, and sulfonate anions can be used as nucleophiles, when a well-paired combination of PC and HAT catalysts is used.
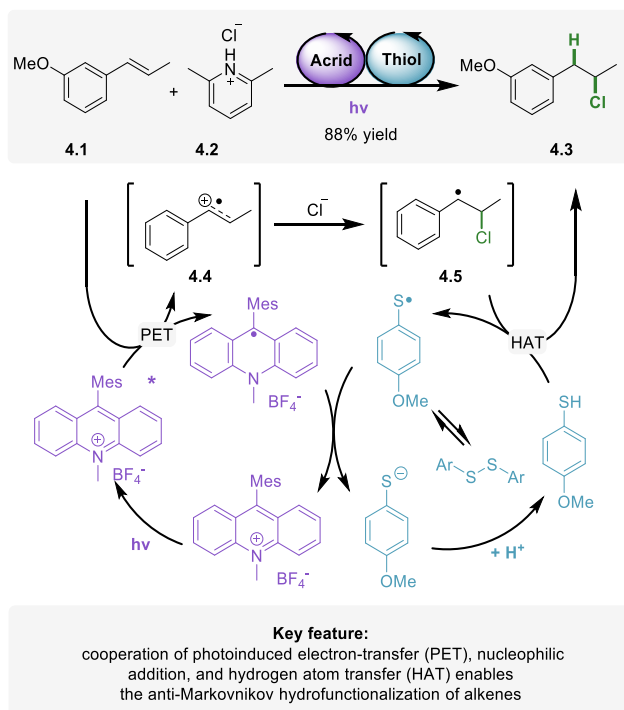
Scheme 4. Merging two organocatalysts enables the light-driven anti-Markovnikov hydrohalogentaion of styrenyl alkenes

The abovementioned photocatalytic strategy using organocatalysts has been extensively studied to afford a range of new reactions, including recent studies on generation and trapping of alkene radical cations[49] in other transformations such as hydroacetoxylation,[50] intra-[51] and intermolecular[52] hydroamination, a range of novel polar radical crossover cycloadditions,[53–55] synthesis of polysubstituted aldehydes,[56] as well as a site-selective arene C-H amination[57] and direct arene C–H fluorination.[58] HAT organocatalysts, such as zwitterionic triazolium amidates, proved also effective in the organo/metal dual-catalytic systems enabling C–H bond alkylation reactions.[59]

Enabling thermodynamically unfeasible transformations

The ability to directly convert a racemic mixture of a compound into its enantiomerically pure form would be attractive from a synthetic standpoint. However, such transformations are thermodynamically unfeasible, due to the prospective increase in entropy (ΔG = +0.42 kcal/mol).[60] To overcome the intrinsic challenges of unfavorable thermodynamics, Miller, Knowles,[60] and co-workers developed an elegant protocol of a light-driven direct deracemization of cyclic ureas **5.1** by the cooperative action of three catalysts namely an (achiral) Ir-photocatalyst, a chiral phosphate catalyst, and a chiral peptide thiol catalyst. The reaction proceeds through the excited-state redox events enabling a kinetic enrichment of one enantiomer (Scheme 5).
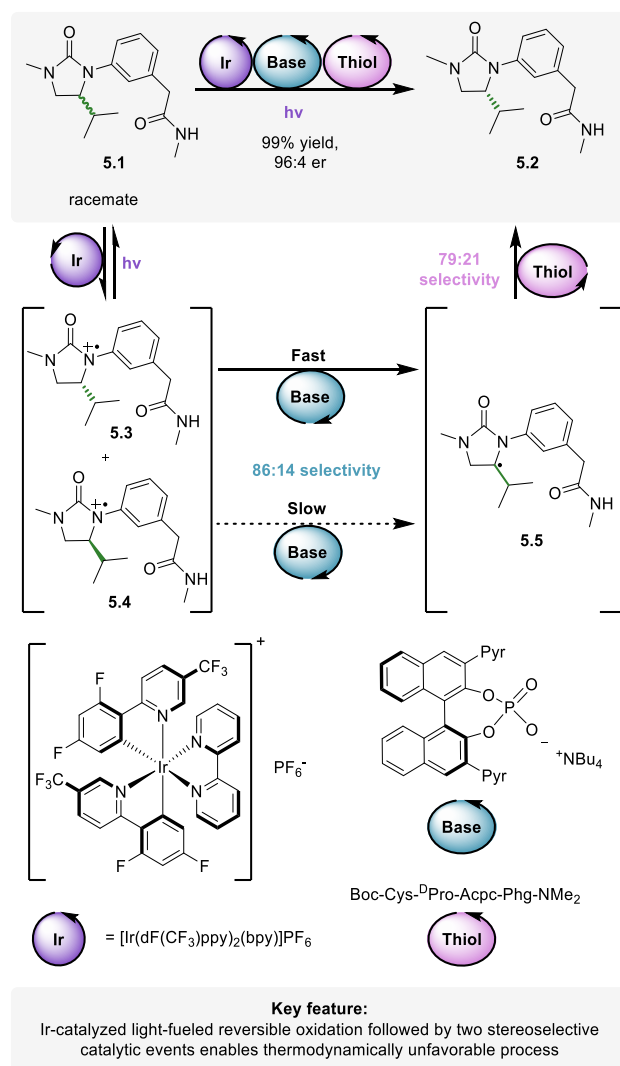
Scheme 5. Ir-/phosphate-/peptide thiol-catalyzed light-driven cooperative deracemization of ureas through stereoselective excited-state processes

First, both enantiomers of cyclic urea **5.1** undergo continuous reversible oxidation by the excited state of the Ir-photocatalyst to form a pair of transient chiral radical cations **5.3** and **5.4**. Then, one enantiomer of the transiently formed **5.3** or **5.4** is preferentially deprotonated by the chiral phosphate catalyst with 86:14 selectivity. In turn, thus-formed α-amino radical **5.5** undergoes enantioselective

hydrogen atom transfer (HAT) in the presence of the chiral thiol catalyst, recovering preferentially the opposite enantiomer of the starting material with 79:21 selectivity. Upon reaching the steady-state level of optical enrichment, the effective overall deracemization is achieved with 96:4 er through the composition of selectivities of chiral oxidation (86:14 er) and chiral hydrogen atom transfer (79:21 er) steps. Overall, the multi-catalytic strategy enables to create the out-of-equilibrium state at the expense of light energy as the fuel.

Cooperation between a series of light-driven organocatalytic processes furnished a kinetically controlled site-selective epimerization of natural sugars to afford rare sugar isomers, as recently reported by Wendlandt[61] and co-workers (Scheme 6). Within the reaction, four organo-catalysts operate in concert, namely a photocatalyst (4-CzIPN), a hydrogen-atom abstraction catalyst (quinuclidine), a HAT catalyst (1-adamantane thiol), and a base (tetrabutylammonium p-chlorobenzoate). First, the blue LED light-excited photocatalyst is quenched by quinuclidine to generate a quinuclidinium radical cation. The latter mediates an irreversible hydrogen-atom abstraction from substrate **6.1** to form sugar radical **6.3**, followed by a diastereoselective HAT from the thiol catalyst to afford the epimerized sugar product **6.2** and the thiyl radical. A series of proton, electron, and hydrogen-atom transfers regenerates catalysts, closing the catalytic cycles.
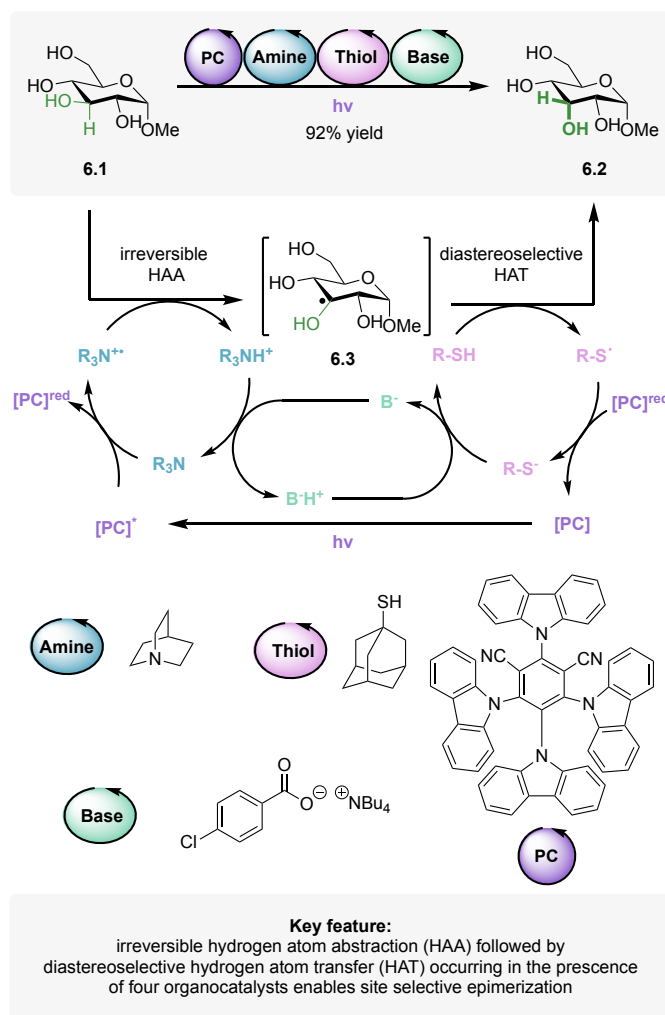
Scheme 6. Cooperative metal-free quadruple-catalytic catalysis enables site-selective epimerization of sugars to form rare sugar isomers

1.4 Domino catalysis

Domino catalysis refers to catalytic systems with typically one catalyst operating in one catalytic cycle to form, modify, or break multiple bonds, i.e., multiple distinct reactions take place within the same catalytic cycle. Considering that a catalyst typically remains bound to the intermediates until the sequence is completed, the accumulation of reaction intermediates is not possible. Because domino reactions have been extensively reviewed in journal articles[62–67] and books,[10,68] below we only discuss representative examples and we further refer the reader to the review literature. However, it is worth noting that some of the reviews do not strictly follow the same definition, sometimes using the term *domino catalysis* in a much broader sense.

It should be noted that *domino catalysis*, featuring only one catalyst that operates in one catalytic cycle, might not belong strictly to the field multi-catalysis. However, the approach represents a stepping stone towards the development of time- and resource-efficient processes with multiple catalytic bond-forming events occurring in one pot. Therefore, we consider its inclusion and a discussion of selected examples as pertinent for this chapter.

Creating multiple bonds within a single linear substrate

Domino reactions were shown to be particularly attractive for natural product synthesis, directly converting relatively simple linear starting materials into complex molecules with high diastereo- and enantioselectivity.
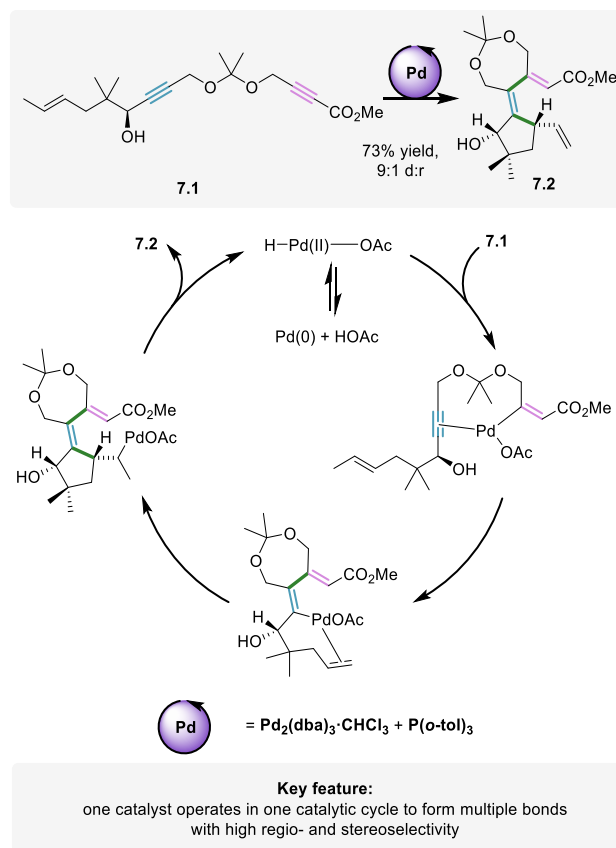
Scheme 7. Pd-catalyzed intramolecular domino polyenyne cycloisomerization for the synthesis of terpene derivatives

The substrates for such processes usually require a high level of design and preorganization for a transformation to be successful; however, the reported examples demonstrate the impressive increase of molecular complexity within a single synthetic step.

For instance, Trost and co-workers[69] employed an intramolecular Pd-catalyzed polyenyne cycloisomerization as the centerpiece of the total synthesis of tremulanes, a group of sesquiterpenes. A linear polyenyne starting material **7.1** containing all the carbon and oxygen atoms in the targeted places undergowent a sequence of reactions through a series of sequential hydropalladation, carbopalladation, and β-hydride elimination steps (Scheme 7). Overall, the Pd-catalyzed domino process resulted in the formation of **7.2** with three new stereocenters, one 5-membered, and one 7-membered ring with high diastereoselectivity and yield in a single synthetic step. In an earlier work from the same group,[70] a Pd-catalyzed polyenyne cycloisomerization led to the formation of six new C-C bonds and seven 5-membered rings, highlighting the synthetic capacity of domino catalysis.

Creating several bonds between multiple substrates

Multiple building blocks can undergo intermolecular reactions to build up molecular complexity under domino catalysis protocols. For instance, Lautens and co-workers[71] recently reported a Co-catalyzed domino transformation, which most likely occurs through a C-H activation of pyridylindole **8.2** followed by a series of insertion steps involving 1,6-enyne **8.1** as the second starting material (Scheme 5). Overall, a pair of simple achiral starting materials are directly converted into pyrrolidine derivatives **8.3** with high regio- and diastereoselectivities and in high yields.
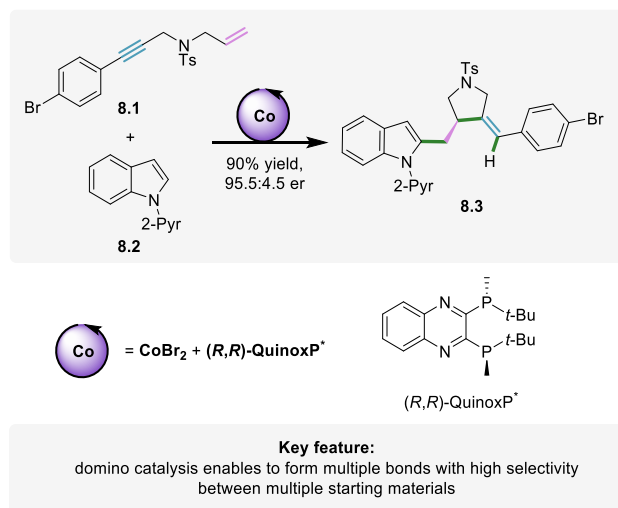
Scheme 8. Co-catalyzed enantioselective hydroarylation of 1,6-enynes through an intermolecular domino reaction

1.5 Relay catalysis

Relay catalysis refers to catalytic transformations occurring in the presence of catalysts, which operate in multiple functionally distinct, non-interfering catalytic cycles to execute a sequence of independent reactions. Importantly, unlike for cooperative catalysis, here catalytic cycles do not share any catalytic intermediates. Therefore, the accumulation of intermediates of the sequence might be possible. It is worth noting that relay catalysis involving two catalysts is often referred to as *tandem catalysis*.

As discussed above, *relay catalysis* covers a range of distinct systems, which we further divided into sub-categories, depending on the number of catalysts and the reaction conditions. In the following chapters, we discuss different types of *relay catalysis*, exemplified by selected examples. Special emphasis is placed on the potential and challenges related to each of the sub-categories.

1.5.1 Orthogonal relay catalysis

Orthogonal relay catalysis refers to catalytic systems exploiting at least two catalysts, which are present and active from the start, with each catalyst mediating only one of multiple consecutive reactions. The strategy requires to address all the common challenges of multi-catalysis, which include (i) the compatibility between all catalysts and reagents, i.e., catalysts and reagents must not inhibit each other or undergo non-productive side reactions; (ii) common conditions, i.e., all reactions need to occur under the same set of reaction conditions; and (iii) reaction ordering, i.e., each catalyst is designed to undergo a selective reaction only with one specific intermediate of the reaction sequence. Despite all the requirements associated, orthogonal relay catalysis represents arguably an ideal case of relay catalysis, providing numerous features inaccessible in other cases. The representative examples that highlight such features are discussed below.

Decreasing overall reaction time for two-step processes

Among typical advantages of orthogonal relay processes are reduction of the reaction time, the amount of work, and resources needed for the overall transformation when compared to the corresponding two-step process.
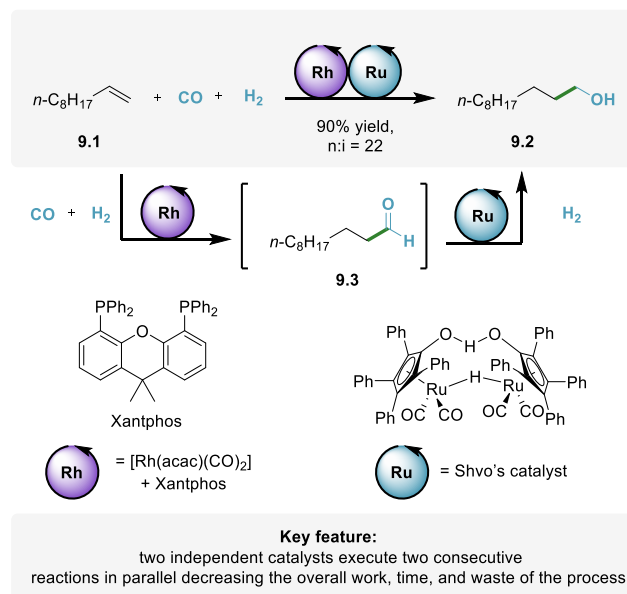
Scheme 9. Rh-/Ru-catalyzed orthogonal relay of hydroformylation-hydrogenation of terminal alkenes to form terminal alcohols

For instance, a large volume of linear aliphatic alcohols in the industry is prepared by a two-step sequence involving hydroformylation of alkenes **9.1** to form aldehydes **9.3**, which are later hydrogenated to the target alcohol products **9.2**. To improve the economy of the process by limiting the overall reaction time of the process, Nozaki and co-workers[72,73] developed the orthogonal relay

of hydroformylation and hydrogenation steps occurring in parallel in the same vessel in the presence of a dual-catalytic Rh-/Ru-system (Scheme 9). The control experiments confirmed that both reactions are fully independent of each other. The overall yield remains the same, irrespectively whether the process is conducted in a one-step or two-step fashion, with the catalysts added sequentially.

Enabling selective sequences under mild conditions

Hydroaminomethylation, a formal combination of hydroformylation of alkenes with reductive amination of aldehyde intermediates, represents an attractive strategy to convert abundant alkenes into value-added aliphatic amines.
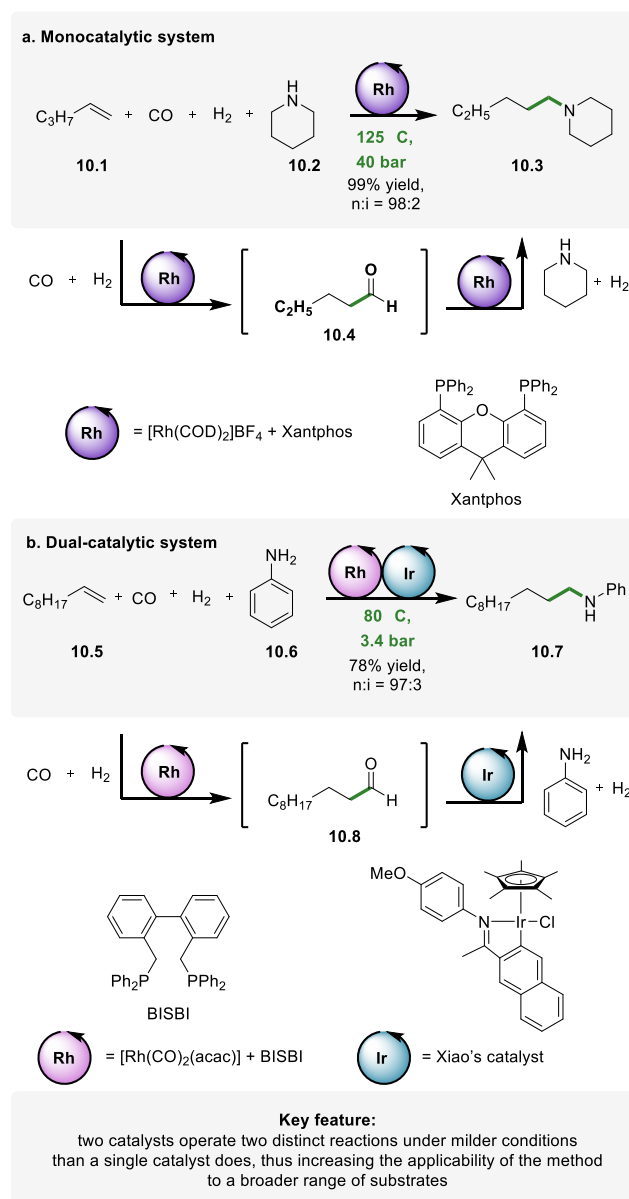
Scheme 10. Comparison of mono-catalytic Rh-catalyzed auto-relay protocol (a) and the bi-catalytic Rh-/Ir-catalyzed orthogonal relay protocol (b) for direct hydroaminomethylation of terminal alkenes to form amines

Beller and co-workers[74] reported that the full sequence can be executed in the presence of a single Rh-complex (auto-relay catalysis, vide infra); however, harsh conditions (>120 °C, 40 bar) are required, which limit the prospective scope of the transformation (Scheme 10a). Because orthogonal relay catalysis enables to select each catalyst for each function independently, the dual-catalytic strategy might facilitate the optimization of the overall activity and selectivity. In that context, Hartwig and co-workers[75] reported an orthogonal relay protocol for hydroaminomethylation of alkenes, which connects Rh-catalyzed hydroformylation of alkenes **10.5** with in situ Ir-catalyzed reductive amination of aldehyde intermediates **10.8** to form amines **10.7** (Scheme 10b).
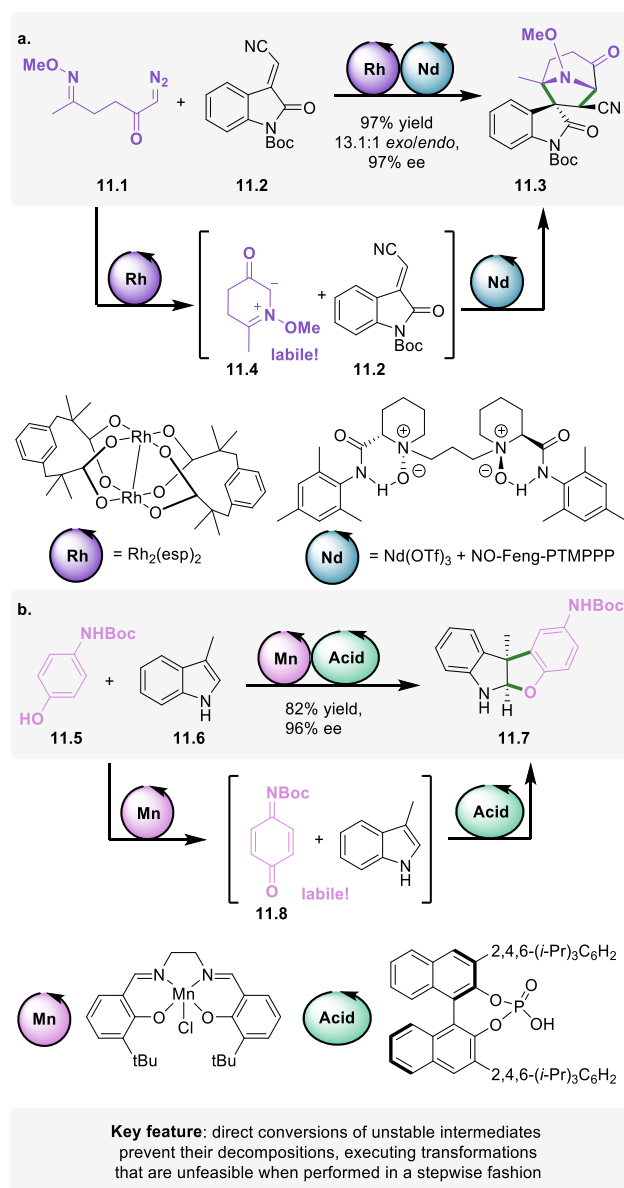
Scheme 11. Orthogonal relay processes occurring through unstable reaction intermediates: (a) Rh-catalyzed formation of labile azomethine ylides followed by Nd-catalyzed enantioselective 1,3-dipolar cycloaddition, and (b) Mn-catalyzed oxidation of phenol to labile N-boc quinone imines followed by CPA-catalyzed enantioselective 1,3-dipolar cycloaddition

Although the approach requires two precious metal catalysts, the full sequence occurs under milder conditions (80 °C, 3.4 bar) with superior regioselectivity, and a broader functional group tolerance, when compared with the sequence in the presence of a single catalyst. The comparison of both protocols underscores the advantages of orthogonal relay catalysis.

Including unstable intermediates

 Under orthogonal relay catalysis, an intermediate can be converted further as soon as it is formed, leading to its short residence time in the reaction mixture.
Therefore, such pathways of reactions can include unstable intermediates, which would be otherwise unfeasible for a stepwise approach. Waldmann and co-workers[76] developed the enantioselective synthesis of the spirotropanyl oxindole scaffold **11.3** proceeding through the Rh-catalyzed reaction of (*E*)-oximino α-diazo ketone **11.1** to form transient azomethine ylide **11.4** that subsequently underwent Nd-catalyzed intermolecular 1,3-dipolar cycloaddition with 3-alkenyl oxindoles **11.2** (Scheme 11a). That one-pot relay approach provides straightforward access to a class of complex biologically active compounds. The synthetic sequence could not be executed in a stepwise manner, due to the instability of the ylide intermediate.
 Zhong and co-workers[77] reported a direct synthesis of benzofuroindolines **11.7**. The sequence occurs thorough Mn-catalyzed oxidation of *N*-Boc aminophenols **11.5** to unstable *N*-Boc quinone imines **11.8**, which subsequently undergo a phosphoric acid-catalyzed enantioselective 1,3-dipolar cycloaddition with indoles **11.6** (Scheme 11b). The strategy was inspired by related phenol oxidation processes occurring in nature, with the Mn-salen complex mimicking natural metalloenzymes.

Preventing secondary reactions of intermediates

In many cases, a primary product of a catalytic reaction remains reactive under catalytic conditions, undergoing secondary side reactions that lower the yield of the target transformation. Because under orthogonal relay catalysis, intermediates might be quickly converted in subsequent reactions, such secondary side reactions can be minimized, increasing the yield of the overall transformation.
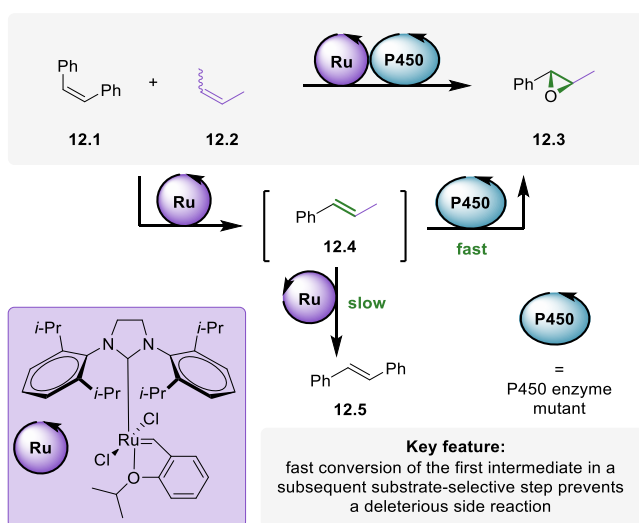
Scheme 12. Ru-/P450-catalyzed orthogonal relay of olefin cross-metathesis and substrate-selective epoxidation of heterocoupling olefin product

To demonstrate the principle, Hartwig, Zhao, and co-workers[78] reported a dual-catalytic system that connects a Ru-catalyzed cross-metathesis of (Z)-stilbene **12.1** with 2-butene **12.2** that forms heterocoupling alkene intermediate **12.4** with a subsequent P450-catalyzed substrate-selective epoxidation of intermediate **12.4** to form selectively arylalkyl epoxide **12.3** (Scheme 12). The fast conversion of alkene intermediate **12.4** outcompetes its slow conversion to (E)-stilbene **12.5** in a secondary reaction of the Ru-catalyzed cross-metathesis, leading to higher yields than a corresponding two-step procedure.

Enabling inaccessible transformations through hydrogen borrowing

Hydrogen borrowing catalysis[79] refers to the process exploiting transition metal-catalyzed reversible oxidation of alcohols, amines or alkanes to form transient aldehydes/ketones, imines or alkenes that can undergo a series of new reactions, including typically alkylation or amination, leading directly to value-added compounds.
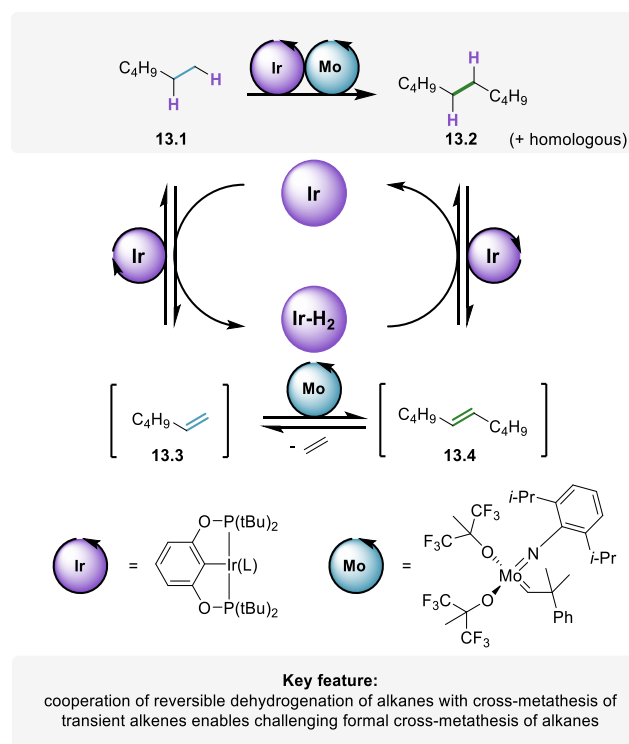
Scheme13. Ir-/Mo-catalyzed orthogonal relay of alkane dehydrogenation-alkene metathesis-alkene hydrogenation for formal alkane cross-metathesis

Attractively, the process eliminates any stochiometric redox reactions required otherwise in a stepwise approach. However, by combining the hydrogen borrowing catalysis with catalytic functionalization reactions into dual-catalytic systems, a broad chemical space of new transformations can be envisioned. In that context, Goldman, Brookhart, and co-workers[80] reported a remarkable dual-catalytic system for the elusive cross-metathesis of linear alkanes (Scheme 13). The sequence involves an Ir-catalyzed reversible dehydrogenation of starting alkane **13.1** to form a transient terminal alkene **13.3**, followed by Mo-catalyzed cross-metathesis to yield new larger alkenes **13.4** (and ethylene), which are lastly hydrogenated back to larger alkanes **13.2** by the initial Ir-catalyst. Although, the system suffers from isomerization reactions and harsh reaction conditions,

17

forming a broad distribution of products, the study underscores the unique potential of cooperating reactions under orthogonal dual catalysis.

Following similar design principles, we devised dual-catalytic transition metal systems for functionalization of unreactive sites.[81] For instance, a relay of reversible oxidation of alcohols and arylation of transient aldehydes enables a general method for direct β-arylation of alcohols.
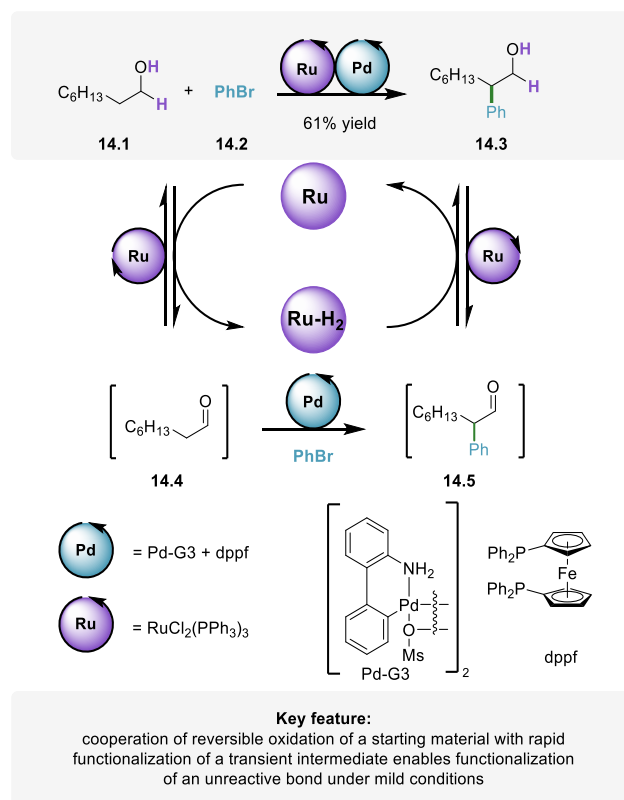
Scheme 14. Ru-/Pd-catalyzed orthogonal relay of alcohol dehydrogenation-aldehyde arylation-aldehyde hydrogenation for direct β-arylation of alcohols

Specifically, in the system, primary alkyl alcohol **14.1** undergoes reversible oxidation by a Ru-catalyst to form transient aldehyde **14.4**. The latter undergoes Pd-catalyzed arylation to form aryl aldehyde **14.5** prior to reduction to the β-aryl alcohol **14.3** by the same hydrogen borrowing Ru-catalyst (Scheme 14). In the same vein, the combination of Fe-catalyzed hydrogen borrowing equilibrium with Rh-catalyzed enantioselective hydroarylation of an α,β-unsaturated aldehydes enables a method for direct enantioselective γ-hydroarylation of allylic alcohols. Importantly, because both reactions building such dual-catalytic systems occur under mild conditions, the overall functionalizations of unreactive sites occur also under mild conditions, enabling the application of such methods to a broad range of starting materials with a high functional group tolerance. Noteworthy, a combination of hydrogen-borrowing catalysis with organocatalysis was reported to enable the control of enantioselectivity of reactions[82,83] that are otherwise racemic under sole hydrogen-borrowing catalysis.[84]

Correcting selectivity of unselective reactions

Sequences of unselective but reversible reactions cooperating in situ with other selective reactions can increase the selectivity of the overall transformations. For instance, cross-metathesis of two olefins typically leads to the formation of a statistical mixture of a heterocoupling product and undesired homocoupling products, lowering the process efficiency. To address this issue, Hartwig, Zhao, and co-workers[85] showed that a combination of an unselective but reversible Ru-catalyzed cross-metathesis of alkenes **15.1** and **15.2** with a substrate-selective P450-catalyzed epoxidation of olefin **15.4** enables to increase the overall efficiency of the sequence (Scheme 15). Specifically, the selective conversion of heterocoupling alkene **15.4** to epoxide **15.3** drives the reversible metathesis reaction to continuously form a new portion of alkene **15.4** at the expense of homocoupling product **15.5** and starting alkene **15.2**. The authors showed that in the dual-catalytic system, the overall yield of the target epoxide product **15.3** was 1.5 times higher, while the end-concentration of the self-metathesis product **15.5** was 40% lower, and the remaining concentration of the starting material **15.2** was 20% lower, than in the stepwise transformation.
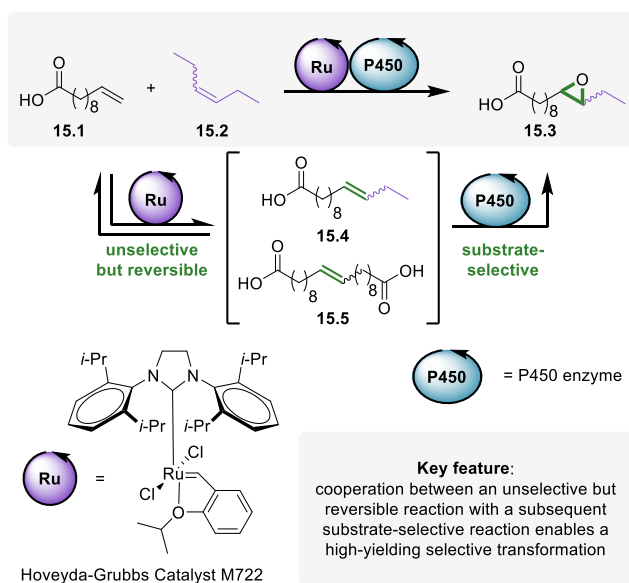
Scheme 15. Ru-/P450-catalyzed orthogonal relay of reversible olefin cross-metathesis and substrate-selective epoxidation of alkenes

The design principles of the above-described system of cooperating reversible olefin metathesis with selective olefin epoxidation resemble the working principles of dynamic kinetic resolution reactions (DKR).[86–89] In the latter, a dynamic equilibrium between two enantiomers of a substrate is maintained, but one enantiomer undergoes a subsequent reaction selectively. For instance, a secondary alcohol continues to be reversibly oxidized-reduced to maintain the racemic composition of the mixture in the presence of a hydrogen-borrowing catalyst, but one enantiomer of the alcohol continuous to undergo a selective acylation in the presence of a lipase, leading in the end to a quantitative conversion of a racemic alcohol to an enantiomerically pure ester. This strategy has been extensively studied for deracemization of alcohols, amines, aldehydes, and ketones. Recently, a combination of photo- and enzymatic catalysis has been reported, opening up the chemical space of DKR to the elusive stereoselective reduction of mixtures of (*E*)- and (*Z*)-alkenes.[90]

Exploiting thermodynamic leveraging

By exploiting the concept of *thermodynamic leveraging,* orthogonal relay catalysis bears the potential to execute reactions in sequence that are thermodynamically unfeasible. In such case, an endothermic reaction is coupled with a subsequent exothermic reaction to create an overall thermodynamically favorable sequence. For instance, Marks and co-workers[91] reported a dual-catalytic method for the etheric C-O bond hydrogenolysis through a combination of Ln(OTf)$_3$-catalyzed endothermic reversible C-O bond scission with a subsequent Pd-catalyzed exothermic C=C bond hydrogenation to generate an overall favorable process (Scheme 16). Such transformations can be used to convert biomass-based materials to alkanes,[92] providing a sustainable alternative to fossil fuels.
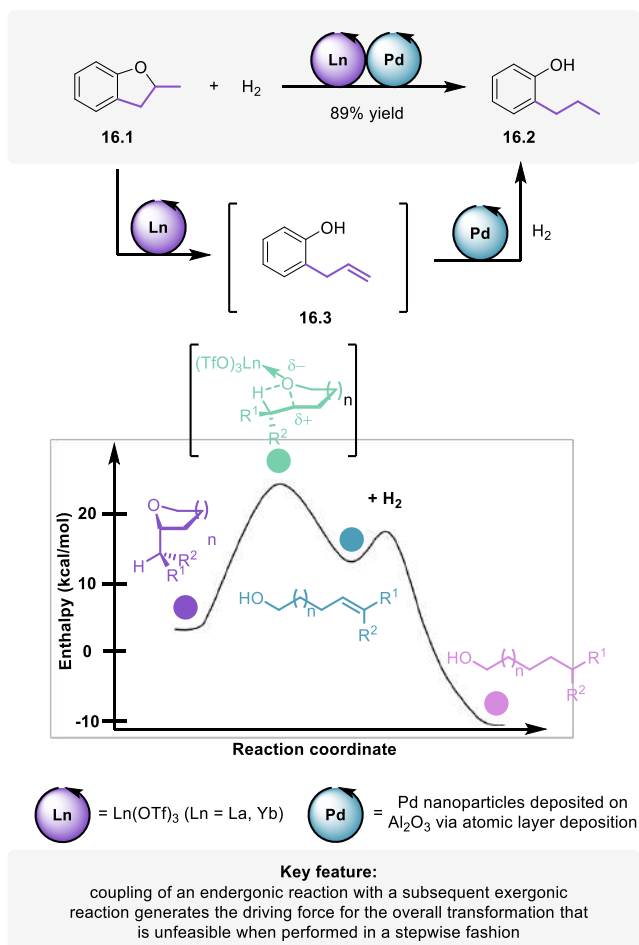
Scheme 16. Thermodynamic leveraging in Ln-/Pd-catalyzed orthogonal relay of retro-hydroalkoxylation of ethers and alkene hydrogenation drives the etheric C-O bond hydrogenolysis

Preventing compatibility issues

One of the major challenges in the development of orthogonal relay-catalyzed transformations is the prospective incompatibility of catalysts that leads to inhibition of catalytic activity, preventing the overall process to occur. One of the common issues in case of transition metal-catalysis is the prospective ligand scrambling. For instance, in the synthesis of dihydroquinolines **17.3** through a

combination of binap-Rh-catalyzed hydroarylation of alkyne **17.1** (with aryl boronic acid **17.2**) followed with Xphos-Pd-catalyzed *N*-arylation (Scheme 17).
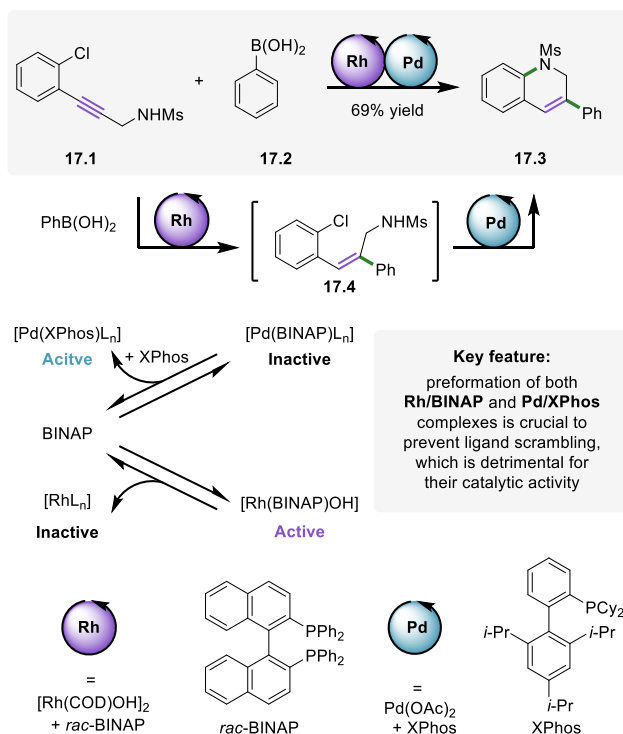
Scheme 17. Synthesis of dihydroquinolines in the orthogonal relay of Rh-catalyzed alkyne hydroarylation followed with Pd-catalyzed intramolecular N-arylation

Lautens and co-workers[93] noted that the formation of mixed ligand complexes is detrimental to the catalytic process. However, the ligand exchange between complexes does not occur under the catalytic conditions (or occurs slowly). Therefore, when suitable complexes are formed prior to adding to the reaction mixture, their catalytic activities are maintained, enabling the formation of product **17.3** in 69% overall yield. Furthermore, this strategy proved effective to prevent premature ligand scrambling in asymmetric variants of orthogonal-relay catalytic reactions in which two metals and two ligands, one chiral and one achiral, are used.[94,95] Although effective, the approach is not general. Therefore, there have been many other strategies studied to address the incompatibility issues with the physical separation of catalysts.[96] In such a case, not only prospective ligand exchange processes are hindered but also any cross-reactivity is prevented. For instance, the physical separation of catalysts within the same vessel can be realized by catalysts immobilization on a solid support.[97]

The incompatibility between reagents of one step with the reagents or catalysts of other steps of the sequence might also be encountered in multi-catalytic systems. Strategies to address such incompatibility issues mainly focus on compartmentalization of different reactions, i.e., the catalysts and reagents for different steps are located in different 'compartments' of the reactor.[2] The compartments can be constructed by phases that are either immiscible,[98] separated by semi-permeable membrane,[99] or physically separated with the volatile intermediates being exchanged through the gas-phase.[100] An elegant example of reaction isolation was reported by Weck and co-workers in a sequence of a Co-catalyzed hydration of alkyne **18.1** to form ketone **18.3** and its

subsequent Rh-catalyzed enantioselective transfer hydrogenation to form enantioenriched secondary alcohol **18.2** (Scheme 18).[101]
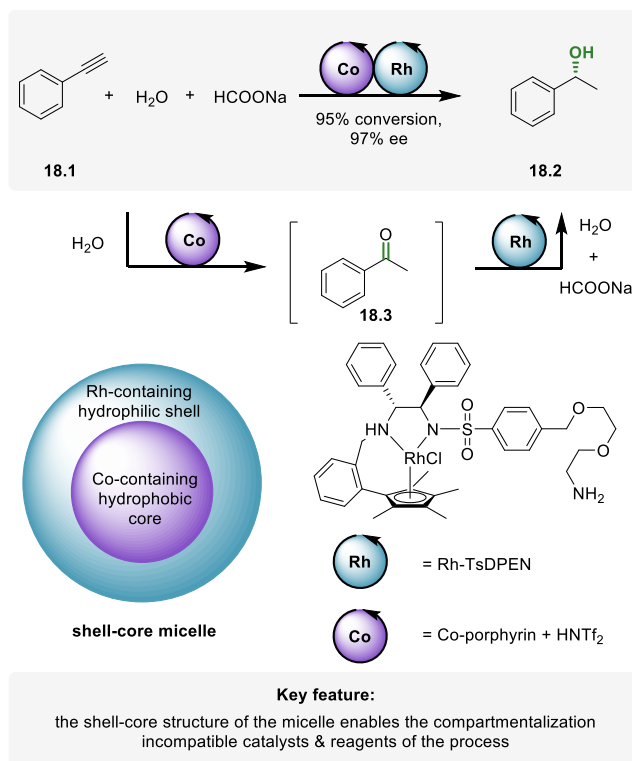
Scheme 18. Co-/Rh-catalyzed orthogonal relay for the enantioselective conversion of terminal alkynes to secondary alcohols enabled by the compartmentalization of incompatible reactions

The reactions are not compatible with each other because HCOONa, that is, the hydrogen source for the Rh-catalyzed transfer hydrogenation, is not compatible with the Co-catalyst. Therefore, the authors designed a core-shell micellar support constructed in an aqueous environment. The Co-catalyzed hydration takes place in the hydrophobic core, which expels detrimental HCOONa, while the Rh-catalyzed hydrogenation takes place in the hydrophilic shell of the micelle. Notably, the fast diffusion of the ketone intermediate within the core-shell micelle containing both catalysts leads to increased yields, when compared to the control reactions in the presence of a mixture of micelles containing one or the other catalyst. Such spatial organization of catalysts mimics the substrate channeling operating in nature.[102]

Noteworthy, when biocatalysis and chemocatalysis are both employed, the sequences are typically executed with the aid of multi-phase systems with catalysts operating in different, non-mixable phases, between which the intermediates are exchanged. For instance, the sequence of Ru-catalyzed olefin metathesis and subsequent P450-catalyzed epoxidation (Scheme 15)[85] was executed in a biphasic system consisting of a dioctylphthalate-phase for the metathetic reaction and an aqueous-phase for the epoxidation reaction. Generally, the strategies for the separation of bio- and chemocatalysts are well-developed, and have been reviewed previously.[2] Also, the use of artificial biocatalysts, including artificial metalloenzymes, has been reviewed.[103,104]

1.5.2 Sequential catalysis

Sequential catalysis refers to catalytic transformations in which the catalysts or reagents for each step are added sequentially. The approach simplifies the way to address the issues of compatibility of catalysts and reagents, optimization of conditions for each step, or synchronization of reactions of the sequence, which are often encountered in orthogonal relay catalysis. However, such an approach prevents exploiting the cooperativity of the reactions, i.e., the enabling feature of relay catalysis that was discussed above. Nevertheless, the main advantage remains in the possibility of performing a target sequence of transformations in one-pot, without the need for costly and tedious isolations and purifications of potentially unstable intermediates.

Preventing side-reactions

The sequential addition of catalysts helps to eliminate side reactions. For instance, Reek[105] and co-workers reported a dual-catalytic transition metal system for branch-selective hydroformylation of terminal alkenes, in which two catalysts are added sequentially and the conditions are adapted for each step. The approach prevents secondary reactivity of the first catalyst and eliminates premature reactivity of the second catalyst over the initial substrate. In the first step of the sequence, terminal alkene **19.1** undergoes a Pd-catalyze mono-isomerization to sub-terminal alkene **19.3** (Scheme 19). Upon completion of the first step, a base is added to stop any further isomerization processes, which would lead to a mixture of internal alkenes, i.e., the secondary products of the isomerization reaction. The Rh-catalyst is added, and the reaction mixture is subjected to a syngas atmosphere (CO/H_2) to undergo the regioselective hydroformylation of the sub-terminal alkene intermediate **19.3**, yielding α-methyl-branched aldehyde **19.2** selectively in high yield.
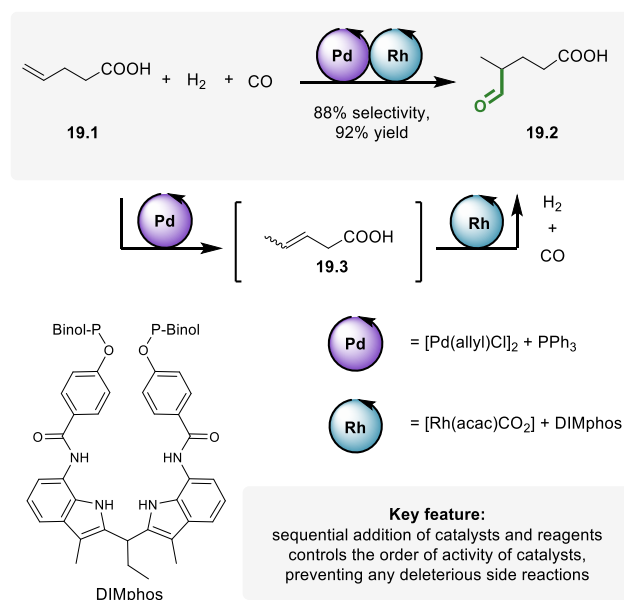
Scheme 19. Pd-/Rh-catalyzed sequential olefin isomerization – hydroformylation for α-branch-selective hydroformylation of terminal alkenes

<u>Eliminating incompatibility issues</u>

The sequential addition of catalysts assists to mitigate the inherent incompatibility between catalysts, such as incompatibility between Brønsted acid and Brønsted base catalysts. For instance, Zhou and co-workers[106] executed a one-pot three-step enantioselective synthesis of spirocyclic indolines **20.3** employing the acid- and base-catalyzed reactions (Scheme 20). The sequence starts with a Pd-catalyzed hydrogenation of nitroarene **20.1** to form aryl amine **20.4**, which is then subjected to a Brønsted acid catalyzed coupling with isatin derivative **20.2** to form ketimine **20.5**. Subsequently, a chiral Brønsted base is added to promote the asymmetric 6π electrocyclization, yielding chiral product **20.3** in 85% yield and 92% ee. Sequential catalysis represents a particular advantage when the stability of intermediates with respect to purification procedures limits the yield of a synthetic route. The authors showed that stepwise synthesis yields the product in only 34% overall yield (with 97% ee), illustrating both the practicality and the increased efficiency of the one-pot procedure over the classic stepwise approach.
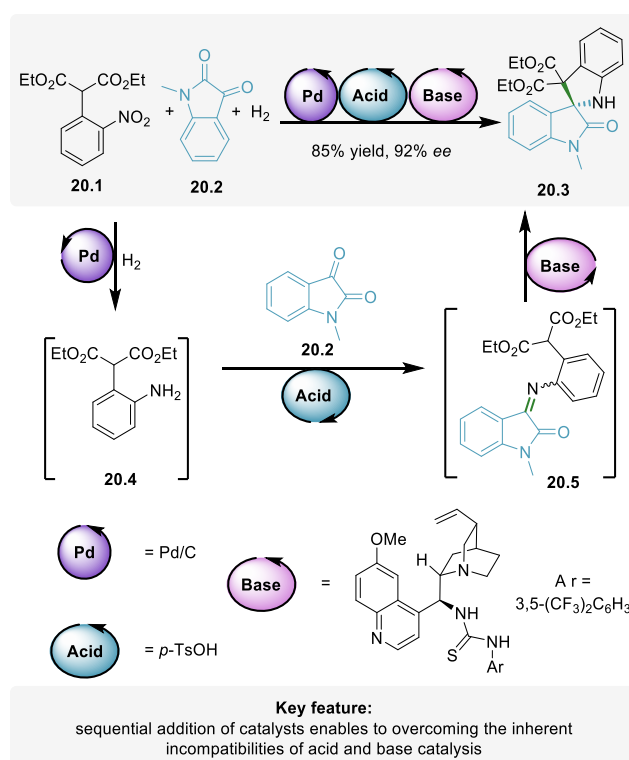
Scheme 20. Pd-/Brønsted acid-/ Brønsted base-catalyzed three step sequence involving reduction, coupling, and asymmetric 6π electrocyclization for the formation of spirocyclic indolines

<u>Exploiting multiple transition metal-catalysts</u>

Although a number of examples of ternary catalytic systems combining transition metal- and organocatalysts operating in a sequential fashion has been reported,[107] three-step sequences occurring in the presence of three transition metal-catalysts remain rare. The main challenges are driven by both the compatibility requirements between all metal complexes and reagents, and the prospective ligand exchanges between the catalysts that are likely to deteriorate their catalytic activities. However, the potential of such multi-catalytic transformations stimulates the development of the ternary transition-metal systems. Ramasatry and co-workers reported one of the first examples of

multi-catalytic protocols with three transition metal-catalysts for the 3-step synthesis of β-carbolines **21.2** (Scheme 21).[108]
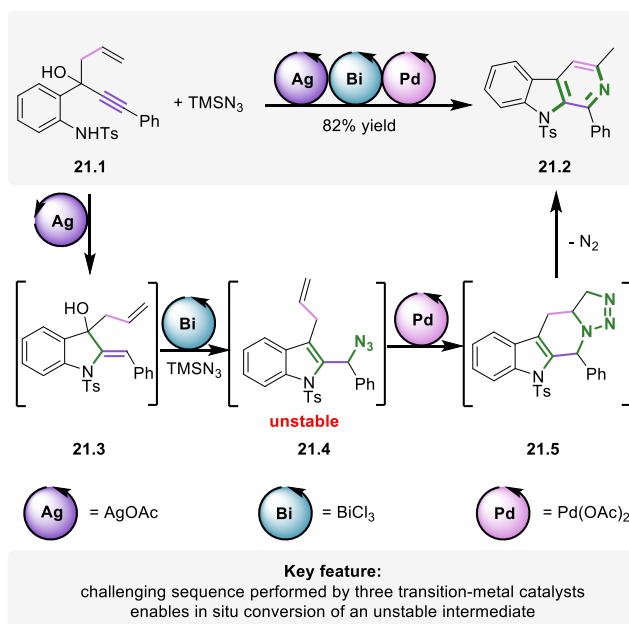
Scheme 21. Ag-/Bi-/Pd-catalyzed three step sequence involving hydroamination, 1,3-allylic alcohol isomerization (AAI), and [3+2] cycloaddition for the formation of β-carbolines

Within the process, starting material **21.1** undergoes first Ag-catalyzed intramolecular hydroamination to form allylic alcohol **21.3**, which is followed by Bi-catalyzed 1,3-allylic alcohol isomerization (AAI) and the Friedel–Crafts-type dehydrative azidation to afford azide intermediate **21.4**. Lastly, the latter undergoes the Pd-catalyzed [3+2]-cycloaddition to form **21.5** followed by nitrogen extrusion to yield β-carbolines **21.2** in overall 82% yield. Noteworthy, azide intermediate **21.4** is unstable and potentially explosive. Hence in situ conversion of **21.4**, without the need for potentially dangerous isolation, is the key factor for the formation of the final product both in high yield and in a safe manner.

Multiple transition metal-catalysts in stereoselective synthesis

Compatibility issues aside, the prospective ligand exchange between multiple transition metal catalysts is particularly problematic in case of stereoselective reactions, because any ligand exchange is likely to deteriorate the stereocontrol of the overall transformation. However, because the efficient preparation of chiral molecules is the key in fine-chemical synthesis, stereoselective multi-catalytic systems remain of high interest. We have recently developed multi-catalytic transition-metal protocols that convert alkenes, unsaturated aliphatic alcohols, and aryl boronic acids to form secondary benzylic alcohols, a prevalent moiety in biologically active molecules and valuable building blocks in organic synthesis, with high stereoselectivities, within one-pot sequences of reactions by integrating transition-metal catalyzed alkene cross-metathesis, isomerization, and nucleophilic addition reactions (Scheme 22a).[109] Because each reaction of the sequence is executed by an independent catalyst, allylic alcohols bearing a prochiral double bond **22.8** can be converted to any stereoisomer of the product **22.9** with high stereoselectivity (>98:2 er and >20:1 dr, for 1,3-syn and 1,3-anti selective synthesis; Scheme 22b). Overall, with the aid of up to four catalysts operating in a single vessel, the protocols directly convert simple starting materials into a range of

valuable products with high stereocontrol. Not only the one-pot protocols are operationally simpler and up to ~3-fold resources more efficient than the stepwise syntheses, but also the overall yield of the product is increased thanks to preventing cumulative losses of materials during subsequent isolations and purifications of the intermediates. Overall, the approach simplifies the synthesis of target motives, increases material efficiency, and limits cost, time, and waste associated with the multi-step procedures.
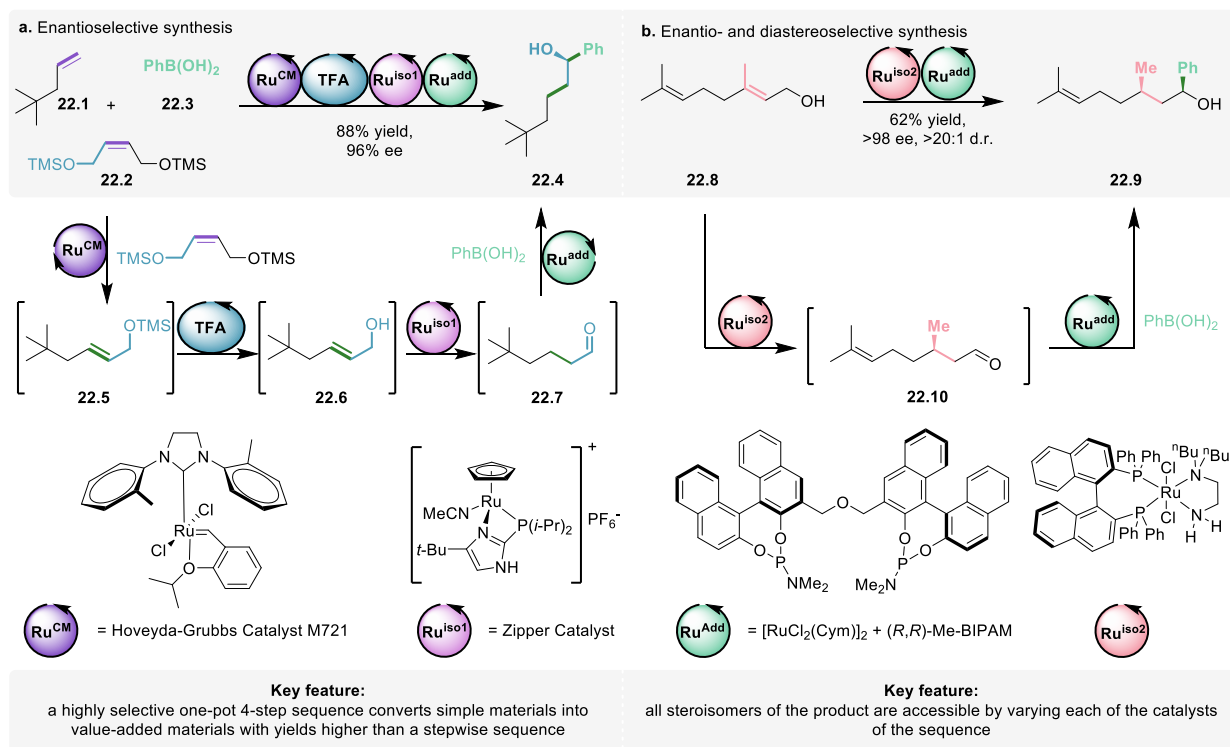
Scheme 22. Multi-catalytic sequences for stereoselective synthesis of secondary benzylic alcohols with up to four catalysts working in the same reaction mixture

1.5.3   Auto-relay catalysis

Auto-relay catalysis, referred to as *auto-tandem catalysis* when two transformations take place, refers to catalytic systems in which a single (pre)-catalyst catalyzes multiple, independent reactions within mechanistically distinct catalytic cycles under the same reaction conditions with all reagents present from the start. The approach faces different challenges than orthogonal relay catalysis. Because a single catalyst is used, incompatibility issues concerning the catalysts are obsolete. The main challenge relates to designing a pre-catalyst that can catalyze two reactions of different catalytic mechanisms in a well-defined manner under the same conditions. The rates of each step are interrelated, and the starting materials and intermediates need to be reactive only in a specific step. Because catalytic activities are promoted by the same pre-catalyst, optimization of each step is challenging with a change of a single parameter affecting all reactions within the sequence. The field has been a subject of a micro-review[110] and conceptual article.[111] Selected examples are discussed below.
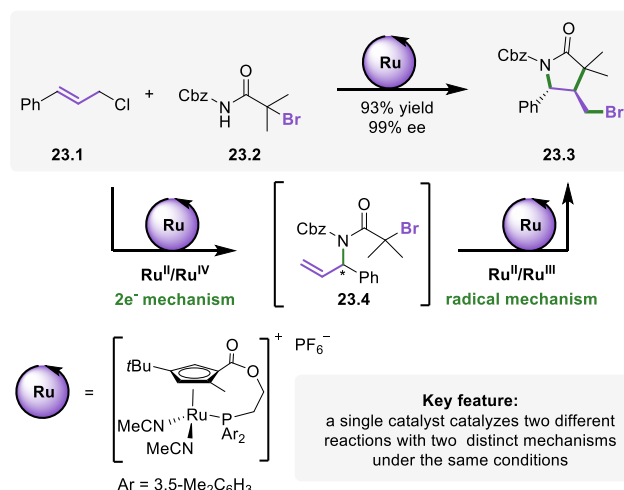
Scheme 23. Ru-catalyzed auto-relay of asymmetric allylic substitution (AAS) and atom transfer radical cyclization (ATRC) for enantioselective synthesis of γ-lactams

The study by Onitsuka and co-workers[112] for the synthesis of enantiomerically enriched γ-lactams **23.3** constitutes an elegant example illustrating the development of auto-relay catalytic systems. The authors envisioned a sequence connecting previously established asymmetric allylic substitution (AAS)[113] of chloroalkene **23.1** with N-nucleophile **23.2** to form bromoalkene intermediate **23.4** with its subsequent atom transfer radical cyclization (ATRC) to yield the final product **23.3** (Scheme 23). Both reactions are catalyzed exclusively by a cyclopentadienylruthenium (Cp'Ru) complex through two different mechanisms. While the AAS reaction occurs through the 2-electron Ru^{II}/Ru^{IV} mechanism, the ATRC cyclization reaction occurs through the radical Ru^{II}/Ru^{III} mechanism. Overall, the protocol directly yields the target γ-lactams **23.3** in excellent yields and enantioselectivities.

The field of auto-relay catalysis is dominated by transition metal-based catalytic systems, including recent elegant studies on Ni-catalyzed direct transformations of dienyl allylic alcohols into chiral 1,3-dinitriles by Fang[114] and Rh-catalyzed dehomologation of alcohols into alkenes by Dong[115]; however, organocatalytic auto-relay catalytic systems have been developed as well. Radosevich[116] and co-workers reported a system based on a single redox-active organophosphorus catalyst, which operates two complementary cycles in the P^{III}/P^{V} couple, to execute a condensation-cyclodehydration sequence for amines **24.1** and carboxylic acids **24.2** as starting materials (Scheme 24). The key common intermediate, bromophosponium cation **24.5**, is generated upon reduction of phosphine oxide pre-catalyst **R₃P=O** by phenylsilane and subsequent halophilic reaction with the oxidant DEBM (diethyl bromomalonate). Condensation involves the activation of acid **24.2** with cation **24.5** to form activated onium intermediated **24.6**, which in turn reacts with amine **24.1** to form amide intermediate **24.4** within the C-N bond forming cycle. Then, amide **24.4** reacts again with catalytic cation **24.5** to form the final product **24.3** through activated onium intermediate **24.7** within the C-C bond forming cycle.
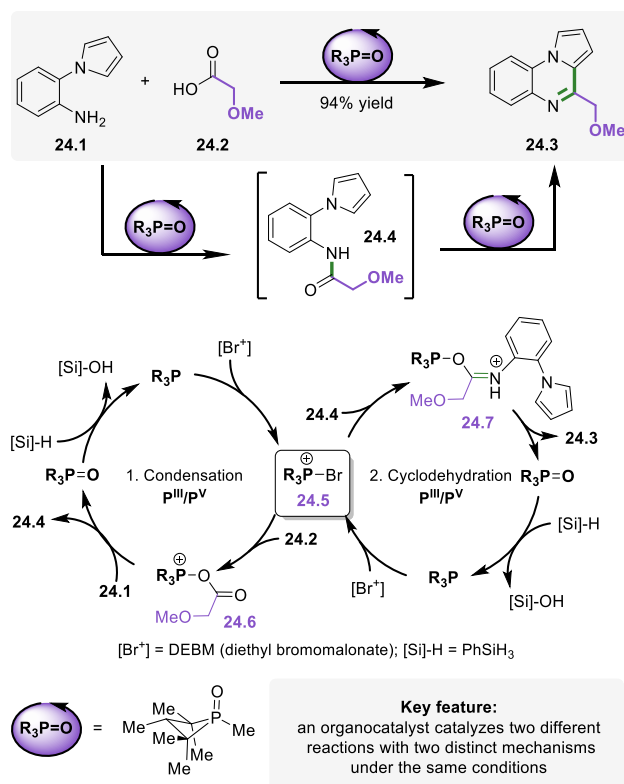
Scheme 24. Condensation-cyclodehydration sequence occurring in the presence of a single organocatalyst that operates two complementary and functionally distinct catalytic cycles

Reaction ordering by 'delay loop'

A major challenge in auto-relay catalysis is to establish kinetic hierarchy for each catalytic cycle involved when the intrinsic reactivity order does not match the required sequence and leads to detrimental side reactions. With the aim to provide an easy access to enantioenriched unprotected homoallylic amines, a valuable building block in organic synthesis, Hoveyda[117] and co-workers studied a single copper-based catalytic system to promote reductive coupling of allenes and nitriles (Scheme 25). Two functionally different catalytic cycles operate simultaneously to catalyze allene **25.1** addition to a nitrile **25.2**, enabled by Cu-B(pin) species, and ketimine **25.5** reduction enabled by Cu–H species. However, premature addition of Cu-H to allene lead to side-products, lowering the efficiency of the overall process. To address this issue, the authors introduced a non-productive 'delay loop' by adding a sacrificial reagent, which reacts with Cu-H faster than the allene does, and hence holds the reduction step just until the ketimine intermediate is formed; the latter reacting with Cu-H faster than the sacrificial reagent. Overall, the delay loop ensures the required order of the catalytic events is kept, albeit at the price of non-productive consumption of sacrificial reagents.
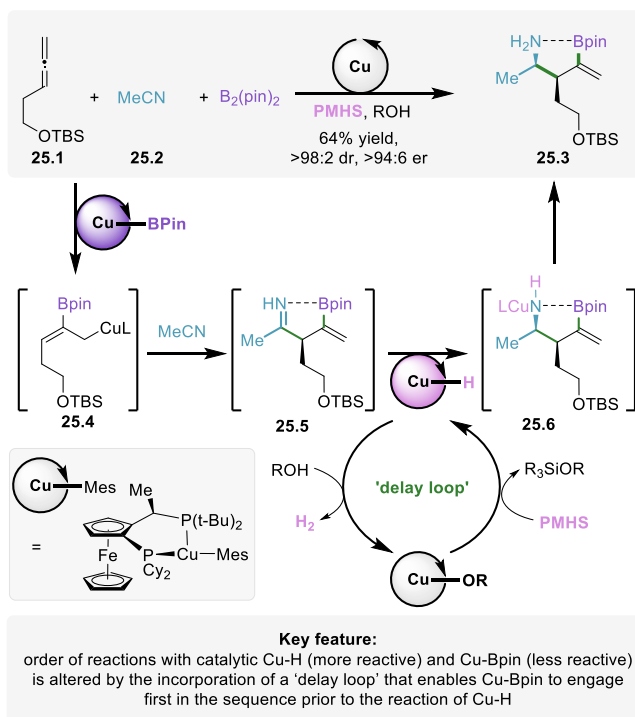
Scheme 25. Cu-catalyzed auto-relay of reductive coupling of allenes and nitriles for the preparation of NH$_2$-amines

Pseudo-allosteric regulation of catalytic activity

   Another strategy to ensure precise ordering of catalytic activities is to separate the operation of different catalytic cycles in the time domain through a pseudo-allosteric control. Herzon[118] and co-workers reported an example in which two catalytic functions of a Ru-complex – hydration and reduction – are separated in time (Scheme 26). The key aspect of this system is that the resting states of the catalyst in each catalytic cycle are metal–substrate complexes. Therefore, the substrate that binds the strongest to the Ru-resting state dominates its catalytic activity until this substrate is consumed. Within the sequence, first a strongly binding alkyne **26.1** undergoes anti-Markovnikov hydration to the corresponding aldehyde **26.4**, which in turn undergoes uncatalyzed Wittig olefination to form 1,4-enone intermediate **26.6**. Because the reduction activity of the catalyst remains latent in the presence of alkyne **26.1**, the side-reduction of the aldehyde **26.4** to the alcohol **26.5** is inhibited, so the intermediate is selectively converted to 1,4-enone **26.6**. When conversion of alkyne **26.1** is finished, 1,4-enone **26.6** can bind to the catalyst to be reduced to the ketone **26.3** through transfer-hydrogenation, forming the product in high yield (up to 75%). The overall control of activity resembles the allosteric mechanism controlling activity of enzymes, that is, one of the key features enabling biosynthetic pathways to be executed through well-orchestrated enzymatic reactions.
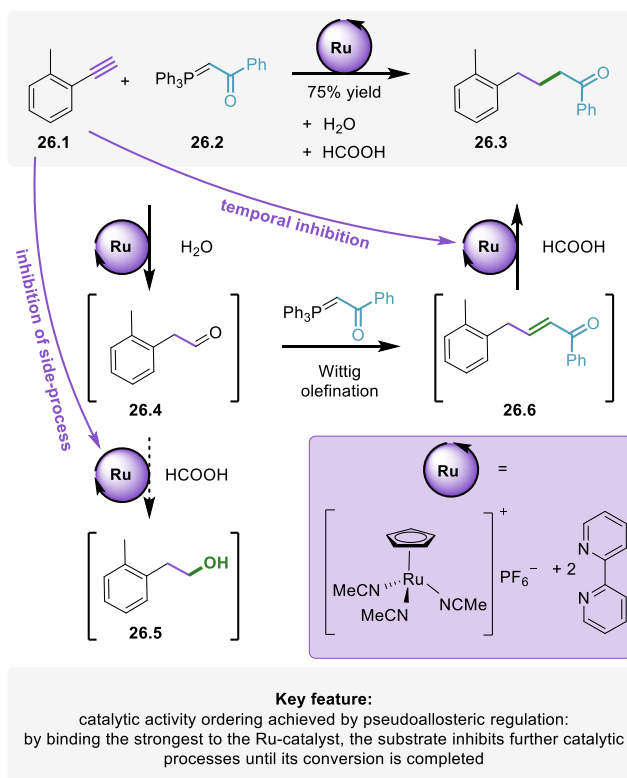
Scheme 26. Ru-catalyzed auto-relay of alkyne hydration, Wittig olefination, and transfer-hydrogenation with a pseudo-allosteric regulation of catalytic activity

1.5.4 Assisted-relay catalysis

Assisted-relay catalysis refers to catalytic systems in which a single catalyst operates multiple reactions within different catalytic cycles, but the subsequent reactions are triggered by the addition of reagents or change in the reaction conditions. Because optimal conditions for each step can be easily adjusted, the order of steps can be controlled. However, because of the time separation of the different catalytic cycles, cooperation between reactions remains excluded.

<u>Temperature trigger</u>

Temperature changes are often used to change the activity of the catalyst. Recently, Ackermann[119] and co-workers reported sequential meta-C−H alkylation and ortho-C−H arylation of aryloxazoline **27.1** occurring in the presence of a single ruthenium(II) complex (Scheme 27). First, the starting material undergoes meta-selective C-H-alkylation with alkyl bromide **27.2** through the radical Ru[II]/Ru[III] mechanism. After completion of the first step, aryl bromide **27.3** is added, and the reaction temperature is increased to trigger Ru-catalyzed ortho-selective C-H-arylation through the two-electron Ru[II]/Ru[IV] mechanism to form the double C−H functionalized product **27.4** in one-pot in 73% overall yields.
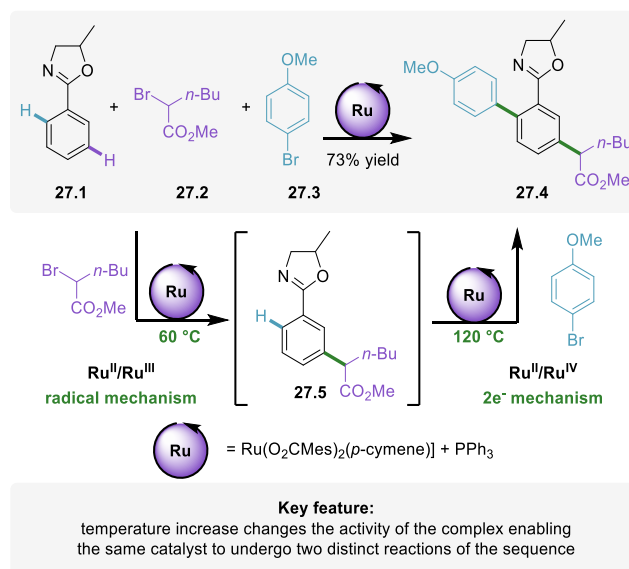
Scheme27. Ru-catalyzed temperature-controlled assisted-relay of sequential C–H alkylation via radical mechanism and ortho-C–H arylation via Ru^{II}/Ru^{IV} mechanism

Chemical trigger

Chemical triggers can be used to trigger the activity change of a catalyst in assisted-relay catalysis. Choudhury[120] and co-workers reported a Ru(II)-complex, which is able to adopt two different states for different catalytic functions: the first state for dehydrogenative coupling of amines, and the second state for hydrogenation of imines (Scheme 28). Both states of the catalyst are switched by the addition of an acid or a base. In a model experiment, 4-methylbenzylamine **28.1** undergoes dehydrogenative coupling to form the corresponding imine intermediate **28.3** in the presence of the catalyst in the first state. Upon addition of a base, the Ru-catalyst adapts the second state, which undergoes hydrogenation of the imine intermediate **28.3** in the presence of hydrogen gas, furnishing the dibenzylamine product **28.2** in 70% yield.
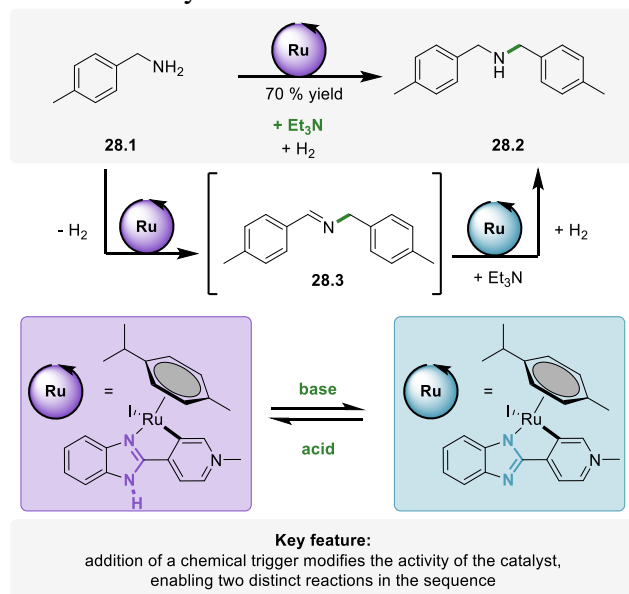
Scheme 28. Ru-catalyzed pH-controlled assisted-relay of sequential dehydrogenative coupling of amines followed with hydrogenation of the imine intermediate

1.6 Complex systems

While most multi-catalytic systems involve just two reactions or two catalysts and can be assigned to a single class of cooperative, domino, or relay catalysis, a higher level of complexity becomes increasingly more common. Although the development of such systems is particularly challenging, due to increasing demand for the precise ordering of the catalytic events and preventing any incompatibility issues or side-reactions between multiple catalysts and reagents, enormous potential for achieving highly efficient synthetic transformations motivates the research in the field. Within this chapter, we discuss selected examples that illustrate various combinations of cooperative, domino, and different types of relay catalysis. The selected studies highlight both increasing complexity and synthetic potential of such multi-catalytic approaches to access increasingly complex architectures from simple starting materials within sequences of precisely orchestrated catalytic events.

We classified the studies of complex systems into two main categories: (a) unassisted complex systems, in which all reactions of the sequence occur without any change to the conditions or any additions of reagents or catalysts, and (b) assisted complex systems, in which the sequence requires the conditions to be modified or reagents/catalysts to be added in the course of the process to trigger subsequent transformations.

1.6.1   Unassisted complex systems

Unassisted complex systems that contain all reagents and catalysts from the start are particularly challenging to design, due to the requirement of compatibility between multiple reagents and catalysts, precise ordering of the catalytic events, and preventing any side-reactions. However, such systems offer the broadest realm of opportunities by merging the advantages of cooperativity between catalysts (i.e., cooperative catalysis) and cooperativity between reactions (i.e., relay catalysis). Below we discuss selected examples of complex systems exploiting either orthogonal- or auto-relay catalysis together with cooperative catalysis.

Orthogonal relay catalysis with the 2nd step involving cooperative catalysis (4 catalysts):

Gong[121] and co-workers reported a protocol exploiting four catalysts to combine hydroformylation of alkenes and asymmetric allylation of aldehydes. The sequence directly converts styrene derivatives, allylic alcohols, and syngas (i.e., CO and H_2) to form α-quaternary aldehydes enantioselectively (Scheme 29). First, styrene **29.1** undergoes hydroformylation with H_2 and CO to form α-branched aldehyde **29.4** in the presence of a Rh-catalyst. In the meantime, the reaction of allylic alcohol **29.2**, a Pd(0)-complex, and a chiral phosphoric acid forms a chiral π-allyl Pd species. The aldehyde intermediate **29.4** reacts with an amine catalyst to form an enamine species **29.5**, which undergoes asymmetric allylation with the π-allyl Pd species, exploiting triple-catalytic cooperative catalysis to form quaternary imine enantioselectively. Upon imine hydrolysis **29.6**, the final α-quaternary chiral aldehyde **29.3** is released. Overall, two C-C bonds are created to form all-carbon quaternary center in a stereoselective fashion with the aid of four catalysts.
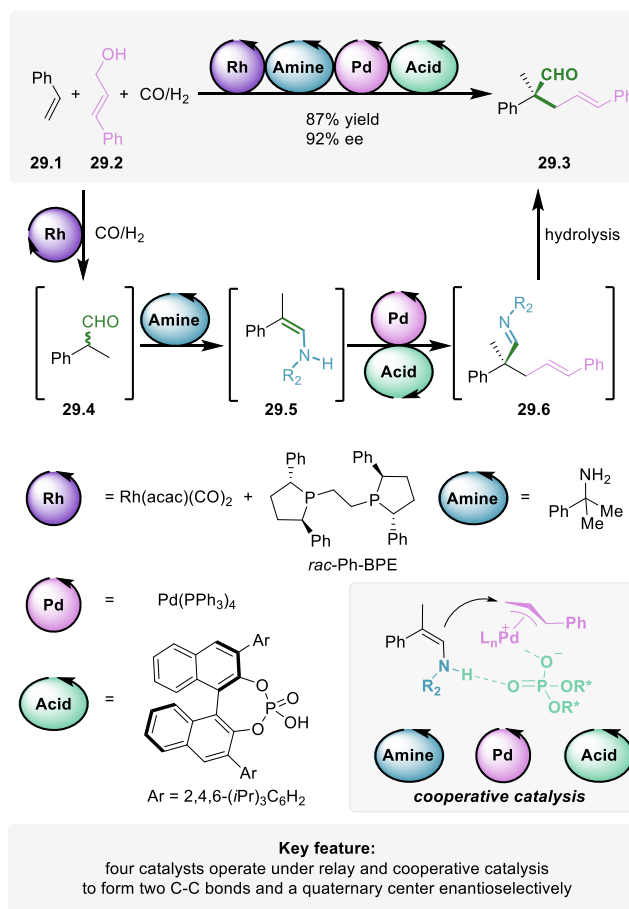
Scheme 29. Rh-/Pd-/Brønsted acid-/amine-catalyzed relay involving hydroformylation and cooperative asymmetric allylation to convert vinyl arenes, allylic alcohols, and syngas to form α-quaternary chiral aldehydes

Gong[122] and co-workers reported a sequence of hydroamination and allylic alkylation reactions occurring in the presence of three catalysts operating under orthogonal relay- and cooperative catalysis (Scheme 30). The sequence starts with an Au-catalyst triggering intramolecular hydroamination of secondary amine-bridged enyne **30.1** to form N-allylic enamine intermediate **30.3**. Then, the N-allylic enamine undergoes intramolecular allylic alkylation under cooperative catalysis of a Pd-complex and a Brønsted acid to yield final pyrrolidine derivative **30.2**.
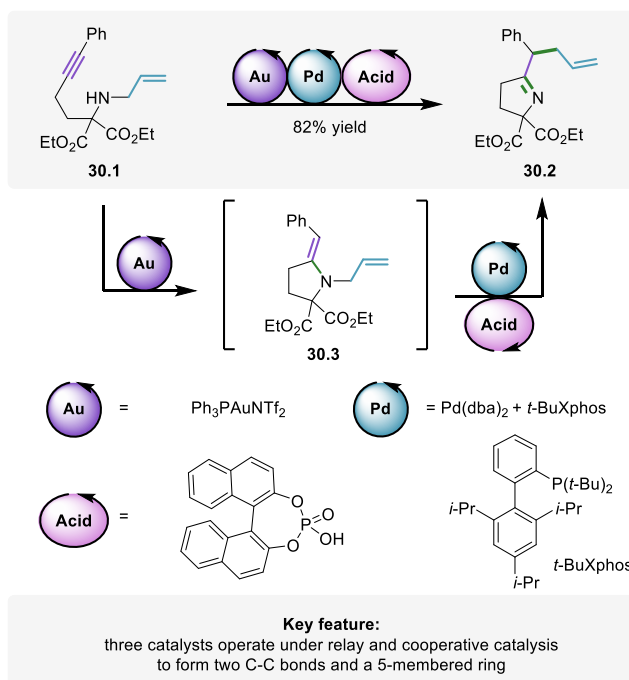
Scheme 30. Au-/Pd-/Brønsted acid-catalyzed relay of intramolecular hydroamination and cooperative allylic alkylation for transforming secondary amine-bridged enynes into pyrrolidine derivatives

Auto-relay catalysis with the 2nd step involving cooperative catalysis (one catalyst acts both cooperatively and non-cooperatively):

Gong[123] and co-workers reported enantioselective one-pot synthesis of julolidine derivatives, exploiting two catalysts that operate under auto-relay and cooperative catalysis (Scheme 31). The synthesis embarks with phosphoric acid-catalyzed enantioselective [4+2] cycloaddition of the aryl imine formed in situ (from **31.1** + **31.2**) and enamine **31.3** to form tetrahydroquinoline intermediate **31.5** bearing an alkyne moiety. Subsequently, the latter undergoes intramolecular hydroamination to form dehydrojulolidine product **31.6** in the presence of cooperative gold phosphate and phosphoric acid catalysts. The synthesis is completed by the stochiometric reduction with a borohydride reagent to form julolidine derivative **31.4** in overall high yield and enantioselectivity.

Cooperative and orthogonal relay catalysis (two independent cooperative systems, consisting of three and two catalysts, respectively, work in relay,):

Merging racemic photoredox/organo dual-catalytic reactions[124] with enzymatic kinetic resolution can serve as a platform for executing elusive stereoselective functionalization reactions at remote, unactivated sites of starting materials. In that context, MacMillan, Hyster, and co-workers[125] recently reported an approach in which a racemic mixture of β-substituted ketone, (*S*)-**32.1** and (*R*)-**32.2**, is converted to nearly enantiopure γ-substituted alcohol **32.3** by merging a substrate-selective reduction process operated by two enzymes with a racemization sequence enabled by three cooperative catalysts (Scheme 32). In the system, (*R*)-**32.2** is reduced stereoselectively to alcohol **32.3** by substrate-selective NADPH-dependent ketoreductase working in combination with glucose dehydrogenase.

Scheme 31. Brønsted acid-/Au-catalyzed auto-relay of enantioselective [4+2] cycloaddition and cooperative intramolecular hydroamination for the synthesis of julolidine derivatives
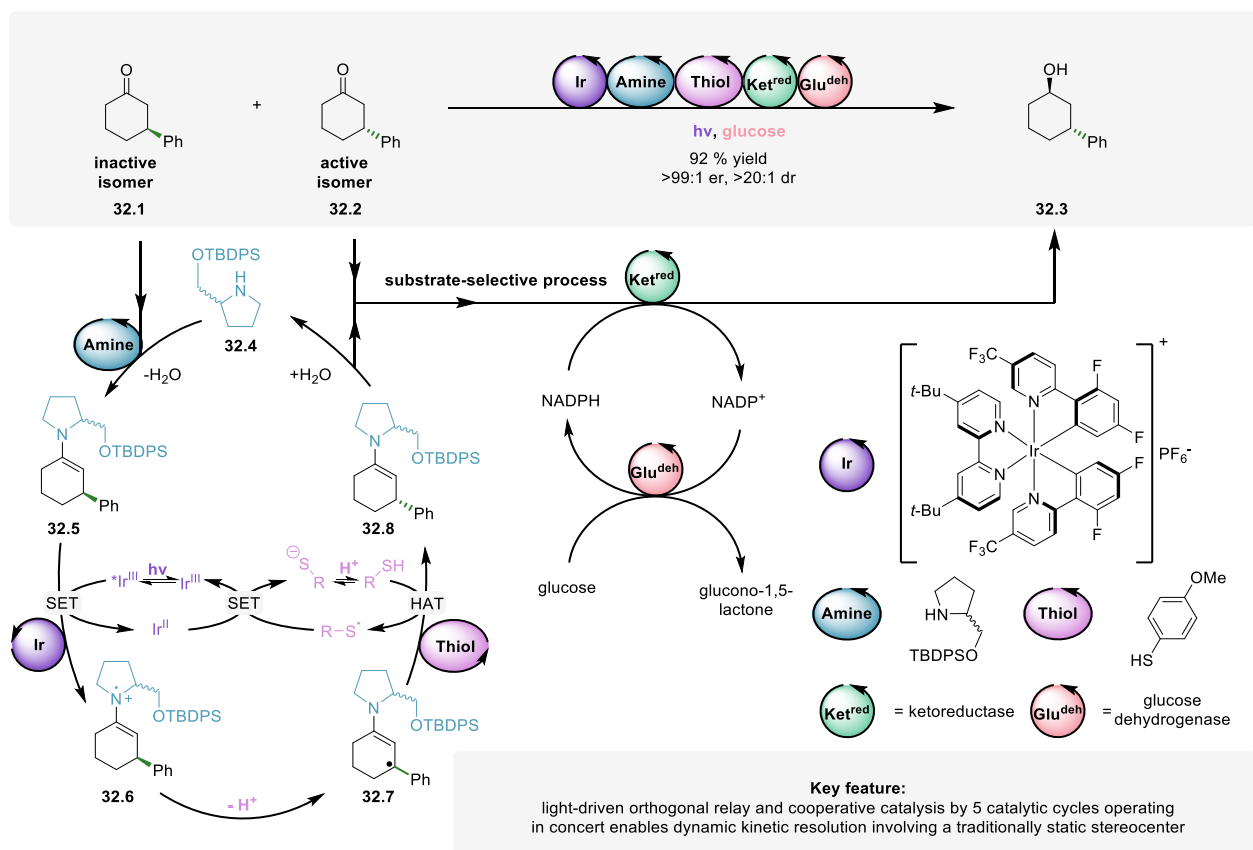
Scheme 32. Merging photocatalysis with enzymatic reactions enables stereoselective reactions at traditionally static stereocentres of racemic starting materials

Importantly, (*S*)-**32.1** remains unreactive to the enzyme. However, (*S*)-**32.1** undergoes continuous racemization in the system with the aid of three cooperating catalysts under light irradiation. First, (*S*)-**32.1** undergoes condensation with amine **32.4** to form enamine (*S*)-**32.5**, which is oxidized to enaminyl radical cation (*S*)-**32.6** by the excited iridium photocatalyst. Upon subsequent deprotonation of (*S*)-**32.6** at its allylic site, the stereochemical information is lost and prochiral radical intermediate **32.7** is formed. An unselective HAT between **32.7** and the thiol catalyst forms a racemic mixture of (*S*)-**32.5** and (*R*)-**32.8**. Upon hydrolysis, (*R*)-**32.2** is formed, which undergoes selective reduction to product **32.3**, and (*S*)-**32.1**, which enters again the racemization cycle. This unique protocol that exploits five catalysts operating in parallel demonstrates the feasibility of catalytic systems of increasing complexity to execute attractive transformations that remain beyond the capabilities of standard systems.

1.6.2   Assisted complex systems

The possibility to modify the conditions of reaction sequence occurring under multi-catalysis expedites the development of such complex systems, however, at the price of preventing the cooperativity between reactions taking place in different phases of the process. Nevertheless, such 'assisted' systems can substantially simplify synthetic processes, increasing their overall efficiency. Bellow we discuss selected examples of assisted complex systems exploiting either sequential or assisted-relay catalysis along with cooperative, auto- or orthogonal-relay catalysis.

Sequential catalysis with the 2ⁿᵈ step involving cooperative catalysis (3 catalysts)

Beller[126] and co-workers developed a triple catalytic system that exploits sequential and cooperative catalysis to directly convert aryl alkynes, anilines, and molecular hydrogen into enantioenriched secondary benzylic amines (Scheme 33). Initially, an Au-catalyst triggers hydroamination of alkyne **33.1** with aniline **33.2** to form an imine, which is subsequently isomerized to ketimine intermediate **33.4**. Upon completion, the inert atmosphere is exchanged for hydrogen, Knölker's complex and a chiral phosphoric acid are added, which catalyze cooperative enantioselective reduction of the ketimine intermediate **33.4** to form the benzylamine **33.3** in high yield and enantioselectivity. Notably, the authors showed that the sequence occurs when all reagents and catalysts are present from the start (i.e., under orthogonal-relay and cooperative catalysis). However, in the latter case, the product was formed in lower yield and selectivity than for the sequential approach (42% yield and 49% ee, versus 80% yield, and 94% ee, respectively), indicating that sequential addition prevents the detrimental side reactions.
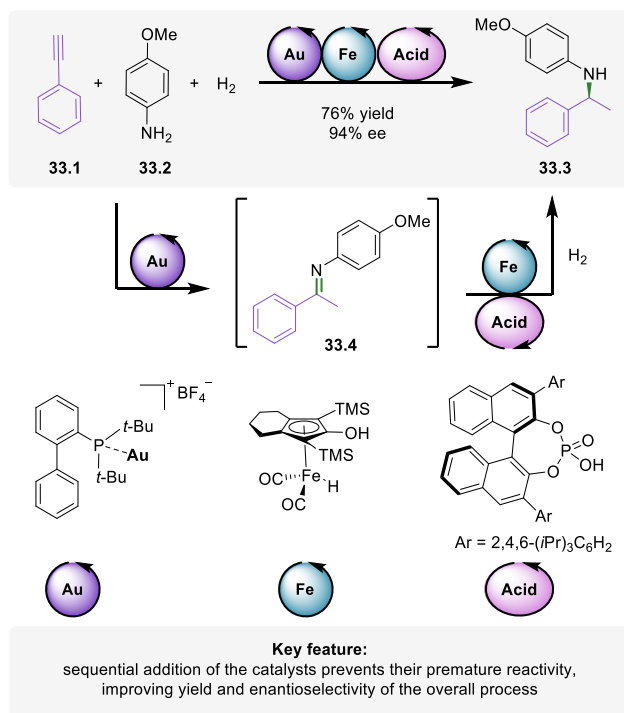
Scheme 33. Au-/ Fe-/Brønsted acid-catalyzed sequential hydroamination of alkynes with primary amines followed by cooperative enantioselective hydrogenation

Sequential catalysis with the 2ⁿᵈ step involving both auto-relay and orthogonal relay catalysis (4 reactions with 3 catalysts)

Combining multiple catalytic activities of several catalysts can ideally provide synthetic sequences that transform abundant chemical commodities into value-added building blocks with high atom- and material-efficiency. Huang[127] and co-workers reported recently a compelling example, where linear alkanes are converted directly into linear alcohols with theoretical 100% atom efficiency within a triple-catalytic, two-step sequence (Scheme 34). In the first step, alkane **34.1** undergoes acceptorless dehydrogenation to form a mixture of alkenes **34.3** and **34.4** in the presence of an Ir-catalyst. In the second step, the alkene intermediates undergo Rh-catalyzed auto-relay isomerization-hydroformylation sequence to form selectively linear aldehyde **34.5**, which in turn directly undergoes Ru-catalyzed hydrogenation to form the linear alcohol product **34.2**. In principle, dihydrogen, the sole by-product of the first step, could be incorporated in the subsequent step, demonstrating the concept of material leveraging in the reaction sequence to improve atom-economy of the synthesis.
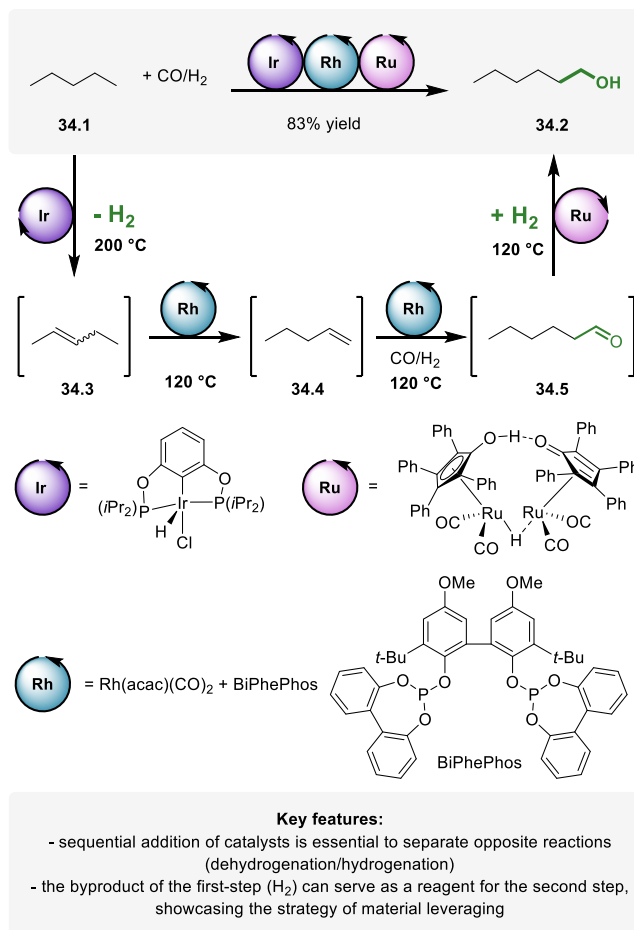
Scheme 34. Ir-/Rh-/Ru-catalyzed sequential dehydrogenation of alkanes followed with orthogonal and auto-relay of olefin isomerization, hydroformylation, and hydrogenation to transform n-alkanes to n-alcohols

It is worth to underscore that all reactions of isomerization-hydroformylation-hydrogenation relay occur in parallel under the same conditions with suitable rates and high chemoselectivity, being the key to form the product in high yield.

Assisted-relay catalysis with the first step involving orthogonal relay catalysis (3 reactions with 2 catalysts)

Chaładaj[128] and co-workers reported a four-component Pd-catalyzed perfluoroalkylative arylation of alkynes, which operates through three functionally distinct catalytic cycles, exploiting relay catalysis and temperature-triggered assisted-relay catalysis (Scheme 35).
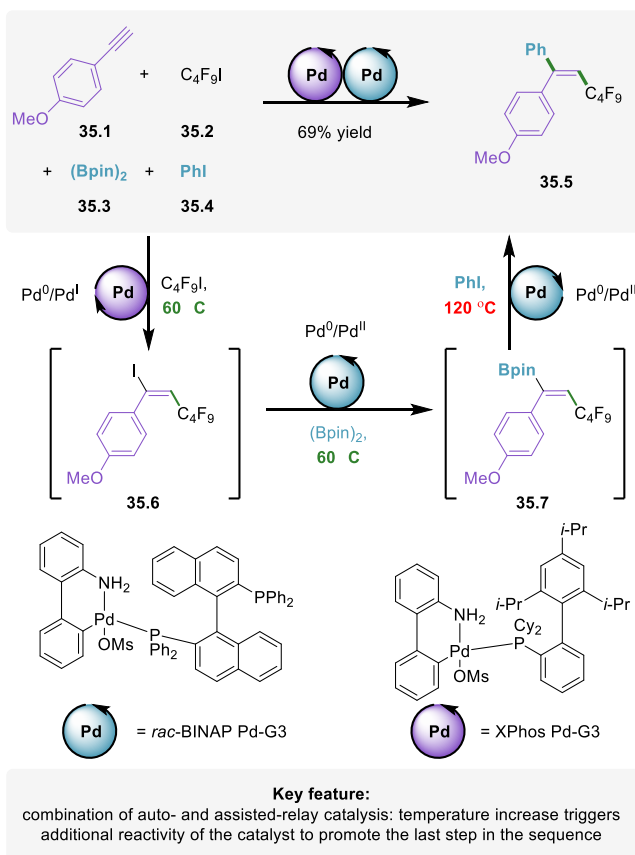
Scheme 35. A four-substrate orthogonal relay of perfluoroalkylative iodination of alkynes and borylation merged with assisted-relay of temperature-triggered Suzuki cross coupling. Two Pd-catalysts operate three functionally distinct catalytic cycles, merging auto-relay and assisted-relay catalysis

Initially, alkyne **35.1** reacts with perfluoroalkyl iodide **35.2** to form vinyl iodide **35.6** through radical Pd^0/Pd^I mechanism involving binap-Pd catalyst. The vinyl iodide **35.6** undergoes directly borylation with $(Bpin)_2$ to form vinyl boronate ester **35.7** within the orthogonal relay through the Pd^0/Pd^{II} mechanism by Xphos-Pd catalyst. Upon completion, the reaction temperature is increased to trigger the Suzuki coupling of the vinyl boronate ester **35.7** with aryl iodide **35.4** to deliver the final product **35.5**.

Assisted-relay catalysis with the 2ⁿᵈ step involving cooperative catalysis (one catalyst acts both cooperatively and non-cooperatively):

Lautens[129] and co-workers reported a three-component synthesis of fully substituted triazoles in the presence of two catalysts operating under assisted-relay and cooperative catalysis (Scheme 36). The sequence starts with a substrate-selective Cu-catalyzed cycloaddition of organic azide **36.1** with iodoalkyne **36.2** to form iodotriazole **36.5**, in the presence of another alkyne **36.3** that remains unreactive under the initial conditions.
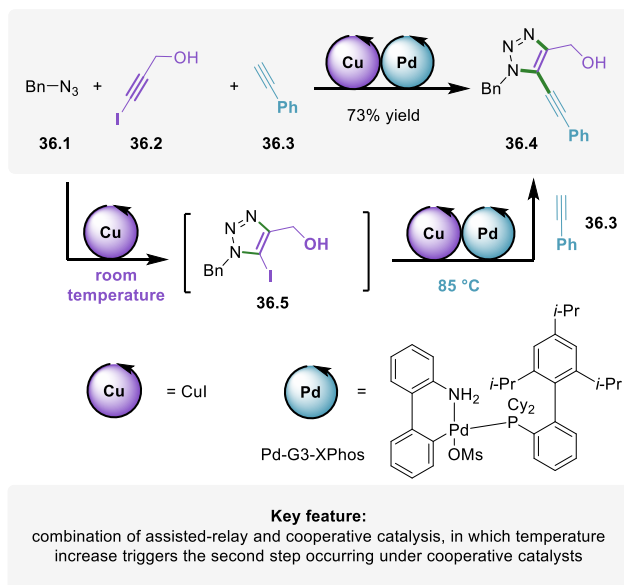
Scheme 36. Cu-/Pd-catalyzed temperature-controlled assisted-relay involving cycloaddition and cooperative Sonogashira coupling to obtain fully substituted triazoles

Upon completion, the temperature is increased from room temperature to 85 °C to trigger the Pd-/Cu-catalyzed Sonogashira reaction of iodotriazole intermediate **36.5** with terminal alkyne **36.3**, yielding fully substituted triazole **36.4** in high overall yield. Although the complete sequence can also be executed directly at 85 °C, the product is formed in significantly lower yield (30% vs. 73%). Careful optimization of the Pd-precatalyst, base, and the temperature program was essential to prevent premature side reactions and ordering the catalytic activity.

Assisted-relay catalysis with the 1st step involving cooperative catalysis and the 2nd step involving divergent catalysis (one catalyst acts both cooperatively and non-cooperatively):

Catalysts with complementary selectivities, such as stereodivergent selectivity, are attractive in the context of diversity-oriented synthesis. The ability to control the activity of complementary catalysts within a sequence represents an appealing strategy for the divergent synthesis. Lalic[130] and co-workers recently reported an elegant dual-catalytic system to perform either (*Z*)- or (*E*)-selective synthesis of vinyl arenes, with the selectivity being controlled by the reaction conditions (Scheme 37). First, a Sonogashira cross-coupling reaction between terminal alkyl alkyne **37.1** and aryl halide **37.2** takes place under cooperative Pd/Cu-catalysis. Then, alkyne intermediate **37.5** undergoes semireduction under assisted-relay catalysis by either Cu- or Pd-complex. While the (*Z*)-selective semi-reduction to furnish **37.3** is promoted by the Cu-complex in the presences of close to stoichiometric amount of methanol as a reductant, the (*E*)-selective semi-reduction to yield **37.4** selectively is conducted by the Pd-complex in the presence of excess methanol. Overall, the possibility to suppress the activity of the Cu-catalyst by excess methanol provides a convenient handle to direct the overall reaction to form either diastereomer of the product in high selectivity and yield.
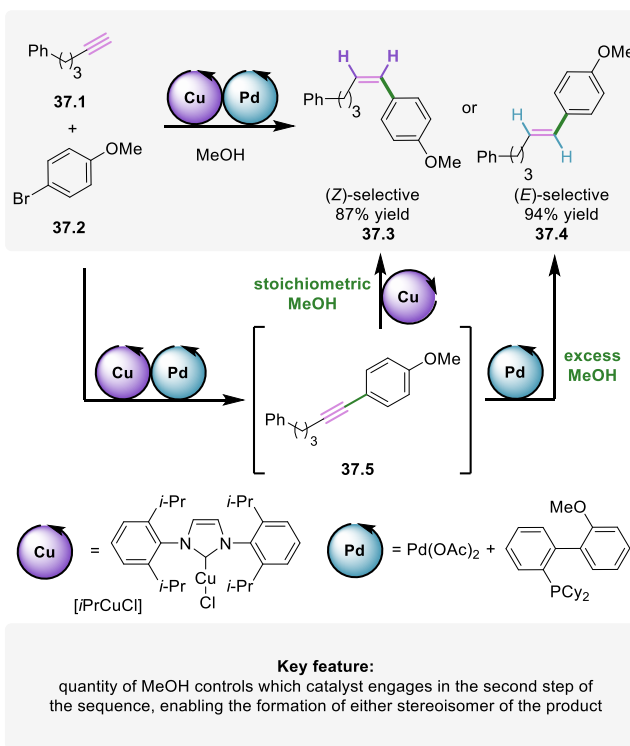
Scheme 37. Cu-/Pd-catalyzed reagent-triggered stereo-divergent assisted-relay of cooperative Sonogashira coupling and semireduction to form either the (*Z*)-alkenes under Cu-catalysis or the (*E*)-alkenes under Pd-catalysis: amount of methanol can divert the activity from Cu- to Pd-catalyst

1.7 Conclusions and perspective of the chapter

Driven by the demand for more efficient and sustainable chemical processes, the field of catalysis continues its rapid development. As illustrated in this chapter, multi-catalysis emerges not only to outcompete the current synthetic protocols, but most importantly also to bring new 'one-pot' transformations that exhibit outstanding resource efficiency. Remarkably, multi-catalytic sequences can undergo through otherwise unfeasible pathways thanks to, for instance, prospectively unstable intermediates being converted as soon as formed. Exemplarily, dual-catalytic systems can enable the direct functionalization of inherently unreactive sites of molecules, thanks to cooperation between reversible catalytic reactions and orthogonal functionalization reactions, opening new valuable short-cuts to the synthetic practitioner.

Despite major challenges that need to be addressed with respect to compatibility issues and catalyst reactivity ordering, recent studies show many competent strategies to address these. For instance, sequential additions of reagents or catalysts, reaction compartmentalization or catalyst encapsulation, proved to be feasible solutions to overcome such incompatibility issues. Likewise, the use of chemical triggers able to induce a change of catalytic activity or stepwise temperature programming of the sequence of reactions, are practical solutions to deliver the correct order of reactions within the targeted sequence. However, these strategies eliminate the advantage of cooperativity between reactions in the sequence, limiting the full potential of multi-catalytic systems. Therefore, novel strategies that address these challenges in situ need to be developed. Recent examples in the literature show that mimicking the features of enzymes, that is, (i) allosteric regulation, (ii) substrate-selective catalysis, or (iii) substrate channeling between consecutive catalytic sites, are plausible ways to solve those issues while maintaining the cooperativity between reactions.

In addition, a fundamental change in approach has to be made in order to improve the development of such complex multi-catalytic systems and to study its emergent properties. In this context, suitable catalysts able to perform with excellent chemo- and reaction-selectivity within a complex mixture are most likely to be different than those performing best in single reaction environments. Linear screening of different parameters for such multivariate systems is rather impractical. Therefore, new strategies to design, analyze and validate the development of such systems are required. Overall, although many challenges remain open, the prospects of multi-catalysis are vast. We envision that future studies will enable the rational design of processes, in which multiple catalysts are orchestrated precisely to transform simple starting materials into valuable products within complex systems of interconnected reactions.

1.8 Aim and outline of the thesis

As above stated, the emergence of transition metal catalysis has had a transformative impact in organic synthesis. In particular, the use of bimetallic systems proved to be a valuable approach toward the improvement of the efficiency, selectivity and atom economy of the overall synthetic process. Besides the significant progress achieved, the development of new bimetallic systems able to outcompete the established classical methods with transformations bearing remarkable features remains challenging. Therefore, is of great interest not only to further develop such systems but also to provide a mechanistic understanding of the processes occurring at a molecular level in order to rationally improve their performance. In **chapter 2** we exploit the power of reversible reactions orthogonal to functionalization reactions, to access non-inherent reactivity of functionalized molecules. Other reversible reactions can be introduced by carefully designing a catalytic sequence of events. **In chapter 3**, we design and develop a reversible catalytic reaction involving a novel Rh-β-boryl elimination step for the transfer borylation reaction. In **chapter 4** we look into the activity-structure relationship of the catalyst by studying computationally xantphos ligand derivates bearing different electronic and steric properties. Cooperativity between two metal species provide unique possibilities to enhance reactivity and selectivity in the hydroformylation reaction as showed by our group recently. In a follow up work, a novel catalytic system based on PdI_2 and PCy_3 presents outstanding iso selectivity for this reaction. In **chapter 5** I describe our computational study that sheds light on the origins of the selectivity by studying different pathways leading to the formation of the product.

1.9 References

(1) Bartholomew, C. H.; Farrauto, R. J. *Fundamentals of Industrial Catalytic Processes*; John Wiley & Sons, Inc.: Hoboken, NJ, USA, 2005.

(2) Rudroff, F.; Mihovilovic, M. D.; Gröger, H.; Snajdrova, R.; Iding, H.; Bornscheuer, U. T. Opportunities and Challenges for Combining Chemo- and Biocatalysis. *Nat. Catal.* **2018**, *1* (1), 12–22.

(3) Galván, A.; Fañanás, F. J.; Rodríguez, F. Multicomponent and Multicatalytic Reactions - A Synthetic Strategy Inspired by Nature. *Eur. J. Inorg. Chem.* **2016**.

(4) Hwang, E. T.; Lee, S. Multienzymatic Cascade Reactions via Enzyme Complex by Immobilization. *ACS Catal.* **2019**, *9* (5), 4402–4425.

(5) Ji, Q.; Wang, B.; Tan, J.; Zhu, L.; Li, L. Immobilized Multienzymatic Systems for Catalysis of Cascade Reactions. *Process Biochem.* **2016**, *51* (9), 1193–1203.

(6) Sperl, J. M.; Sieber, V. Multienzyme Cascade Reactions—Status and Recent Advances. *ACS Catal.* **2018**, *8* (3), 2385–2396.

(7) Ricca, E.; Brucher, B.; Schrittwieser, J. H. Multi-Enzymatic Cascade Reactions: Overview and Perspectives. *Adv. Synth. Catal.* **2011**, *353* (13), 2239–2262.

(8) Fogg, D. E.; dos Santos, E. N. Tandem Catalysis: A Taxonomy and Illustrative Review. *Coord. Chem. Rev.* **2004**, *248* (21–24), 2365–2379.

(9) Patil, N. T.; Shinde, V. S.; Gajula, B. A One-Pot Catalysis: The Strategic Classification with Some Recent Examples. *Org. Biomol. Chem.* **2012**, *10* (2), 211–224.

(10) Tietze, L. F.; Brasche, G.; Gericke, K. M. Domino Reactions in Organic Synthesis. In *Domino Reactions in Organic Synthesis*; Wiley: Weinheim, 2006; pp 1–541.

(11) Allen, A. E.; MacMillan, D. W. C. Synergistic Catalysis: A Powerful Synthetic Strategy for New Reaction Development. *Chem. Sci.* **2012**, *3* (3), 633.

(12) Inamdar, S. M.; Shinde, V. S.; Patil, N. T. Enantioselective Cooperative Catalysis. *Org. Biomol. Chem.* **2015**, *13* (30), 8116–8162.

(13) Kim, D.-S.; Park, W.-J.; Jun, C.-H. Metal–Organic Cooperative Catalysis in C–H and C–C Bond Activation. *Chem. Rev.* **2017**, *117* (13), 8977–9015.

(14) Afewerki, S.; Córdova, A. Combinations of Aminocatalysts and Metal Catalysts: A Powerful Cooperative Approach in Selective Organic Synthesis. *Chem. Rev.* **2016**, *116* (22), 13512–13570.

(15) Peters, R. *Cooperative Catalysis*; Peters, R., Ed.; Wiley: Weinheim, 2015.

(16) Romiti, F.; del Pozo, J.; Paioti, P. H. S.; Gonsales, S. A.; Li, X.; Hartrampf, F. W. W.; Hoveyda, A. H. Different Strategies for Designing Dual-Catalytic Enantioselective Processes: From Fully Cooperative to Non-Cooperative Systems. *J. Am. Chem. Soc.* **2019**, *141* (45), 17952–17961.

(17) Krautwald, S.; Sarlah, D.; Schafroth, M. A.; Carreira, E. M. Enantio- and Diastereodivergent Dual Catalysis: -Allylation of Branched Aldehydes. *Science* **2013**, *340* (6136), 1065–1068.

(18) Krautwald, S.; Schafroth, M. A.; Sarlah, D.; Carreira, E. M. Stereodivergent α-Allylation of Linear Aldehydes with Dual Iridium and Amine Catalysis. *J. Am. Chem. Soc.* **2014**, *136* (8), 3020–3023.

(19) Sandmeier, T.; Krautwald, S.; Zipfel, H. F.; Carreira, E. M. Stereodivergent Dual Catalytic α-Allylation of Protected α-Amino- and α-Hydroxyacetaldehydes. *Angew. Chemie Int. Ed.* **2015**, *54* (48), 14363–14367.

(20) He, R.; Huo, X.; Zhao, L.; Wang, F.; Jiang, L.; Liao, J.; Zhang, W. Stereodivergent Pd/Cu Catalysis for the Dynamic Kinetic Asymmetric Transformation of Racemic Unsymmetrical 1,3-Disubstituted Allyl Acetates. *J. Am. Chem. Soc.* **2020**, *142* (18), 8097–8103.

(21) Huo, X.; Zhang, J.; Fu, J.; He, R.; Zhang, W. Ir/Cu Dual Catalysis: Enantio- and Diastereodivergent Access to α,α-Disubstituted α-Amino Acids Bearing Vicinal Stereocenters. *J. Am. Chem. Soc.* **2018**, *140* (6), 2080–2084.

(22) Jiang, X.; Boehm, P.; Hartwig, J. F. Stereodivergent Allylation of Azaaryl Acetamides and Acetates by Synergistic Iridium and Copper Catalysis. *J. Am. Chem. Soc.* **2018**, *140* (4), 1239–1242.

(23) Wei, L.; Zhu, Q.; Xu, S.-M.; Chang, X.; Wang, C.-J. Stereodivergent Synthesis of α,α-Disubstituted α-Amino Acids via Synergistic Cu/Ir Catalysis. *J. Am. Chem. Soc.* **2018**, *140* (4), 1508–1513.

(24) He, Z.-T.; Jiang, X.; Hartwig, J. F. Stereodivergent Construction of Tertiary Fluorides in Vicinal Stereogenic Pairs by Allylic Substitution with Iridium and Copper Catalysts. *J. Am. Chem. Soc.* **2019**, *141* (33), 13066–13073.

(25) Xu, S.-M.; Wei, L.; Shen, C.; Xiao, L.; Tao, H.-Y.; Wang, C.-J. Stereodivergent Assembly of Tetrahydro-γ-Carbolines via Synergistic Catalytic Asymmetric Cascade Reaction. *Nat. Commun.* **2019**, *10* (1), 5553.

(26) Zhang, Q.; Yu, H.; Shen, L.; Tang, T.; Dong, D.; Chai, W.; Zi, W. Stereodivergent Coupling of 1,3-Dienes with Aldimine Esters Enabled by Synergistic Pd and Cu Catalysis. *J. Am. Chem. Soc.* **2019**, *141* (37), 14554–14559.

(27) Sandmeier, T.; Carreira, E. M. Enantioselective Iridium-Catalyzed α-Allylation with Aqueous Solutions of Acetaldehyde. *Org. Lett.* **2020**, *22* (3), 1135–1138.

(28) Singha, S.; Serrano, E.; Mondal, S.; Daniliuc, C. G.; Glorius, F. Diastereodivergent Synthesis of Enantioenriched α,β-Disubstituted γ-Butyrolactones via Cooperative N-Heterocyclic Carbene and Ir Catalysis. *Nat. Catal.* **2020**, *3* (1), 48–54.

(29) Zhang, M.-M.; Wang, Y.-N.; Wang, B.-C.; Chen, X.-W.; Lu, L.-Q.; Xiao, W.-J. Synergetic Iridium and Amine Catalysis Enables Asymmetric [4+2] Cycloadditions of Vinyl Aminoalcohols with Carbonyls. *Nat. Commun.* **2019**, *10* (1), 2716.

(30) Kim, B.; Kim, Y.; Lee, S. Y. Stereodivergent Carbon–Carbon Bond Formation between Iminium and Enolate Intermediates by Synergistic Organocatalysis. *J. Am. Chem. Soc.* **2021**, *143* (1), 73–79.

(31) Tellis, J. C.; Primer, D. N.; Molander, G. A. Single-Electron Transmetalation in Organoboron Cross-Coupling by Photoredox/Nickel Dual Catalysis. *Science* **2014**, *345* (6195), 433–436.

(32) Twilton, J.; Le, C.; Zhang, P.; Shaw, M. H.; Evans, R. W.; MacMillan, D. W. C. The Merger of Transition Metal and Photocatalysis. *Nat. Rev. Chem.* **2017**, *1* (7), 0052.

(33) Zuo, Z.; Ahneman, D. T.; Chu, L.; Terrett, J. A.; Doyle, A. G.; MacMillan, D. W. C. Merging Photoredox with Nickel Catalysis: Coupling of -Carboxyl Sp3-Carbons with Aryl Halides. *Science* **2014**, *345* (6195), 437–440.

(34) Jouffroy, M.; Primer, D. N.; Molander, G. A. Base-Free Photoredox/Nickel Dual-Catalytic Cross-Coupling of Ammonium Alkylsilicates. *J. Am. Chem. Soc.* **2016**, *138* (2), 475–478.

(35) Nakajima, K.; Nojima, S.; Nishibayashi, Y. Nickel- and Photoredox-Catalyzed Cross-Coupling Reactions of Aryl Halides with 4-Alkyl-1,4-Dihydropyridines as Formal Nucleophilic Alkylation Reagents. *Angew. Chemie Int. Ed.* **2016**, *55* (45), 14106–14110.

(36) Milligan, J. A.; Phelan, J. P.; Badir, S. O.; Molander, G. A. Alkyl Carbon–Carbon Bond Formation by Nickel/Photoredox Cross-Coupling.
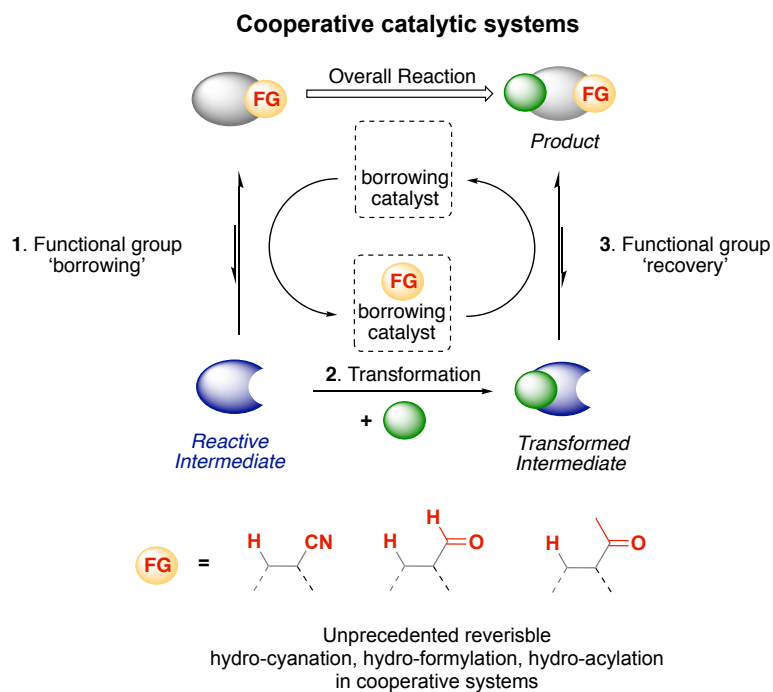
Angew. Chemie Int. Ed. **2019**, *58* (19), 6152–6163.

(37)   Shaw, M. H.; Shurtleff, V. W.; Terrett, J. A.; Cuthbertson, J. D.; MacMillan, D. W. C. Native Functionality in Triple Catalytic Cross-Coupling: Sp3 C-H Bonds as Latent Nucleophiles. *Science* **2016**, *352* (6291), 1304–1308.

(38)   Le, C.; Liang, Y.; Evans, R. W.; Li, X.; MacMillan, D. W. C. Selective Sp3 C–H Alkylation via Polarity-Match-Based Cross-Coupling. *Nature* **2017**, *547* (7661), 79–83.

(39)   Zhang, X.; MacMillan, D. W. C. Direct Aldehyde C–H Arylation and Alkylation via the Combination of Nickel, Hydrogen Atom Transfer, and Photoredox Catalysis. *J. Am. Chem. Soc.* **2017**, *139* (33), 11353–11356.

(40)   Heitz, D. R.; Tellis, J. C.; Molander, G. A. Photochemical Nickel-Catalyzed C–H Arylation: Synthetic Scope and Mechanistic Investigations. *J. Am. Chem. Soc.* **2016**, *138* (39), 12715–12718.

(41)   Shields, B. J.; Doyle, A. G. Direct C(Sp 3)–H Cross Coupling Enabled by Catalytic Generation of Chlorine Radicals. *J. Am. Chem. Soc.* **2016**, *138* (39), 12719–12722.

(42)   Perry, I. B.; Brewer, T. F.; Sarver, P. J.; Schultz, D. M.; DiRocco, D. A.; MacMillan, D. W. C. Direct Arylation of Strong Aliphatic C–H Bonds. *Nature* **2018**, *560* (7716), 70–75.

(43)   Lee, G. S.; Won, J.; Choi, S.; Baik, M.-H.; Hong, S. H. Synergistic Activation of Amides and Hydrocarbons for Direct C(Sp 3)–H Acylation Enabled by Metallaphotoredox Catalysis. *Angew. Chemie Int. Ed.* **2020**, *59* (39), 16933–16942.

(44)   Thullen, S. M.; Treacy, S. M.; Rovis, T. Regioselective Alkylative Cross-Coupling of Remote Unactivated C(Sp 3)–H Bonds. *J. Am. Chem. Soc.* **2019**, *141* (36), 14062–14067.

(45)   Cao, H.; Kuang, Y.; Shi, X.; Wong, K. L.; Tan, B. B.; Kwan, J. M. C.; Liu, X.; Wu, J. Photoinduced Site-Selective Alkenylation of Alkanes and Aldehydes with Aryl Alkenes. *Nat. Commun.* **2020**, *11* (1), 1956.

(46)   Shaw, M. H.; Twilton, J.; MacMillan, D. W. C. Photoredox Catalysis in Organic Chemistry. *J. Org. Chem.* **2016**, *81* (16), 6898–6926.

(47)   Hamilton, D. S.; Nicewicz, D. A. Direct Catalytic Anti-Markovnikov Hydroetherification of Alkenols. *J. Am. Chem. Soc.* **2012**, *134* (45), 18577–18580.

(48)   Wilger, D. J.; Grandjean, J.-M. M.; Lammert, T. R.; Nicewicz, D. A. The Direct Anti-Markovnikov Addition of Mineral Acids to Styrenes. *Nat. Chem.* **2014**, *6* (8), 720–726.

(49)   Margrey, K. A.; Nicewicz, D. A. A General Approach to Catalytic Alkene Anti-Markovnikov Hydrofunctionalization Reactions via Acridinium Photoredox Catalysis. *Acc. Chem. Res.* **2016**, *49* (9), 1997–2006.

(50)   Perkowski, A. J.; Nicewicz, D. A. Direct Catalytic Anti-Markovnikov Addition of Carboxylic Acids to Alkenes. *J. Am. Chem. Soc.* **2013**, *135* (28), 10334–10337.

(51)   Nguyen, T. M.; Nicewicz, D. A. Anti-Markovnikov Hydroamination of Alkenes Catalyzed by an Organic Photoredox System. *J. Am. Chem. Soc.* **2013**, *135* (26), 9588–9591.

(52)   Nguyen, T. M.; Manohar, N.; Nicewicz, D. A. Anti -Markovnikov Hydroamination of Alkenes Catalyzed by a Two-Component Organic Photoredox System: Direct Access to Phenethylamine Derivatives. *Angew. Chemie Int. Ed.* **2014**, *53* (24), 6198–6201.

(53)   Zeller, M. A.; Riener, M.; Nicewicz, D. A. Butyrolactone Synthesis via Polar Radical Crossover Cycloaddition Reactions: Diastereoselective Syntheses of Methylenolactocin and Protolichesterinic Acid. *Org. Lett.* **2014**, *16* (18), 4810–4813.

(54)   Cavanaugh, C. L.; Nicewicz, D. A. Synthesis of α-Benzyloxyamino-γ-Butyrolactones via a Polar Radical Crossover Cycloaddition Reaction. *Org. Lett.* **2015**, *17* (24), 6082–6085.

(55)   Gesmundo, N. J.; Grandjean, J.-M. M.; Nicewicz, D. A. Amide and Amine Nucleophiles in Polar Radical Crossover Cycloadditions: Synthesis of γ-Lactams and Pyrrolidines. *Org. Lett.* **2015**, *17* (5), 1316–1319.

(56)   Wu, F.; Wang, L.; Chen, J.; Nicewicz, D. A.; Huang, Y. Direct Synthesis of Polysubstituted Aldehydes via Visible-Light Catalysis. *Angew. Chemie Int. Ed.* **2018**, *57* (8), 2174–2178.

(57)   Romero, N. A.; Margrey, K. A.; Tay, N. E.; Nicewicz, D. A. Site-Selective Arene C-H Amination via Photoredox Catalysis. *Science* **2015**, *349* (6254), 1326–1330.

(58)   Chen, W.; Huang, Z.; Tay, N. E. S.; Giglio, B.; Wang, M.; Wang, H.; Wu, Z.; Nicewicz, D. A.; Li, Z. Direct Arene C–H Fluorination with 18 F – via Organic Photoredox Catalysis. *Science* **2019**, *364* (6446), 1170–1174.

(59)   Ohmatsu, K.; Suzuki, R.; Furukawa, Y.; Sato, M.; Ooi, T. Zwitterionic 1,2,3-Triazolium Amidate as a Catalyst for Photoinduced Hydrogen-Atom Transfer Radical Alkylation. *ACS Catal.* **2020**, *10* (4), 2627–2632.

(60)   Shin, N. Y.; Ryss, J. M.; Zhang, X.; Miller, S. J.; Knowles, R. R. Light-Driven Deracemization Enabled by Excited-State Electron Transfer. *Science* **2019**, *366* (6463), 364–369.

(61)   Wang, Y.; Carder, H. M.; Wendlandt, A. E. Synthesis of Rare Sugar Isomers through Site-Selective Epimerization. *Nature* **2020**, *578* (7795), 403–408.

(62)   Pellissier, H. Stereocontrolled Domino Reactions. *Chem. Rev.* **2013**, *113* (1), 442–524.

(63)   Grossmann, A.; Enders, D. N-Heterocyclic Carbene Catalyzed Domino Reactions. *Angew. Chemie Int. Ed.* **2012**, *51* (2), 314–325.

(64)   Pellissier, H. Recent Developments in Enantioselective Metal-Catalyzed Domino Reactions. *Advanced Synthesis and Catalysis*. 2016, pp 2194–2259.

(65)   Clavier, H.; Pellissier, H. Recent Developments in Enantioselective Metal-Catalyzed Domino Reactions. *Adv. Synth. Catal.* **2012**, *354* (18), 3347–3403.

(66)   Pellissier, H. Recent Developments in Enantioselective Metal-Catalyzed Domino Reactions. *Adv. Synth. Catal.* **2019**, *361* (8), 1733–1755.

(67)   Chanda, T.; Zhao, J. C. G. Recent Progress in Organocatalytic Asymmetric Domino Transformations. *Adv. Synth. Catal.* **2018**, *360* (1), 2–79.

(68)   Tietze, L. F. Domino Reactions. In *Domino Reactions: Concepts for Efficient Organic Synthesis*; Tietze, L. F., Ed.; Wiley-VCH Verlag GmbH & Co. KGaA: Weinheim, Germany, 2014; pp 1–621.

(69)   Trost, B. M.; Min, C. Total Synthesis of Terpenes via Palladium-Catalysed Cyclization Strategy. *Nat. Chem.* **2020**, *12* (6), 568–573.

(70)   Trost, B. M.; Shi, Y. Palladium-Catalyzed Cyclizations of Polyenynes. A Palladium Zipper. *J. Am. Chem. Soc.* **1993**, *115* (21), 9421–9438.

(71)   Whyte, A.; Torelli, A.; Mirabi, B.; Prieto, L.; Rodríguez, J. F.; Lautens, M. Cobalt-Catalyzed Enantioselective Hydroarylation of 1,6-Enynes. *J. Am. Chem. Soc.* **2020**, *142* (20), 9510–9517.

(72)   Takahashi, K.; Yamashita, M.; Nozaki, K. Tandem Hydroformylation/Hydrogenation of Alkenes to Normal Alcohols Using Rh/Ru Dual Catalyst or Ru Single Component Catalyst. *J. Am. Chem. Soc.* **2012**, *134* (45), 18746–18757.

(73)   Takahashi, K.; Yamashita, M.; Ichihara, T.; Nakano, K.; Nozaki, K. High-Yielding Tandem Hydroformylation/Hydrogenation of a Terminal Olefin to Produce a Linear Alcohol Using a Rh/Ru Dual Catalyst System. *Angew. Chemie Int. Ed.* **2010**, *49* (26), 4488–4490.

(74)   Ahmed, M.; Seayad, A. M.; Jackstell, R.; Beller, M. Amines Made Easily: A Highly Selective Hydroaminomethylation of Olefins. *J. Am. Chem. Soc.* **2003**, *125* (34), 10311–10318.

(75)   Hanna, S.; Holder, J. C.; Hartwig, J. F. A Multicatalytic Approach to the Hydroaminomethylation of A-Olefins. *Angew. Chemie Int. Ed.* **2019**, *58* (11), 3368–3372.

(76)   Jia, Z.-J.; Shan, G.; Daniliuc, C. G.; Antonchick, A. P.; Waldmann, H. Enantioselective Synthesis of the Spirotropanyl Oxindole Scaffold through Bimetallic Relay Catalysis. *Angew. Chemie Int. Ed.* **2018**, *57* (44), 14493–14497.

(77)   Yu, Q.; Fu, Y.; Huang, J.; Qin, J.; Zuo, H.; Wu, Y.; Zhong, F. Enantioselective Oxidative Phenol-Indole [3 + 2] Coupling Enabled by Biomimetic Mn(Iii)/Brønsted Acid Relay Catalysis. *ACS Catal.* **2019**, *9* (8), 7285–7291.

(78)   Denard, C. A.; Bartlett, M. J.; Wang, Y.; Lu, L.; Hartwig, J. F.; Zhao, H. Development of a One-Pot Tandem Reaction Combining Ruthenium-Catalyzed Alkene Metathesis and Enantioselective Enzymatic Oxidation to Produce Aryl Epoxides. *ACS Catal.* **2015**, *5* (6), 3817–3822.

(79)   Corma, A.; Navas, J.; Sabater, M. J. Advances in One-Pot Synthesis through Borrowing Hydrogen Catalysis. *Chem. Rev.* **2018**, *118* (4), 1410–1459.

(80)   Goldman, A. S. Catalytic Alkane Metathesis by Tandem Alkane Dehydrogenation-Olefin Metathesis. *Science* **2006**, *312* (5771), 257–261.

(81)   Lichosyt, D.; Zhang, Y.; Hurej, K.; Dydio, P. Dual-Catalytic Transition Metal Systems for Functionalization of Unreactive Sites of Molecules. *Nat. Catal.* **2019**, *2* (2), 114–122.

(82)   Quintard, A.; Constantieux, T.; Rodriguez, J. An Iron/Amine-Catalyzed Cascade Process for the Enantioselective Functionalization of Allylic Alcohols. *Angew. Chemie Int. Ed.* **2013**, *52* (49), 12883–12887.

(83)   Roudier, M.; Constantieux, T.; Quintard, A.; Rodriguez, J. Triple Iron/Copper/Iminium Activation for the Efficient Redox Neutral Catalytic Enantioselective Functionalization of Allylic Alcohols. *ACS Catal.* **2016**, *6* (8), 5236–5244.

(84)   Black, P. J.; Harris, W.; Williams, J. M. J. Catalytic Electronic Activation: Indirect Addition of Nucleophiles to an Allylic Alcohol This Work Was Supported by the University of Bath and Roche Discovery (P.J.B.). *Angew. Chemie Int. Ed.* **2001**, *40* (23), 4475.

(85)   Denard, C. A.; Huang, H.; Bartlett, M. J.; Lu, L.; Tan, Y.; Zhao, H.; Hartwig, J. F. Cooperative Tandem Catalysis by an Organometallic Complex and a Metalloenzyme. *Angew. Chemie Int. Ed.* **2014**, *53* (2), 465–469.

(86)   Bhat, V.; Welin, E. R.; Guo, X.; Stoltz, B. M. Advances in Stereoconvergent Catalysis from 2005 to 2015: Transition-Metal-Mediated Stereoablative Reactions, Dynamic Kinetic Resolutions, and Dynamic Kinetic Asymmetric Transformations. *Chem. Rev.* **2017**, *117* (5), 4528–4561.

(87)   Verho, O.; Bäckvall, J. E. Chemoenzymatic Dynamic Kinetic Resolution: A Powerful Tool for the Preparation of Enantiomerically Pure Alcohols and Amines. *J. Am. Chem. Soc.* **2015**, *137* (12), 3996–4009.

(88)   Pàmies, O.; Bäckvall, J. E. Combination of Enzymes and Metal Catalysts. A Powerful Approach in Asymmetric Catalysis. *Chem. Rev.* **2003**, *103* (8), 3247–3261.

(89)   Chen, Z.; Aota, Y.; Nguyen, H. M. H.; Dong, V. M. Dynamic Kinetic Resolution of Aldehydes by Hydroacylation. *Angew. Chemie Int. Ed.* **2019**, *58* (14), 4705–4709.

(90)   Litman, Z. C.; Wang, Y.; Zhao, H.; Hartwig, J. F. Cooperative Asymmetric Reactions Combining Photocatalysis and Enzymatic Catalysis. *Nature* **2018**, *560* (7718), 355–359.

(91)   Atesin, A. C.; Ray, N. A.; Stair, P. C.; Marks, T. J. Etheric C–O Bond Hydrogenolysis Using a Tandem Lanthanide Triflate/Supported Palladium Nanoparticle Catalyst System. *J. Am. Chem. Soc.* **2012**, *134* (36), 14682–14685.

(92)   Lohr, T. L.; Li, Z.; Marks, T. J. Thermodynamic Strategies for C–O Bond Formation and Cleavage via Tandem Catalysis. *Acc. Chem. Res.* **2016**, *49* (5), 824–834.

(93)   Panteleev, J.; Zhang, L.; Lautens, M. Domino Rhodium-Catalyzed Alkyne Arylation/Palladium-Catalyzed N Arylation: A Mechanistic Investigation. *Angew. Chemie Int. Ed.* **2011**, *50* (39), 9089–9092.

(94)   Friedman, A. A.; Panteleev, J.; Tsoung, J.; Huynh, V.; Lautens, M. Rh/Pd Catalysis with Chiral and Achiral Ligands: Domino Synthesis of Aza-Dihydrodibenzoxepines. *Angew. Chemie Int. Ed.* **2013**, *52* (37), 9755–9758.

(95)   Zhang, L.; Qureshi, Z.; Sonaglia, L.; Lautens, M. Sequential Rhodium/Palladium Catalysis: Enantioselective Formation of Dihydroquinolinones in the Presence of Achiral and Chiral Ligands. *Angew. Chemie Int. Ed.* **2014**, *53* (50), 13850–13853.

(96)   Lohr, T. L.; Marks, T. J. Orthogonal Tandem Catalysis. *Nat. Chem.* **2015**, *7* (6), 477–482.

(97)   Huang, H.; Denard, C. A.; Alamillo, R.; Crisci, A. J.; Miao, Y.; Dumesic, J. A.; Scott, S. L.; Zhao, H. Tandem Catalytic Conversion of Glucose to 5-Hydroxymethylfurfural with an Immobilized Enzyme and a Solid Acid. *ACS Catal.* **2014**, *4* (7), 2165–2168.

(98)   Cybulski, O.; Dygas, M.; Mikulak-Klucznik, B.; Siek, M.; Klucznik, T.; Choi, S. Y.; Mitchell, R. J.; Sobolev, Y. I.; Grzybowski, B. A. Concentric Liquid Reactors for Chemical Synthesis and Separation. *Nature* **2020**, *586* (7827), 57–63.

(99)   Sato, H.; Hummel, W.; Gröger, H. Cooperative Catalysis of Noncompatible Catalysts through Compartmentalization: Wacker Oxidation and Enzymatic Reduction in a One-Pot Process in Aqueous Media. *Angew. Chemie Int. Ed.* **2015**, *54* (15), 4488–4492.

(100)   Huff, C. A.; Sanford, M. S. Cascade Catalysis for the Homogeneous Hydrogenation of CO 2 to Methanol. *J. Am. Chem. Soc.* **2011**, *133* (45), 18122–18125.

(101)   Lu, J.; Dimroth, J.; Weck, M. Compartmentalization of Incompatible Catalytic Transformations for Tandem Catalysis. *J. Am. Chem. Soc.* **2015**, *137* (40), 12984–12989.

(102)   Wheeldon, I.; Minteer, S. D.; Banta, S.; Barton, S. C.; Atanassov, P.; Sigman, M. Substrate Channelling as an Approach to Cascade Reactions. *Nat. Chem.* **2016**, *8* (4), 299–309.

(103)   Bornscheuer, U. T.; Huisman, G. W.; Kazlauskas, R. J.; Lutz, S.; Moore, J. C.; Robins, K. Engineering the Third Wave of Biocatalysis. *Nature* **2012**, *485* (7397), 185–194.

(104)   Hyster, T. K.; Ward, T. R. Genetic Optimization of Metalloenzymes: Enhancing Enzymes for Non-Natural Reactions. *Angew. Chemie Int. Ed.* **2016**, *55* (26), 7344–7357.

(105)   Dydio, P.; Ploeger, M.; Reek, J. N. H. Selective Isomerization–Hydroformylation Sequence: A Strategy to Valuable α-Methyl-Branched Aldehydes from Terminal Olefins. *ACS Catal.* **2013**, *3* (12), 2939–2942.

(106)   Yin, X.-P.; Zeng, X.-P.; Liu, Y.-L.; Liao, F.-M.; Yu, J.-S.; Zhou, F.; Zhou, J. Asymmetric Triple Relay Catalysis: Enantioselective Synthesis of Spirocyclic Indolines through a One-Pot Process Featuring an Asymmetric 6π Electrocyclization. *Angew. Chemie Int. Ed.* **2014**, *53* (50), 13740–13745.

(107)   Sancheti, S. P.; Urvashi; Shah, M. P.; Patil, N. T. Ternary Catalysis: A Stepping Stone toward Multicatalysis. *ACS Catal.* **2020**, *10* (5), 3462–3489.

(108)   Dhiman, S.; Mishra, U. K.; Ramasastry, S. S. V. One-Pot Trimetallic Relay Catalysis: A Unified Approach for the Synthesis of β-Carbolines and Other [c]-Fused Pyridines. *Angew. Chemie Int. Ed.* **2016**, *55* (27), 7737–7741.

(109)   Casnati, A.; Lichosyt, D.; Lainer, B.; Veth, L.; Dydio, P. Multicatalytic Approach to One-Pot Stereoselective Synthesis of Secondary Benzylic Alcohols. *Org. Lett.* **2021**, *23* (9), 3502–3506.

(110) Camp, J. E. Auto-Tandem Catalysis: Activation of Multiple, Mechanistically Distinct Process by a Single Catalyst. *European J. Org. Chem.* **2017**, *2017* (3), 425–433.

(111) Shindoh, N.; Takemoto, Y.; Takasu, K. Auto-Tandem Catalysis: A Single Catalyst Activating Mechanistically Distinct Reactions in a Single Reactor. *Chem. - A Eur. J.* **2009**, *15* (45), 12168–12179.

(112) Kanbayashi, N.; Takenaka, K.; Okamura, T.; Onitsuka, K. Asymmetric Auto-Tandem Catalysis with a Planar-Chiral Ruthenium Complex: Sequential Allylic Amidation and Atom-Transfer Radical Cyclization. *Angew. Chemie Int. Ed.* **2013**, *52* (18), 4897–4901.

(113) Matsushima, Y.; Onitsuka, K.; Kondo, T.; Mitsudo, T.; Takahashi, S. Asymmetric Catalysis of Planar-Chiral Cyclopentadienylruthenium Complexes in Allylic Amination and Alkylation. *J. Am. Chem. Soc.* **2001**, *123* (42), 10405–10406.

(114) Long, J.; Yu, R.; Gao, J.; Fang, X. Access to 1,3-Dinitriles by Enantioselective Auto-tandem Catalysis: Merging Allylic Cyanation with Asymmetric Hydrocyanation. *Angew. Chemie Int. Ed.* **2020**, *59* (17), 6785–6789.

(115) Wu, X.; Cruz, F. A.; Lu, A.; Dong, V. M. Tandem Catalysis: Transforming Alcohols to Alkenes by Oxidative Dehydroxymethylation. *J. Am. Chem. Soc.* **2018**, *140* (32), 10126–10130.

(116) Lecomte, M.; Lipshultz, J. M.; Kim-Lee, S.-H.; Li, G.; Radosevich, A. T. Driving Recursive Dehydration by P III /P V Catalysis: Annulation of Amines and Carboxylic Acids by Sequential C–N and C–C Bond Formation. *J. Am. Chem. Soc.* **2019**, *141* (32), 12507–12512.

(117) Zhang, S.; del Pozo, J.; Romiti, F.; Mu, Y.; Torker, S.; Hoveyda, A. H. Delayed Catalyst Function Enables Direct Enantioselective Conversion of Nitriles to NH 2 -Amines. *Science* **2019**, *364* (6435), 45–51.

(118) Li, L.; Herzon, S. B. Temporal Separation of Catalytic Activities Allows Anti-Markovnikov Reductive Functionalization of Terminal Alkynes. *Nat. Chem.* **2014**, *6* (1), 22–27.

(119) Korvorapun, K.; Kaplaneris, N.; Rogge, T.; Warratz, S.; Stückl, A. C.; Ackermann, L. Sequential Meta-/Ortho-C–H Functionalizations by One-Pot Ruthenium(II/III) Catalysis. *ACS Catal.* **2018**, *8* (2), 886–892.

(120) Semwal, S.; Choudhury, J. Switch in Catalyst State: Single Bifunctional Bi-State Catalyst for Two Different Reactions. *Angew. Chemie Int. Ed.* **2017**, *56* (20), 5556–5560.

(121) Meng, J.; Fan, L.-F.; Han, Z.-Y.; Gong, L.-Z. α-Quaternary Chiral Aldehydes from Styrenes, Allylic Alcohols, and Syngas via Multi-Catalyst Relay Catalysis. *Chem* **2018**, *4* (5), 1047–1058.

(122) Wu, H.; He, Y.-P.; Gong, L.-Z. The Combination of Relay and Cooperative Catalysis with a Gold/Palladium/Brønsted Acid Ternary System for the Cascade Hydroamination/Allylic Alkylation Reaction. *Adv. Synth. Catal.* **2012**, *354* (6), 975–980.

(123) Wang, C.; Han, Z.-Y.; Luo, H.-W.; Gong, L.-Z. Highly Enantioselective Relay Catalysis in the Three-Component Reaction for Direct Construction of Structurally Complex Heterocycles. *Org. Lett.* **2010**, *12* (10), 2266–2269.

(124) Pirnot, M. T.; Rankic, D. A.; Martin, D. B. C.; MacMillan, D. W. C. Photoredox Activation for the Direct -Arylation of Ketones and Aldehydes. *Science* **2013**, *339* (6127), 1593–1596.

(125) DeHovitz, J. S.; Loh, Y. Y.; Kautzky, J. A.; Nagao, K.; Meichan, A. J.; Yamauchi, M.; MacMillan, D. W. C.; Hyster, T. K. Static to Inducibly Dynamic Stereocontrol: The Convergent Use of Racemic β-Substituted Ketones. *Science* **2020**, *369* (6507), 1113–1118.

(126) Fleischer, S.; Werkmeister, S.; Zhou, S.; Junge, K.; Beller, M. Consecutive Intermolecular Reductive Hydroamination: Cooperative Transition-Metal and Chiral Brønsted Acid Catalysis. *Chem. - A Eur. J.* **2012**, *18* (29), 9005–9010.

(127) Tang, X.; Gan, L.; Zhang, X.; Huang, Z. N-Alkanes to n -Alcohols: Formal Primary C─H Bond Hydroxymethylation via Quadruple Relay Catalysis. *Sci. Adv.* **2020**, *6* (47), eabc6688.

(128) Domański, S.; Gatlik, B.; Chaładaj, W. Pd-Catalyzed Boroperfluoroalkylation of Alkynes Opens a Route to One-Pot Reductive Carboperfluoroalkylation of Alkynes with Perfluoroalkyl and Aryl Iodides. *Org. Lett.* **2019**, *21* (13), 5021–5025.

(129) Yamamoto, K.; Bruun, T.; Kim, J. Y.; Zhang, L.; Lautens, M. A New Multicomponent Multicatalyst Reaction (MC) 2 R: Chemoselective Cycloaddition and Latent Catalyst Activation for the Synthesis of Fully Substituted 1,2,3-Triazoles. *Org. Lett.* **2016**, *18* (11), 2644–2647.

(130) Armstrong, M. K.; Goodstein, M. B.; Lalic, G. Diastereodivergent Reductive Cross Coupling of Alkynes through Tandem Catalysis: Z - and E -Selective Hydroarylation of Terminal Alkynes. *J. Am. Chem. Soc.* **2018**, *140* (32), 10233–10241.

CHAPTER 2

Cooperative catalysis engaging hydro-functional group borrowing unlocking non-inherent reactivity

Cooperative catalytic systems

FG = Unprecedented reverisble
hydro-cyanation, hydro-formylation, hydro-acylation
in cooperative systems

2.1 Introduction

Reversible catalytic reactions can transiently change the reactivity of organic molecules and therefore unlock their non-inherent reactivity (Figure 1A). By establishing an equilibrium between two different functionalities, the reactivity of the neighboring atoms can be temporarily changed, opening the access for functionalization reactions to occur at initially non-reactive sites of the target molecule (Figure 1B top).[1] A diverse set of such reversible transformations have been exploited as catalytic transfer functionalization reactions[2] (known as 'shuttle catalysis'), in which chemical entities such as H_2[3,4], CO[5], $H-CN$[6], $R-CHO$[7,8], or $HR-C=O$,[9] among others, are transferred between two substrates by controlling the direction of the equilibrium with a thermodynamic driving force (e.g., gas release, string release, polymerization or precipitation of one of the components of the equilibrium).
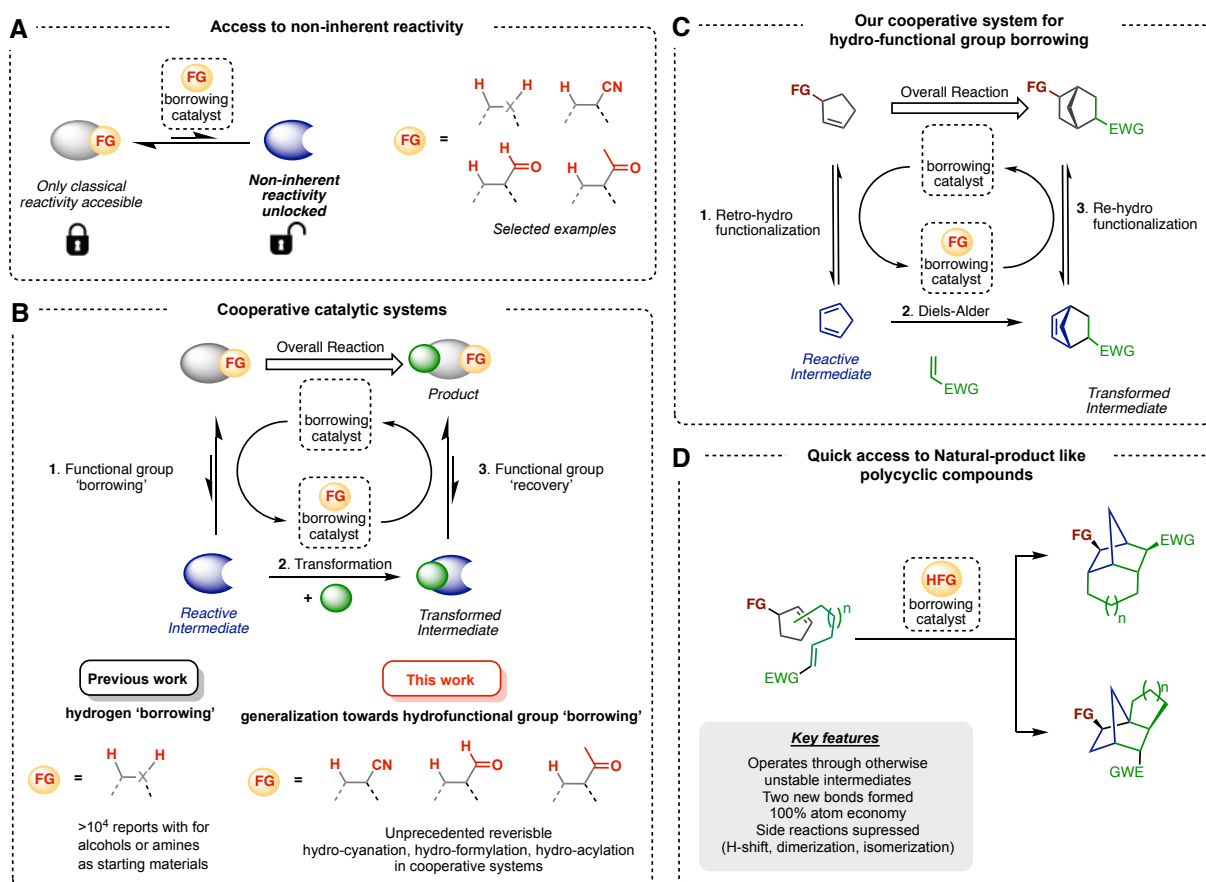
Figure 1. **Development of cooperative systems engaging hydro-functional group borrowing.** (**A**) Access to non-inherent reactivity via catalytic functional group borrowing. (**B**) Envisioned general approach towards cooperative systems engaging functional group borrowing. (**C**) Our design for a cooperative system exploiting reversible hydro-functionalization and orthogonal Diels-Alder reaction. (**D**) Synthetic potential for modular access to natural product-like polycyclic compounds.

When reversible catalytic reactions cooperate with other transformations, networks of reactions can be developed to carry out transformations that cannot be accomplished efficiently with these reactions performed sequentially.[1] However, such cooperative systems are difficult to develop

because all individual reactions must be operating simultaneously under the same conditions and with adequate rates for overall catalytic turnover, and all plausible deactivation processes and side-reactions involving intermediates and reagents must be suppressed.[10] Owing to these constraints, the vast majority of cooperative systems engaging reversible catalysis that have been reported over the past 40 years use reversible dehydrogenation reaction, which is often referred to as 'hydrogen borrowing' reactivity (Figure 1B bottom left).[11,12] While hydrogen borrowing catalysis created a number of highly valuable chemical transformations for alcohols and amines, which today represent state-of-art methods in synthesis, new approaches for the development of such cooperative systems are needed to unlock the full potential of networks exploiting reversible catalysis and enable novel transformations for other starting materials beyond the limited established scope (Figure 1B bottom right). Here we report a class of cooperative systems that engage, for the first time, reversible hydrofunctionalization reactions to unlock diene-like non-inherent reactivity of functionalized alkene starting materials together with orthogonal Diels-Alder reactions to access functionalized (poly)cyclic compounds in one step with 100% atom economy (Figure 1C). Moreover, our approach proved to be successful to facilitate the access to natural product-like polycyclic compounds (Figure 1D).

2.2 Results and Discussion

2.2.1   Reaction design

 We considered that diene reactivity of (homo)allyl nitrile starting material **1a** or **1b** can be accessed by catalytic retro-hydrocyanation in presence of a catalytic system based on Ni-DPEPhos-AlMe$_2$Cl[6] to form *in situ* cyclopentadiene intermediate **2**. Then, this transient reactivity will be seized by a dienephile, such as crotonate **3**, which will engage with **2** in a Lewis Acid catalyzed Diels-Alder reaction to form intermediate **4**. Lastly, the catalytic re-hydrocyanation reaction of **4** will lead to the formation of the target product **5**, closing the cycle and regenerating the H-CN borrowing catalyst (Figure 2A).

 The success of this particular design relies in the following key points: 1) all three reactions in the network need to occur efficiently under the exact same set of conditions (as above-stated for all cooperating systems), 2) direction must be thermodynamically driven towards formation of the product (in this case, conjugation drives step **I** and string release drives step **III**), and 3) the following competing side reactions need to be suppressed: dimerization of **2** to form **6**; transfer of the functional group to **6** forming **7**; back transfer of functional group to the initial starting material **1a** or **1b**; transfer of the functional group to the dienophile **3** (Figure 2A).

 To identify a suitable ranged of catalytic conditions for the devised network of reactions, we studied each step independently with similar model reactions and evaluated the performance of all of them under identical catalytic conditions (Figure 2B). The first step (**I**), the retro-hydrocyanation of either **1a** or **1b** to form **2**, was emulated as the transfer of H-CN between **1a** or **1b** and the known efficient acceptor **8**, forming **9**. The second step (**II**), the Diels-Alder reaction was studied as the reaction of **2** and **3**. The third step (**III**), the re-hydrocyanation of intermediate **4** to form **5** was studied as the transfer of H-CN between the efficient donor **10** to the independently prepared intermediate **4** to form **5**.

 In Table 1, I present the yields and conversions for the model reactions (after 4 h reaction time) corresponding to retro-hydrocyanation (**I**), Diels-Alder (**II**), and re-hydrocyanation (**III**). At ambient temperature using 20 mol% AlMe$_2$Cl, that is, under standard retro-hydrocyanation conditions[6] (entry 1), only **1b** reacts quantitatively in step **I**, step **II** is rather sluggish, barely forming any product **4**,

while step **III** occurs cleanly, albeit not quantitatively. Upon increasing the reaction temperature to 50 ºC (entry 2), reaction emulating step **I** occurs in quantitative yields for both starting materials **1a** and **1b**, the rate of step **II** increases, but the yield and the conversion remain low, while step **III** occurs nearly quantitatively. Further increase of the temperature to 80 ºC or 130 ºC (i.e., standard retro-hydrocyanation conditions)[6] was found to be detrimental in general (entries 3 and 4), indicating that many side processes start taking place under these conditions. To further improve the performance of step **II**, I studied increasing the amount of the Lewis acid (entries 5 to 8). I found that in the presence of 5 mol% Ni(cod)$_2$, 5 mol% DPEPhos, and 40 mol% AlMe$_2$Cl at 50 ºC (entry 6), all steps occurred with high yields, indicating that these are the conditions suitable for exploration of the full system.

C Proof of concept model reaction

Table 2. Optimization of the model reaction.

entry	variations from standard conditions	Yield (conversion)% from **1a** or [**1b**]	Observations
1	none	99 (99), [99 (99)]	-
2	24 hours	50 (50), [44 (44)]	Traces of **4**
3	at 28 ºC	16	Traces of **4**
4	at 80 ºC	99	-
5	at 100 ºC	34	Formation of **4**, **6** and **7**
6	at 130 ºC	24	Formation of **4**, **6** and **7**
7	**1M** instead of 0.5M	88	Formation of **7**
8	**0.25M** instead of 0.5M	60	-
9	**20% AlMe$_2$Cl** instead of 40%	5	-
10	**80% AlMe$_2$Cl** instead of 40%	86	-
11	**AlMe$_3$ 40%** instead of AlMe$_2$Cl	2	Formation of **7**
12	**AlCl$_3$ 40%** instead of AlMe$_2$Cl	0	Traces of **4**
13	No lewis acid	0	No reaction
14	10% of Ni(cod)$_2$/DPEPhos	79	Formation of **7**

Table 1. Optimization of reactions **I**, **II** and **III**.

entry	% Lewis Acid + [Ni]	T (ºC)	Reaction I from **1a**	Reaction I from **1b**	Reaction II	Reaction III)
1	20	28	68 (82)	99 (99)	13 (19)	88 (90)
2	20	50	99 (99)	99 (99)	32 (42) $^{\$}$53(66)	98 (99)
3	20	80	79 (99)	97 (99)	62 (83)	84 (93)
4	20	130	68 (99)	82 (99)	28 (71)	76 (92)
5	40	28	88 (99)	99 (99)	23 (29)	74 (77)
6	40	50	99 (99)	99 (99)	51 (62) $^{\$}$77(93)	97 (99)
7	40	130	62 (99)	84 (99)	37 (97)	65 (99)
8	80	50	99 (99)	99 (99)	64 (82)	93 (99)

Figure 2. **Reaction design, exploratory studies, and proof-of-concept model reaction.** (**A**) Proposed reaction design to unlock diene reactivity of unsaturated and functionalized cyclopentenes. (**B**) Model reactions to explore catalytic conditions in which retro-hydrocyanation, Diels-Alder and re-hydrocyanation reactions can operate simultaneously. [Ni] = Ni(cod)$_2$ 5 mol%, DPEPhos 5 mol%. LA = AlMe$_2$Cl. $^{\$}$16 h. Reaction **I**: yield of **9**, conversion of **1a** or **1b**; Reaction **II**: yield of **4**, conversion of **3**. Reaction **III**: yield of **5**, conversion of **4**. (**C**) Successful combination of reversible hydrocyanation and the Diels-Alder reaction.

Conditions: 3.0 equiv. of **1a** or **1b**, 1 equiv. of **3**, 0.0625 mmol scale. [a] Values of combined yields of **5** isomers and conversion of **3**, determined by GC analysis of the reaction mixture with an internal standard. [b] NMR yield. For details see experimental section.

2.2.2 Model reaction

Next, we evaluated the model reaction between **1a** or **1b** and *n*-butyl crotonate **3** as a dienophile for the Diels-Alder cycloaddition under the catalytic conditions found in the exploratory studies (Figure 2C). We found that nitrile **1a** or **1b** and dienophile **3** reacted to form the target bridged bicyclic nitrile **5** in 99% yield, in the presence of 5 mol% of Ni(cod)$_2$, 5 mol% of DPEPhos, and 40 mol% of AlMe$_2$Cl, after 72 hours, at 50 ºC (Table 2, entry 1). The *endo*:*exo* 87:13 selectivity of product **5** resembles the typical selectivity of the Lewis Acid catalyzed Diels-Alder reaction (87:13, see the experimental section) Also, during the reaction, we observed formation of unsaturated bicyclic intermediate **4** – the Diels-Alder adduct, which was quantitatively converted to product **5** by the end of the reaction. These results are consistent with the envisioned transformation occurring through a sequence of independent *retro*-hydrocyanation – Diels-Alder cycloaddition – *re*-hydrocyanation.

The overall efficiency of the network of reactions is strongly affected by temperature and the loading and type of Lewis acid. For instance, significantly lower yields of the product were observed when conducting the reaction at high temperatures (entries 5 and 6), due to the formation of side products, which arise from an unproductive pathway of dimerization of **2** to form **6** and hydrocyanation of **6** to form **7**. Concentration changes from standard conditions were also found to be detrimental for the reaction (entry 7 and 8). Variation of the Lewis acid loading (entry 9 and 10) lead to poor to moderate yields. Different types of Lewis acids, such as AlMe$_3$ or AlCl$_3$, or its absence (entry 11 to 13) led to formation of only traces of the product or no reaction.

To evaluate the substrate sensitivity of the system, we evaluated other classes of dienophiles such as methacrylate, carboxiamide, and maleimide, all of which also engaged successfully in the envisioned network and formed products **11-13** in 48-70% yields (Figure 2D).

2.2.3 Intramolecular reactions

Bolstered by the possibility of merging the Diels-Alder reactions with reversible retro-hydrocyanation reaction, we focused on intramolecular transformations that offer the potential to quickly assemble natural product-like, bridged polycyclic compounds (Figure 3). Depending on the relative positions of the functional group and the group bearing the dienophile on the cyclopentene ring, the reaction may furnish tricyclic frameworks **A**, **B**, or **C**, with [3.3.1.13,9], [5.2.1.01,6], or [4.4.0.05,9] connectivity (isomers of octahydromethanoindene), respectively (Figure 3). Noteworthy, in a classic approach with a direct Diels-Alder reaction, the control over the different connectivities is not possible, as reported by Grubbs and collegues[13]. This limitation is imposed by rapid interconversions of the different cyclopentadiene intermediates via hydride shift processes, which lead the formation of the most stable isomer(s) of the starting diene prior the actual Diels-Alder reaction can occur.

We surmised that the challenge of preparing tricyclic frameworks **A**, **B**, or **C** via the Diels-Alder reaction can be overcome with our strategy. We envisioned each required cyclopentadiene isomer can be generated in situ under the conditions suitable for the Diels-Alder reaction, thereby it can quickly engage in the target cycloaddition step prior to the isomerization processes. To verify the feasibility of our hypothesis, we first evaluated computationally the corresponding Diels-Alder cycloadditions and the hydride shift reactions. The computed Gibbs free energy barriers suggest that reactions to form frameworks **A**, **B**, and **C** are feasible ($\Delta G^{\ddagger}_{\text{non-catalyzed}}$ 22.3 − 25.5 kcal/mol) and that

the energetic barriers can be significantly lowered by a Lewis acid catalyst ($\Delta G^{\ddagger}_{catalyzed}$ 16.1 − 18.1 kcal/mol). Moreover, the computed energy barriers for the Diels-Alder reaction catalyzed by a Lewis acid (AlMe$_2$Cl) were found to be lower than the energy barriers for the [1,5]-sigmatropic rearrangements of the diene intermediates ($\Delta G^{\ddagger}_{sigmatropic\ rearrangements}$ 26.2 − 26.9 kcal/mol). Therefore, our computational studies indicate that the Diels-Alder reactions should outcompete the hydride shift processes, as initially hypothesized.
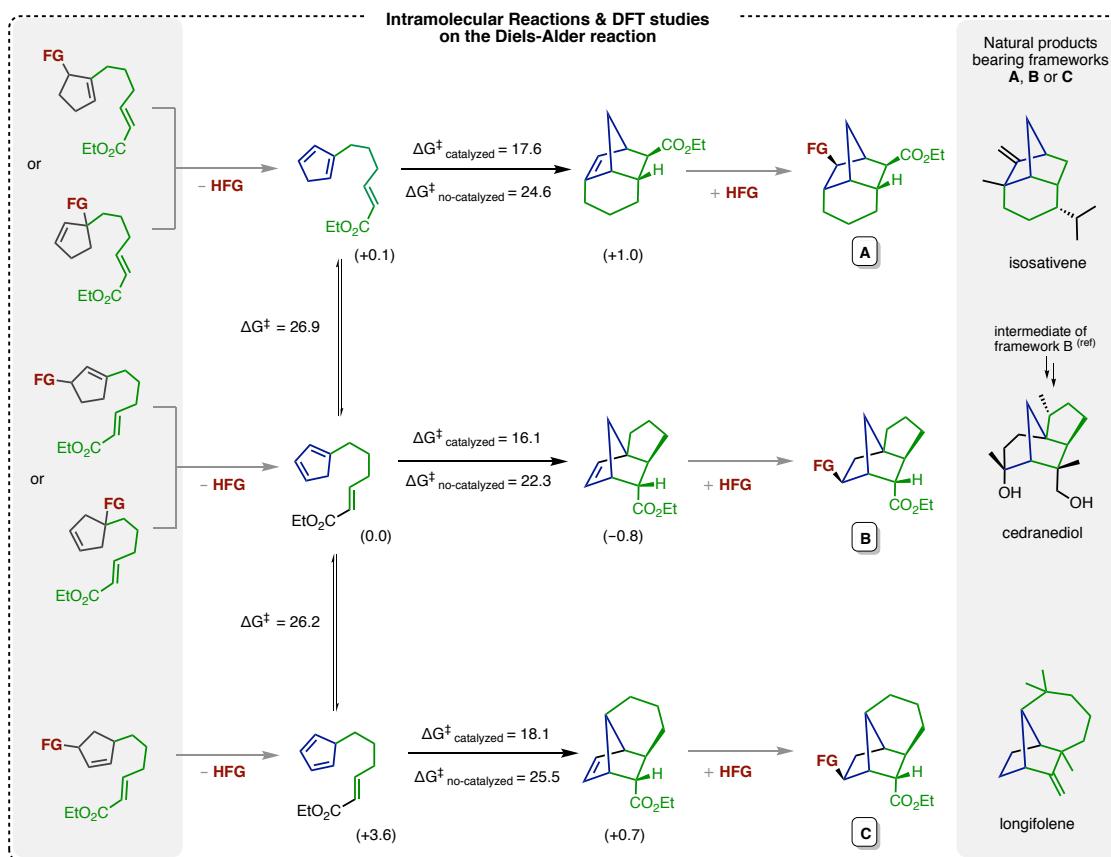
Figure 3. Envisioned network for intramolecular reactions. DFT studies on intramolecular reactions of substituted cyclopentadienes generated *in situ* upon hydro-functional group borrowing. The values shown correspond to Gibbs free energy in kcal/mol. ref = [14]. For details see computational studies section.

Catalytic experiments confirmed that products bearing frameworks **A** and **B** are formed in reactions of suitable starting materials (Figure 4). Specifically, the reaction of 2-substituted allyl nitrile derivative **15** in the presence of 5 mol% of Ni(cod)$_2$, 5 mol% of DPEPhos, and 40 mol% of AlMe$_2$Cl, after 24 h, at 50 ºC, readily furnished tricyclic nitrile **16** of framework **A** in 91% yield, as the only product of the reaction. In turn, compound **17**, a 3-substituted allyl nitrile derivative, furnished tricyclic nitrile **18** of framework **B** in 94% yield and 54:46 regioselectivity. Compound **19**, quaternary homoallyl nitrile analogue of **17**, reacted to form **18** of framework **B** in 81% yield and identical selectivity, showcasing that conveniently different starting materials can be used to generate in situ the same diene intermediates. Additionally, compound **20**, (*Z*)-isomer of **17**, also furnished **18** of framework **B** in 93% yield and 53:47 selectivity, showing stereoconvergence of the approach. (The synthesis of the starting material required to furnish product of framework **C** has not been completed prior to the submission of my PhD thesis; this work is in progress).

In addition to different frameworks, the structure of the bridged tricyclic products can be further modulated by using a modified starting material, prepared via a similar synthetic pathway. First, the size of one of new rings can be controlled by adjusting the length of the linker between the cyclopentene and dienophile moiety. For instance, 3-substituted allyl nitrile derivative **21**, bearing a longer chain length than its analogue **15**, reacted to form **22** of framework **B**, in 79% yield and 64:16:20 selectivity (*2* endo regioisomers, 1 exo regioisomer). Second, different dienophile moieties can be present in the starting material, and these can be easily introduced at the cross-metathesis step (see experimental section). For instance, compound **23**, analogue of **15** bearing a methacrylate-like dienophile motif, reacted to form **24** in 92% yield and 85:15 regioselectivity.
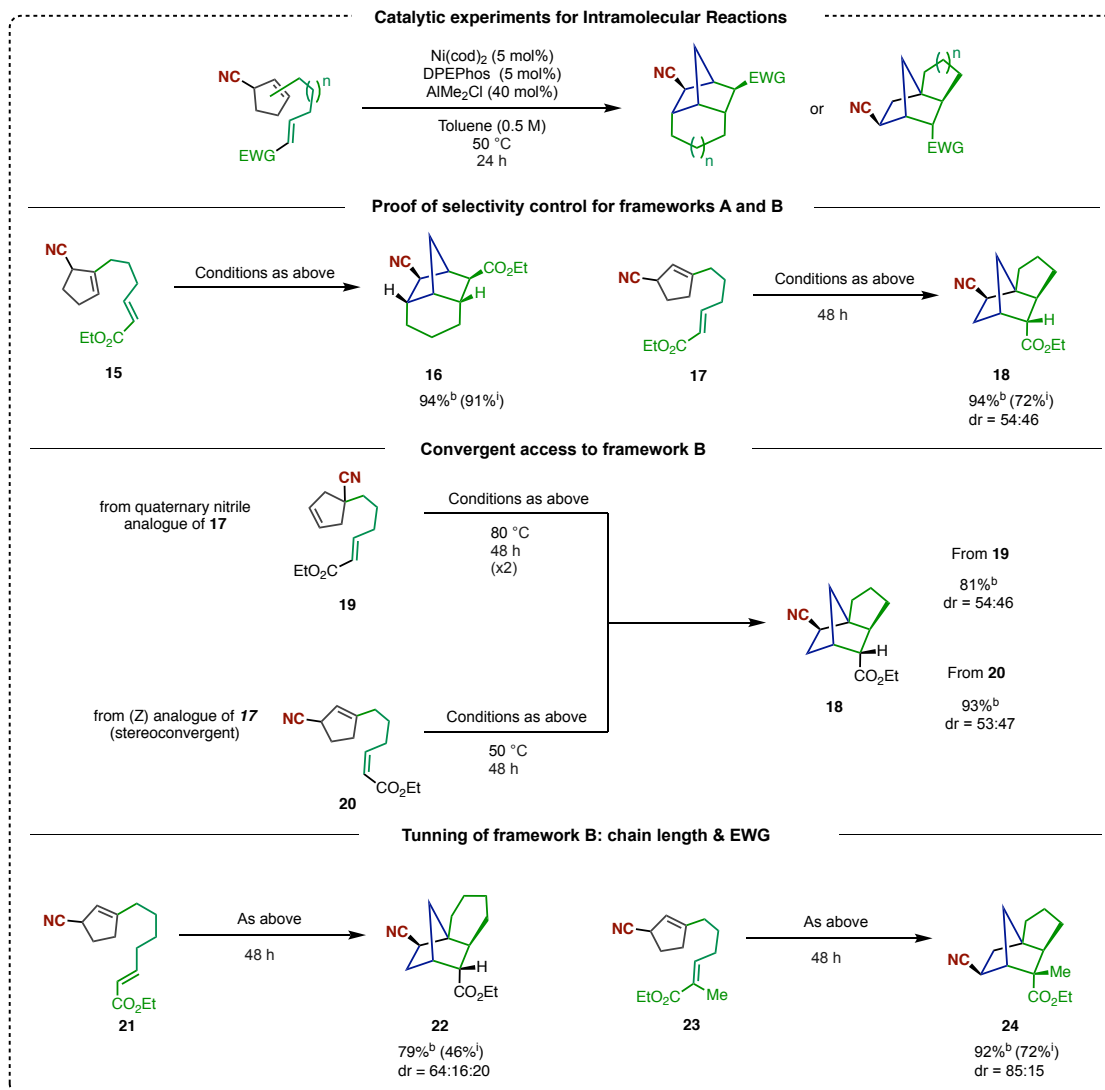
Figure 4. Synthetic potential of the intramolecular reactions. Synthesis of the targeted functionalized polycyclic frameworks A and B, selectivity control, convergent access, and tunning of framework B. [i] Isolated yield. [b] NMR yield. For details see experimental section.

2.2.4 Exploiting other hydro-functional group borrowing.

Finally, to assess the breadth of the strategy, we tested the feasibility of reversible retro-hydroformylation and retro-hydroacylation reactions as partners for the Diels-Alder reaction to build the prospective systems of cooperating reactions (Figure 5). Upon developing suitable catalytic conditions employing a similar strategy than the one used for retro-hydrocyanation systems, we found that cyclopent-2-ene aldehyde **1c**, the aldehyde analogue of nitrile **1a**, reacted with (*E*)-1,2-bis(Bpin)ethene to form bridged bicyclic aldehyde **25** in 72% yield, in the presence of 4 mol% of [Rh(cod)OMe]$_2$, 8 mol% of xantphos, and 8 mol% of 3-methyoxybenzoic acid, after 48 hours, at 90 °C (Figure 5A). Besides, aldehyde **1c** reacted with ethyl 2,3-dimethylmaleimide to form the aldehyde analogue of **13,** compound **26** in 46 % yield. Furthermore, reaction of **1c** with dimethyl maleate furnished **27** in 45 % yield.

In turn, cyclopent-2-ene-methyl ketone **1d**, the methyl ketone analogue of nitrile **1a**, reacted with diethyl fumarate to form bridged bicyclic ketone **29** in 12% yield, in the presence of 5 mol% of [Rh(ethylene)$_2$Cl$_2$], 20 mol% of tris[3,5-bis(trifluoromethyl)phenyl]phosphine, and 20 mol% of 4-methyl-2-aminopyridine, after 40 hours, at 150 °C (Figure 5B).
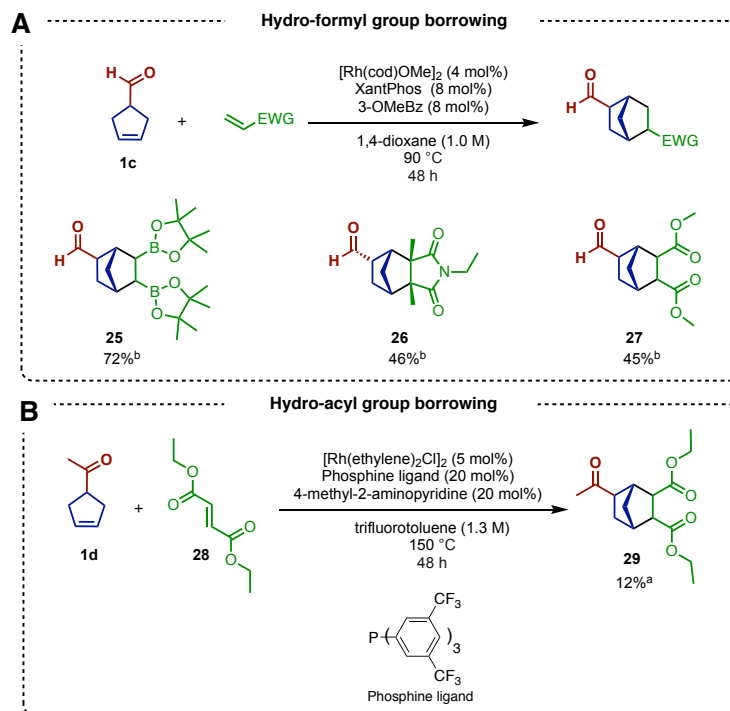
Figure 5. Development of additional cooperative systems involving hydro-functional group borrowing. (**A**) Hydro-formyl group borrowing examples. (**B**) Hydro-acyl group borrowing example. [a] Value of combined yield of isomers determined by GC analysis of the reaction mixture with an internal standard. [b] NMR yield. For details see experimental section.

2.3 Conclusions

In conclusion, our studies provide a proof-of-concept series of transformations that engage reversible catalytic hydrofunctionalization reactions to enable unprecedented one-step transformations.

The developed strategy provides facile access to a series of polycyclic compound bearing natural product-like frameworks, highlighting the synthetic potential of the approach.

Considering the remarkable success of hydrogen borrowing strategy in generating various valuable transformations, which find numerous applications in academic laboratories and chemical industry, we foresee that our studies provide a blueprint for the discovery of many other yet unknown transformations for common organic molecules by exploiting the newly generated non-inherent reactivities with numerous reversible functionalization reactions and thus greatly empowering organic synthesis.

2.4 Experimental Section

2.4.1   Experimental Methods

Unless stated otherwise, all reactions and manipulations were conducted on the laboratory bench or in a well-ventilated fume hood in air with reagent grade solvents. Reactions under inert gas atmosphere were carried out in oven-dried glassware in a nitrogen-filled glove box or by standard Schlenk techniques under nitrogen. Unless noted otherwise, all reagents and solvents were purchased from commercial suppliers and used without further purification. For experiments under inert gas atmosphere, dried and degassed solvents were purchased from commercial suppliers, stored in a nitrogen-filled glove box and used as received. Column chromatography was carried out with the aid of a CombiFlash EZ Prep Chromatography System with integrated ELSD using the RediSep Rf (Gold) Silica Gel Disposable Flash columns. TLC was carried out on Merck Kieselgel F254 plates. TLC visualization was carried out with ultraviolet light (254 nm), followed by staining with a 1% aqueous $KMnO_4$ solution. NMR spectra were acquired on the 400 MHz or 500 MHz Bruker instruments at the Institute of Science and Supramolecular Engineering (ISIS). NMR spectra were processed using the MestReNova 14.2 software. Chemical shifts are reported in parts per million (ppm) and referenced to residual solvent peaks or tetramethylsilane (TMS). Coupling constants are reported in hertz (Hz). GC-FID analysis was obtained on a Shimadzu GC-2010 Plus instrument equipped with a SH-Rxi-5MS column (25 m x 0.20 mm ID x 0.33 μm film) connected to a FID detector. GC-MS analysis was obtained on a Shimadzu QP2020 (EI) instrument equipped with a SH-Rxi-5MS column (25 m x 0.20 mm ID x 0.33 μm film). GC-FID and NMR yields were calculated using dodecane or 1,3,5-trimethoxybenzene as the internal standards. GC-FID yields were corrected for response factors for all compounds. High-resolution electrospray ionization mass spectra (HR-MS ESI) were obtained at the Analytical Facility of the Department of Chemistry, University of Strasbourg. High-resolution atmospheric pressure photoionization mass spectra (HR-MS APPI) were obtained on a Thermo Exactive Plus EMR instrument with a MasCom GC-APPI Interface (at ISIS).

2.4.2   Exploratory Studies

In Table 3 and Table 4, I present the complete list of results for the exploratory studies regarding the model reactions for the retrohydrocyanation step (reaction **I**), the Diels-Alder step (reaction **II**), and the re-hydrocyanation step (reaction **III**), upon 4 and 16 hours reaction time, respectively.

entry	mol% Lewis Acid + [Ni]	T (°C)	Yield (conversion) %			
			Reaction I		Reaction II	Reaction III
			From **1a**	From **1b**		
1	20	28	99 (99)	68 (82)	13 (19)	88 (90)
2	20	50	99 (99)	99 (99)	32 (42)	98 (99)
3	20	80	97 (99)	79 (99)	62 (83)	84 (93)
4	20	130	82 (99)	68 (99)	28 (71)	76 (92)
5	40	28	99 (99)	88 (99)	23 (29)	74 (77)
6	40	50	99 (99)	99 (99)	51 (62)	97 (99)
7	40	80	99 (99)	79 (99)	62 (86)	94 (99)
8	40	130	84 (99)	62 (99)	37 (97)	65 (99)
9	80	28	99 (99)	69 (99)	38 (51)	59 (99)
10	80	50	99 (99)	99 (99)	64 (82)	93 (99)
11	80	80	95 (99)	85 (99)	73 (95)	85 (99)
12	80	130	76 (99)	63 (99)	17 (96)	32 (99)

Table 3: Optimization of reactions I, II and III (4 hours reaction time). Values of yield and conversion determined by GC analysis. Conditions: [Ni/DPEPhos] = Ni(cod)$_2$ 5 mol%, DPEPhos 5 mol%, Lewis Acid =AlMe$_2$Cl (indicated mol%), toluene 0.5 M, 0.0625 mmol scale. Values of yield and conversion determined by GC-analysis: Reaction I, yield of **9**, conversion of **1a** or **1b**; Reaction II, yield of **4**, conversion of **3**. Reaction III, yield of **5** conversion of **4.**

entry	mol% Lewis Acid + [Ni]	T (°C)	Yield (conversion) %			
			Reaction I		Reaction II	Reaction III
			From **1a**	From **1b**		
1	20	28	99 (99)	97 (99)	26 (43)	98 (99)
2	20	50	99 (99)	94 (99)	53 (66)	92 (99)
3	20	80	95 (99)	71 (99)	68 (96)	80 (99)
4	20	130	81 (99)	53 (99)	38 (89)	65 (99)
5	40	28	99 (99)	99 (99)	55 (73)	86 (99)
6	40	50	99 (99)	99 (99)	77 (93)	93 (99)
7	40	80	89 (99)	66 (99)	72 (97)	94 (99)
8	40	130	72 (99)	39 (99)	31 (97)	52 (99)
9	80	28	99 (99)	99 (99)	63 (82)	95 (99)
10	80	50	99 (99)	87 (99)	80 (95)	83 (99)
11	80	80	89 (99)	69 (99)	69 (98)	69 (99)
12	80	130	68 (99)	25 (99)	9 (82)	17 (99)

Table 4: Optimization of reactions I, II and III (16 hours reaction time). Values of yield and conversion determined by GC analysis. Conditions: [Ni/DPEPhos] = Ni(cod)$_2$ 5 mol%, DPEPhos 5 mol%, Lewis Acid =AlMe$_2$Cl (indicated mol%), toluene 0.5 M, 0.0625 mmol scale. Values of yield and conversion determined by GC-analysis: Reaction I, yield of **9**, conversion of **1a** or **1b**; Reaction II, yield of **4**, conversion of **3**. Reaction III, yield of **5** conversion of **4.**

2.4.2.1 General procedure for the retro-hydrocyanation reactions (Reaction **I**)

In a nitrogen-filled glove box, an oven-dried 4 mL vial was charged sequentially with a solution of Ni(cod)$_2$ (1.7 mg, 6.1 μmol, 5.0 mol%) and DPEphos (3.4 mg, 6.1 μmol, 5.0 mol%) in toluene (250 μL), unsaturated nitrile substrate **1a** or **1b** (11.6 mg, 125 μmol, 1.0 equiv.), norbornene **8** (11.8 mg, 125 μmol, 1.0 equiv.) and the corresponding amount of 0.9 M solution of AlMe$_2$Cl in hexane (27.8 μL, 25 μmol, 0.20 equiv. *or* 55.6 μL, 50 μmol, 0.40 equiv. *or* 111 uL, 100 μmol, 0.80 equiv.). The vial was closed tightly with a screw-cap was placed in a pre-heated heating plate and allowed to stir at the corresponding temperature (28 °C, 50 °C, 80 °C, 130 °C) for 4 hours or 16 hours. Upon completion of the corresponding reaction time, the mixture was cooled to room temperature and dodecane was added as an internal standard. The reaction mixture was diluted with 2 mL of acetonitrile and filtrated through a plug of silica using ethyl acetate as an eluent. The yield was determined by GC analysis based on calibration of the product **9**. The results are listed in table 3 and table 4.

2.4.2.2 General procedure for the Diels-Alder reactions (Reaction **II**)

In a nitrogen-filled glove box, an oven-dried 4 mL vial was charged sequentially with a solution of Ni(cod)$_2$ (1.7 mg, 6.1 μmol, 5.0 mol%) and DPEphos (3.4 mg, 6.1 μmol, 5.0 mol%) in toluene (250 μL), freshly cracked cyclopentadiene **2** (8.3 mg, 10.3 μL, 125 μmol, 1.0 equiv.), *n*-butyl crotonate **3** (17.8 mg, 19.8 μL, 125 μmol, 1.0 equiv.) and the corresponding amount of 0.9 M solution of AlMe$_2$Cl in hexane (27.8 uL, 25 μmol, 0.20 equiv. *or* 55.6 uL, 0.050 mmol, 0.40 equiv. *or* 111 uL, 0.100 mmol, 0.80 equiv.). The vial was closed tightly with a screw-cap was placed in a pre-heated heating plate and allowed to stir at the corresponding temperature (28 °C, 50 °C, 80 °C, 130 °C) for 4 hours or 16 hours. Upon completion of the corresponding reaction time, the mixture was cooled to room temperature and dodecane was added as an internal standard. The reaction mixture was diluted with 2 mL of acetonitrile and filtrated through a plug of silica using ethyl acetate as an eluent. The yield was determined by GC analysis based on calibration of a mixture of diastereoisomers of product **4**.

2.4.2.3 General procedure for the hydrocyanation of the Diels-Alder adduct (Reaction **III**)

In a nitrogen-filled glove box, an oven-dried 4 mL vial was charged sequentially with a solution of Ni(cod)$_2$ (1.7 mg, 6.1 μmol, 5.0 mol%) and DPEphos (3.4 mg, 6.1 μmol, 5.0 mol%) in toluene (250 μL), isovaleronitrile **10** (10.4 mg, 13.1 μL, 125 μmol, 1.0 equiv.), Diels-Alder adduct **4** (26.0 mg, 125 μmol, 1.0 equiv.) and the corresponding amount of 0.9 M solution of AlMe$_2$Cl in hexane (27.8 uL, 25 μmol, 0.20 equiv. *or* 55.6 μL, 50 μmol, 0.40 equiv. *or* 111 uL, 0.100 mmol, 0.80 equiv.). The vial was closed tightly with a screw-cap was placed in a pre-heated heating plate and allowed to stir at the corresponding temperature (28 °C, 50 °C, 80 °C, 130 °C) for 4 hours or 16 hours. Upon completion of the corresponding reaction time, the mixture was cooled to room temperature and dodecane was added as an internal standard. The reaction mixture was diluted with 2 mL of acetonitrile and filtrated through a plug of silica using ethyl acetate as an eluent. The yield was determined by GC analysis based on calibration of a mixture of diastereoisomers the product **5**.

2.4.3 Preparation and characterization of starting materials

### 2.4.3.1 General procedure for the metathesis reactions
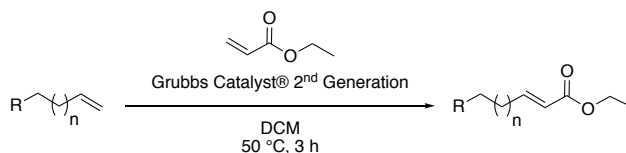
Inside a nitrogen filled glovebox, a screw-cap vial equipped with a stirring bar was charged sequentially with substrate (4.00 mmol, 1.00 equiv.), Grubbs Catalyst® 2nd Generation (170 mg, 0.20 mmol, 5.0 mol%), anhydrous DCM (8.00 mL), and coupling partner ethyl acrylate (872 μL, 800 mg, 8.00 mmol, 2.00 equiv.). The vial was placed in a pre-heated heating plate and allowed to stir at 50 °C for 3 hours. After completion of the reaction, the vial was removed from the glovebox, Celite® was added, the reaction mixture was concentrated *in vacuo,* and subjected to flash column chromatography (silica, 0 - 20% methyl t-butyl ether in petroleum ether). Fractions containing the product (judged by GC-MS analysis) were combined and the solvent was evaporated, yielding the corresponding product.

2.4.3.2 General procedure for halogen exchange reactions
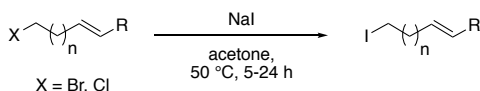
A screw-cap vial was charged sequentially with chloride or bromide substrate (1.00 equiv.), NaI (3.00 equiv.), dry acetone (until a concentration of 0.5 M was reached) and a magnetic stirring bar. The vial was closed tightly and heated to 50 °C for the indicated time. The reaction mixture was concentrated *in vacuo* until the volume was reduced to 1/3. Then water was added (equal volume than acetone), the organic material was extracted with Et$_2$O (3 x 3-times the volume of acetone), and passed through a pad of basic alumina, with abundant Et$_2$O. The organic phase was dried over anhydrous MgSO$_4$, filtered, concentrated *in vacuo* over Celite® yielding the product, which was used without further purification.

2.4.3.3 General procedure for Negishi cross-coupling reactions
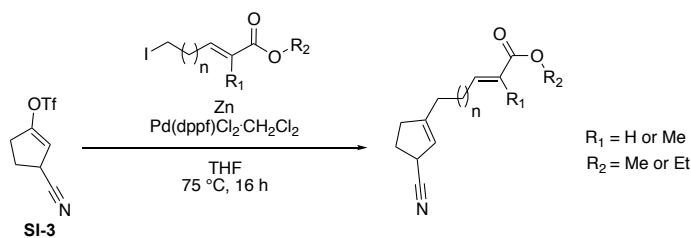
Preparation of the ZnI-reagent
Zn powder (95.4 mg, 1.50 mmol, 3.00 equiv.) was placed in a 4 mL vial and dried under vacuum at 150 °C for 20 min. Anhydrous THF (0.66 mL), ethylene dibromide (7.5 mg, 3.4 μL, 40 μmol), and TMSCl (2.2 mg, 2.6 μL, 20 μmol) were sequentially added under a nitrogen atmosphere. The mixture was allowed to stir at 65 °C for 20 min. The corresponding iodide (0.80 mmol, 1.60 equiv.) was added neat at RT to the Zn suspension. The mixture was allowed to stir at 65 °C for 2 hours. After cooling to rt, the upper solution is carefully removed from residual Zn dust using a syringe and used directly in the next step without further purification.

Negishi coupling
To a solution of 3-cyanocyclopent-1-en-1-yl trifluoromethanesulfonate **SI-3** (0.50 mmol, 121 mg, 1.00 equiv.) and Pd(dppf)Cl$_2$·DCM (8.2 mg, 10 μmol, 0.2 equiv.) in THF (3.0 mL) was added the freshly prepared solution of the zinc reagent. The reaction vial was sealed and allowed to stir at 75 °C for 16 h. Afterwards, the reaction was cooled to room temperature and filtered over a Celite® pad with copious washing with diethyl ether. Celite® was added to the filtrate, all volatiles were removed in vacuo, and the residue was subjected to flash column chromatography (silica). Fractions containing the product (judged by GC-MS analysis) were combined and the solvent was evaporated, yielding the corresponding product.

2.4.3.4 Synthesis of starting materials

cyclopent-3-ene-1-carbonitrile 1a

The compound was prepared according to a literature procedure.[15] To a solution of cyclopent-3-en-1-ol (10.0 g, 9.10 mL, 119 mmol, 1.00 equiv.) in pyridine (125 mL), tosyl chloride (28.0 g, 146 mmol, 1.22 equiv.) was added in one portion at 0 °C. The resulting mixture was allowed to stir for 5 hours at this temperature and placed in a refrigerator at -18 ºC overnight. The mixture was then slowly poured into a stirring mixture of 12 M hydrochloric acid (200 mL) and 300 g of crushed ice. Filtration of the mixture gave cyclopent-3-en-1-yl 4-methylbenzenesulfonate as a white solid (27.3 g, 115 mmol, 95%) which was used in the next step without further purification. To a solution of NaCN (11.2 g, 0.228 mmol, 2.0 equiv.) in 250 mL of DMSO at 100 ºC was added cyclopent-3-en-1-yl 4-methylbenzenesulfonate (27.3, 0.114 mol, 1.0 equiv.) and the reaction mixture was allowed to stir at 100 ºC for 5 hours. After completion of the reaction, the reaction mixture was cooled down to room temperature and quenched by addition of water. The aqueous phase was extracted with diethyl ether (3 x 300 mL), the combined organic layers were washed with brine and dried over MgSO₄. The solution was concentrated *in vacuo* and the residue was subjected to column chromatography (silica, 0 - 30% ethyl acetate in petroleum ether) yielding the title product **(**3.50 g, 37.6 mmol, 33%) as a yellowish oil. The pure compound was dried over molecular sieves (3Å) for 24 hours at room temperature before being used in the catalytic experiments. The NMR data match previously reported data for the title product.[15]

¹H NMR (500 MHz, CDCl₃) δ 5.73 (s, 2H), 3.09 (quint, J = 8.4, 7.9 Hz, 1H), 2.85 – 2.76 (m, 2H), 2.71 (dd, J = 15.0, 6.5 Hz, 2H).

cyclopent-2-ene-1-carbonitrile 1b

The compound was prepared according to a literature procedure.[16–18] A mixture of cyclopentene (6.80 g, 100 mmol, 1.00 equiv.), NBS (17.0 g, 92.0 mmol, 0.92 equiv.) and benzoyl peroxide (243 mg, 0.863 mmol, 0.01 equiv.) in CCl₄ (50 mL) was allowed to stir at 40 ºC for 5 hours. The reaction mixture was cooled down to 0 ºC and then filtered through a pad of Celite® (eluent hexane). The filtrate was washed with 5% aq. NaHCO₃ (50 mL) and concentrated *in vacuo* (100 mbar, 20 ºC) yielding 3-bromocyclopent-1-ene (7.51 g, 51.4 mmol, 56%) as a yellowish liquid which was used in next step without further purification. A suspension of NaCN (2.94 g, 60.0 mmol, 1.20 equiv.) in 50 mL of DMSO was allowed to stir at 100 ºC until a clear solution was formed, which was cooled down to room temperature and added in one portion to 3-bromocyclopent-1-ene (7.30 g, 50.0 mmol, 1.00 equiv.) at 0 °C while stirring. The reaction mixture was allowed to stir vigorously for 10 min at 0 °C and quenched by addition of water. The aqueous phase was extracted with diethyl ether (3 x 100 mL), the combined organic layers were washed with brine and dried over MgSO₄. The solution was concentrated *in vacuo*, and the crude product was subjected to flash column chromatography (silica, 0 - 10% diethyl ether in pentane), yielding cyclopent-2-ene-1-carbonitrile **1b** (1.02 g, 11.0 mmol, 22%) as a yellowish oil. The pure compound was dried over molecular sieves 3 Å for 24 hours at room temperature before being used in the catalytic experiments. The NMR data match previously reported data for the title product.[18]

¹H NMR (500 MHz, CDCl₃) δ 6.04 – 5.99 (m, 1H), 5.69 – 5.64 (m, 1H), 3.60 – 3.52 (m, 1H), 2.62 – 2.52 (m, 1H), 2.47 – 2.38 (m, 1H), 2.38 – 2.28 (m, 1H), 2.24 – 2.12 (m, 1H).

4-formylcyclopent-1-ene 1c

The compound was prepared according to a literature procedure.[19,20] To a stirred suspension of LiAlH₄ (5.10 g, 134 mmol, 1.50 equiv.) in dry diethyl ether (120 mL) was added dropwise a solution of 3-cyclopentene-1-carboxylic acid (10.0 g, 9.3 mL, 89.0 mmol, 1.00 equiv.) in dry diethyl ether (30 mL) at 0 °C under a nitrogen atmosphere. The resulting mixture was allowed to warm up to room temperature and allowed to stir for 16 hours. Upon careful quenching with water and 5% NaOH_aq, the suspension was filtered through Celite®. The organic layer was separated, dried over anhydrous Na₂SO₄ and the volatiles were removed under reduced pressure to furnish 4-(Hydroxymethyl)cyclopent-1-ene as a colorless liquid (8.75 g, 89.0 mmol, 100%). To a stirred suspension of Dess-Martin-Periodinane (38.0 g, 89.1 mmol, 1.15 equiv.) in DCM (220 mL) was added a solution of 4-(hydroxymethyl)cyclopent-1-ene (7.60 g, 77.4 mmol, 1.00 equiv.) in DCM (40 mL). The mixture was allowed to stir at room temperature for 2 h, quenched by addition of 5% NaOH_aq and filtered through celite (washed with diethyl ether). The organic layer was separated and washed with 5% NaOH_aq (100 mL) and brine (2 x 100 mL), dried over anhydrous Na₂SO₄, and the volatiles were removed under reduced pressure (CAUTION: Remove solvent carefully since product forms azeotropic mixtures with common solvents. Temperature of heating bath: 40 °C, pressure: up to 500 mbar for max. 5 min to prevent significant evaporation of product). The residue was purified by Kugelrohr distillation (115 °C, 28 mbar), obtaining the title product as a colorless liquid (3.64 g, 37.9 mmol, 49%), which was stored at -30 °C under nitrogen. The NMR data match previously reported data for the title product.[19,20]

¹H NMR (500 MHz, CDCl₃) δ = 9.65 (d, J = 2.1 Hz, 1H), 5.68 (s, 2H), 3.08 (ttd, J = 9.5, 4.8, 2.1 Hz, 1H), 2.80 – 2.48 (m, 4H)

1-(cyclopenten-3-en-1-yl)ethanone 1d

The compound was prepared according to a literature procedure.[21,22] To a cooled solution of 3-cyclopentenecarboxylic acid (9.26 mL, 10.0 g, 89.2 mmol, 1.00 equiv.) in dichloromethane (270 mL) at 0 °C under a nitrogen atmosphere was added dropwise oxalyl chloride (11.5 mL, 17.0 g, 133 mmol, 1.50 equiv.) followed by 10 drops of DMF. The mixture was slowly warmed to room temperature and stirred for 2 hours. The reaction mixture was then concentrated under reduced pressure to give crude acyl chloride intermediate. To a solution of N-methoxy-N-methylamine hydrochloride (13.1 g, 133 mmol, 1.50 equiv.) in dichloromethane (330 mL) was added Et3N (37.3 mL, 27.1 g, 267 mmol, 3.00 equiv.) and the mixture was stirred at room temperature for 1 hours. A solution of the above prepared acyl chloride in DCM (30 mL) was added. The reaction mixture was stirred at room temperature for 6 hours. The mixture was washed with HCl (1 M, 2 x 100 mL), saturated NaHCO3 solution (2 x 100 mL) and brine (2 x 100 mL), dried over MgSO4, concentrated in vacuo, and the crude product was subjected to flash column chromatography (silica, 0 – 20% ethyl acetate in petroleum ether), yielding N-methoxy-N-methylcyclopent-3-ene-1-carboxamide (12.0 g, 77.0 mmol, 86%) as a yellowish oil. To a solution of above prepared amide intermediate (4.87 g, 31.4 mmol, 1.00 equiv.) in dry diethyl ether (105 mL) was added a solution of MeMgBr (10.5 mL, 3.74 g, 31.4 mmol, 1.00 equiv.) at 0 °C under a nitrogen atmosphere. The reaction mixture was then allowed to reach room temperature. After 6 hours, the reaction mixture was quenched by the addition of saturated NH4Cl solution (100 mL) and washed with diethyl ether (3 x 20 mL). The organic phase was washed with brine, dried over MgSO4, filtered, concentrated in vacuo over Celite®, and the residue was subjected to flash column chromatography (silica, 5% diethyl ether in pentane), yielding the title product (2,31 g, 20. 9 mmol, 67%) as a yellowish oil. The NMR data match previously reported data for the title product.[21]

¹H NMR (500 MHz, CDCl3) δ 5.64 (s, 2H), 3.24 (q, 1H, J = 8.0 Hz), 2.59 (d, 4H, J = 8.0 Hz), 2.18 (s, 3H).

Preparation of butyl 3-methylbicyclo[2.2.1]hept-5-ene-2-carboxylate 4a-b

endo:exo = 87:13
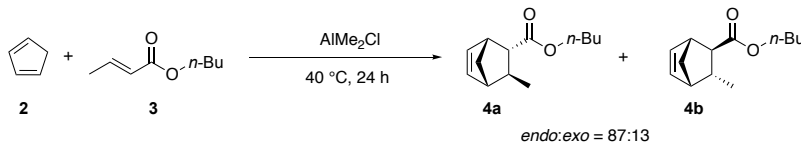
Under a nitrogen atmosphere, an oven-dried 25 mL scintillation vial was charged sequentially with *n*-butyl crotonate (1.42 g, 1.58 mL, 10.0 mmol, 1.00 equiv.), freshly cracked cyclopentadiene (0.990 g, 1.24 mL, 15.0 mmol, 1.50 equiv.) and AlMe₂Cl (0.9 M in heptane, 2.22 mL, 2.00 mmol, 0.20 equiv.). The vial was sealed with a Teflon-lined screw cap, placed in a pre-heated aluminum block and stirred at 40 °C for 24 hours. After cooling down to room temperature, the reaction was quenched by the addition of 2 mL methanol, filtered through a pad of celite, *concentrated in vacuo* and purified via flash column chromatography (silica, 0-5% ethyl acetate in petroleum ether) to give the title compounds (1.89 g, 9.1 mmol, 91%, endo:exo 87:13) as a colorless oil.

¹H NMR of the mixture of endo- (en) and exo-diastereoisomer (ex):

¹H NMR (500 MHz, CDCl₃) δ = 6.26 (dd, J = 5.7, 3.1 Hz, 1H, en), 6.21 (dd, J = 5.7, 3.1 Hz, 1H, ex), 6.10 (dd, J = 5.7, 2.9 Hz, 1H, ex), 5.98 (dd, J = 5.6, 2.9 Hz, 1H, en), 4.13 – 3.96 (m, 4H, en+ex), 3.13 – 3.08 (m, 1H, en), 2.98 – 2.90 (m, 1H,ex), 2.70 (dq, J = 3.5, 1.7 Hz, 1H, ex), 2.48 – 2.43 (m, 1H, en), 2.39 – 2.32 (m, 2H, en+ex), 1.89 – 1.76 (m, 2H, en+ex), 1.69 – 1.51 (m, 6H, en+ex), 1.46 – 1.32 (m, 6H, en+ex), 1.17 (d, J = 7.0 Hz, 6H, en+ex), 0.97 – 0.87 (m, 6H, en+ex).

¹³C-NMR of the mixture of endo- (en) and exo-diastereoisomer (ex):

¹³C{¹H} NMR (126 MHz, CDCl₃) δ = 176.5 (ex), 175.0 (en), 138.8 (en), 136.8 (ex), 135.4 (ex), 133.4 (en), 64.3 (ex), 64.1 (en), 52.7 (en), 51.5 (ex), 48.9 (en), 48.3 (ex), 47.4 (ex), 47.3 (ex), 46.1 (en), 46.1 (en), 39.3 (ex), 37.9 (en), 30.9 (ex), 30.9 (en), 21.1 (en + ex), 19.3 (ex), 19.3 (en), 13.9 (ex), 13.9 (en).

HRMS (ESI) m/z calcd for C₁₃H₂₁O₂ ([M+H]⁺): 209.1536, found 209.1536.

N-ethyl-2,3-dimethylmaleimide SI-0
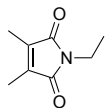
The compound was prepared according to a literature procedure.[23] To a solution of dimethyl maleic anhydride (3.00 g, 23.8 mmol, 1.0 equiv.) in toluene (100 mL) was added ethylamine (2 M in THF, 11.9 mL, 23.8 mmol, 1.00 equiv.). The reaction mixture was heated to reflux for 16 hours. After cooling down to room temperature, the volatiles were removed under reduced pressure. The resulting residue was subjected to column chromatography (silica, 0 - 10% ethyl acetate in petroleum ether) yielding the title compound as colorless liquid (3.20 g, 20.9 mmol, 88%). The NMR data match previously reported data for the title product.[23]

¹H NMR (400 MHz, CDCl₃) δ = 3.53 (q, J = 7.2 Hz, 2H), 1.95 (s, 6H), 1.16 (t, J = 7.2 Hz, 3H).

Preparation of ethyl (*E*)-6-(1-cyanocyclopent-3-en-1-yl)hex-2-enoate 19
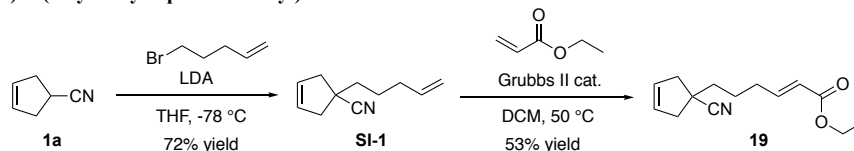
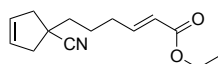**1-(pent-4-en-1-yl)cyclopent-3-ene-1-carbonitrile SI-1**
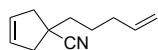
A solution of cyclopent-3-ene-1-carbonitrile (372 mg, 4.00 mmol, 1.00 equiv.) in THF (8.00 mL) was added to a solution of LDA at -78 °C prepared from diisopropylamine (672.7 μL, 4.80 mmol, 1.20 equiv.), 1.6 M solution of butyllithium in hexanes (2.75 mL, 4.40 mmol, 1.10 equiv.) and THF (13 mL). After 50 min at -78 °C, a solution of 5-bromopent-1-ene (569 μL, 715 mg, 4.80 mmol, 1.20 equiv.) in THF (4 mL) was added. The reaction mixture was allowed to stir for 1 hour at -78 °C and allowed to warm up to room temperature and stirred overnight. Then, 40 mL of saturated aqueous NH₄Cl solution were added and the aqueous phase was washed with diethyl ether (3 x 50 mL). The organic phase was washed with water (1 x 25 mL) and brine (1 x 25 mL), and then dried over anhydrous MgSO₄. The solution was concentrated *in vacuo* and the residue was subjected to column chromatography (silica, 0-10% ethyl acetate in petroleum ether) yielding the title product (465 mg, 2.89 mmol, 72%).

¹H NMR (500 MHz, CDCl₃) δ 5.79 (ddt, J = 16.9, 10.2, 6.7 Hz, 1H), 5.67 (s, 2H), 5.07 – 5.01 (m, 1H), 5.01 – 4.95 (m, 1H), 2.94 – 2.85 (m, 2H), 2.52 – 2.43 (m, 2H), 2.15 – 2.06 (m, 2H), 1.70 – 1.59 (m, 4H).

¹³C{¹H} NMR (126 MHz, CDCl₃) δ 138.0, 128.3, 125.8, 115.4, 44.7, 40.8, 38.4, 33.6, 25.3.

HRMS (ESI) m/z calcd for C₁₁H₁₆N ([M+H]⁺): 162.1277, found 162.1288.

Ethyl (*E*)-6-(1-cyanocyclopent-3-en-1-yl)hex-2-enoate 19

Prepared according to the general procedure for metathesis reactions **2.4.3.1** starting from 1-(pent-4-en-1-yl)cyclopent-3-ene-1-carbonitrile **SI-1** (242 mg, 1.50 mmol, 1.00 equiv.) and ethyl acrylate (327 μL, 300 mg, 3.00 mmol, 2.00 equiv.). The crude product was subjected to flash column chromatography (silica, 0 - 20% methyl t-butyl ether in petroleum ether), yielding the title product (184 mg, 0.79 mmol, 53%) as a colorless oil.

¹H NMR (500 MHz, CDCl₃) δ 6.93 (dt, J = 15.6, 6.9 Hz, 1H), 5.84 (dt, J = 15.7, 1.6 Hz, 1H), 5.72 – 5.61 (m, 2H), 4.19 (q, J = 7.1 Hz, 2H), 2.96 – 2.85 (m, 2H), 2.51 – 2.43 (m, 2H), 2.30 – 2.22 (m, 2H), 1.76 – 1.63 (m, 4H), 1.33 – 1.24 (m, 3H).

¹³C{¹H} NMR (126 MHz, CDCl₃) δ 166.6, 147.8, 128.3, 125.5, 122.3, 60.4, 44.6, 40.7, 38.4, 32.0, 24.5, 14.4.

HRMS-pAPCI (m/z): [M+H]⁺ calcd for C₁₄H₂₀NO₂ 234.1494, found 234.1445.

Preparation of 3-cyanocyclopent-1-en-1-yl trifluoromethanesulfonate SI-3
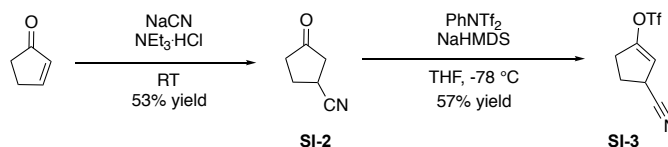
3-Oxocyclopentane-1-carbonitrile SI-2

The compound was prepared according to a literature procedure.[24] NaCN (5.64 g, 115 mmol, 1.15 equiv.) and trimethylaminehydrochloride (11.2 g, 81.6 mmol, 0.82 equiv.) were dissolved in a mixture of methanol (200 mL) and water (240 mL). A solution of cyclopenten-2-one (8.20 g, 8.37 mL, 100 mmol, 1.00 equiv.) in methanol (16 mL) was added dropwise over 30 min at rt. The reaction mixture was allowed to stir at rt for 24 hours and concentrated *in vacuo*. 4 M hydrochloric acid was added until a neutral pH was reached and the aqueous phase was washed with CHCl$_3$ immediately (6 x 250 mL). The organic phase was dried over MgSO$_4$, filtered, concentrated *in vacuo* and the residue was subjected to flash column chromatography (silica, 0 - 40% ethyl acetate in petroleum ether) yielding the title product (5.78 g, 52.8 mmol, 53%). The NMR data match previously reported data for the title product.[25]

^{1}H NMR (500 MHz, CDCl$_3$) δ 3.24 – 3.14 (m, 1H), 2.70 – 2.57 (m, 1H), 2.57 – 2.38 (m, 3H), 2.35 – 2.20 (m, 2H).

3-cyanocyclopent-1-en-1-yl trifluoromethanesulfonate SI-3

The compound was prepared according to a modified literature procedure.[26] To a solution of 3-oxocyclopentane-1-carbonitrile (328 mg, 3.00 mmol, 1.00 equiv.) in anhydrous THF (14 mL) was added a freshly prepared NaHMDS solution (0.9 M in THF, 3.60 mmol, 4.00 mL, 1.20 equiv,) at -78 °C. The reaction mixture was allowed to stir for 1 hour at this temperature, before a solution of PhNTf$_2$ (1.50 g, 4.20 mmol, 1.40 equiv.) in anhydrous THF (10 mL) was added to the reaction mixture at -78 °C in a dropwise manner. The resulting solution was allowed to warm to rt over a period of 4 hours, after which it was allowed to stir for additional 12 hours. After the completion of the reaction (TLC), the resulting solution was treated with saturated aqueous NH$_4$Cl solution (10 mL) and the aqueous phase was washed with diethyl ether (3 × 10 mL). The organic phase was washed with saturated aqueous Na$_2$CO$_3$ solution (10 mL), dried over anhydrous MgSO$_4$, filtered, concentrated *in vacuo* over Celite®, and the residue was subjected to flash column chromatography (silica, 0 - 20% methyl t-butyl ether in petroleum ether) yielding the title product (412 mg, 1.71 mmol, 57%) as a colorless oil.

^{1}H NMR (500 MHz, CDCl$_3$) δ 5.67 (d, *J* = 2.1 Hz, 1H), 3.79 – 3.64 (m, 1H), 2.86 – 2.75 (m, 1H), 2.74 – 2.63 (m, 1H), 2.58 – 2.47 (m, 1H), 2.42 – 2.32 (m, 1H).
^{13}C{^{1}H} NMR (126 MHz, CDCl$_3$) δ 153.1, 119.9 (q, *J*$_{19F-13C}$ 321 Hz), 119.7, 112.5, 30.9, 30.5, 26.5.
^{19}F{^{1}H} NMR (471 MHz, CDCl$_3$) δ -73.3.
HRMS (ESI) m/z calcd for C$_7$H$_5$O$_2$NF$_3$S ([M–H$_2$O]$^-$): 239.9999, found 239.9992.

5-iodopent-1-ene SI-4

The compound was prepared according to the general procedure for halogen exchange reactions **2.4.3.2**, starting from 5-bromo-1-pentene (10.0 g, 77.5 mmol, 1.00 equiv.) and NaI (30.4 g, 202.5 mmol, 3.00 equiv.), yielding the title product (12.5 g, 63.6 mmol, 82%) as a colorless oil. The NMR data match previously reported data for the title product. [27]

^{1}H NMR (500 MHz, CDCl$_3$) δ 5.75 (ddt, *J* = 17.0, 10.2, 6.7 Hz, 1H), 5.08 (dd, *J* = 17.2, 1.7 Hz, 1H), 5.02 (dd, *J* = 10.2, 1.4 Hz, 1H), 3.19 (t, *J* = 6.9 Hz, 2H), 2.21 – 2.11 (m, 2H), 1.96 – 1.87 (m, 2H).

6-iodohex-1-ene SI-5

The compound was prepared according to the general procedure for halogen exchange reactions **2.4.3.2**, starting from 6-bromo-1-hexene (10.0 g, 61.7 mmol, 1.00 equiv.) and NaI (27.7 g, 185.1 mmol, 3.00 equiv.), yielding the title product (10.4 g, 49.5 mmol, 80%) as a colorless oil. The NMR data match previously reported data for the title product. [27]

^{1}H NMR (500 MHz, CDCl$_3$) δ 5.79 (ddt, *J* = 16.9, 10.2, 6.7 Hz, 1H), 5.02 (dd, *J* = 17.2, 1.8 Hz, 1H), 4.99 – 4.93 (m, 1H), 3.19 (t, *J* = 7.0 Hz, 2H), 2.13 – 2.02 (m, 2H), 1.88 – 1.79 (m, 2H), 1.54 – 1.46 (m, 2H).

ethyl (*E*)-6-iodohex-2-enoate SI-6

The compound was prepared according to the general procedure for metathesis reactions **2.4.3.1**, starting from 5-Iodopent-1-ene (784 mg, 4.00 mmol, 1.00 equiv.) and ethyl acrylate (871 μL, 800 mg, 8.00 mmol, 2.00 equiv). The crude product was subjected to flash column chromatography (silica, 0 - 20% methyl t-butyl ether in petroleum ether), yielding the title product (739 mg, 2.76 mmol, 69%) as a colorless oil. The NMR data match previously reported data for the title product.[28]

^{1}H NMR (500 MHz, CDCl$_3$) δ 6.89 (dt, *J* = 15.7, 7.0 Hz, 1H), 5.88 (dt, *J* = 15.6, 1.6 Hz, 1H), 4.19 (q, *J* = 7.1 Hz, 2H), 3.19 (t, *J* = 6.8 Hz, 2H), 2.36 – 2.28 (m, 2H), 2.03 – 1.93 (m, 2H), 1.29 (t, *J* = 7.1 Hz, 3H).

ethyl (*E*)-7-iodohept-2-enoate SI-7

The compound was prepared according to the general procedure for metathesis reactions **2.4.3.1**, starting from 5-Iodopent-1-ene (840 mg, 4.00 mmol, 1.00 equiv.) and ethyl acrylate (871 μL, 800 mg, 8.00 mmol, 2.00 equiv.). The crude product was subjected to flash column chromatography (silica, 0 - 20% methyl t-butyl ether in petroleum ether), yielding the title product (828 mg, 2.94 mmol, 73%) as a colorless oil. The NMR data match previously reported data for the title product.[28]
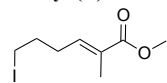
^{1}H NMR (500 MHz, CDCl$_3$) δ 6.94 (dt, *J* = 15.6, 6.9 Hz, 1H), 5.83 (dt, *J* = 15.6, 1.6 Hz, 1H), 4.19 (q, *J* = 7.2 Hz, 2H), 3.19 (t, *J* = 6.9 Hz, 2H), 2.26 – 2.19 (m, 2H), 1.88 – 1.81 (m, 2H), 1.63 – 1.53 (m, 2H), 1.29 (t, *J* = 7.1 Hz, 3H).

methyl (*E*)-6-iodo-2-methylhex-2-enoate SI-8

The compound was prepared according to the general procedure for metathesis reactions **2.4.3.1**, with the following modifications: methyl methacrylate was used as a coupling partner (5.52 mL, 5.16 g, 60.0 mmol, 20.0 equiv.), 5-iodo-1-pentene (587 mg, 3.00 mmol, 1.00 equiv.), toluene (6.00 mL), Grubbs Catalyst® 2nd Generation (382 mg, 0.45 mmol, 15 mol%), and 90 °C for 24 hours. The crude product was subjected to flash column chromatography (silica, 0 - 20% methyl t-butyl ether in petroleum ether), yielding the title product (837 mg, 3.12 mmol, 52%) as a yellowish oil. The NMR data match previously reported data for the title product.[29]

^{1}H NMR (500 MHz, CDCl$_3$) δ 6.73 – 6.67 (m, 1H), 3.74 (s, 3H), 3.20 (t, *J* = 6.8 Hz, 2H), 2.34 – 2.25 (m, 2H), 2.01 – 1.94 (m, 2H), 1.87 (s, 3H).

**Preparation of ethyl (*Z*)-6-iodohex-2-enoate SI-11**
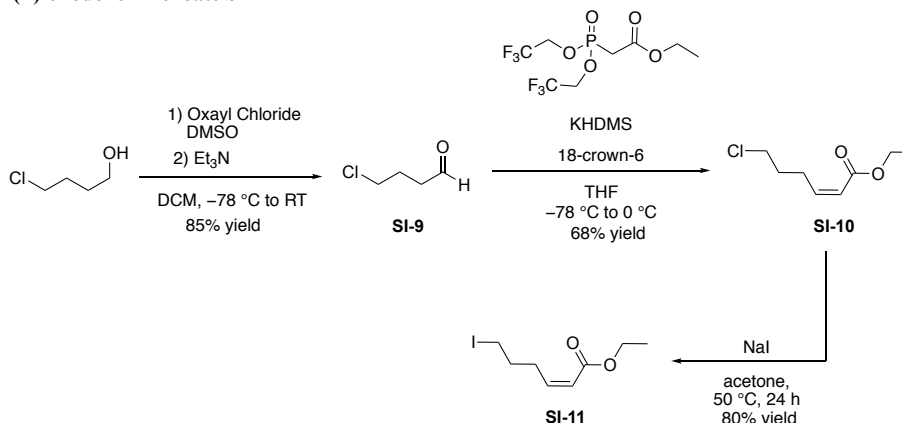
4-chlorobutanal SI-9
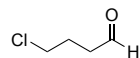
The compound was prepared according to a literature procedure.[30] To a solution of freshly distilled oxalyl chloride (2.10 mL, 24.0 mmol, 1.20 equiv.) in DCM (60 mL) at −78 °C was added a solution of DMSO (3.40 mL, 48.0 mmol, 2.40 equiv.) in DCM (10 mL). After 10 min, a solution of 4-chlorobutan-1-ol (2.07 mL, 2.16 g, 20.0 mmol, 1.00 equiv.) in DCM (10 mL) was added dropwise. After 30 min, triethylamine (13.9 mL, 100 mmol, 5.00 equiv.) was added. The mixture was allowed to warm to room temperature and then DCM (20 mL) and water (20 mL) were added. The aqueous phase was washed with DCM (3 × 50 mL). The organic phase was dried over anhydrous MgSO$_4$, filtered, concentrated *in vacuo*, and the residue was subjected to flash column chromatography (silica, 100% DCM) yielding the title product (1.80 g, 17.0 mmol, 85%) as a colorless oil. The NMR data match previously reported data for the title product.[30]

^{1}H NMR (500 MHz, CDCl$_3$) δ 9.82 (t, *J* = 1.1 Hz, 1H), 3.60 (t, *J* = 6.3 Hz, 2H), 2.68 (td, *J* = 7.0, 1.0 Hz, 2H), 2.15 – 2.05 (m, 2H).
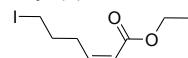

ethyl (*Z*)-6-chlorohex-2-enoate SI-10
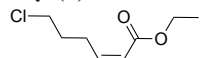
The compound was prepared using a modified literature procedure.[31] To a solution of (CF$_3$CH$_2$O)$_2$(O)PCH$_2$CO$_2$Et (624 μL, 875 mg, 2.64 mmol, 1.00 equiv.) and 18-crown-6 (2.09 g, 7.92 mmol, 2.50 equiv.) in THF (10 mL) was added KHMDS solution (0.5 M in toluene, 5.00 mL, 2.64 mmol, 1.00 equiv.) under N$_2$ atmosphere at −78 °C. After stirring at −78 °C for 30 min, a solution of 4-chlorobutanal (309 μL, 308 mg, 2.90 mmol, 1.10 equiv.) in THF (5.00 mL) was added. The mixture was allowed to stir at −78 °C for 20 min, warmed to 0 °C, poured into a solution of saturated NaHCO$_3$, and washed with diethyl ether. The organic phase was washed with brine, dried over MgSO$_4$, filtered, concentrated *in vacuo* over Celite®, and the residue was subjected to flash column chromatography (silica, 0 - 20% methyl t-butyl ether in petroleum ether), yielding the title product (316 mg, 1.79 mmol, 68%) as a colorless oil.

^{1}H NMR (500 MHz, CDCl$_3$) δ 6.20 (dt, *J* = 11.6, 7.7 Hz, 1H), 5.82 (dt, *J* = 11.5, 1.7 Hz, 1H), 4.17 (q, *J* = 7.1 Hz, 2H), 3.56 (t, *J* = 6.8 Hz, 2H), 2.80 (qd, *J* = 7.6, 1.7 Hz, 2H), 1.99 – 1.88 (m, 2H), 1.29 (t, *J* = 7.1 Hz, 3H).
^{13}C{^{1}H} NMR (126 MHz, CDCl$_3$) δ 166.4, 148.0, 121.1, 60.1, 44.5, 32.1, 26.6, 14.4.
HRMS (ESI) m/z calcd for C$_8$H$_{14}$ClO$_2$ ([M+H]$^+$): 177.0677, found 177.0678.

ethyl (*Z*)-6-iodohex-2-enoate SI-11

The compound was prepared according to the general procedure halogen exchange reactions **2.4.3.2**, starting from ethyl (*Z*)-6-chlorohex-2-enoate (316 mg, 1.69 mmol, 1.00 equiv.), NaI (758 mg, 5.06 mmol, 3.00 equiv.), acetone (2 mL) and a reaction time of 24 hours. Upon extraction, the organic phase was dried over anhydrous MgSO$_4$, filtered, concentrated *in vacuo* over Celite®, and the residue was subjected to flash column chromatography (silica, 0 - 10% methyl t-butyl ether in petroleum ether), yielding the title product (363 mg, 1.35 mmol, 80%) as a yellowish oil.

^{1}H NMR (500 MHz, CDCl$_3$) δ 6.18 (dt, *J* = 11.5, 7.6 Hz, 1H), 5.82 (dt, *J* = 11.4, 1.7 Hz, 1H), 4.18 (q, *J* = 7.1 Hz, 2H), 3.20 (t, *J* = 7.2 Hz, 2H), 2.76 (qd, *J* = 7.5, 1.7 Hz, 2H), 1.99 (quint, *J* = 7.2 Hz, 2H), 1.29 (t, *J* = 7.1 Hz, 3H).
^{13}C{^{1}H} NMR (126 MHz, CDCl$_3$) δ 166.4, 147.7, 121.2, 60.2, 33.0, 30.1, 14.4, 5.7.
HRMS (ESI) m/z calcd for C$_8$H$_{14}$O$_2$I ([M+H]$^+$): 269.0033, found 269.0026.

Preparation of ethyl (*E*)-6-(5-cyanocyclopent-1-en-1-yl)hex-2-enoate 15
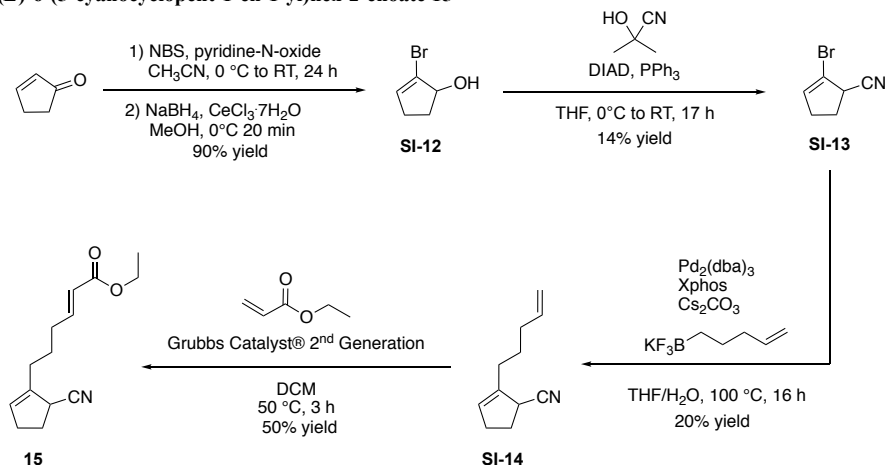
2-bromocyclopent-2-ene-1-carbonitrile SI-13

The intermediate SI-12 was prepared according to a literature procedure.[32] To a solution of cyclopentenone (500 mg, 6.09 mmol, 1.00 equiv.) and pyridine-N-oxide (870 mg, 9.14 mmol, 1.50 equiv.) in CH_3CN (30 mL) was added NBS (1.08 g, 6.09 mmol, 1.00 equiv.) at 0 °C. The reaction mixture was warmed to room temperature, stirred for 24 hours, concentrated *in vacuo* and the residue was subjected to flash column chromatography (silica, 0 - 15% ethyl acetate in petroleum ether), yielding a brominated intermediate (877 mg, 5.48 mmol, 90%) as a brown oil. To a solution of the brominated intermediate (100 mg, 0.62 mmol, 1.00 equiv.) and $CeCl_3 \cdot 7H_2O$ (278 mg, 0.75 mmol, 1.20 equiv.) in MeOH (6.2 mL) was added $NaBH_4$ (35 mg, 0.93 mmol, 1.50 equiv.) at 0 °C. The resulting mixture was stirred for 20 min at the same temperature and then saturated aqueous NH_4Cl solution (3 mL) was added. The organic phase was dried over anhydrous Na_2SO_4, filtered, concentrated *in vacuo*, yielding quantitatively alcohol intermediate SI-12, which was used in the next step without purification.

Under a nitrogen atmosphere, DIAD (16.3 mL, 16.8 g, 83.2 mmol, 1.50 equiv.) was added to a solution of alcohol SI-12 (9.04 g, 55.5 mmol, 1.00 equiv.), PPh_3 (21.8 g, 83.2 mmol, 1.50 equiv.) and acetone cyanohydrine (7.61 mL, 7.08 g, 83.2 mmol, 1.50 equiv.) in THF (126 mL) at 0 °C in a dropwise manner. The reaction mixture was allowed to warm to room temperature and stirred for 17 hours. Et_2O (200 mL) and celite were added and the volatiles were removed under reduced pressure. The residue was divided into two parts and subjected to column chromatography (silica gel, 0-100% ethyl acetate in petroleum ether) in parallel. The product containing fractions of the two purifications were collected, combined, and subjected to column chromatography (silica, 90-0% n-pentane in Et_2O) to isolate a fraction containing the title compound (1.32 g, 7.68 mmol, 14%) as an orange oil.

^{1}H NMR (500 MHz, $CDCl_3$) δ = 6.12 (q, *J* = 2.3 Hz, 1H), 3.78 – 3.69 (m, 1H), 2.65 – 2.228 (m, 4H)
^{13}C NMR (126 MHz, CDCl3) δ = 136.2, 119.5, 114.6, 41.6, 31.9, 29.2
HRMS (ESI) m/z calcd. for C_6H_7BrN ([M+H]$^+$): 171.9756; found: 171.9768; m/z calcd. for C_6H_7BrN ([M+H]$^+$): 173.9736; found: 173.9748.

ethyl (*E*)-6-(5-cyanocyclopent-1-en-1-yl)hex-2-enoate 15

The *Suzuki-coupling* procedure is adapted from a literature procedure.[33] In a nitrogen-filled glove box, a 20 mL screw-cap vial equipped with a magnetic stir bar was charged with $Pd_2(dba)_3$ (22.9 mg, 30.0 µmol, 2.50 mol%), XPhos (71.5 mg, 150 µmol, 15.0 mol%), Cs_2CO_3 (1.47 g, 4.50 mmol, 4.50 equiv.), potassium trifluoro(pent-4-en-1-yl)borate [34] (264 mg, 1.50 mmol, 1.50 equiv.), dry THF (5.45 mL), 2-bromocyclopent-2-ene-1-carbonitrile **SI-15** (172 mg, 1.00 mmol, 1.00 equiv.) and H_2O (550 µL). The vial was sealed with a Teflon-lined screw cap, removed from the glove box, placed in a preheated aluminum block at 100 °C, and allowed to stir for 16 hours (800 rpm). After cooling down to room temperature, H_2O (20 mL) and DCM (20 mL) were added, and the layers were separated. The aqueous phase was washed with DCM (2 x 20 mL) and the organic phase was dried over Na_2SO_4. The volatiles were removed under reduced pressure and the resulting crude product was used in the next step without further purification. The crude yield was approximately 20%.

Olefin metathesis

Ethyl (E)-6-(5-cyanocyclopent-1-en-1-yl)hex-2-enoate **15** was prepared according to the general procedure for metathesis reactions **2.4.3.1**, starting from the crude product of the Suzuki coupling (ca. 0.2 mmol) and ethyl acrylate (43.8 µL, 40.2 mg, 4.00 mmol, 2.0 equiv.). The resulting residue was subjected to flash column chromatography (silica, 0 - 10% ethyl acetate in petroleum ether), yielding the title product (23.7 mg, 102 µmol, 50%) as a yellowish oil.

^{1}H NMR (400 MHz, $CDCl_3$) δ 6.95 (dt, *J* = 15.8, 7.0 Hz, 1H), 5.83 (d, *J* = 15.7 Hz, 1H), 5.60 (dd, *J* = 4.0, 2.0 Hz, 1H), 4.19 (q, *J* = 7.2 Hz, 2H), 3.56 – 3.21 (m, 1H), 2.58 – 2.07 (m, 8H), 1.79 – 1.47 (m, 2H), 1.29 (t, *J* = 7.2 Hz, 3H).
^{13}C{^{1}H} NMR (126 MHz, $CDCl_3$) δ 166.8, 148.4, 138.4, 128.8, 122.0, 121.4, 60.4, 37.2, 31.8, 31.5, 29.4, 28.8, 25.8, 14.4.
HRMS (ESI) m/z calcd. for $C_{12}H_{19}O_5$ ([M+H]$^+$): 243.1227; found: 243.1239.

Ethyl (*E*)-6-(3-cyanocyclopent-1-en-1-yl)hex-2-enoate 17
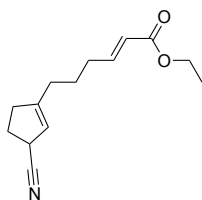
Ethyl (*E*)-6-(3-cyanocyclopent-1-en-1-yl)hex-2-enoate **17** was prepared according to the general procedure for Negishi cross-coupling reactions **2.4.3.3**, starting from 3-cyanocyclopent-1-en-1-yl trifluoromethanesulfonate **SI-6** (0.50 mmol, 121 mg, 1.00 equiv.) and Ethyl (E)-6-iodohex-2-enoate **SI-9** (214 mg, 0.80 mmol, 1.60 equiv.). The residue was subjected to flash column chromatography (silica, 0 - 20% methyl t-butyl ether in petroleum ether), yielding the title product (147 mg, 0.63 mmol, 63%) as a colorless oil.

^{1}H NMR (500 MHz, CDCl$_3$) δ 6.93 (dt, *J* = 15.7, 7.0 Hz, 1H), 5.82 (dt, *J* = 15.7, 1.6 Hz, 1H), 5.30 (d, *J* = 1.9 Hz, 1H), 4.18 (q, *J* = 7.2 Hz, 2H), 3.61 – 3.50 (m, 1H), 2.51 – 2.39 (m, 1H), 2.38 – 2.25 (m, 2H), 2.24 – 2.16 (m, 3H), 2.16 – 2.09 (m, 2H), 1.68 – 1.57 (m, 2H), 1.28 (t, *J* = 7.1 Hz, 3H).

^{13}C{^{1}H} NMR (126 MHz, CDCl$_3$) δ 166.7, 150.0, 148.4, 122.1, 122.0, 118.8, 60.4, 34.5, 34.4, 31.8, 30.3, 29.1, 25.8, 14.4.

HRMS (ESI) m/z calcd for C$_{14}$H$_{20}$O$_2$N ([M+H]$^+$): 234.1489, found 234.1481.

ethyl (*Z*)-6-(3-cyanocyclopent-1-en-1-yl)hex-2-enoate (20)
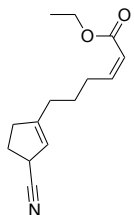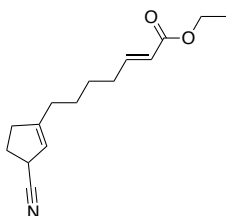
Ethyl (*Z*)-6-(3-cyanocyclopent-1-en-1-yl)hex-2-enoate **20** was prepared according to the general procedure for Negishi cross-coupling reactions **2.4.3.3** starting from 3-cyanocyclopent-1-en-1-yl trifluoromethanesulfonate **SI-6** (0.25 mmol, 60.3 mg, 1.00 equiv.) and ethyl (*Z*)-6-iodohex-2-enoate **SI-14** (107 mg, 0.40 mmol, 1.60 equiv.). The residue was subjected to flash column chromatography (silica, 0 - 20% methyl t-butyl ether in petroleum ether), yielding the title product (32.0 mg, 135 µmol, 54%) as a colorless oil.

^{1}H NMR (500 MHz, CDCl$_3$) δ 6.20 (dt, *J* = 11.6, 7.6 Hz, 1H), 5.79 (dt, *J* = 11.6, 1.7 Hz, 1H), 5.32 – 5.25 (m, 1H), 4.17 (q, *J* = 7.1 Hz, 2H), 3.59 – 3.51 (m, 1H), 2.70 – 2.62 (m, 2H), 2.49 – 2.41 (m, 1H), 2.37 – 2.28 (m, 2H), 2.23 – 2.11 (m, 3H), 1.65 – 1.58 (m, 2H), 1.29 (t, *J* = 7.1 Hz, 3H).

^{13}C{^{1}H} NMR (126 MHz, CDCl$_3$) δ 166.5, 150.3, 149.5, 122.2, 120.4, 118.5, 60.0, 34.5, 34.3, 30.5, 29.1, 28.7, 26.8, 14.4.

HRMS (ESI) m/z calcd for C$_{14}$H$_{20}$O$_2$N ([M+H]$^+$): 234.1489 found 234.1480.
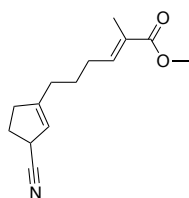
ethyl (*E*)-7-(3-cyanocyclopent-1-en-1-yl)hept-2-enoate 21

Ethyl (*E*)-7-(3-cyanocyclopent-1-en-1-yl)hept-2-enoate **21** was prepared according to the general procedure for Negishi cross-coupling reactions **2.4.3.3** starting from 3-cyanocyclopent-1-en-1-yl trifluoromethanesulfonate **SI-6** (0.50 mmol, 120 mg, 1.00 equiv.) and Ethyl (*E*)-7-iodohept-2-enoate **SI-10** (226 mg, 0.80 mmol, 1.60 equiv.). The residue was subjected to flash column chromatography (silica, 0 - 20% methyl t-butyl ether in petroleum ether), yielding the title product (46.0 mg, 185 µmol, 37%) as a colorless oil.

^{1}H NMR (500 MHz, CDCl$_3$) δ 6.94 (dt, *J* = 15.7, 7.0 Hz, 1H), 5.81 (dt, *J* = 15.6, 1.6 Hz, 1H), 5.33 – 5.24 (m, 1H), 4.18 (q, *J* = 7.1 Hz, 2H), 3.62 – 3.51 (m, 1H), 2.49 – 2.40 (m, 1H), 2.37 – 2.28 (m, 2H), 2.26 – 2.16 (m, 3H), 2.15 – 2.05 (m, 2H), 1.54 – 1.42 (m, 4H), 1.29 (t, *J* = 7.1 Hz, 3H).

^{13}C{^{1}H} NMR (126 MHz, CDCl$_3$) δ 166.8, 150.4, 148.9, 122.2, 121.7, 118.5, 60.4, 34.5, 34.4, 32.1, 30.7, 29.2, 27.9, 27.0, 14.4.

HRMS (ESI) m/z calcd for C$_{15}$H$_{22}$O$_2$N ([M+H]$^+$): 248.1645, found 248.1670.

Methyl (*E*)-6-(3-cyanocyclopent-1-en-1-yl)-2-methylhex-2-enoate 23

Methyl (*E*)-6-(3-cyanocyclopent-1-en-1-yl)-2-methylhex-2-enoate **23** was prepared according to the general procedure for Negishi cross-coupling reactions **2.4.3.3** starting from 3-cyanocyclopent-1-en-1-yl trifluoromethanesulfonate **SI-6** (0.50 mmol, 120 mg, 1.00 equiv.) and Methyl (*E*)-6-iodo-2-methylhex-2-enoate **SI-11** (214 mg, 0.80 mmol, 1.60 equiv.). The residue was subjected to flash column chromatography (silica, 0 - 20% methyl t-butyl ether in petroleum ether), yielding the title product (90.0 mg, 387 µmol, 77%) as a colorless oil.

^{1}H NMR (500 MHz, CDCl$_3$) δ 6.73 (td, *J* = 6.0, 1.5 Hz, 1H), 5.30 (d, *J* = 1.9 Hz, 1H), 3.73 (s, 3H), 3.59 – 3.48 (m, 1H), 2.52 – 2.40 (m, 1H), 2.37 – 2.26 (m, 2H), 2.23 – 2.08 (m, 5H), 1.83 (s, 3H), 1.65 – 1.58 (m, 2H).

^{13}C{^{1}H} NMR (126 MHz, CDCl$_3$) δ 168.8, 150.1, 141.8, 128.2, 122.1, 118.7, 51.9, 34.5, 34.4, 30.5, 29.2, 28.3, 26.4, 12.6.

HRMS (ESI) m/z calcd for C$_{14}$H$_{20}$NO$_2$ ([M+H]$^+$): 234.1489, found 234.1501.

## 2.4.4 Intermolecular catalytic reactions and isolation procedures

2.4.4.1 Hydro-cyanide group borrowing

2.4.4.1.1 General procedure for intermolecular reactions

In a nitrogen-filled glove box, an oven-dried 4 mL vial was charged sequentially with a solution of Ni(cod)$_2$ (0.86 mg, 3.13 µmol, 5 mol%) and DPEPhos (1.68 mg, 3.13 µmol, 5 mol%) in toluene (125 µL), unsaturated nitrile substrate **1a** (17.4 mg, 188 µmol, 3.00 equiv.), dienophile (62.5 µmol, 1.00 equiv.) and 0.9 M solution of AlMe$_2$Cl in hexane (27.7 µL, 25 µmol, 0.40 equiv.) or 1.0 M solution of AlMe$_3$ in toluene (27.7 µL, 25 µmol, 0.40 equiv.). The vial was closed tightly with a screw-cap and placed in a pre-heated heating plate at the indicated temperature for the indicated amount of hours. After cooling to room temperature, the reaction mixture was diluted with 2 mL of acetonitrile and 1,3,5-trimethoxybenzene was added as an internal standard. The mixture was filtrated through a plug of silica using ethyl acetate as an eluent and a sample for GC analysis was taken. The GC-yield was determined based on a calibration of the mixture of isomers. The mixture was concentrated *in vacuo* over Celite® and the residue was subjected to flash column chromatography, yielding the corresponding product.

2.4.4.1.2 Intermolecular reactions

Reaction of **1a** and **3** leading to compounds **8a-c**
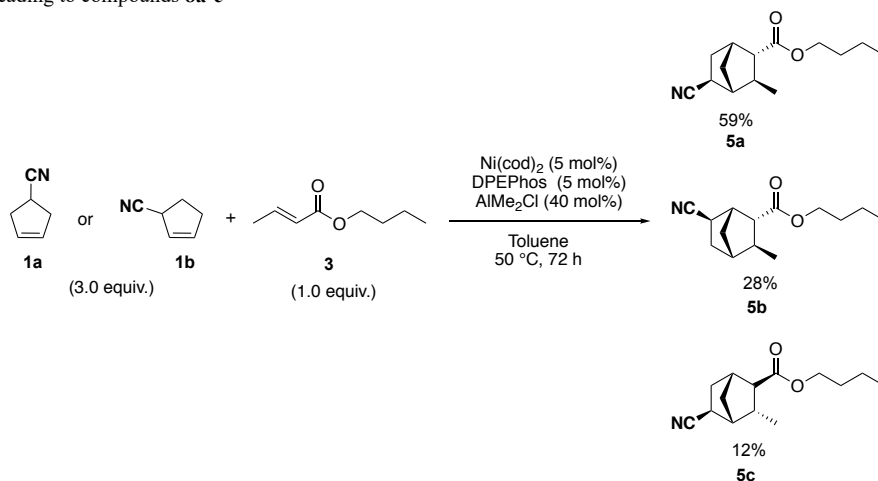
The reaction was performed according to the general procedure for hydrogen-cyanide borrowing reactions **2.4.4.1.1**, starting from unsaturated nitrile substrate **1a** or **1b** (17.4 mg, 188 µmol, 3.00 equiv.), *n*-butyl crotonate **3** (8.80 mg, 9.79 µL, 62.5 µmol, 1.00 equiv.), and 0.9 M solution of AlMe$_2$Cl in hexane (27.7 µL, 25.0 µmol, 0.40 equiv.) at 50 °C for 72 hours. The crude yield as determined by GC-analysis was: **5a** (59%), **5b** (28%), **5c** (12%). For the isolation of the products, the reaction mixture (a triplicate) was subjected to flash column chromatography (silica, 0 - 20% methyl t-butyl ether in petroleum ether) yielding the title products **5a** (18.3 mg, 77.8 µmol, 41%) as a colorless oil, **5b** (7.8 mg, 33.2 µmol, 18%) as a colorless oil, and **5c** (2.1 mg, 8.9 µmol, 5%) as a colorless oil. Due to the low yield, the analytical sample for the isomer **5c** was obtained by isolation of several reaction batches.

5a
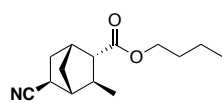
^{1}H NMR (500 MHz, CDCl$_3$) δ 4.12 – 4.02 (m, 2H), 2.65 (s, 1H), 2.47 (ddd, *J* = 9.1, 4.9, 1.6 Hz, 1H), 2.31 – 2.28 (m, 1H), 2.28 – 2.25 (m, 1H), 1.99 – 1.92 (m, 1H), 1.87 – 1.80 (m, 1H), 1.75 – 1.69 (m, 2H), 1.69 – 1.65 (m, 1H), 1.64 – 1.58 (m, 2H), 1.41 – 1.32 (m, 2H), 1.01 (d, *J* = 7.1 Hz, 3H), 0.94 (t, *J* = 7.4 Hz, 3H).
^{13}C{^{1}H} NMR (126 MHz, CDCl$_3$) δ 173.8, 123.2, 64.7, 54.3, 48.5, 40.6, 38.5, 35.8, 31.0, 30.8, 30.6, 21.2, 19.3, 13.8.
HRMS (ESI) m/z calcd for C$_{14}$H$_{22}$NO$_2$ ([M+H]$^+$): 236.1645, found 236.1651.

5b
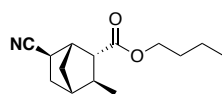
^{1}H NMR (500 MHz, CDCl$_3$) δ 4.09 (td, *J* = 6.7, 1.2 Hz, 2H), 2.83 – 2.79 (m, 1H), 2.72 (ddd, *J* = 9.0, 5.1, 1.6 Hz, 1H), 2.27 (dd, *J* = 5.4, 4.1 Hz, 1H), 2.10 – 2.05 (m, 1H), 1.88 – 1.77 (m, 3H), 1.72 – 1.64 (m, 2H), 1.64 – 1.59 (m, 2H), 1.43 – 1.33 (m, 2H), 1.00 (d, *J* = 7.0 Hz, 3H), 0.95 (t, *J* = 7.4 Hz, 3H).
^{13}C{^{1}H} NMR (126 MHz, CDCl$_3$) δ 173.7, 123.5, 64.8, 53.9, 45.5, 43.2, 38.9, 36.2, 35.7, 30.8, 26.1, 21.5, 19.3, 13.8.
HRMS (ESI) m/z calcd for C$_{14}$H$_{22}$NO$_2$ ([M+H]$^+$): 236.1645, found 236.1650

5c
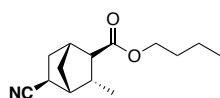
¹H NMR (500 MHz, CDCl₃) δ 4.07 (t, *J* = 6.6 Hz, 2H), 2.74 – 2.68 (m, 1H), 2.63 – 2.57 (m, 1H), 2.51 – 2.46 (m, 1H), 2.34 – 2.28 (m, 1H), 1.93 – 1.88 (m, 1H), 1.78 – 1.65 (m, 4H), 1.63 – 1.58 (m, 2H), 1.42 – 1.34 (m, 2H), 1.06 (d, *J* = 7.0 Hz, 3H), 0.94 (t, *J* = 7.4 Hz, 3H).
¹³C{¹H} NMR (126 MHz, CDCl₃) δ 174.7, 123.7, 64.7, 53.6, 47.1, 41.1, 38.7, 37.4, 36.2, 30.8, 24.3, 19.3, 16.5, 13.9.
HRMS (ESI) m/z calcd for C₁₄H₂₂NO₂ ([M+H]⁺): 236.1645, found 236.1655.

Reaction of **1a** and **SI-16** leading to compounds **11a-d**
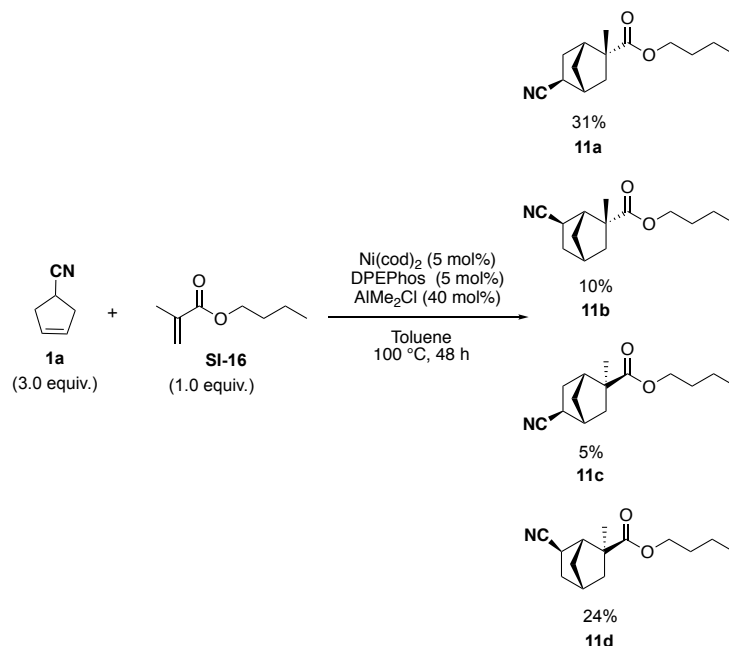
The reaction was performed according to the general procedure for hydrogen-cyanide borrowing reactions **2.4.4.1.1**, starting from unsaturated nitrile substrate **1a** (17.4 mg, 188 µmol, 3.00 equiv.), *n*-butyl methacrylate **SI-16** (8.80 mg, 9.84 µL, 62.5 µmol, 1.00 equiv.), and 0.9 M solution of AlMe₂Cl in hexane (27.7 µL, 25.0 µmol, 0.40 equiv.) at 100 °C for 48 hours. The crude yield as determined GC-analysis was: **11a** (31%), **11b** (10%), **11c** (5%), **11d** (24%).
For the isolation of the products, the reaction mixture (a triplicate) was subjected to flash column chromatography (silica, 0 - 20% methyl t-butyl ether in petroleum ether) yielding the title products **11a** (8.7 mg, 37.0 µmol, 20%) as a colorless oil, **11b** (1.8 mg, 7.7 µmol, 4%) as a colorless oil, **10c** (1.5 mg, 6.4 µmol, 3%) as a colorless oil and **11d** (7.0 mg, 29.8 µmol, 16%) as a colorless oil. Due to the low yield, the analytical samples for the minor isomers **11b** and **11c** were obtained by isolation of several reaction batches.

11a

¹H NMR (500 MHz, CDCl₃) δ 4.13 – 3.99 (m, 2H), 2.66 – 2.57 (m, 1H), 2.45 – 2.36 (m, 1H), 2.36 – 2.28 (m, 1H), 2.14 (dd, *J* = 13.4, 2.7 Hz, 1H), 1.82 – 1.64 (m, 3H), 1.64 – 1.56 (m, 3H), 1.42 – 1.35 (m, 2H), 1.34 – 1.29 (m, 1H), 1.27 (s, 3H), 0.94 (t, *J* = 7.4 Hz, 3H).
¹³C{¹H} NMR (126 MHz, CDCl₃) δ 176.6, 123.3, 64.8, 49.9, 46.1, 42.8, 39.7, 36.3, 33.0, 30.9, 29.6, 26.4, 19.3, 13.8.
HRMS (ESI) m/z calcd for C₁₄H₂₂O₂N ([M+H]⁺): 236.1645, found 236.1653.
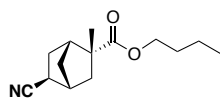
11b
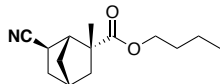
¹H NMR (500 MHz, CDCl₃) δ 4.12 – 4.06 (m, 2H), 2.91 – 2.85 (m, 1H), 2.82 – 2.77 (m, 1H), 2.45 – 2.38 (m, 2H), 1.90 – 1.82 (m, 1H), 1.71 – 1.60 (m, 4H), 1.53 – 1.49 (m, 1H), 1.42 – 1.36 (m, 2H), 1.24 (s, 3H), 0.94 (t, *J* = 7.4 Hz, 3H), 0.91 – 0.87 (m, 1H).
¹³C{¹H} NMR (126 MHz, CDCl₃) δ 177.1, 123. 6, 65.2, 49.4, 48.9, 40.8, 37.8, 37.1, 35.6, 30.8, 25.9, 22.6, 19.3, 13.9.
HRMS (ESI) m/z calcd for C₁₄H₂₂O₂N ([M+H]⁺): 236.1645, found 236.1661.

11c
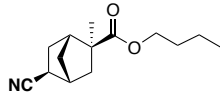
¹H NMR (500 MHz, CDCl₃) δ 4.16 – 4.01 (m, 2H), 2.55 – 2.50 (m, 1H), 2.44 – 2.37 (m, 2H), 2.05 (dd, *J* = 13.1, 2.5 Hz, 1H), 1.84 – 1.74 (m, 2H), 1.73 – 1.65 (m, 2H), 1.65 – 1.60 (m, 2H), 1.44 – 1.35 (m, 2H), 1.33 – 1.29 (m, 1H), 1.28 (s, 3H), 0.95 (t, *J* = 7.4 Hz, 3H).
¹³C{¹H} NMR (126 MHz, CDCl₃) δ 176.4, 123.2, 65.0, 50.9, 50.1, 39.9, 37.0, 36.1, 34.7, 30.8, 28.3, 26.7, 19.3, 13.8.
HRMS (ESI) m/z calcd for C₁₄H₂₂O₂N ([M+H]⁺): 236.1645, found 236.1653.

11d
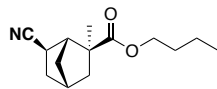
¹H NMR (500 MHz, CDCl₃) δ 4.12 – 4.03 (m, 2H), 2.67 – 2.62 (m, 1H), 2.62 – 2.57 (m, 1H), 2.49 (dd, J = 13.5, 5.0 Hz, 1H), 2.37 – 2.29 (m, 1H), 2.15 (ddd, 1H), 1.76 (ddd, J = 13.6, 5.5, 4.4 Hz, 1H), 1.65 – 1.58 (m, 3H), 1.55 – 1.50 (m, 1H), 1.42 – 1.33 (m, 2H), 1.20 (s, 3H), 0.96 – 0.87 (m, 4H).
¹³C{¹H} NMR (126 MHz, CDCl₃) δ 177.7, 123.3, 65.0, 48.4, 44.4, 42.8, 40.6, 37.6, 30.8, 30.7, 30.0, 22.4, 19.3, 13.9.
**HRMS** (ESI) m/z calcd for C₁₄H₂₂O₂N ([M+H]⁺): 236.1645, found 236.1738.

Reaction of **1a** and **SI-17** leading to compounds **12a-c**
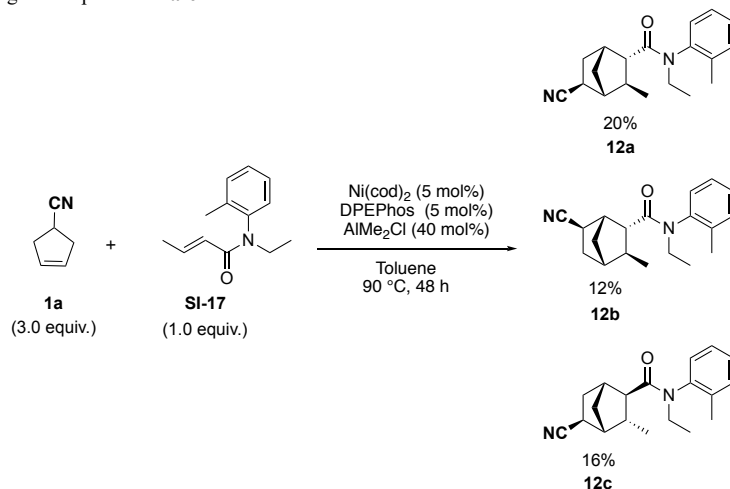
The reaction was performed according to the general procedure for hydrogen-cyanide borrowing reactions **2.4.4.1.1**, starting from unsaturated nitrile substrate **1a** (17.4 mg, 188 µmol, 3.00 equiv.), crotamiton **SI-17** (12.7 mg, 62.5 µmol, 1.00 equiv.), and 0.9 M solution of AlMe₂Cl in hexane (27.7 µL, 25.0 µmol, 0.40 equiv.) at 90 °C for 48 hours. The crude yield as determined GC-analysis was: **12a** (20%), **12b** (12%), **12c** (16%).
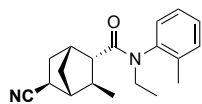For the isolation of the products, the reaction mixture (a triplicate) was subjected to flash column chromatography (silica, 0 - 40% ethyl acetate in petroleum ether) yielding a mixture of isomers **12a-c** (15.6 mg, 52.7 µmol 28%, **12a/12b/12c** = 42/25/33) as a colorless oil. The analytical sample of each isomer was obtained by isolation of several reaction batches.

12a

Two rotamers. Ratio R1/R2: 1.00 / 0.47
¹H NMR (500 MHz, DMSO-d_6) δ 7.42 – 7.35 (m, 1H, R1; 1H, R2), 7.35 – 7.24 (m, 2H, R1; 2H, R2), 7.24 – 7.16 (m, 1H, R1), 7.14 – 7.08 (m, 1H, R2), 4.16 – 4.04 (m, 1H, R2), 3.96 – 3.85 (m, 1H, R1), 3.19 – 3.08 (m, 1H, R1), 2.97 – 2.87 (m, 1H, R2), 2.71 – 2.56 (m, 1H, R1; 1H, R2), 2,16 (s, 3H, R2), 2.14 – 2.07 (m, 5H, R1), 2.07 – 1.98 (m, 1H, R1; 2H, R2), 1.98 – 1.84 (m, 1H, R1; 2H, R2), 1.72 – 1.65 (m, 1H, R1), 1.49 – 1.17 (m, 3H, R1; 4H, R2), 1.31 – 1.18 (m, 3H, R1; 3H, R2), 0.79 – 0.71 (m, 3H, R1; 3H, R2).
¹³C{¹H} NMR (126 MHz, DMSO-d_6) δ 171.3 (R2), 171.1 (R1), 140.4 (R1), 140.2 (R2), 135.6 (R2), 135.3 (R1), 131.6 (R2), 131.4 (R1), 130.1 (R2), 129.6 (R1), 128.5 (R1), 128.4 (R2), 127.1 (R1), 127.0 (R2), 123.5 (R1), 123.5 (R2), 52.4 (R1), 51.8 (R2), 48.1 (R1), 47. 9 (R2), 43.0 (R1), 42.7 (R2), 40.8 (R2), 40.6 (R1), 38.2 (R2), 38.0 (R1), 36.1 (R1), 36. 0 (R2), 29.9 (R2), 29.8 (R1), 29.6 (R1, R2), 21.1 (R2), 20.7 (R1), 17.3 (R2), 17.2 (R1), 13.0 (R1), 12.5 (R2).
HRMS (ESI) m/z calcd for C₁₉H₂₄ON₂ ([M]⁺): 296.1883 found 296.1884

12b
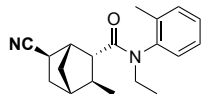
Two rotamers: Ratio R1/R2: 1.00 / 0.57
¹H NMR (500 MHz, DMSO-d_6) δ 7.43 – 7.36 (m, 1H, R1; 1H, R2), 7.36 – 7.27 (m, 3H, R1; 2H, R2), 7.14 (dd, J = 7.7, 1.5 Hz, 1H, R2), 4.10 (dq, J = 14.3, 7.1 Hz, 1H, R2), 3.90 (dq, J = 14.2, 7.1 Hz, 1H, R1), 3.19 (dq, J = 14.2, 7.1 Hz, 1H, R1), 3.03 – 2.95 (m, 2H, R2), 2.93 – 2.87 (m, 1H, R1), 2.26 – 2.23 (m, 1H, R1), 2.22 (s, 3H, R2), 2.14 (s, 3H, R1), 2.07 – 2.00 (m, 2H, R2), 1.94 – 1.84 (m, 2H, R1; 2H, R2), 1.83 – 1.75 (m, 1H, R1; 1H, R2), 1.75 – 1.72 (m, 1H, R1), 1.69 – 1.62 (m, 1H, R1; 1H, R2), 1.46 – 1.26 (m, 2H, R1; 2H, R2), 1.06 – 0.98 (m, 3H, R1; 3H, R2), 0.73 (d, J = 6.6 Hz, 3H, R1), 0.75 (d, J = 6.6 Hz, 3H, R2).
¹³C{¹H} NMR (126 MHz, DMSO-d_6) δ 171.0 (R1), 171.2 (R2), 140.3 (R1), 140.0 (R2), 135.5 (R2), 135.2 (R1), 131.6 (R2), 131.4 (R1), 130.0 (R2), 129.5 (R1), 128.6 (R1), 128.5 (R2), 127.3 (R1), 127.1 (R2), 123.9 (R1), 123.6 (R2), 52.0 (R1), 51.4 (R2), 45.4 (R1), 44.7 (R2), 43.0 (R1), 42.9 (R1), 42.8 (R2), 42.7 (R2), 38.3 (R2), 38.2 (R1), 36.0 (R1, R2), 35.3 (R1), 35.3 (R2), 25.0 (R1, R2), 21.0 (R1), 20.5 (R2), 17.2 (R1), 17.2 (R2), 12.8 (R1), 12.4 (R2).
HRMS (ESI) m/z calcd for C₁₉H₂₄ON₂ ([M]⁺): 296.1883 found 296.1884

12c
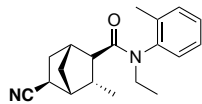
Two rotamers: Ratio R1/R2: 1.00 / 0.50
¹H NMR (500 MHz, DMSO-d_6) δ 7.41 – 7.34 (m, 1H, R1; 1H, R2), 7.34 – 7.25 (m, 2H, R1; 2H, R2), 7.24 – 7.18 (m, 1H, R1), 7.15 – 7.08 (m, 1H, R2), 4.00 – 3.88 (m, 1H, R1), 3.88 – 3.79 (m, 1H, R2), 3.27 – 3.19 (m, 1H, R1), 3.19 – 3.09 (m, 1H, R2), 2.72 – 2.64 (m, 1H, R1; 1H, R2), 2.45 – 2.36 (m, 1H, R1), 2.35 – 2.23 (m, 2H, R1; 1H, R2), 2.22 – 2.15 (m, 4H, R2), 2.11 (s, 3H, R1), 2.09 – 1.86 (m, 1H, R2), 1.86 – 1.79 (m, 1H, R1), 1.55 – 1.19 (m, 2H, R1; 3H, R2), 1.18 – 1.09 (m, 1H, R1; 1H, R2), 1.06 – 0.96 (m, 3H, R1; 3H, R2), 0.95 – 0.86 (m, 1H, R1; 1H, R2), 0.73 (d, J = 7.1 Hz, 3H, R1), 0.69 (d, J = 7.0 Hz, 3H, R2).

¹³C{¹H} NMR (126 MHz, DMSO-d_6) δ 173.7 (R2), 172.9 (R1), 140.6 (R1), 140.6 (R2), 135.5 (R2), 135.4 (R1), 131.4 (R1), 131.3 (R2), 129. 8 (R2), 129.5 (R1), 128.3 (R1), 128.3 (R2), 127.1 (R1), 127.0 (R2), 124.1 (R2), 124.1 (R1), 51.1 (R1), 50.2 (R2), 46.4 (R1), 46.1 (R2), 42.8 (R2), 42.5 (R1), 42.5 (R1), 42.2 (R2), 36.9 (R1), 36.8 (R2), 36.1 (R1, R2), 36.1 (R1, R2), 23.4 (R2), 23.3 (R1), 17.4 (R2), 17.2 (R1), 15.4 (R1), 15.0 (R2), 12.8 (R1), 12.7 (R2).

HRMS (ESI) m/z calcd for $C_{19}H_{24}ON_2$ ([M]$^+$): 296.1883 found 296.1883

Reaction of **1a** and **SI-0** leading to compound **13**
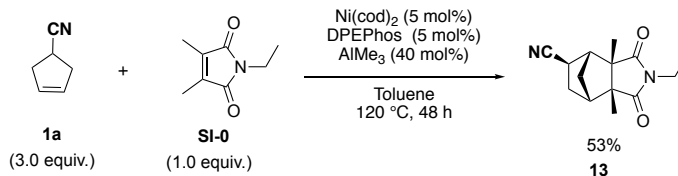
The reaction was performed according to the general procedure for hydrogen-cyanide borrowing reactions **2.4.4.1.1**, starting from unsaturated nitrile substrate **1a** (17.4 mg, 188 µmol, 3.00 equiv.), maleimide **13** (9.6 mg, 62.5 µmol, 1.00 equiv.) and 1.0 M solution of AlMe₃ in toluene (27.7 µL, 25.0 µmol, 0.40 equiv.) at 120 °C for 48 hours. The crude yield as determined by NMR spectroscopy was: **14** (51%).
For the isolation of the product, the reaction mixture (a duplicate) was subjected to column chromatography (silica, 0 - 40% ethyl acetate in petroleum ether) yielding the title product (9.2 mg, 37.4 µmol, 30%) as a colorless oil.

13
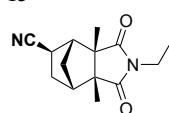
¹**H NMR** (500 MHz, CDCl₃) δ 3.53 (q, *J* = 7.2 Hz, 2H), 2.64 – 2.59 (m, 1H), 2.47 – 2.43 (m, 1H), 2.43 – 2.38 (m, 1H), 2.08 – 2.02 (m, 1H), 1.91 – 1.83 (m, 2H), 1.76 – 1.70 (m, 1H), 1.26 (s, 3H), 1.24 (s, 3H), 1.17 (t, *J* = 7.2 Hz, 3H).
¹³C{¹H} NMR (126 MHz, CDCl₃) δ 179.9, 179.7, 121.9, 54.6, 54.5, 51.7, 46.9, 36.7, 33.8, 31.9, 28.0, 17.8, 17.7, 13.3.
HRMS (pAPCI) m/z: calcd for $C_{14}H_{19}N_2O_2$ ([M+H]$^+$): 247.1447, found 247.1441.

2.4.4.2 Hydro-formyl group borrowing

2.4.4.2.1   General procedure for intermolecular reactions

In a nitrogen-filled glove box, a 4 mL screw-cap scintillation vial equipped with a magnetic stir bar was charged with [Rh(cod)OMe]₂ (3.9 mg, 0.008 mmol, 0.04 equiv.), xantphos (9.3 mg, 0.016 mmol, 0.08 equiv.), 3-methoxybenzoic acid (2.4 mg, 0.016 mmol, 0.08 equiv.), dry solvent (200 µL), 4-formylcyclopent-1-ene **1c** and dienophile (0.2 mmol, 1.0 equiv.). The vial was sealed with a Teflon-lined screw-cap, removed from the glove box, placed in a preheated aluminium block at 90 °C, and allowed to stir at 800 rpm for the indicated time. Upon completion of the reaction, internal standard (1,3,5-trimethoxybenzene) was added, and the crude yield was determined via NMR spectroscopy.

Procedure for isolation as aldehydes
After cooling down to room temperature, the reaction mixture was filtered through a pad of celite, and the volatiles were removed. The residue was subjected to column chromatography to isolate the corresponding product.

Procedure for isolation as alcohols
After cooling down to room temperature, MeOH (200 µL) and NaBH₄ (11.3 mg, 0.3 mmol, 1.0 equiv.) were added to the reaction and it was allowed to stir for 3 hours at room temperature. Subsequently, water (5 mL) and DCM (8 mL) were added. The phases were separated, and the aqueous phase was washed with DCM (2 x 8 mL). The organic phase was dried with Na₂SO₄ and filtered. The volatiles of the filtrate were removed under reduced pressure and the residue was subjected to column chromatography to isolate the corresponding product.

2.4.4.2.2 Intermolecular reactions

Reaction of **1c** and **vinyl bpin dimer** leading to compound **29**
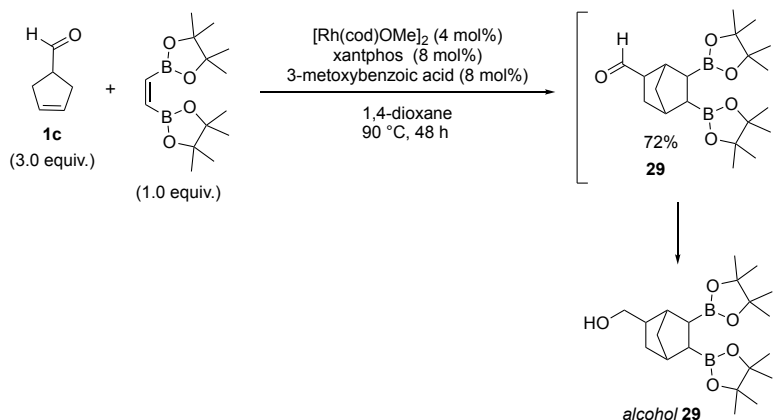
The reaction was performed according to the general procedure for hydro-formyl group borrowing reactions **2.4.4.2.1**, starting from 4-formylcyclopent-1-ene **1c** (57.7 mg, 600 µmol, 3.00 equiv.) and vinyl Bpin dimer (56.0 mg, 200 µmol, 1.00 equiv.) in 1,4-dioxane (200 µL) at 90 °C for 48 hours. The crude yield as determined by NMR spectroscopy was: 72% (mixture of isomers). The crude product was isolated as an alcohol following the procedure 4.2.1.2, and the residue was subjected to column chromatography (silica gel, 0 - 40% ethyl acetate in petroleum ether) yielding the title product (21.0 mg, 56 µmol, 28%) as an orange oil consisting of two isomers in a ratio of 63/37 = major(mj) / minor (mn) as determined by NMR. As the isomers were isolated as an inseparable mixture and due to the complexity of the corresponding NMR spectra, no assignment of the relative configuration was postulated.

alcohol **29**
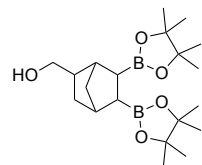
^{1}H NMR (500 MHz, CDCl$_3$) δ 3.39 – 3.32 (m, 1H, mj+mn), 3.30 – 3.21 (m, 1H, mj+mn), 2.37 – 2.35 (m, 0.7H, mj), 2.30 – 2.24 (m, 0.6H, mn), 2.20 (m, 0.7H, mj), 2.16 (m, 0.5H, mn), 1.73 (qd, J = 8.6, 4.4 Hz, 2H, mj+mn), 1.51 (ddd, J = 12.6, 8.5, 2.4 Hz, 0.6H, mj), 1.44 (ddd, J = 11.5, 8.5, 2.4 Hz, 0.4H, mn), 1.35 – 1.26 (m, 3H, mj+mn), 1.25 – 1.14 (m, 24H, mj+mn), 1.08 – 0.83 (m, 2H, mj+mn)

^{13}C{^{1}H} NMR (126 MHz, CDCl$_3$) δ 83.1 (mn), 83.0 (mj), 82.9 (mj), 82.9 (mn), 67.2 (mn), 67.1 (mj), 47.4 (mj), 42.9 (mn), 41.2 (mj), 39.3 (mn), 39.1 (mj), 37.6 (mj), 37.6 (mn), 36.8 (mn), 32.1 (mj), 31.1 (mn), 25.2 (mn), 25.0 (mj), 25.0 (mj), 25.0 (mn), 24.9 (mj), 24.8 (mn), 24.8 (mn), 24.8 (mj) [Note: the carbon atom attached to the boron atom was not observed due to quadrupole broadening or relaxation delay caused by the ^{11}B nucleus.][35]

HRMS (ESI) m/z calcd. for C$_{20}$H$_{37}$O$_5$B$_2$ ([M+H]$^+$): 379.2822; found: 379.2840.

Reaction of **1c** and **13** leading to compound **30**
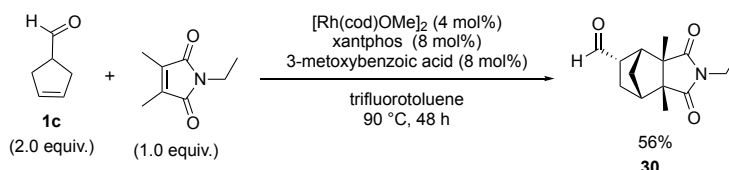
The reaction was performed according to the general procedure for hydro-formyl group borrowing reactions **2.4.4.2.1**, starting from 4-formylcyclopent-1-ene **1c** (38.5 mg, 400 µmol, 2.00 equiv.) and ethyl 2,3-dimethylmaleimide (30.6 mg, 200 µmol, 1.00 equiv.) in trifluorotoluene (200 µL) at 90 °C for 48 hours. The crude yield as determined by NMR spectroscopy was 46%. The crude product was isolated as an alcohol following the procedure 4.2.1.1, and the residue was subjected to column chromatography (silica gel, 0 - 25% ethyl acetate in petroleum ether) yielding the title product (16.9 mg, 68.0 µmol, 34%) as an orange oil.

30
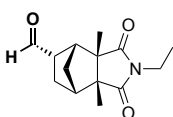
^{1}H NMR (500 MHz, CDCl$_3$) δ 9.59 (s, 1H), 3.53 (q, J = 7.2 Hz, 2H), 2.62 – 2.60 (m, 1H), 2.40 – 2.33 (m, 2H), 2.05 – 1.96 (m, 1H), 1.79 (ddd, J = 11.0, 2.8, 1.6 Hz, 1H), 1.36 – 1.28 (m, 2H), 1.26 (s, 3H), 1.22 (s, 3H), 1.16 (t, J = 7.2 Hz, 3H).

^{13}C{^{1}H} NMR (126 MHz, CDCl$_3$) δ 200.6, 180.7, 180.7, 55.1, 54.7, 50.0, 48.1, 47.1, 35.3, 33.6, 25.4, 17.7, 17.7, 13.3.

HRMS (ESI) m/z calcd. for C$_{14}$H$_{20}$O$_3$N ([M+H]$^+$): 250.1438; found: 250.1452.

Reaction of **1c** and **dimethyl maleate** leading to compound **31**
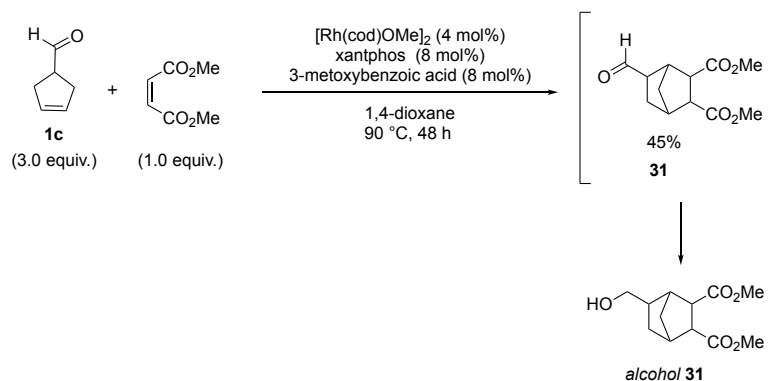
The reaction was performed according to the general procedure for hydro-formyl group borrowing reactions **2.4.4.2.1**, starting from 4-formylcyclopent-1-ene **1c** (38.5 mg, 400 μmol, 2.00 equiv.) and dimethyl maleate (28.8 mg, 25.1 μL, 200 μmol, 1.00 equiv.) in 1,4-dioxane (200 μL) at 90 °C for 72 hours. The crude yield as determined by NMR spectroscopy was: 45% (mixture of isomers). The crude product was isolated as an alcohol following the procedure 4.2.1.2, and the residue was subjected to flash column chromatography (silica gel, 0 - 50% ethyl acetate in petroleum ether) yielding the title product (17.5 mg, 72.0 μmol, 36%) as an orange oil consisting of three isomers. Apart from one trace isomer (tr), the ratio of the other two isomers was determined to be 60/40 = major(mj) / minor (mn) by NMR. As the isomers were isolated as an inseparable mixture and due to the complexity of the corresponding NMR spectra, no assignment of the relative configuration was postulated. In case of the trace isomer, some signals in the carbon NMR spectrum could not be identified due to overlap with the two other isomers.

alcohol **31**

^{1}H NMR (500 MHz, CDCl$_3$) δ 3.74 – 3.59 (m, 6H), 3.39 – 3.37 (m, 2H), 3.25 – 3.22 (m, 1H), 2.86 (dd, J = 5.1, 1.7 Hz, 0.5H, mj), 2.81 (dd, J = 5.8, 1.6 Hz, 0.4H, mn), 2.68 – 2.47 (m, 2H), 1.88 – 1.77 (m, 0.8H), 1.76 – 1.59 (m, 1.5H), 1.57 – 1.51 (m, 0.5H), 1.49 – 1.42 (m, 1.2H), 1.41 – 1.34 (m, 1.4H), 1.15 (dt, J = 12.7, 4.8 Hz, 0.5H), 0.97 (dddd, J = 13.2, 5.8, 4.2, 2.0 Hz, 0.6H).

^{13}C{^{1}H} NMR (126 MHz, CDCl$_3$) δ 175.6 (tr), 175.1 (mj), 174.9 (mn), 173.9 (mn), 173.7 (mj), 66.2 (mn), 66.0 (mj), 63.1 (tr), 52.3 (tr), 52.2 (mn), 52.2 (mj), 52.2 (mn), 52.1 (mj), 52.0 (tr), 49.7 (tr), 49.7 (mn), 49.1 (mj), 49.0 (mj), 48.3 (mn), 44.1 (mj), 43.4 (tr), 43.4 (mj), 42.1 (tr), 41.9 (mn), 41.7 (mn), 41.7 (tr), 40.6 (tr), 40.1 (mj), 39.4 (mn), 39.4 (tr), 35.2 (mj), 35.1 (mn), 33.4 (mn), 28.9 (mj), 27.4 (tr).

HRMS (ESI) m/z calcd. for C$_{12}$H$_{19}$O$_5$ ([M+H]$^+$): 243.1227; found: 243.1239.

2.4.4.3 Hydro-acyl group borrowing

Reaction of **1d** and **28** leading to compound **29**
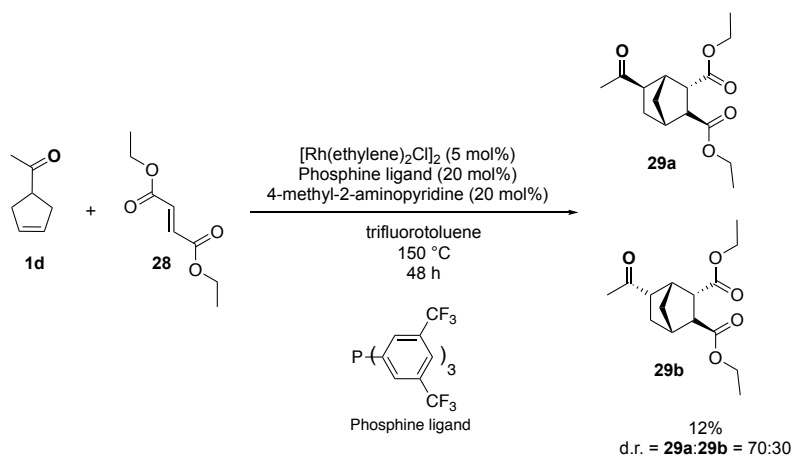
In a nitrogen filled glove box, four identical reactions were set up in parallel according to the following procedure: a 4 mL screw-cap vial was filled with 4-methyl-2-aminopyridine (4.3 mg, 40.0 μmol, 0.20 equiv.), [Rh(ethylene)$_2$Cl]$_2$ (3.9 mg, 10.0 μmol, 0.05 equiv.), tris[3,5-bis(trifluoromethyl)phenyl]phosphine (26.8 mg, 40.0 μmol, 0.20 equiv.), trifluorotoluene (150 μL), ketone **1d** (44.1 mg, 400 μmol, 2.00 equiv.), and diethyl fumarate **28** (34.4 mg, 32.7 μL, 200 μmol, 1.00 equiv.). The vial was removed from the glove box and placed in a pre-heated aluminum block (150 °C). The mixture was stirred at this temperature for 48 hours, before it was cooled to room temperature. The reaction solution was filtered over a small plug of silica, and the filter cake was washed with ethyl acetate (5 mL). The solvent was removed and a stock solution of hexadecane in CHCl$_3$ (0.5 M, 100 μL, 0.25 equiv.) was added. Calibrated GC analysis for the four reaction set ups was performed, leading to an average crude yield of 12%. As the determination of the crude d.r. proved to be difficult due to the complexity of the crude mixtures, the reaction set-ups were combined and subjected to column chromatography (silica, 0-50% ethyl acetate in petroleum ether). All fractions containing product were combined and analyzed by NMR spectroscopy to give a d.r. of two isomers **29a:29b** = 70/30.

29a

¹**H NMR** (500 MHz, CDCl₃) δ 4.27 – 4.10 (m, 4H), 3.33 – 3.25 (m, 1H), 2.87 – 2.83 (m, 1H), 2.81 – 2.76 (m, 1H), 2.63 – 2.58 (m, 1H), 2.55 – 2.47 (m, 1H), 2.15 (s, 3H), 2.04 – 1.95 (m, 1H), 1.54 – 1.40 (m, 2H), 1.32 – 1.24 (m, 7H).
¹³**C NMR** (126 MHz, CDCl₃) δ 208.73, 174.33, 173.04, 61.07, 61.00, 49.39, 49.20, 48.44, 43.26, 41.86, 35.57, 31.59, 28.82, 14.52, 14.33.

29b

¹**H NMR** (500 MHz, CDCl₃) δ 4.20 – 4.11 (m, 4H), 3.25 – 3.20 (m, 1H), 2.91 – 2.87 (m, 1H), 2.84 – 2.82 (m, 1H), 2.70 – 2.65 (m, 1H), 2.63 – 2.58 (m, 1H), 2.18 (s, 3H), 1.81 – 1.71 (m, 1H), 1.48 – 1.42 (m, 2H), 1.38 – 1.31 (m, 1H), 1.30 – 1.24 (m, 6H).
¹³**C NMR** (126 MHz, CDCl₃) δ 208.73, 173.93, 173.47, 61.17, 60.99, 53.54, 48.93, 48.92, 44.26, 40.19, 36.26, 29.01, 27.70, 14.47, 14.38.

2.4.5 Intramolecular catalytic reactions and isolation procedures

2.4.5.1 General procedure

In a nitrogen-filled glove box, an oven-dried 4 mL vial was charged sequentially with a solution of Ni(cod)₂ (0.86 mg, 3.13 µmol, 5 mol%) and DPEPhos (1.68 mg, 3.13 µmol, 5 mol%) in toluene (125 µL), unsaturated nitrile substrate (62.5 µmol, 1.00 equiv.) and 0.9 M solution of AlMe₂Cl in hexane (27.7 µL, 25.0 µmol, 40 mol%). The vial was closed tightly with a screw-cap and placed in a pre-heated heating plate at 50 °C for 48 hours. After cooling to room temperature, TMB was added as an internal standard. The reaction mixture was diluted with 2 mL of acetonitrile and filtrated through a plug of silica using ethyl acetate as an eluent. The crude yield was determined by NMR spectroscopy integrating the ester signal. The reaction mixture was concentrated *in vacuo* over Celite® and the residue subjected to flash column chromatography (silica, 0 - 20% methyl t-butyl ether in petroleum ether) yielding the corresponding product.

2.4.5.2 Catalytic reactions

Reaction of **15** leading to compound **16**
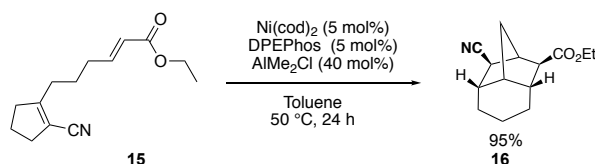
The reaction was performed according to the general procedure for intramolecular reactions **2.4.5.1**, starting from ethyl (*E*)-6-(5-cyanocyclopent-1-en-1-yl)hex-2-enoate **15** (14.6 mg, 62.5 µmol, 1.00 equiv.) and a reaction time of 24 hours. The crude yield as determined by NMR spectroscopy was 95%. After purification, the compound **16** (13.3 mg, 56.8 µmol, 91%) was isolated as a colorless oil.

16

¹**H NMR** (500 MHz, CDCl₃) δ 4.16 – 4.09 (m, 2H), 2.89 – 2.78 (m, 1H), 2.42 – 2.34 (m, 2H), 2.18 – 2.14 (m, 1H), 2.10 – 2.06 (m, 1H), 2.04 – 1.99 (m, 1H), 1.79 – 1.62 (m, 6H), 1.54 – 1.46 (m, 2H), 1.25 (td, *J* = 7.0, 1.9 Hz, 3H).
¹³**C{¹H} NMR** (126 MHz, CDCl₃) δ 174.3, 123.0, 60.9, 48.7, 46. 0, 41.3, 41.1, 38.5, 38.1, 34.2, 25.6, 25.6, 14.5, 14.4.
HRMS (ESI) m/z calcd for C₁₄H₂₀O₂N ([M+H]⁺): 234.1489, found 234.1487.
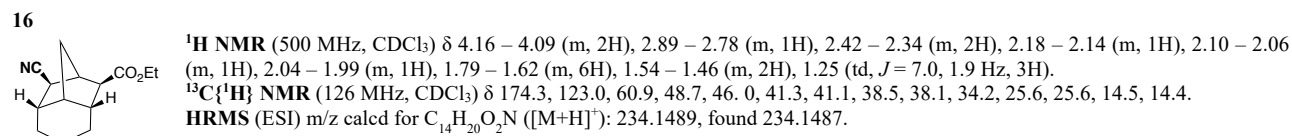
Reaction of **17** leading to compounds **18a-b**

The reaction was performed according to the general procedure for intramolecular reactions **2.4.5.1**, starting from ethyl (*E*)-6-(3-cyanocyclopent-1-en-1-yl)hex-2-enoate **17** (14.6 mg, 62.5 µmol, 1.00 equiv.) and a reaction time of 48 hours. The crude yield as determined by NMR spectroscopy was 94% (r.r. **18a**:**18b** = 46:54 (GC-FID)). After purification, compound **18a** (4.8 mg, 20.6 µmol, 33%) was isolated as a colorless oil, alongside compound **18b** (5.7 mg, 24.3 µmol, 39%) as a colorless oil.

18a
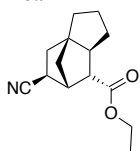
¹H NMR (500 MHz, CDCl₃) δ 4.15 (q, *J* = 7.1 Hz, 2H), 2.90 – 2.77 (m, 2H), 2.66 – 2.59 (m, 1H), 2.06 – 1.98 (m, 1H), 1.97 – 1.91 (m, 2H), 1.91 – 1.71 (m, 4H), 1.63 – 1.53 (m, 3H), 1.30 – 1.25 (m, 4H).
¹³C{¹H} NMR (126 MHz, CDCl₃) δ 173.7, 123. 6, 61.0, 57.2, 54.0, 49.4, 47.5, 41.2, 39.4, 32.7, 28.0, 26.9, 26.4, 14.4.
HRMS (ESI) m/z calcd for C₁₄H₂₀O₂N ([M+H]⁺): 234.1489 found 234.1486.

18b

¹H NMR (500 MHz, CDCl₃) δ 4.13 (q, *J* = 7.1 Hz, 2H), 2.69 – 2.56 (m, 2H), 2.53 – 2.44 (m, 1H), 2.11 – 2.00 (m, 2H), 1.99 – 1.72 (m, 6H), 1.66 – 1.57 (m, 2H), 1.28 – 1.23 (m, 4H).
¹³C{¹H} NMR (126 MHz, CDCl₃) δ 173.8, 122.8, 60.8, 60.4, 54.5, 49.7, 42.2, 41.1, 34.6, 32.7, 31.6, 27.5, 25.9, 14. 4.
HRMS (ESI) m/z calcd for C₁₄H₂₀O₂N ([M+H]⁺): 234.1489 found 234.1487.

Reaction of **19** leading to compounds **18a-b**
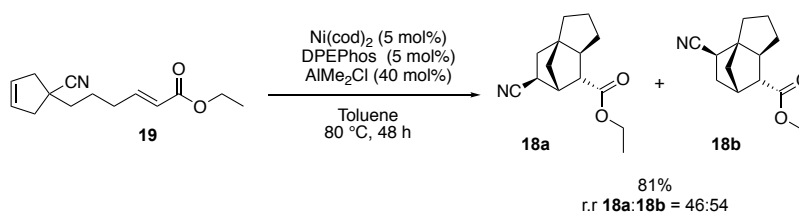
The reaction was performed according to the general procedure for intramolecular reactions **2.4.5.1**, starting from ethyl (*E*)-6-(1-cyanocyclopent-3-en-1-yl)hex-2-enoate **19** (14.6 mg, 62.5 µmol, 1.00 equiv.) with the following modifications: reaction was stirred at 80°C; after completion of 48 hours of reaction, the mixture was filtrated over a plug of basic alumina using diethyl ether as an eluent. The filtrate was evaporated, and the crude mixture resubmitted to identical reaction conditions at 80°C for another 48 hours due to incomplete conversion of the starting material. The crude yield as determined by NMR spectroscopy was 81% (r.r. **18a**:**18b** = 46:54 (GC-FID)).

Reaction of **20** leading to compounds **18a-b**
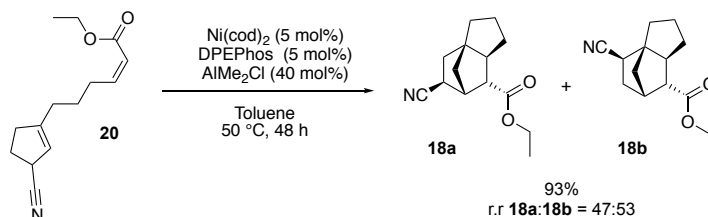
The reaction was performed according to the general procedure for intramolecular reactions **2.4.5.1**, starting from ethyl (*Z*)-6-(3-cyanocyclopent-1-en-1-yl)hex-2-enoate **20** (14.6 mg, 62.5 µmol, 1.00 equiv.) and a reaction time of 48 hours. The crude yield as determined by NMR spectroscopy was 93% (r.r. **18a**:**18b** = 47:53 (GC-FID)). After purification, compound **18a** (4.7 mg, 20.0 µmol, 32%) was isolated as a colorless oil, alongside compound **18b** (5.4 mg, 23.0 µmol, 37%) as a colorless oil.

Reaction of **21** leading to compounds **22a-c**
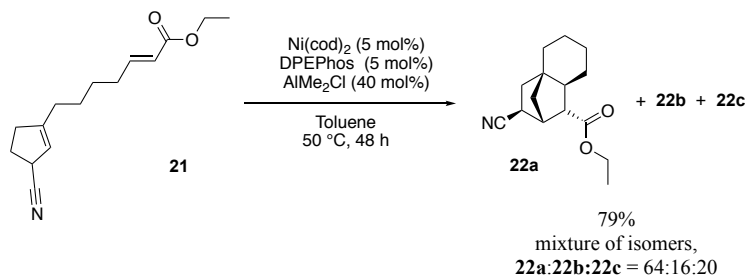
The reaction was performed according to the general procedure for intramolecular reactions **2.4.5.1**, starting from ethyl (*E*)-7-(3-cyanocyclopent-1-en-1-yl)hept-2-enoate **21** (15.4 mg, 62.5 µmol, 1.00 equiv.) and a reaction time of 48 hours. The crude yield as determined by NMR spectroscopy was 79% (mixture of isomers, **22a**:**22b**:**22c** = 64:16:20 (GC-FID)). After purification, only compound **22a** (7.1 mg, 28.7 µmol, 46%) was isolated as a colorless oil.

22a
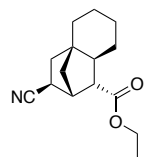
^{1}H NMR (500 MHz, CDCl$_3$) δ 4.14 (q, *J* = 7.2 Hz, 2H), 2.82 – 2.75 (m, 1H), 2.72 – 2.65 (m, 1H), 2.41 – 2.34 (m, 1H), 1.91 – 1.82 (m, 2H), 1.79 – 1.61 (m, 6H), 1.49 – 1.38 (m, 2H), 1.29 – 1.25 (m, 4H), 1.16 – 1.07 (m, 1H), 1.01 – 0.92 (m, 1H).
^{13}C{^{1}H} NMR (126 MHz, CDCl$_3$) δ 173.6, 123.5, 60.9, 53.8, 47.2, 45.7, 43.6, 43.0, 38.2, 33.5, 30.5, 27.4, 25.7, 24.0, 14.4.
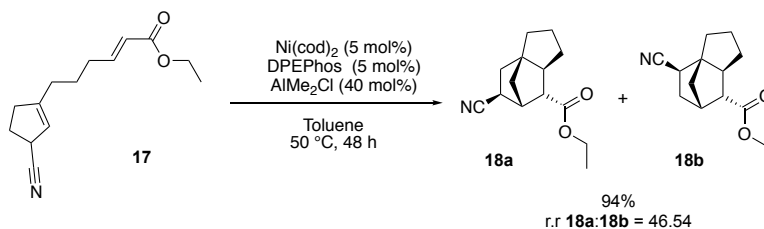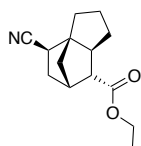**HRMS** (ESI) m/z calcd for C$_{15}$H$_{22}$O$_2$N ([M+H]$^+$): 248.1645, found 248.1655.

Reaction of **23** leading to compounds **24a-b**
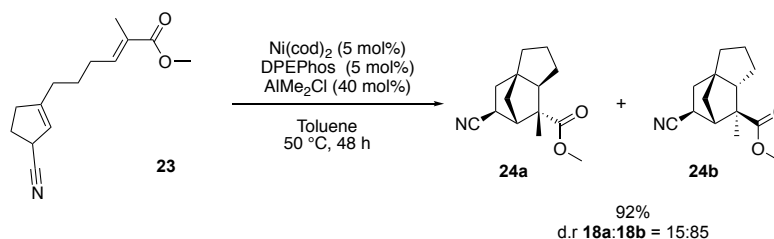
The reaction was performed according to the general procedure for intramolecular reactions **2.4.5.1**, starting from (*E*)-6-(3-cyanocyclopent-1-en-1-yl)-2-methylhex-2- **23** (14.6 mg, 62.5 µmol, 1.00 equiv.) and a reaction time of 48 hours. The crude yield as determined by NMR spectroscopy was 92% (d.r. **24a**:**24b** = 15:85 (GC-FID)). For the quantification of the isolated yield, two independent reaction batches (scale: 62.5 µmol) were combined yielding compound **24a** (4.6 mg, 19.7 µmol, 16%) as a colorless oil, alongside with compound **24b** (16.4 mg, 70.3 µmol, 56%) as a colorless oil after purification.

24a
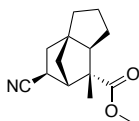
^{1}H NMR (500 MHz, CDCl$_3$) δ 3.71 (s, 3H), 2.56 – 2.51 (m, 1H), 2.50 – 2.47 (m, 1H), 2.32 – 2.25 (m, 1H), 1.89 – 1.64 (m, 7H), 1.61 – 1.54 (m, 1H), 1.52 – 1.48 (m, 1H), 1.45 – 1.38 (m, 1H), 1.23 (s, 3H).
^{13}C{^{1}H} NMR (126 MHz, CDCl$_3$) δ 177.4, 123.5, 56.8, 53. 5, 53.1, 53.0, 52.4, 39.1, 39.0, 28.9, 27.9, 27.1, 26.6, 21.6.
HRMS (ESI) m/z calcd for C$_{14}$H$_{20}$O$_2$N ([M+H]$^+$): 234.1489, found 234.1497.

24b
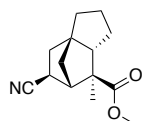
^{1}H NMR (500 MHz, CDCl$_3$) δ 3.68 (s, 3H), 2.50 – 2.42 (m, 1H), 2.42 – 2.36 (m, 1H), 2.28 – 2.22 (m, 1H), 1.90 – 1.66 (m, 8H), 1.54 – 1.50 (m, 1H), 1.47 – 1.40 (m, 1H), 1.22 (s, 3H).
^{13}C{^{1}H} NMR (126 MHz, CDCl$_3$) δ 177.6, 123.0, 60.2, 53.7, 53.2, 52.2, 47.8, 38.9, 34.3, 33.4, 27.4, 26.8, 26.7, 21.3.
HRMS (ESI) m/z calcd for C$_{14}$H$_{20}$O$_2$N ([M+H]$^+$): 234.1489, found 234.1498.

2.5 Computational studies

2.5.1 Density functional theory calculations

All DFT calculations[36] were performed with the *Gaussian09*[37] suite of programs. Geometries were optimized with the B3LYP functional[38–40] and the 6-31+G(d,p) basis set[41–47]. Stationary points were probed through vibrational analysis and Gibbs free energy corrections were performed under standard conditions (298.15 K, 1.0 atm). Transition states have been verified through Intrinsic Reaction Coordiante calculations (IRC) or optimization to minima at both sides of the frequency. Single point energy calculations including the effect of toluene as a solvent were performed with the B3LYP-D3BJ[38–40,48] functional including dispersion corrections, the SMD solvation model[49], and the larger 6-311+G(d,p)[41,43,47,50,51] basis set.

2.5.2 Computed Gibbs free energies values for Intramolecular Diels-Alder and H-shift reactions.

The feasibility of the intramolecular Diels-Alder reactions of substituted cyclopentadienes generated *in situ* upon retro-hydrofunctionalization was studied by DFT. The computed free energy barriers for the Diels-Alder reactions, non-catalyzed and catalyzed by AlMe2Cl for a model substrate leading to the three possible connectivities are shown in Figure 6. The predicted products for each pathway when catalyzed by AlMe2Cl are highlighted with dashed rectangular. All the computed structures are presented in charts 1 to 4.
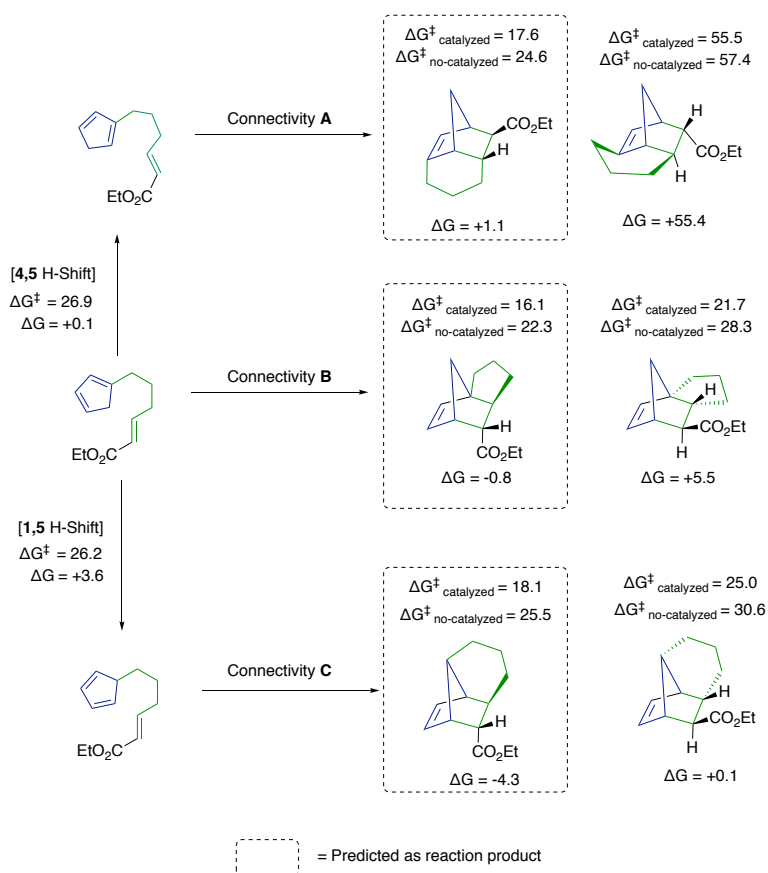
Figure 6. Intramolecular reactions of substituted cyclopentadienes generated *in situ* upon hydro-functional group borrowing, leading to three possible connectivities A, B or C. Free energy barriers in kcal/mol for Intramolecular Diels-Alder and H-shift reactions. Calculations have been performed at the B3LYP-D3BJ/6-311++G(d,p)(SMD)//B3LYP/6-31+G(d,p) level of theory in toluene as solvent; SMD, solvation model based on density.

Connectivity	Structure	Imaginary Freq. (cm-1)	Gcorr	G$_{298}$ gas phase	E0, toluene	G$_{298}$toluene
A	A1	-	0.235293	-656.454705	-656.8951093	-656.6598163
	TSA1_endo	-258.30	0.245878	-656.354577	-656.8142654	-656.5683874
	PA1_endo	-	0.247369	-656.358618	-656.8187566	-656.5713876
	TSA1_exo	-411.58	0.242546	-656.406027	-656.8631466	-656.6206006
	PA1_exo	-	0.247791	-656.445692	-656.9058473	-656.6580563
	A1_LA	-	0.349855	-1517.557561	-1518.228673	-1517.878818
	TSA1_endo_LA	-243.86	0.362659	-1517.458383	-1518.1532	-1517.790541
	PA1_endo_LA	-	0.362645	-1517.458803	-1518.152877	-1517.790232
	TSA1_exo_LA	-312.65	0.358374	-1517.515906	-1518.209188	-1517.850814
	PA1_exo_LA	-	0.363666	-1517.544494	-1518.239425	-1517.875759
B	B1	-	0.235581	-656.455049	-656.8954852	-656.6599042
	TSB1_endo	-446.23	0.242428	-656.409534	-656.8667653	-656.6243373
	PB1_endo	-	0.246199	-656.449497	-656.9073758	-656.6611768
	TSB1_exo	-439.36	0.242228	-656.400137	-656.8570997	-656.6148717
	PB1_exo	-	0.2468	-656.439373	-656.8980036	-656.6512036
	B1_LA	-	0.349634	-1517.557131	-1518.228258	-1517.878624
	TSB1_endo_LA	-370.27	0.358215	-1517.518741	-1518.211251	-1517.853036
	PB1_endo_LA	-	0.362291	-1517.549158	-1518.241969	-1517.879678
	TSB1_exo_LA	-345.22	0.357625	-1517.509505	-1518.201646	-1517.844021
	PB1_exo_LA	-	0.362415	-1517.539357	-1518.232608	-1517.870193
C	C1	-	0.236299	-656.449323	-656.8905235	-656.6542245
	TSC1_endo	-427.85	0.243098	-656.397142	-656.8567538	-656.6136558
	PC1_endo	-	0.247611	-656.447386	-656.9087554	-656.6611444
	TSC1_exo	-459.83	0.243749	-656.389019	-656.8492069	-656.6054579
	PC1_exo	-	0.248674	-656.439633	-656.9027174	-656.6540434
	C1_LA	-	0.35056	-1517.550966	-1518.223322	-1517.872762
	TSC1_endo_LA	-363.41	0.35785	-1517.507417	-1518.201836	-1517.843986
	PC1_endo_LA	-	0.363586	-1517.547554	-1518.244056	-1517.88047
	TSC1_exo_LA	-279.74	0.360082	-1517.40269	-1518.097403	-1517.737321
	PC1_exo_LA	-	0.36179	-1517.409214	-1518.102351	-1517.740561
[4,5]-H-shift	A1_B1_TS	-1238.92	0.231577	-656.41202	-656.8485884	-656.6170114
[1,5]-H-shift	B1_C1_TS	-1194.05	0.232256	-656.41324	-656.8504488	-656.6181928

Table 5. Computed values of imaginary frequencies (for transition states). G_{corr} is the thermal correction to Gibbs Free Energy. $G_{298\ gas\ phase}$ is the sum of electronic and thermal free energies at B3LYP/6-31+G(d,p) in gas phase; E_0 is the electronic energies obtained at B3LYP-D3BJ/6-311++G(d,p)(SMD) level of theory in toluene as solvent; SMD, solvation model based on density. $G_{298\ toluene}$ is the sum of E_0 and G_{corr}.

2.6 References

(1)   Lichosyt, D.; Zhang, Y.; Hurej, K.; Dydio, P. Dual-Catalytic Transition Metal Systems for Functionalization of Unreactive Sites of Molecules. *Nat. Catal.* **2019**, *2* (2), 114–122.

(2)   Bhawal, B. N.; Morandi, B. Catalytic Transfer Functionalization through Shuttle Catalysis. *ACS Catal.* **2016**, *6* (11), 7528–7535.

(3)   Wang, D.; Astruc, D. The Golden Age of Transfer Hydrogenation. *Chem. Rev.* **2015**, *115* (13), 6621–6686.

(4)   Baráth, E. Hydrogen Transfer Reactions of Carbonyls, Alkynes, and Alkenes with Noble Metals in the Presence of Alcohols/Ethers and Amines as Hydrogen Donors. *Catalysts* **2018**, *8* (12), 671.

(5)   Morimoto, T.; Fuji, K.; Tsutsumi, K.; Kakiuchi, K. CO-Transfer Carbonylation Reactions. A Catalytic Pauson−Khand-Type Reaction of Enynes with Aldehydes as a Source of Carbon Monoxide. *J. Am. Chem. Soc.* **2002**, *124* (15), 3806–3807.

(6)   Fang, X.; Yu, P.; Morandi, B. Catalytic Reversible Alkene-Nitrile Interconversion through Controllable Transfer Hydrocyanation. *Science* **2016**, *351* (6275), 832–836.

(7)   K., M. S.; Jung-Woo, P.; A., C. F.; M., D. V. Rh-Catalyzed C–C Bond Cleavage by Transfer Hydroformylation. *Science* **2015**, *347* (6217), 56–60.

(8)   Tan, G.; Wu, Y.; Shi, Y.; You, J. Syngas-Free Highly Regioselective Rhodium-Catalyzed Transfer Hydroformylation of Alkynes to α,Β-Unsaturated Aldehydes. *Angew. Chem. Int. Ed.* **2019**, *58* (22), 7440–7444.

(9)   Jun, C.-H.; Lee, H. Catalytic Carbon−Carbon Bond Activation of Unstrained Ketone by Soluble Transition-Metal Complex. *J. Am. Chem. Soc.* **1999**, *121* (4), 880–881.
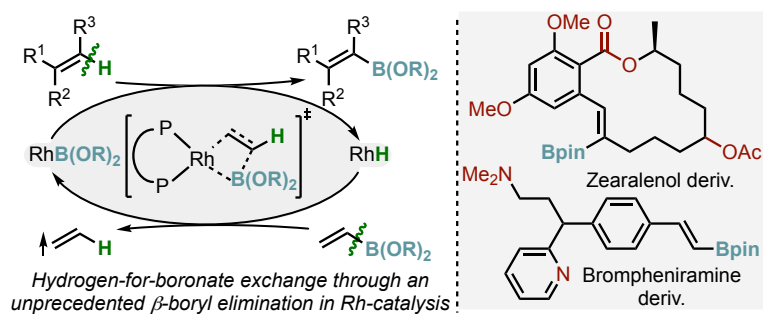
(10)   Martínez, S.; Veth, L.; Lainer, B.; Dydio, P. Challenges and Opportunities in Multicatalysis. *ACS Catal.* **2021**, *11* (7), 3891–3915.

(11)   Reed-Berendt, B. G.; Latham, D. E.; Dambatta, M. B.; Morrill, L. C. Borrowing Hydrogen for Organic Synthesis. *ACS Cent. Sci.* **2021**, *7* (4), 570–585.

(12)   Corma, A.; Navas, J.; Sabater, M. J. Advances in One-Pot Synthesis through Borrowing Hydrogen Catalysis. *Chem. Rev.* **2018**, *118* (4), 1410–1459.

(13)   Stille, J. R.; Grubbs, R. H. Intramolecular Diels-Alder Reaction of .Alpha.,.Beta.-Unsaturated Ester Dienophiles with Cyclopentadiene and the Dependence on Tether Length. *J. Org. Chem.* **1989**, *54* (2), 434–444.

(14)   Landry, D. W. Total Synthesis of 14-Cedranediol. *Tetrahedron* **1983**, *39* (17), 2761–2768.

(15)   Johnson, C. R.; Keiser, J. E.; Sharp, J. C. Chemistry of Sulfoxides and Related Compounds. XIII. Synthesis of 2-Thiabicyclo[2.2.1]Heptane Derivatives. *J. Org. Chem.* **1969**, *34* (4), 860–864.

(16)   Emmons, W. D. The Preparation and Properties of Oxaziranes. *J. Am. Chem. Soc.* **1957**, *79* (21), 5739–5754.

(17)   Cui, X.-Y.; Ge, Y.; Tan, S. M.; Jiang, H.; Tan, D.; Lu, Y.; Lee, R.; Tan, C.-H. (Guanidine)Copper Complex-Catalyzed Enantioselective Dynamic Kinetic Allylic Alkynylation under Biphasic Condition. *J. Am. Chem. Soc.* **2018**, *140* (27), 8448–8455.

(18)   Colombini, M.; Crotti, P.; Di Bussolo, V.; Favero, L.; Gardelli, C.; Macchia, F.; Pineschi, M. Regiochemical Control of the Ring Opening of 1,2-Epoxides by Means of Chelating Processes.9. Synthesis and Ring Opening Reactions of Cis- and Trans-Oxides Derived from 3-(Benzyloxymethyl)Cyclopentene and Methyl 2-Cyclopenten-1-Carboxylate 1. *Tetrahedron* **1995**, *51* (29), 8089–8112.

(19)   Olah, G. A.; Prakash, G. K. S.; Arvanaghi, M.; Anet, F. A. L. High-Field 1H and 13C NMR Spectroscopic Study of the 2-Norbornyl Cation1a. *J. Am. Chem. Soc.* **1982**, *104* (25), 7105–7108.

(20)   Depres, J. P.; Greene, A. E. Improved Selectivity in the Preparation of Some 1,1-Difunctionalized 3-Cyclopentenes. High Yield Synthesis of 3-Cyclopentenecarboxylic Acid. *J. Org. Chem.* **1984**, *49* (5), 928–931.

(21)   Hu, H.; Faraldos, J. A.; Coates, R. M. Scope and Mechanism of Intramolecular Aziridination of Cyclopent-3-Enyl-Methylamines to 1-Azatricyclo[2.2.1.02,6]Heptanes with Lead Tetraacetate. *J. Am. Chem. Soc.* **2009**, *131* (33), 11998–12006.

(22)   Wu, H.; Wang, Q.; Zhu, J. Copper-Catalyzed Enantioselective Arylative Desymmetrization of Prochiral Cyclopentenes with Diaryliodonium Salts. *Angew. Chem. Int. Ed Engl.* **2018**, *57* (10), 2721–2725.

(23)   Zoutendam, P. H.; Kissinger, P. T. Novel Electrohydrodimerization of N-Substituted Maleimides in Aqueous Media. *J. Org. Chem.* **1979**, *44* (5), 758–761.

(24)   Yamashita, Y.; Maki, D.; Sakurai, S.; Fuse, T.; Matsumoto, S.; Akazome, M. Preparation of Chiral 3-Oxocycloalkanecarbonitrile and Its Derivatives by Crystallization-Induced Diastereomer Transformation of Ketals with Chiral 1,2-Diphenylethane-1,2-Diol. *RSC Adv.* **2018**, *8* (57), 32601–32609.

(25)   Farcasiu, D.; Schleyer, P. V. R.; Ledlie, D. B. Ring Enlargements by Thallium(III) Oxidation of Double Bonds. Application to Adamantane Systems. *J. Org. Chem.* **1973**, *38* (20), 3455–3459.

(26)   Stanislawski, P. C.; Willis, A. C.; Banwell, M. G. New Protocols for the Assembly of the Tetracyclic Framework Associated with the Aromatic Erythrina Alkaloids. *Org. Lett.* **2006**, *8* (10), 2143–2146.

(27)   Ingenito, R.; Burton, C.; Langella, A.; Chen, X.; Zytko, K.; Pessi, A.; Wang, J.; Bianchi, E. Novel Potent ApoA-I Peptide Mimetics That Stimulate Cholesterol Efflux and Pre-β Particle Formation in Vitro. *Bioorg. Med. Chem. Lett.* **2010**, *20* (1), 236–239.

(28)   Bunce, R. A.; Peeples, C. J.; Jones, P. B. Tandem SN2-Michael Reactions for the Preparation of Simple Five- and Six-Membered-Ring Nitrogen and Sulfur Heterocycles. *J. Org. Chem.* **1992**, *57* (6), 1727–1733.

(29)   Bhat, V.; Welin, E. R.; Guo, X.; Stoltz, B. M. Advances in Stereoconvergent Catalysis from 2005 to 2015: Transition-Metal-Mediated Stereoablative Reactions, Dynamic Kinetic Resolutions, and Dynamic Kinetic Asymmetric Transformations. *Chem. Rev.* **2017**, *117* (5), 4528–4561.

(30)   Nikitas, N. F.; Triandafillidi, I.; Kokotos, C. G. Photo-Organocatalytic Synthesis of Acetals from Aldehydes. *Green Chem.* **2019**, *21* (3), 669–674.

(31)   Suzuki, J.; Miyano, N.; Yashiro, S.; Umezawa, T.; Matsuda, F. Total Synthesis of (−)-Kainic Acid and (+)-Allo-Kainic Acid through SmI2-Mediated Intramolecular Coupling between Allyl Chloride and an α,β-Unsaturated Ester. *Org. Biomol. Chem.* **2017**, *15* (31), 6557–6566.

(32)   Ohfusa, T.; Nishida, A. Reactivity and Stereoselectivity of the Diels–Alder Reaction Using Cyclic Dienophiles and Siloxyaminobutadienes. *Tetrahedron* **2011**, *67* (10), 1893–1906.

(33)   Bull, J. A.; Charette, A. B. Intramolecular Simmons−Smith Cyclopropanation. Studies into the Reactivity of Alkyl-Substituted Zinc Carbenoids, Effect of Directing Groups and Synthesis of Bicyclo[n.1.0]Alkanes. *J. Am. Chem. Soc.* **2010**, *132* (6), 1895–1902.

(34)   Molander, G. A.; Yokoyama, Y. One-Pot Synthesis of Trisubstituted Conjugated Dienes via Sequential Suzuki−Miyaura Cross-Coupling with Alkenyl- and Alkyltrifluoroborates. *J. Org. Chem.* **2006**, *71* (6), 2493–2498.

(35)   Wrackmeyer, B. Organoboron Chemistry. In *Modern Magnetic Resonance*; Springer, 2008; pp 455–457.

(36)   Cramer, C. J.; Truhlar, D. G. Density Functional Theory for Transition Metals and Transition Metal Chemistry. *Phys. Chem. Chem. Phys.* **2009**, *11* (46), 10757–10816.

(37)   Frisch, M. J.; Trucks, G. W.; Schlegel, H. B.; Scuseria, G. E.; Robb, M. A.; Cheeseman, J. R.; Scalmani, G.; Barone, V.; Mennucci, B.; Petersson, G. A.; Nakatsuji, H.; Caricato, M.; Li, X.; Hratchian, H. P.; Izmaylov, A. F.; Bloino, J.; Zheng, G.; Sonnenb, D. J. *Gaussian 09*; Gaussian, Inc: Wallingford CT, 2009.

(38)   Becke, A. D. Density-Functional Thermochemistry. III. The Role of Exact Exchange. *J. Chem. Phys.* **1993**, *98*, 5648–5652.

(39)   Becke, A. D. Density-Functional Exchange-Energy Approximation with Correct Asymptotic Behavior. *Phys. Rev. A* **1988**, *38* (6), 3098–3100.

(40)   Lee, C.; Yang, W.; Parr, R. G. Development of the Colle-Salvetti Correlation-Energy Formula into a Functional of the Electron Density. *Phys. Rev. B* **1988**, *37* (2), 785–789.

(41)   Clark, T.; Chandrasekhar, J.; Spitznagel, G. W.; Schleyer, P. V. R. Efficient Diffuse Function-Augmented Basis Sets for Anion Calculations. III. The 3-21+G Basis Set for First-Row Elements, Li–F. *J. Comput. Chem.* **1983**, *4* (3), 294–301.

(42)   Ditchfield, R.; Hehre, W. J.; Pople, J. A. Self-Consistent Molecular-Orbital Methods. IX. An Extended Gaussian-Type Basis for Molecular-Orbital Studies of Organic Molecules. *J. Chem. Phys.* **1971**, *54* (2), 724–728.

(43)   Francl, M. M.; Pietro, W. J.; Hehre, W. J.; Binkley, J. S.; Gordon, M. S.; DeFrees, D. J.; Pople, J. A. Self-consistent Molecular Orbital Methods. XXIII. A Polarization-type Basis Set for Second-row Elements. *J. Chem. Phys.* **1982**, *77* (7), 3654–3665.

(44)   Gordon, M. S.; Binkley, J. S.; Pople, J. A.; Pietro, W. J.; Hehre, W. J. Self-Consistent Molecular-Orbital Methods. 22. Small Split-Valence Basis Sets for Second-Row Elements. *J. Am. Chem. Soc.* **1982**, *104* (10), 2797–2803.

(45)   Hariharan, P. C.; Pople, J. A. The Influence of Polarization Functions on Molecular Orbital Hydrogenation Energies. *Theor. Chim. Acta* **1973**, *28* (3), 213–222.

(46)   Hehre, W. J.; Ditchfield, R.; Pople, J. A. Self—Consistent Molecular Orbital Methods. XII. Further Extensions of Gaussian—Type Basis Sets for Use in Molecular Orbital Studies of Organic Molecules. *J. Chem. Phys.* **1972**, *56* (5), 2257–2261.

(47)   Spitznagel, G. W.; Clark, T.; von Ragué Schleyer, P.; Hehre, W. J. An Evaluation of the Performance of Diffuse Function-Augmented Basis Sets for Second Row Elements, Na-Cl. *J. Comput. Chem.* **1987**, *8* (8), 1109–1116.

(48)   Grimme, S.; Ehrlich, S.; Goerigk, L. Effect of the Damping Function in Dispersion Corrected Density Functional Theory. *J. Comput. Chem.* **2011**, *32* (7), 1456–1465.

(49)   Marenich, A. V.; Cramer, C. J.; Truhlar, D. G. Universal Solvation Model Based on Solute Electron Density and on a Continuum Model of the Solvent Defined by the Bulk Dielectric Constant and Atomic Surface Tensions. *J. Phys. Chem. B* **2009**, *113* (18), 6378–6396.

(50)   Krishnan, R.; Binkley, J. S.; Seeger, R.; Pople, J. A. Self-consistent Molecular Orbital Methods. XX. A Basis Set for Correlated Wave Functions. *J. Chem. Phys.* **1980**, *72* (1), 650–654.

(51)   McLean, A. D.; Chandler, G. S. Contracted Gaussian Basis Sets for Molecular Calculations. I. Second Row Atoms, Z=11–18. *J. Chem. Phys.* **1980**, *72* (10), 5639–5648.

CHAPTER 3

Transfer C-H Borylation of Alkenes under Rh(I)-Catalysis: Insight into the Synthetic Capacity, Mechanism & Selectivity-Control

3.1 Introduction

   Given the pharmacophoric properties of boronic acid derivatives[1–3] as well as the multitude of methods to convert a C−B bond into a C−C or C−X bond,[4–7] the ability to install a boronic ester group by a selective functionalization of one of the C−H bonds in available starting materials is highly appealing for both modular synthesis of functional materials and late-stage functionalization of complex molecules.[8] While the borylation of aromatic and aliphatic C−H bonds has been extensively studied,[9–14] the direct borylation of vinylic C−H bonds remains underdeveloped with no general method being available, despite the presence of these motifs in various synthetic and natural compounds (Figure 1a).[15–17]
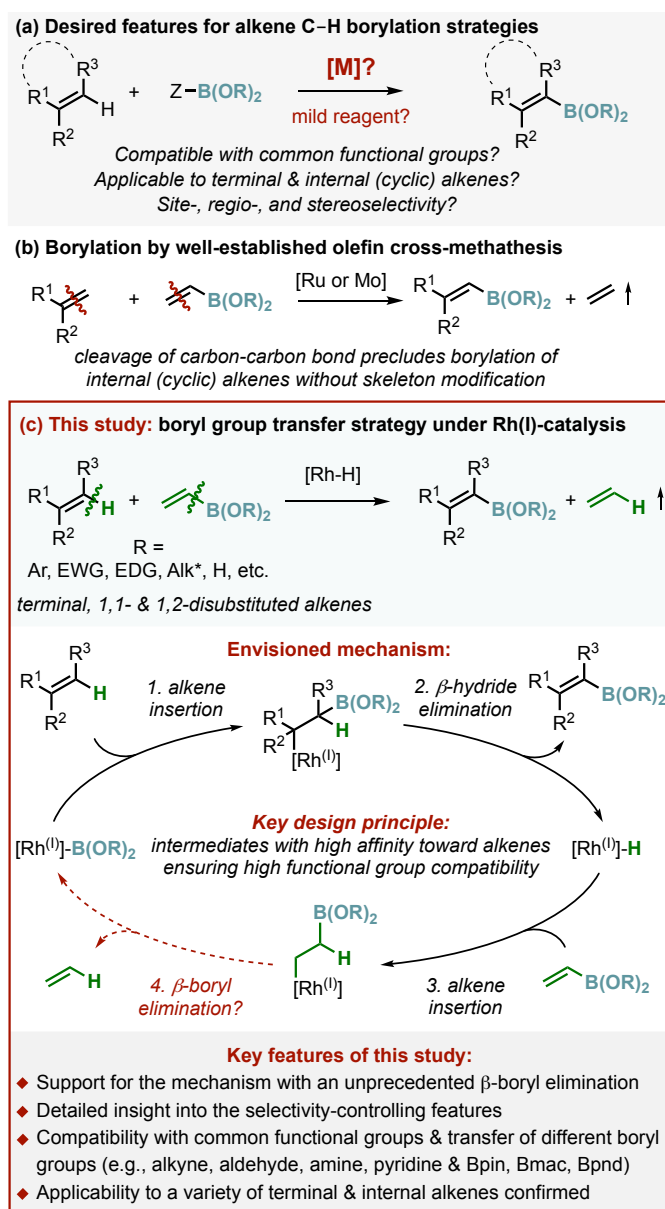

Figure 1. Context of this work. (a) C–H borylation of alkenes with appealing features for fine-chemical synthesis, (b) state of the art – alkene cross-metathesis, (c) transfer borylation reaction under Rh(I)-catalysis – summary of this work. * When thermodynamically favored, the isomerization of the double bond across an alkyl group is detrimental for the reaction.

In that context, alkene cross-metathesis employing a simple vinyl boronate ester as a reagent[18–22] enables formal C−H bond borylation of terminal alkenes under mild conditions and with high atom-economy (Figure 1b); thereby the strategy has found numerous applications in fine-chemical synthesis.[23–27] However, when the initial carbon skeleton is to be maintained, the approach is unsuitable for the borylation of substrates bearing internal alkenes, e.g., many (macrocyclic) natural products. In contrast, the boryl-Heck[28–30] and dehydrogenative[31–44] protocols were reported to be applicable to the C−H borylation of terminal and internal alkene starting materials. Still, the synthetic utility of these reactions is often limited. In the case of the boryl-Heck reaction, the use of Cl-Bcat or Br-Bcat as the borylation reagent leads to the inevitable incompatibility with many nucleophilic functional groups, including soft nucleophiles, such as enolizable ketones or esters, in addition to amines or alcohols. Also, the involvement of multiple reagents and a post-synthetic transesterification of unstable Bcat products further diminishes the atom-economy of the protocol. In turn, dehydrogenative borylation methods often suffer from competitive hydrogenation and hydroboration side-reactions. In addition, these processes involve high-valent metal-hydride intermediates, which need to be either quenched by a sacrificial reagent or undergo an extrusion of dihydrogen. Therefore, starting materials bearing functional groups of high reactivity towards such metal-hydrides are inherently incompatible.

Functional group transfer catalysis[45] that would mediate the exchange of hydrogen for a boryl group between starting materials could enrich the scope of strategies for C−H bond borylation by being applicable to both terminal and internal alkene starting materials, while at the same time employing a benign reagent as a boryl group donor, ensuring a tolerance toward a broad range of functional groups and high atom-economy of the process (Figure 1c).[46] Although, Marciniec[47,48] and Wu[44] reported a boryl group transfer between boryl group donors and alkenes in the presence of [RuHCl(CO)(PCy$_3$)$_2$] or [Cp$_2$ZrH$_2$], the reported scopes of these methods remain restricted to simple monosubstituted alkenes, such as styrene and its derivatives bearing a limited range of functional groups (i.e., halogens, alkyl, and alkoxy substituents).[44,47,49–51] For instance, no examples of starting materials containing an internal double bond or bearing other common functional groups, such as alkynes, aldehydes, ketones, amides, or any heterocycles, were reported to be productive, and thus these methods found no practical applications in fine-chemical synthesis so far. Further, limited mechanistic insight into the boryl group transfer catalysis hinders rational development of these protocols toward synthetic applications.[52]

We hypothesized that phosphine-Rh(I)-complexes would be the catalysts of choice for a chemoselective boryl group transfer that would occur in a proposed catalytic cycle involving a series of alkene insertion and β-elimination steps, as shown in Figure 1c. Our reasoning was as follows: (i) In stoichiometric experiments, a Rh(I)-boryl complex reacted with styrene to form Rh(I)-hydride and styryl boronate ester,[53] indicating the feasibility of two elementary steps of the proposed catalytic cycle (steps 1,2). In turn, (ii) Rh(I)-hydrides are known to react selectively with alkenes to form Rh(I)-alkyl species tolerating a broad range of functional groups (step 3).[54–57] (iii) Although the final elementary step, the β-boryl elimination, (step 4), is unreported for Rh-complexes, microscopic reversibility for the reverse step, i.e., an alkene insertion into a Rh(I)-B bond,[53,58] supported its feasibility.[59–61] (iv) Lastly, the engagement of only low-valent Rh(I)-intermediates obviates otherwise impeding side-reactions based on reductive-elimination reactivity of high-valent complexes, such as competitive hydroboration or hydrogenation. The chemoselectivity of the alkene insertion into a Rh(I)-B bond remained an open question.[62–67]

Here we report our studies establishing the development, mechanism, and key features of transfer C−H borylation of alkenes under Rh(I)-catalysis. The method proved to be applicable not only to terminal but also to so far challenging internal alkene starting materials and compatible with a broad range of functional groups, including motifs that are typically problematic using established approaches. A series of experimental mechanistic studies, corroborated by DFT calculations, provided insight into the details of the catalytic cycle that introduces the thus far unreported yet relatively fast β-boryl elimination step engaging the Rh(I)-(β-borylalkyl) intermediate. Further, the studies revealed the rate and selectivity determining aspects of the reaction. The studies set the stage for developing new valuable hydrogen-for-functional group exchange transformations for fine-chemical synthesis.

3.2 Results and Discussion

3.2.1 Catalyst formulation

We commenced our studies by evaluating the feasibility of the devised reactivity in a model reaction of styrene **1a** with vinyl boronate pinacol ester **2** forming product **3a**. To identify a suitable catalyst, we considered precursors that could form the prospective species that operate in the catalytic cycle, i.e., either a Rh(I)-hydride or a Rh(I)-boryl complex (Figure 1c). We selected phosphine-Rh(I)-alkoxide complexes, which were reported to form coordinatively unsaturated Rh(I)-hydride species through migratory insertion of an olefin into the Rh−O bond and subsequent β-hydride elimination.[68,69]
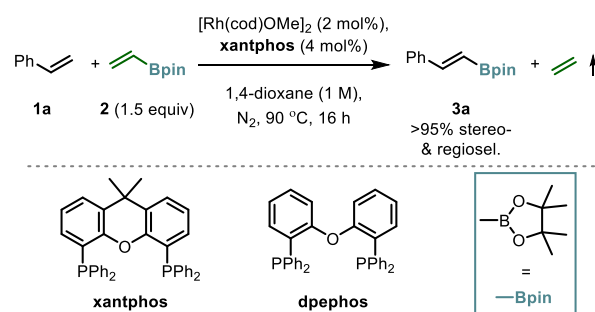
entry	variations from standard conditions	yield (%)[a]
1	none	92 (81)[b]
2	[Rh(cod)Cl]$_2$ as precursor[c]	<2
3	[Rh(cod)Cl]$_2$ + NaOMe as precursor[c]	92
4	[Rh(cod)Cl]$_2$ + NaOtBu as precursor[c]	92
5	no [Rh(cod)OMe]$_2$	<2
6	no xantphos	18
7	**dpephos** instead of **xantphos**	<2
8	1/2 cat. loading	<2
9	1/2 cat. loading + 5 mol% B$_2$pin$_2$	92
10	1/8 cat. loading + 1.2 mol% B$_2$pin$_2$	81

Table 1. Evaluation of reaction conditions [a] Yield determined by ^{1}H NMR analysis of the reaction mixture with an internal standard; [b] yield of isolated material by a column chromatography purification; [c] instead of [Rh(cod)OMe]$_2$; 1 : 1 ratio of Rh to sodium alkoxide. For reactions with other phosphine ligands and reaction conditions, see section 3.5.2.2 and Table 3.

Upon evaluation of a range of complexes of different phosphine ligands and conditions (Table 1, Tables 2-4), we found that the model reaction of **1a** with **2** (1.5 equiv) in the presence of [Rh(cod)OMe]$_2$ and xantphos formed product **3a** in 92% NMR yield (81% yield of isolated material; entry 1), confirming the successful reaction design. Importantly, no other isomers of the product were observed. It should be noted that, because this isodesmic reaction is merely exergonic (ΔG^o = -0.57 kcal/mol),[70] the release of the gaseous ethene by-product is a driving force of the reaction. The formation of ethene was confirmed by in situ NMR spectroscopy.[70]

The phosphine-Rh(I)-alkoxide complex is key to the catalytic activity, as confirmed in a series of control experiments (Table 1). No reaction was observed with [Rh(cod)Cl]$_2$ in place of [Rh(cod)OMe]$_2$ (entry 2). However, the catalytic activity was recovered when [Rh(cod)Cl]$_2$ was used with a variety of alkoxide salts (entries 3-4 and Table 2) that formed the rhodium(I)-alkoxide complexes in situ. No reaction occurred in the absence of the rhodium precursor (entry 5), but low activity of the rhodium(I)-alkoxide precursor was maintained in the absence of any phosphine ligand (18% yield, entry 6).
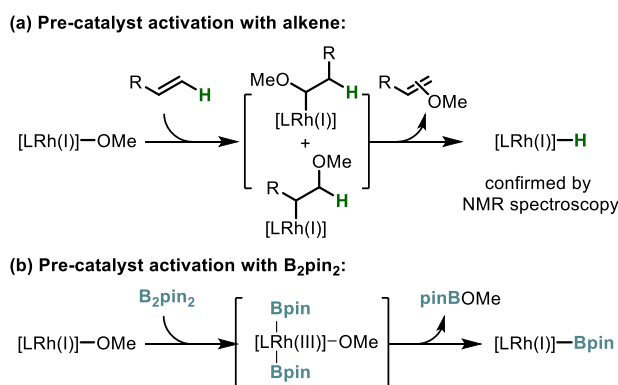
Scheme 1. Different modes of pre-catalyst activation

The formation of a catalytic Rh(I)-hydride species via migratory insertion of an alkene into the Rh(I)-alkoxide bond and β-hydride elimination was confirmed in stochiometric NMR experiments (Scheme 1a); however, the process is not quantitative. As judged by the characteristic hydride signal at -12.4 ppm in the ^{1}H NMR spectrum, up to 16% of a Rh-hydride species was formed after 2 h at 22 °C in the stoichiometric reactions of alkene **1a** with xantphos-Rh(I)-alkoxide containing either the MeO or tBuO ligand. No increase of the yield of the Rh-hydride was observed upon further reaction at this or elevated temperatures, but a mixture of other unidentified complexes was formed as judged by ^{31}P NMR spectroscopy.[70]

We found that catalytic amounts of B$_2$pin$_2$ are beneficial for the rate of the catalytic reaction. Most likely, the addition of B$_2$pin$_2$ enables an alternative pathway of the pre-catalyst activation by the facile formation of the other catalytic intermediate of the cycle, i.e. the Rh(I)-Bpin complex, in a sequence of oxidative addition of B$_2$pin$_2$ and reductive elimination of MeOBpin (Scheme 1b).[71] Noteworthy, a control catalytic reaction of **1a** with a stoichiometric amount of B$_2$pin$_2$ in the absence of vinyl Bpin **2** formed only trace of product **3a**, in line with B$_2$pin$_2$ acting as a pre-catalyst activator rather than an alternative stochiometric boryl group donor. Most importantly, the use of co-catalytic amounts of B$_2$pin$_2$ additive enables to lower the catalyst loading substantially (Table 1, entries 1 and 8-10).

3.2.2 Synthetic Capacity

With the established conditions in hand, we evaluated the reaction with respect to its functional group compatibility, its applicability to sterically and electronically varied olefines, including natural products and bioactive materials, as well as its ability to transfer different boryl groups (Figure 2). We established the following:

The method is compatible with a broad variety of functional groups (**1b-1q**) and heteroaromatic moieties (**1r-1u**). Particularly noteworthy is the compatibility with aldehydes **1b**, alkynes **1p**, **1q**, amines **1c**, **1d**, and pyridines **1r**, **1s**, which are often problematic in borylation protocols,[15] due to either their ability to inhibit the catalyst or their intrinsic incompatibility with reagents (e.g., HBpin) or catalytic intermediates (e.g., Ru(II)- or Rh(III)-hydrides). We found that although acidic NH, OH, or CH groups are problematic (Figure 14), they can be effectivly protected, as observed in experiments with alkenes **1d**, **1k**, **1l**, and **1q**. It is worth noting that in initial reactions of alkynes **1p** or **1q** with donor **2**, a competitive ene-yne coupling was observed;[72,73] however, the use of vinyl (*E*)-1,2-bisboronate **4** in place of donor **2** prevented these side-reactions. Inter se, alkene **1v** that contains an alkyl-benzyl alkyne moiety reacted to form boryl derivative **3v** bearing a (non-borylated) 1,3-diene motif, revealing the alkyne-isomerization activity[74] of this Rh-catalyst as well as a high selectivity of the catalyst towards terminal mono alkenes over dienes.

The method is applicable to a range of olefins bearing electronically (**1w-1aa**) and sterically (e.g., **1ab**) varied double bonds and different substitution patterns, including 1,1- and 1,2-disubstituted alkenes **1ac-1an**. It is noteworthy that the borylation of enamides like **1x-1aa** have been thus far rather underdeveloped, with only a single substrate being borylated in a synthetically useful yield.[37,38,47,75] In reactions of starting materials **1ab-1an**, the presence of co-catalytic B$_2$pin$_2$ was essential for the efficient catalytic activity; presumably alkenes **1ab-1an** are not able to activate the pre-catalyst efficiently due to their hindered insertion into the Rh−O bond. In case of 1,1-disubstituted alkenes, the stereoselectivity of the reaction seems to be controlled by steric effects. Unsymmetric alkenes **1ag-1aj** bearing two aryl rings of similar size, that is, phenyl rings with varied substituents in (remote) para or meta positions, reacted to form close to equimolar mixtures of stereoisomeric products irrespectively of the electronic effects. On the other hand, alkenes **1ac**, **1ae**, and **1ak** bearing one phenyl and one methyl, trifluoromethyl, or 2-thiophene ring furnished one isomer of the product preferentially with a synthetically useful stereoselectivity (77 to 90%). Similarly, 1,2-disubstituted alkenes **1al-1n** reacted with a substantial stereoselectivity (77 to >95%); however, the electronic effect on the selectivity was pronounced. While both (*E*)- and (*Z*)-β-methylstyrene **1al** reacted to form the same stereoisomer of **3al** with 83% selectivity (39% yield), (*E*)-methylisoeugenol **1am** furnished **3am** with excellent selectivity (>95%), with only traces of the other isomer. It should be noted that internal aliphatic alkenes, such as cyclooctene, alkenes that tend to isomerize to internal or trisubstituted alkenes, such as 1-octene or α-ethylstyrene, or alkenes bearing highly congested double bonds, such as α-tert-butylstyrene, failed to form the target products in substantial amounts, establishing the current limitations of the method (for details, see Figure 14).

The method is applicable to transfer different boronate ester groups, including Bmac (**3ao**), or the chiral α-pinene-based Bpnd group (**3ap**), providing an easy access to boronic acid derivatives of varied reactivity for tailored synthetic applications.[76–79] It is also worth noting that the method employs only simple readily available reagents and is easily scalable (1.1 g of **3aq** (76% yield) furnished using just 0.24 mol% of [Rh(cod)OMe]$_2$).

Diverse functional groups:

3o: 86%

3p:[b] R³ = tBu, 53%
3q:[b] R³ = TMS, 42%

Heteroaromatic groups:

3r: 2-Py: 76%
3s: 3-Py: 80%

3t: 88%

3u: 98%

FG:	Yield:
3b: 4-CHO	80%
3c: 4-NMe₂	69%
3d: 4-N(Boc)Me	80%
3e: 4-COMe	58%
3f: 4-Cl	87%
3g: 4-CF₃	82%
3h: 3,5-bisCF₃	83%
3i: 4-F	76%[a]
3j: 4-CN	74%
3k: 4-CO₂Me	70%
3l: 4-OAc	92%
3m: 4-OMe	66%[a]
3n: 2-Me	90%

Electronically varied alkenes:

3w: 54%

3x: 80%

3y: 97%

3z: 93%

3aa: 85%

1v

3v: 55%

Different boronic esters:

3ao: 86%

3ap: 92%

Scale-up:

- 0.20 mmol: 96% yield with 2 mol% of [Rh]
- 5.0 mmol: 76% yield[a,c] with 0.24 mol% of [Rh]

3aq

Different substitution patterns & congested double bonds:

3ab:[c] 52%

3ac:[c] 81% (90:10 E:Z)

3ad:[c] 77% (87:13 E:Z)

3ae:[c] 50% (90:10 Z:E)

	R⁴:	Yield:
3af:[c]	H	88%
3ag:[a,c]	CO₂Me	47% (53:47 dr)[e]
3ah:[c]	OMe	51% (55:45 dr)[e]
3ai:[c]	SMe	47% (53:47 dr)[e]

3aj:[c] 81% (53:47 dr)[e]

3ak:[c] 39% (77:23 E:Z)

3al:[c,d] 39%[a] (83:17 Z:E)

3am:[a,c] 42% (>95:5 Z:E)

3an:[a,c] 37% (77:23 Z:E)

Figure 2. Compatibility of the method with different functional groups, heteroaromatic motifs, electronically and sterically varied terminal and internal alkenes, and different boronic esters. For an overview of the reaction conditions, including the comparison between the analytical yields determined by ¹H NMR analysis of the reaction mixture with an internal standard and the yields of isolated materials, see Table 5. Because vinylboronic esters tend to partially decompose during chromatography on silica gel,[28,80,81] the analytical yields are reported here to indicate the actual reaction performance; [a] isolated yield; [b] **4** (1.0 equiv) instead of **2**; [c] B₂pin₂ as an additive; [d] starting from *cis*-**1al**, starting from *trans*-**1al**: 38% isolated yield (83:17 Z:E); [e] dr, diastereomeric ratio between (E)- and (Z)-products; major stereoisomer was not assigned.

Typical motifs of drug molecules with multiple strongly coordinating *N*- or *S*-sites that could chelate to the metal center and hence impede the reaction, often represent a significant challenge in transition metal catalysis (Figure 3). Nonetheless, we observed that derivatives of antihistamine Brompheniramine **1ar**, antipsychotic Chlorpromazine **1as**, and agonist of retinoid receptor CD3254 **3au** underwent transfer borylation efficiently, establishing a powerful entry point for the synthesis

of large libraries of such bioactive molecules. Additionally, boronic acids are bioisosteres of carboxylic acids that find diverse applications in pharmacology.[1–3] In this context, the protocol proved effective in the concise synthesis of the boronic acid bioisostere of antiplatelet drug Ozagrel **5** through its Bpin ester **3at.**

Complex natural products of macrocyclic structure are particularly challenging. Gratifyingly, our protocol furnished boryl derivative **3av** of Zearalenol, a nonsteroidal mycoestrogen found in *Fusarium spp*. Albeit the product was formed in modest yield, this example demonstrates the unique synthetic capacity of the transfer borylation strategy for the late-stage functionalization of complex substrates.

3ar[b]: Brompheniramine deriv.   **3as**: Chlorpromazine deriv.   **5**: Ozagrel bioisostere[c]
76%[a]   80%   (**3at**: Bpin ester: 85%)

3au: CD3254 deriv.   **3av**:[b,d] Zearalenol deriv.
89%   11% (33% rsm)
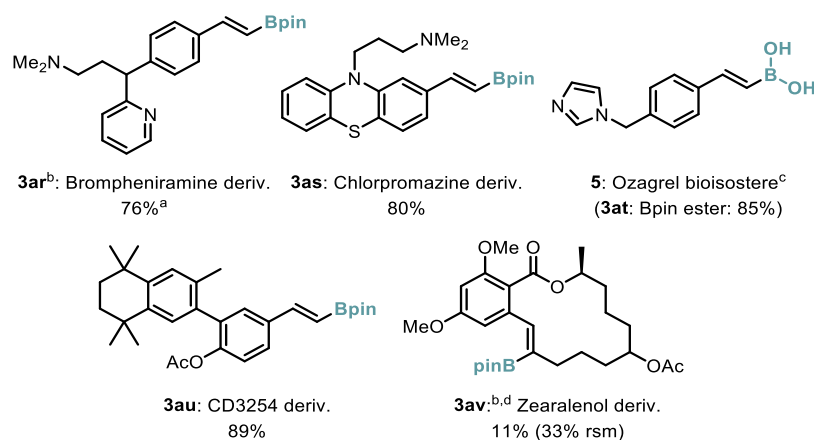
Figure 3. Compatibility of the method with polyfunctionalized bioactive compounds. [a] isolated yield; [b] B₂pin₂ as an additive; [c] The ester **3at** was readily hydrolyzed to the boronic acid **5** (68% yield);[70] [d] the catalyst solution was added portion-wise (in total 8.75 mol% of Rh-precursor);[70] deriv, derivative, rsm, recovered starting material.

3.2.3   Experimental mechanistic studies

Having established the boryl group transfer between alkenes under phosphine-Rh(I)-alkoxide catalysis and its broad applicability with an excellent functional group tolerance, open questions arose regarding the mechanistic aspects of the reaction that could assist further rational development of the method. In particular, we wondered whether the reaction occurred in the proposed catalytic cycle involving Rh(I)-hydride and Rh(I)-boryl intermediates with the Rh(I)-(β-borylalkyl) intermediates engaging in the so far unreported β-boryl elimination step (see Figure 1c) or whether an alternative mechanism involving a Rh-alkoxide mediated C(sp²)−H bond activation was operating.[82–84] The origin of the excellent regio- and stereoselectivity remained to be solved as well. To shed light on the above questions, we performed a series of experimental studies, which we further corroborated by DFT calculations.

Probing Alternative Catalytic Cycles. Stereochemical considerations for the formation of the product involving either a sequence of alkene insertion into a Rh-B bond and β-hydride elimination or a direct C-H activation implied different fate of the olefinic hydrogen atoms of alkene **1a** depending on the mechanism of the reaction (paths I-II, Figure 4a). Furthermore, because the earlier mechanism operates through the formation of a Rh−H species, this pathway might also lead to a proton scrambling throughout different positions of the alkene starting materials, depending on

selectivity, rates, and reversibility of alkene insertion steps (paths III-IV, Figure 4a). To differentiate between these scenarios, we performed catalytic experiments with deuterium-labeled starting materials (Figure 4b).

(a) Implications of alkene insertion & -elimination sequence or alternative C H bond activation mechanism

path I. insertion into a Rh–B bond - β–H elim. removes H^Z & inverts H^E to the (Z)-side   path III. reversible alkene insertion into a Rh–H scrambles H^Z & H^E

path II. C–H bond activation removes H^E & retains H^Z at the (Z)-side   path IV. reversible inverted alkene insertion into a Rh–H scrambles H
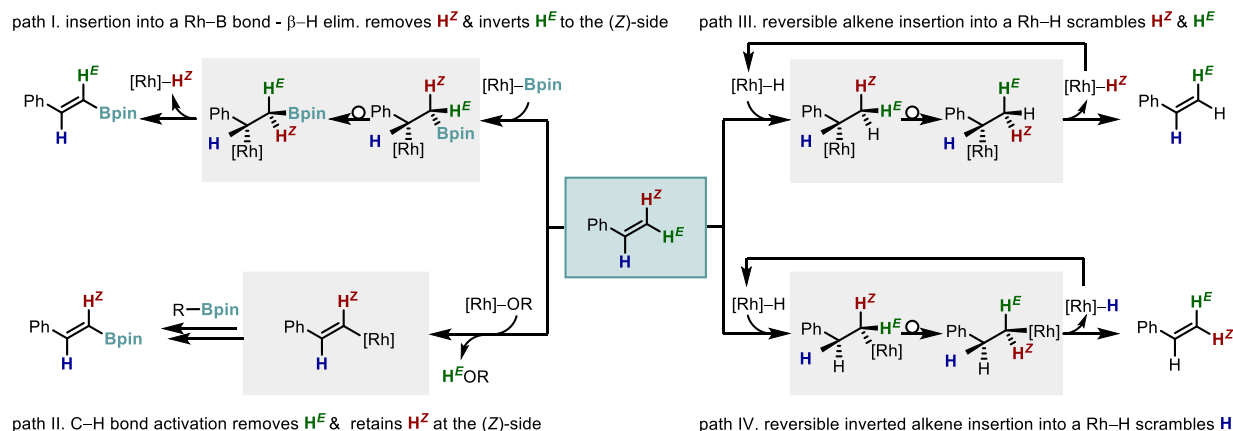
(b) Experiments with isotope-labeled starting materials probing the mechanism of the reaction
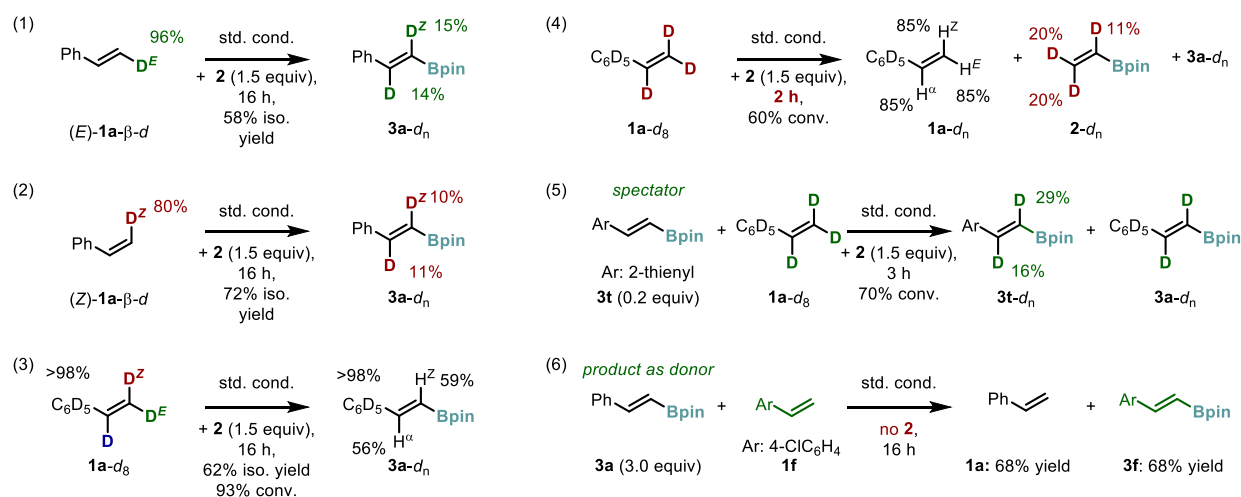
Figure 4 Mechanistic experiments probing the prospective catalytic cycle for the boryl group transfer. (1-2): Partial deuterium retaining in **3a** in the reaction of (*E*)-**1a**-β–*d* is consistent with the mechanism involving alkene insertion into a Rh−B bond & β-hydride elimination sequence; (1-4): H/D scrambling between starting materials indicates fast & reversible alkene insertion into the Rh−H intermediate; (5): Deuterium incorporation into **3t** indicates that the product re-enters the cycle; (6): Boryl group transfer between **3a** and **1f** indicates that the reaction is reversible. For standard conditions, see Table 1; for further details, see section 3.5.3.

The reaction of (*E*)-β-deuteriostyrene **1a**-β-*d* furnished product **3a** that partially retained deuterium labeling, which was scrambled between both vinylic C−H bonds (reaction 1). This outcome of **3a** maintaining some deuterium is inconsistent with the mechanism involving a direct C−H bond activation by the Rh(I)-alkoxide species (path II, Figure 4a), but it is consistent with the mechanism involving an alkene insertion into the Rh(I)−Bpin followed with a β-hydride elimination to form the product and a Rh-hydride (path I). In this reaction, the deuterium scrambling results most likely from a fast and reversible alkene insertion into the Rh-H bond (paths III-IV). In fact, both (*E*)- or (*Z*)-β-deuteriostyrene **1a**-β-*d* reacted with **2** forming product **3a** with similar content and relative

distribution of deuterium at the α- and β-sites (reactions 1-2). Furthermore, in situ NMR spectroscopy and GC-MS analysis of the reaction of styrene-d_8 **1a**-d_8 with **2** revealed the extensive hydrogen/deuterium scrambling not only throughout the α- and β-sites of product **3a**, but also between both alkene starting materials **1a**-d_8 and **2** occurring already early in the process (reactions 3-4). This result indicates that the reversible insertions into the Rh-H/Rh-D bonds are faster than the actual transfer of the boryl group. We also found that the product re-enters the cycle during the catalytic reaction. Compound **3t**, the analogue of **3a** bearing a different aryl ring, added to the reaction of **1a**-d_8 and **2** as a 'spectator' underwent partial deuterium incorporation into its α- and β-positions, implying its reversible insertion into the Rh-H/Rh-D bond occurring also early in the process (3 h; reaction 5). Lastly, utilizing compound **3a** as the boryl group donor instead of vinyl boronate **2** in the reaction of 4-chlorostyrene **1f**, we observed the formation of **3f**, 4-chloro analogue of **3a**, and styrene **1a** (reaction 6), indicating the reversibility of all steps of the catalytic cycle. It should be noted that these experiments confirmed the reversibility of all steps in the catalytic cycle forming **3a**, i.e., (E)-product; however, the relative rates between the steps (e.g., alkene insertion into the Rh-B versus β-boryl elimination) as well as the feasibility of the catalytic cycle forming alternative products, i.e., (Z)- and α-isomers, had yet to be investigated.

Insight into the Rate Limiting Step. With the observed fast hydrogen/deuterium scrambling (Figure 4b), we considered that both the insertion of alkenes into the Rh(I)-hydride and β-hydride elimination must be fast, and hence the overall rate of the reaction is limited by either the alkene insertion into the Rh(I)-boryl intermediate or the β-boryl elimination step (Figure 1c). To differentiate between these scenarios, we studied the reactivity of the independently prepared Rh(I)-boryl intermediate, **LRhBpin** (Figure 5).[70,71] First, we found that **LRhBpin** reacted with alkene **1a** to form product **3a** gradually in time, implying a rather slow alkene insertion into the Rh−B bond (Figure 5a).

(a) Reactivity of Rh(I)-Bpin intermediate with an alkene

conditions	yield
22 °C, 16 h:	50%
45 °C, 5 h:	74%

(b) Catalytic activity of Rh(I)-Bpin intermediate

phase (time):	TOF/ h^{-1}	TON
< 1st turnover (5 h):	0.09(1)	0.44
> 1st turnover (16 h):	0.09(1)	1.52
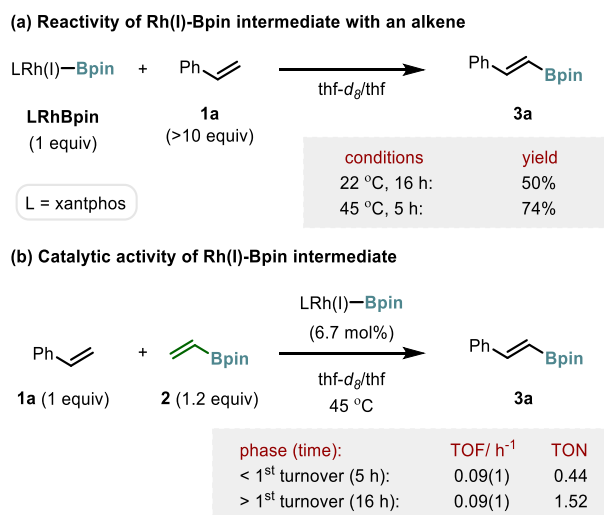
Figure 5. Reactivity of independently prepared xantphos-Rh(I)-Bpin intermediate. **LRhBpin** reacts with **1a** rather slowly and is catalytically active under similar conditions; the formation of **3a** with similar rates in the different phases of the catalytic reaction suggests that the alkene insertion is rate-liming. TOF, turnover frequency; TON, turnover number.

In turn, we observed that **LRhBpin** is catalytically active in the model reaction, with similar rates of the formation of **3a** early in the reaction, i.e., before the first catalytic turnover, and later in the

reaction, i.e., after the first catalytic turnover (Figure 5b). Most importantly, the formation of **3a** before the first turnover involves only the insertion of alkene into the Rh−B bond of *starting* **LRhBpin** (and the fast β-hydride elimination), while the formation of **3a** in the later phase of the reaction requires all steps of the cycle, including the β-boryl elimination step. Thus, similar rates in the different phases of the reaction indicate that the alkene insertion into the Rh−B bond is slower than the β-boryl elimination, and hence is most likely the rate-limiting step of the catalytic process.

Probing Stereo- and Regiocontrol of the Reaction. Because product **3a** is more stable than isomers (*Z*)-**3a** and (α)-**3a** (0.0 vs. +4.2 and +5.0 kcal/mol, respectively),[70] the stereo- and regioselectivity of the reaction might be either under thermodynamic control, that is, when the formation of different isomers of the product is similarly fast, but isomers quickly interconvert to form the product of the lowest energy, or under kinetic control, that is, when the formation of one isomer is much faster than that of the other isomers. To shed light on these scenarios, we studied the reactivity of independently prepared isomers (*Z*)-**3a** and (α)-**3a** under catalytic conditions. We observed that stereoisomer (*Z*)-**3a** underwent fast conversion to (*E*)-isomer **3a**, when present as a spectator of a catalytic reaction of substrate **1aq** under otherwise standard conditions (Figure 6, reaction 1). This observation indicates that stereoselectivity might be indeed thermodynamically controlled.[28,35] However, the quick formation of (*Z*)-**3a** along with **3a** would need to be confirmed to exclude the possibility of kinetic control operating, where the reaction forms **3a** much faster than (*Z*)-**3a**. In contrast, in an analogous experiment, the α-regioisomer of **3a**, (α)-**3a** was rather reluctant to the isomerization: only 11% of (α)-**3a** converted to **3a** after 3 h, while at the same time the (β-selective) catalytic reaction was nearly finished (84% yield of **3m**; Figure 6, reaction 2). This experiment clearly showed that the formation of (*E*)-isomer is much faster than the formation of the α-isomer, in line with kinetic control of the regioselectivity. Overall, the conversions of (*Z*)-**3a** and (α)-**3a** to **3a** indicate that both prospective products of the reaction can enter the catalytic cycle, and hence, due to the principle of microscopic reversibility, they could be formed in the reaction as well. However, the slower conversion of the α-isomer to the (*E*)-isomer compared to the rate of the actual catalytic formation of the (*E*)-isomer implies that the regioselectivity of the reaction is kinetically controlled, a rather unusual feature in functional group transfer catalysis.[85] Most importantly, because the kinetic control depends on the catalyst, the data suggest the feasibility of accessing different isomers using different catalysts.
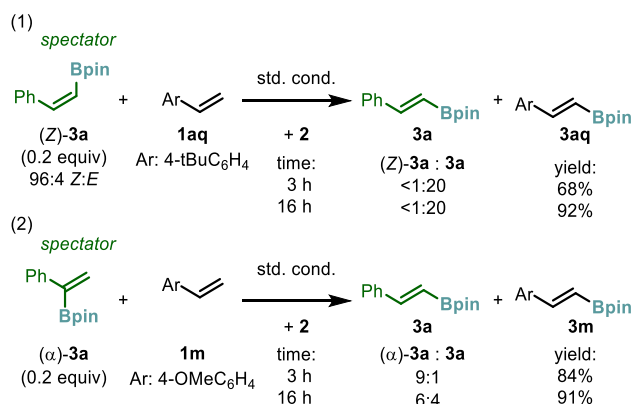
Figure 6. Mechanistic experiments probing the pathways toward formation of stereo- and regioisomeric products. (1): Fast isomerization of (*Z*)-**3a** to **3a** indicates that the stereoselectivity of the reaction might be thermodynamically controlled or kinetically controlled at the β-hydride elimination step. (2): As the isomerization of (α)-**3a** to **3a** is slower than the catalytic reaction, the regioselectivity is controlled kinetically. For standard conditions, see Table 1; for details, see section 3.5.3.

3.2.4 Computational mechanistic studies

The experimental mechanistic findings were corroborated by DFT calculations performed at the M06-L/def2-TZVP(SMD,1,4-dioxane)//M06-L/def2-SVP level of theory. The computed free energy surfaces for the formation of **3a**, (*Z*)-**3a** and (α)-**3a** (Figure 7) demonstrated the feasibility of the initially considered catalytic cycle (Figure 1c) and further supported the alkene insertion into the Rh−B bond as the rate-limiting step of the reaction.
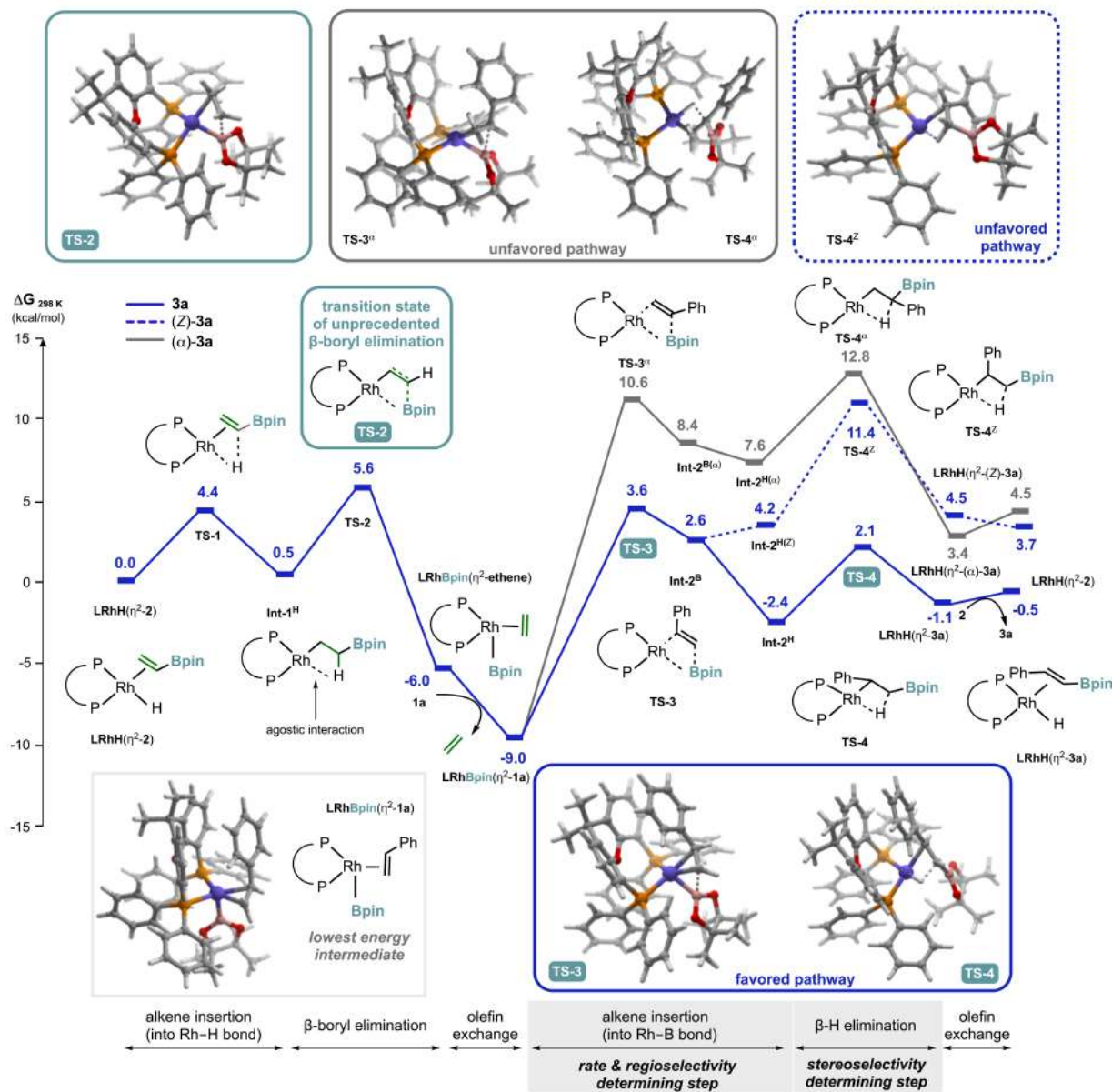
Figure 7. DFT investigation of the free energy surfaces for the reaction pathways leading to products **3a**, (*Z*)-**3a**, or (α)-**3a**. Calculations have been performed at the M06-L/def2-TZVP(SMD)//M06-L/def2-SVP level of theory in 1,4-dioxane as solvent (SMD solvation model); SMD, solvation model based on density; Int, intermediate, TS, transition state.

Importantly, our computations not only support that the regioselectivity is kinetically controlled but also suggested that the stereoselectivity is also under kinetic control. Additionally, we provided an

insight into the preferential P-P coordination mode of xantphos during the reaction (section 3.2.4.1), as well as a detailed analysis on the unprecedented β-boryl elimination process (section 3.2.4.2).

Specifically, the initial xantphos-Rh(I)-hydride complex coordinated by boryl group donor **2**, **LRhH**(η^2-**2**) is predicted to readily form the Rh(I)-boryl intermediate, **LRhBpin**(η^2-ethene) in an exergonic process (ΔG_{rel} = -6.0 kcal/mol) through an alkene insertion (via transition state 1, **TS-1**) – β-boryl elimination (**TS-2**) sequence with a low free energy barrier of +5.6 kcal/mol. Noteworthy, the oxygen atom of the xantphos ligand does not interact with the metal center during the process, while such an interaction was found to be important in other Rh-catalyzed reactions.[67] Parallel calculations indicate that such a pathway would lead to a significantly higher free energy barrier (ΔG_{rel} = +10.5 kcal/mol vs +5.6 kcal/mol; see section 3.2.4.1). Therefore, the activity of the **xantphos**-Rh(I) complex originates most likely from the distinct wide bite angle of the ligand rather than the presence of the oxygen atom. In accordance, no activity was observed for the analogous complex bearing flexible **dpephos** (cf. Table 1).

The borylation of **1a** with the thus-formed **LRhBpin**(η^2-ethene) intermediate embarks upon a ligand exchange to form **LRhBpin**(η^2-**1a**) (along with the extrusion of ethene), which is the lowest energy intermediate of the catalytic cycle (ΔG_{rel} = -9.0 kcal/mol; see section 3.2.4.4 for full discussion on olefin exchange processes). The subsequent alkene insertion into its Rh(I)−B bond is predicted to be rate-limiting with the free energy barrier of +12.6 kcal/mol (**TS-3**). The following β-hydride elimination to form product **3a** through **TS-4** proceeds with a low barrier (+4.5 kcal/mol). Product **3a** is released from **LRhH**(η^2-**3a**) upon the ligand exchange with another molecule of **2**, closing the catalytic cycle. Notably, the alternative β-hydride elimination step toward the formation of stereoisomeric product (*Z*)-**3a** involves a significantly higher energy barrier (**TS-4**^{Z}), even greater than that for the alkene insertion into the Rh–B bond (**TS-3**), accounting for the overall barrier of +20.4 kcal/mol (from **LRhBpin**(η^2-**1a**); dotted blue line in Figure 7), in line with kinetic control of the stereoselectivity. Further, the reaction pathway toward the formation of regioisomeric product (α)-**3a** involves higher energy transition states for both alkene insertion (**TS-3**$^\alpha$) and β-hydride elimination (**TS-4**$^\alpha$) with the overall barrier of +21.8 kcal/mol (grey line in Figure 7), in line with kinetic control of the regioselectivity. Noteworthy, computations also predict that both (*Z*)-**3a** and (α)-**3a** can enter the catalytic cycle with energy barriers of +6.9 and +9.4 kcal/mol, respectively. These results correlate well with the observed interconversions of (*Z*)-**3a** and (α)-**3a** to product **3a**, which were found to be fast and slow in comparison to the rate of the actual catalytic reaction, respectively (cf. Figure 6). Overall, although isomer **3a** is thermodynamically more stable than (*Z*)-**3a** and (α)-**3a**, the calculations suggest that its formation is kinetically controlled.

It is worth mentioning that a stepwise analysis of the β-boryl elimination process revealed that prior to the transition state, there is an intermediate engaging an interaction between boron and Rh atoms, which leads to the C–B bond weakening and its elongation prior to the bond breaking event, and hence facilitating this unprecedented elementary reaction (see section 3.2.4.2).

3.2.4.1 Influence of the coordination mode of Xantphos on the free energy surfaces

Because of the oxygen of the xanthene fragment, xantphos can serve as either a bidentate or tridentate ligand.[86] To discriminate whether the oxygen atom plays an important role in the title transformation, we studied the alkene insertion into a Rh-H bond and the β-boron elimination steps for both coordination modes of the ligand: the **P–O–P** mode with the involvement of the oxygen atom in the coordination towards Rh and the **P–P** mode without this interaction (Figure 8).
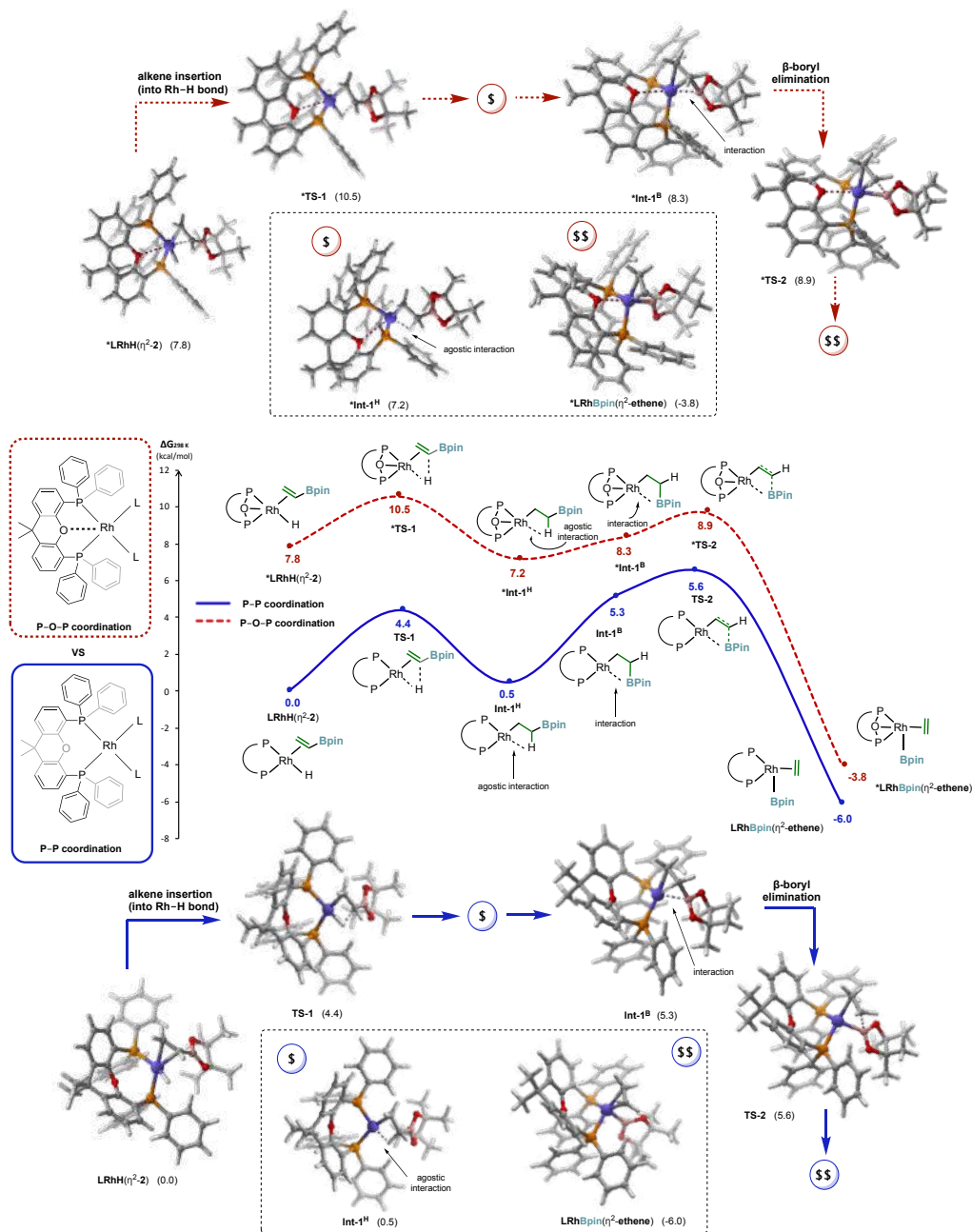
Figure 8. DFT investigation on the coordination mode of xantphos and its influence on the free energy surface. Calculations have been performed at the M06-L/def2-TZVP(SMD)//M06-L/def2-SVP level of theory in 1,4-dioxane as solvent (SMD solvation model); SMD, solvation model based on density; **Int**, intermediate, **TS**, transition state. Free energy surfaces in blue and red dashed line correspond to **P–P** and **P–O–P** coordination modes, respectively.

Our studies revealed that the **P–P** coordination mode is preferred over the **P–O–P** mode in all cases (Figure 8, see **P–P** blue line and **P–O–P** red dashed line). For instance, the ***LRhH(η^2-2)** complex of the **P–O–P** mode is 7.8 kcal/mol less stable than its analogue **LRhH(η^2-2)** of the **P–P** mode. The same trend was observed for all other intermediates studied, resulting in the following free energy differences (in favor of the **P–P** mode) for analogue intermediates: **Int-1^H** 6.7 kcal/mol, **Int-1^B** 3.0 kcal/mol and **LRhBpin(η^2-2)** 2.2 kcal/mol. Further, the energy barriers for the alkene insertion into Rh–H bond and the β-boryl elimination process are also significantly higher when the oxygen is interacting with the Rh center: 10.5 kcal/mol vs 4.4 kcal/mol, for the alkene insertion into Rh–H bond, and 8.4 kcal/mol vs 5.1 kcal/mol, for the β-boryl elimination process. Because subsequent steps of the cycle occur through analogues elementary reactions, no coordination of oxygen to Rh was considered in later stages of the mechanism.

3.2.4.2 The β-boryl elimination process

The β-boryl elimination process occurs in two stages. Initially, intermediate **Int-1^H** in which one alkyl C-H bond interacts with the Rh center through an agostic interaction, undergoes conversion through the rotation of the alkyl chain to form intermediate **Int-1^B** in which the boron group interacts with the Rh center. Population analysis of **Int-1^B** revealed that p-atomic orbital of the boron atom and d-atomic orbital of the Rh atom contribute significantly to the HOMO molecular orbital of **Int-1^B** (Figure 9), evidencing shared electron density between both atoms. This interaction causes the length of the C–B bond to increase from 1.56 Å (**Int-1^H**) to 1.67 Å (**Int-1^B**), therefore weakening the bond prior to its breaking during the β-boryl elimination event (endergonic process, **Int-1^H** to **Int-1^B**, +4.81 kcal/mol).

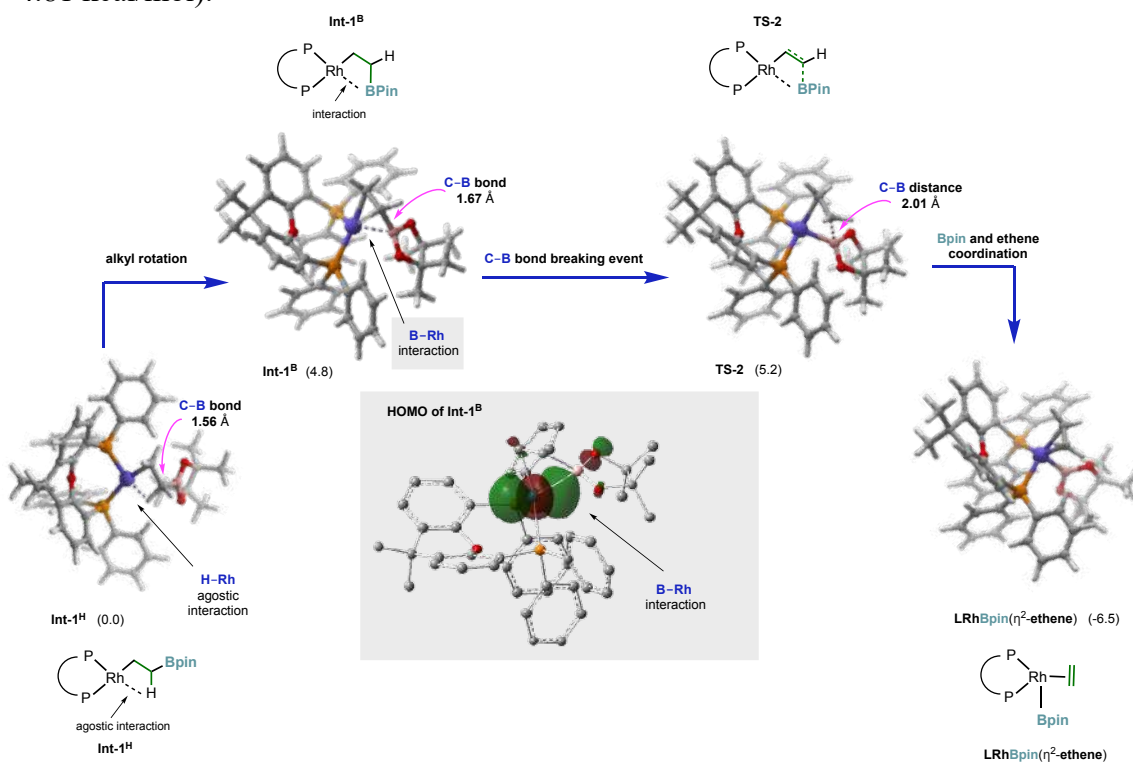**Figure 9. A stepwise analysis of the β-boryl elimination process.** Calculations have been performed at the M06-L/def2-TZVP(SMD)//M06-L/def2-SVP level of theory in 1,4-dioxane as solvent (SMD solvation model); SMD, solvation model based on density; **Int**, intermediate, **TS**, transition state. Spatial distribution of the HOMO for **Int-1^B** at isodensity value of 0.004 e (H atoms omitted for clarity).

In principle, this interaction of Rh with the C-B bond resembles the agostic interaction of Rh with the C-H bond found in analogous intermediate for the β-hydride elimination process. Finally, the transition state **TS-2** is reached at the expense of additional +0.36 kcal/mol (accounting for a total of +5.16 kcal/mol for the overall β-boryl elimination process) to form the **LRhBpin(η^2-ethene)** complex (exergonic process **TS-2** to **LRhBpin(η^2-ethene)**, -11.63 kcal/mol).

3.2.4.3 Formation of ground state complex LRhH(η2-2)

The putative **LRh-H** complex generated in situ upon the pre-catalyst activation should readily react with vinyl Bpin **2** to form the alkene complex **LRhH(η^2-2)**. The process was found to be exergonic of −5.2 kcal/mol (Figure 10).
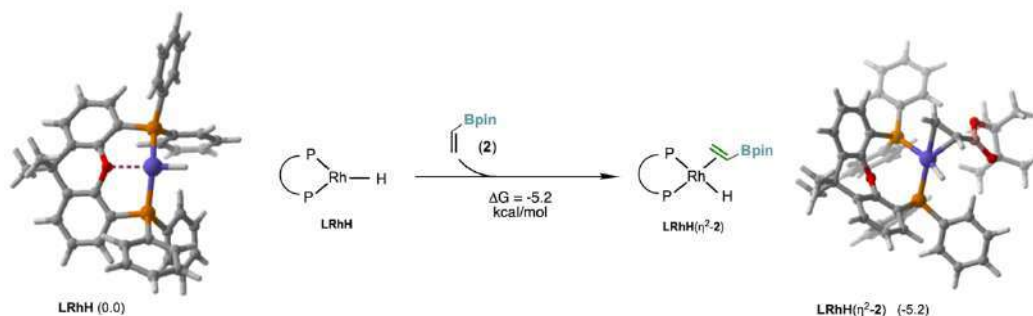
Figure 10. Formation of ground state complex LRhH(η^2-2) complex. Calculations have been performed at the M06-L/def2-TZVP(SMD)//M06-L/def2-SVP level of theory in 1,4-dioxane as solvent (SMD solvation model); SMD, solvation model based on density.

3.2.4.4 Olefin exchange processes leading to the overall lowest energy intermediate

We examined several olefin exchange processes departing from the complex **LRhBpin(η^2-ethene)** in order to find the plausible lowest energy intermediate or a dormant complex possible in the overall catalytic cycle. We considered the exchange of ethene with the olefins present in the reaction mixture, namely, styrene (**1a**), vinyl Bpin (**2**), vinyl (*E*)-1,2-bisboronate (**4**), and the product (**3a**) (Figure 11). We found that the most favored exchange occurs for **1a**, leading to the lowest energy complex **LRhBpin(η^2-1a)** (exergonic process, -3.0 kcal/mol). In addition, exchange of ethene for vinyl Bpin **2** leading to the complex **LRhBpin(η^2-2)** is also thermodynamically favored (-1.8 kcal/mol). On the contrary, exchange of ethene for vinyl (*E*)-1,2-bisboronate (**4**) is disfavored (endergonic process, +2.6 kcal/mol).

It is worth noting that the olefin exchange process occurs most likely through the associative mechanism, which is typically fast and commonly operating in the chemistry of d^8 square planar metal complexes.[87] In agreement, we found that decoordination of ethene from **LRhBpin(η^2-ethene)** to form **LRhBpin** species is thermodynamically unfavorable (highly endergonic process, +11.9 kcal/mol), indicating that the dissociative mechanism is rather unlikely.
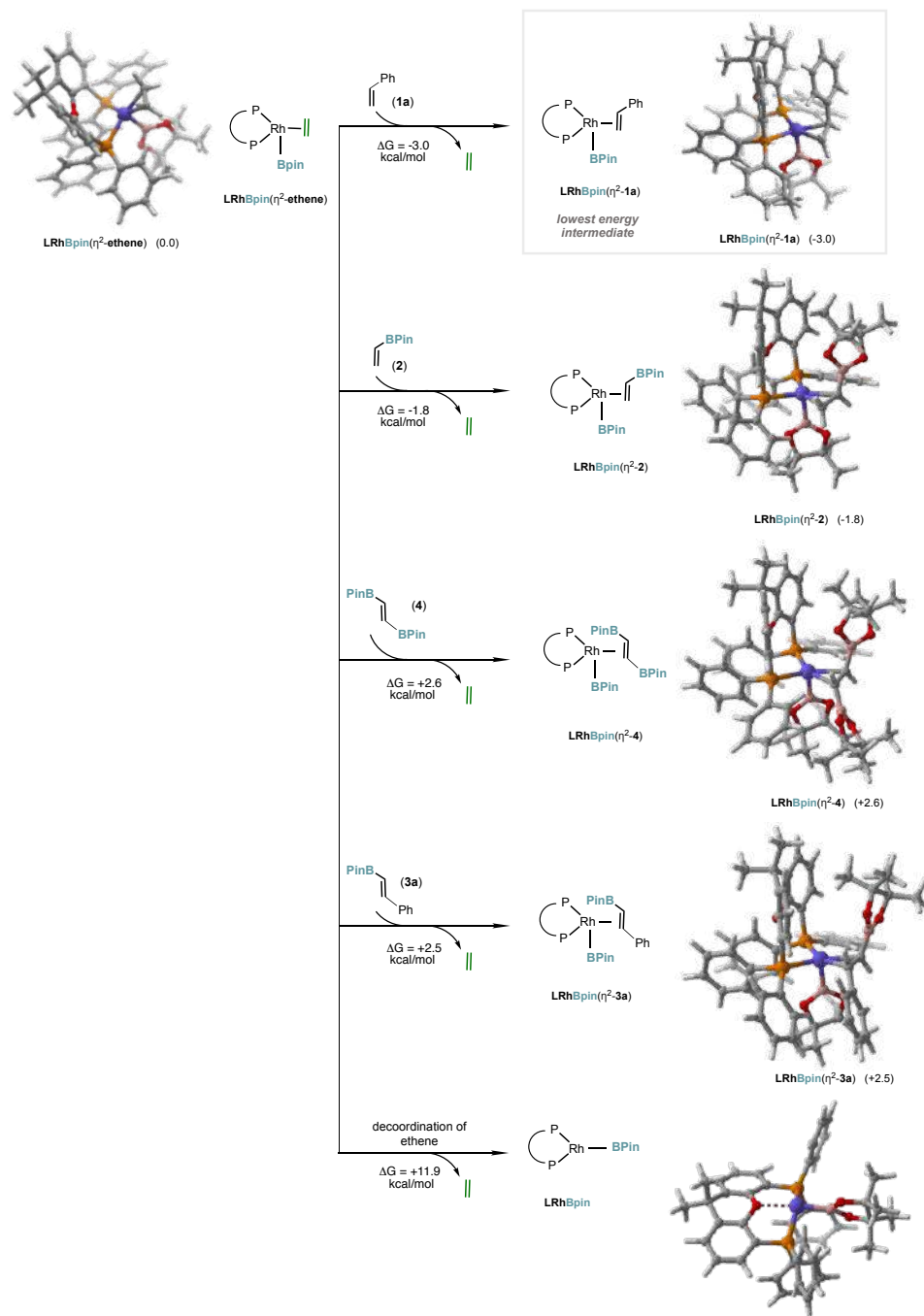
Figure 1. Olefin exchange processes from LRhBpin(η^2-ethene) complex. Calculations have been performed at the M06-L/def2-TZVP(SMD)//M06-L/def2-SVP level of theory in 1,4-dioxane as solvent (SMD solvation model); SMD, solvation model based on density; **Int**, intermediate.

3.3 Summarized Mechanistic Proposal

Based on the collected data we propose that Rh(I)-catalyzed transfer borylation of alkenes occurs as shown in Figure 12. The key mechanistic features are:

The Rh(I)-alkoxide pre-catalyst enters the catalytic cycle either through the alkene insertion into the Rh−O bond – β-hydride elimination sequence forming the catalytic Rh-hydride species (path a) or through its reaction with co-catalytic B_2pin_2 additive to form the catalytic Rh(I)-boryl complex along with pinBOMe under B_2pin_2-based activation (path b).
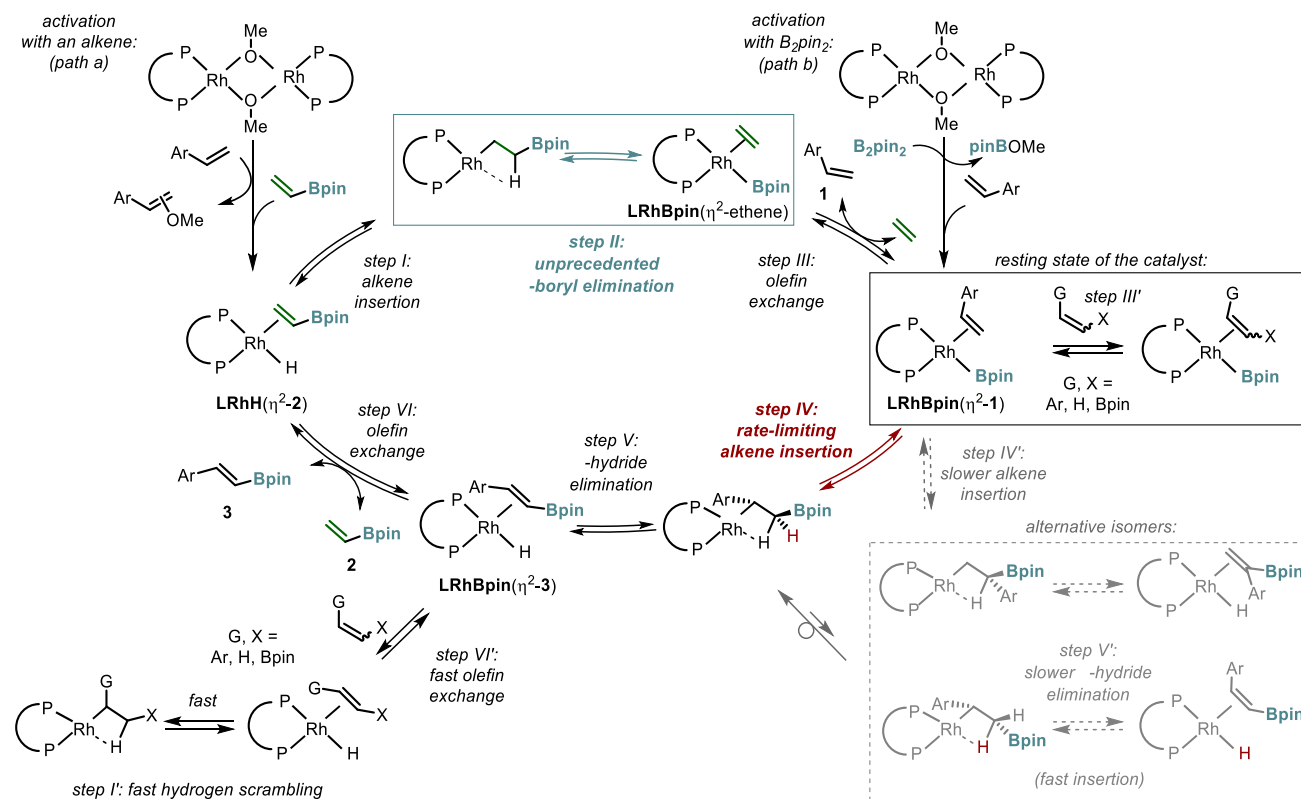
Figure 12. Full proposal of the mechanism of Rh(I)-catalyzed transfer borylation of alkenes.

In the catalytic cycle, the Rh(I)-hydride intermediate with coordinated Bpin-donor **2**, **LRhH**(η^2**-2**), reacts readily to form the Rh(I)-boryl species, **LRhBpin**(η^2**-ethene**), through an alkene insertion into the Rh−H bond – β-boryl elimination sequence (steps I-II).

LRhBpin(η^2**-1**), formed upon olefin exchange of ethene for starting material **1**, is the lowest energy intermediate of the catalytic cycle (step III), which is in equilibrium engaging other alkenes in the mixture (step III'). The complex undergoes rate-limiting regioselective alkene insertion (step IV), followed by a fast and stereoselective β-hydride elimination (step V), and the release of product **3** through an olefin exchange, which completes the cycle (step VI).

The relatively low free energy barriers for all steps of the catalytic cycle forming the (*E*)-isomer of the product have two main consequences: First, many elementary steps are reversible, which can lead to isomerization and scrambling processes (through steps I' and IV'). Second, the free energy surface for the overall transformation is relatively flat, which is essential for effective catalysis in isodesmic processes with a limited energetic driving force. However, the study shows that a catalyst might impose high energy barriers (e.g., competitive steps IV' or V') for the formation of different isomers of the products, creating the prospects for the kinetic control of selectivity in functional group transfer catalysis.[85]

3.4 Conclusions

In conclusion, the herein disclosed Rh(I)-catalyzed boryl group transfer reaction proved to be applicable not only to simple alkenes but also to more complex settings of polyfunctionalized molecules with multiple groups that could inhibit the catalyst. Therefore, such reactivity together with an excellent functional group tolerance indicates its possible applicability to late-stage modifications of complex fine chemicals. Further, the mechanistic studies provided insight into the features controlling the selectivity setting the stage for the development of methods to access different regio- and stereoisomers of the products by C−H borylation; a feature that remains elusive with current strategies.

The studies revealed that an uncommon β-boryl elimination step engaged in the reaction is notably easy, especially in contrast to the well-documented reverse step – an alkene insertion into a Rh−B bond. Considering the number of known alkene insertion elementary reactions into different metal-heteroatom bonds, the mechanistic approach carries the potential for the development of other hydrogen-functional group exchange reactions of high value to organic synthesis. The research to uncover the full capacity of the strategy continues in our laboratories.

3.5 Experimental Details

3.5.1 Experimental methods

Unless stated otherwise, all reactions and manipulations were conducted on the laboratory bench or in a well-ventilated fume hood in air with reagent grade solvents. Reactions under inert gas atmosphere were carried out in oven-dried glassware in a nitrogen-filled glove box or by standard Schlenk techniques under nitrogen. Unless noted otherwise, all reagents and solvents were purchased from commercial suppliers and used without further purification. [Rh(COD)OMe]$_2$ was synthesized according to a literature procedure.[88] For experiments under inert gas atmosphere, dried and degassed solvents were purchased from commercial suppliers, stored in a nitrogen-filled glove box and used as received. Column chromatography was carried out with the aid of a CombiFlash EZ Prep Chromatography System with integrated ELSD using the RediSep Rf (Gold) Silica Gel Disposable Flash columns. TLC was carried out on Merck Kieselgel F254 plates. TLC visualization was carried out with ultraviolet light (254 nm), followed by staining with a 1% aqueous KMnO$_4$ solution. NMR spectra were acquired on the 400 MHz (Bruker 400 MHz NMR UltraShield Magnet, Console Avance III, equipped by a standard probe BBFO ^{1}H-X inverse 5 mm (with ^{31}P < X < ^{15}N)) or 500 MHz (Bruker 500 MHz NMR Ascend Magnet, Console Avance Neo equipped by a Cryo-Probe Prodigy ^{1}H-X 5 mm (with ^{31}P < X < ^{15}N) with a 24-positions auto-sampler) instruments at the Institute of Science and Supramolecular Engineering (ISIS). NMR spectra were processed using the MestReNova 14.1 software. Chemical shifts are reported in parts per million (ppm) and referenced to residual solvent peaks or tetramethylsilane (TMS). Coupling constants are reported in hertz (Hz). GC-FID analysis was obtained on a Shimadzu GC-2010 Plus instrument equipped with a SH-Rxi-5MS column (25 m x 0.20 mm ID x 0.33 mm film) connected to a FID detector. GC-MS analysis was obtained on a Shimadzu QP2020 (EI) instrument equipped with a SH-Rxi-5MS column (25 m x 0.20 mm ID x 0.33 mm film). GC-FID and NMR yields were calculated using dodecane, 1,3,5-trimethoxybenzene, mesitylene or isochroman as the internal standards. GC-FID yields were corrected for response factors for all compounds. High-resolution electrospray ionization mass spectra (HR-ESI-MS) were obtained at the Analytical Facility of the Department of Chemistry, University of Strasbourg or at the Institute of Science and Supramolecular Engineering using a ThermoFisher Orbitrap Exactive Plus with Extend Mass Range(source HESI II) with a Vanquish PDA (VF-XX) detector. Preparative HPLC was carried out with an Agilent semi-preparative HPLC system equipped with: a 1260 Infinity II Binary pump, a 1260 Infinity II Variable Wavelength Detector equipped with a 3 mm preparative cell, a 1290 Infinity II Preparative Open-Bed Sampler/Collector with a 20 mL injection loop, and an Agilent 5 Prep C18 50*21.2 mm column 5 μm particle size.

3.5.2 Evaluation of reaction parameters

3.5.2.1 Evaluation of different rhodium pre-catalysts and additives
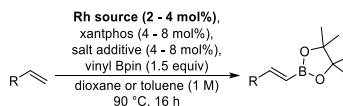
Entry	R =	Rh source	Salt additive	Yield %
1^a	Ph	[Rh(COD)OMe]$_2$	-	92
2^a	Ph	[Rh(COD)Cl]$_2$	-	n.d.
3^a	Ph	[Rh(COD)Cl]$_2$	NaOMe	92
4^a	Ph	[Rh(COD)Cl]$_2$	KOMe	92
5^a	Ph	[Rh(COD)Cl]$_2$	NaOEt	92
6^a	Ph	[Rh(COD)Cl]$_2$	NaOtBu	92
7^a	Ph	[Rh(COD)Cl]$_2$	NaF	n.d.
8^b	Ph	[RhCp*Cl$_2$]$_2$	NaOMe	n.d.
9^c	Ph	[RhCp*Cl$_2$]$_2$	NaOMe	n.d.
10^{a,e}	Ph	[Rh(xantphos)Cl]$_2$	NaOtBu + B$_2$pin$_2$	93
11^d	CO$_2$Et	[Rh(COD)OMe]$_2$	-	54
12^d	CO$_2$Et	[Rh(C$_2$H$_4$)$_2$Cl]$_2$	AgBF$_4$	n.d.
13^d	CO$_2$Et	[Rh(COD)(MeCN)$_2$]BF$_4$	-	n.d.
14^d	CO$_2$Et	[Rh(COD)]SbF$_6$	-	n.d.

Table 2. Evaluation of different rhodium pre-catalysts and additives.

a) Conditions: 0.2 mmol of styrene, 0.3 mmol vinyl Bpin, 2 mol% Rh source, 4 mol% xantphos, 4 mol% of salt additive, dioxane (200 μL, 1 M), 90 °C, 16 h. Yields were determined by analysis of ^{1}H NMR spectra using 1,3,5-trimethoxybenzene as an internal standard. b) Conditions: 0.2 mmol of styrene, 0.3 mmol vinyl Bpin, 4 mol% [RhCp*Cl$_2$]$_2$, 8 mol% xantphos, 16 mol% of NaOMe, dioxane (200 μL, 1 M), 90 °C, 16 h. Yields were determined by analysis of ^{1}H NMR spectra using 1,3,5-trimethoxybenzene as an internal standard. n.d.: not detected. c) Conditions: 0.2 mmol of styrene, 0.3 mmol vinyl Bpin, 4 mol% [RhCp*Cl$_2$]$_2$, 8 mol% xantphos, 16 mol% of NaOMe, toluene (200 μL, 1 M), 90 °C, 16 h. Yields were determined by analysis of ^{1}H NMR spectra using 1,3,5-trimethoxybenzene as an internal standard. n.d.: not detected. d) Conditions: 0.2 mmol of ethyl acrylate, 0.6 mmol vinyl Bpin, 8 mol% Rh source (4 mol% for dimeric Rh source), 8 mol% xantphos, 8 mol% of salt additive, toluene (200 μL, 1 M), 110 °C, 24 h. Yields were determined by analysis of ^{1}H NMR spectra using 1,3,5-trimethoxybenzene as an internal standard. e) Additional B$_2$pin$_2$ (5 mol%) was used.

3.5.2.2 Evaluation of ligands

L₁ xantphos   L₂ N-xantphos   L₃ binap   L₄ DPEPhos

L₅ DPPF   L₆ DPPE   L₇ BISBI   L₈ tBu-xantphos   L₉ Cy-DPEPhos
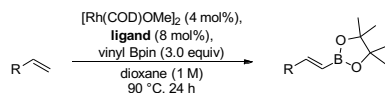
Entry	R =	Ligand	Yield %
1ᵃ	Ph	L₁	92
2ᵃ	Ph	L₃	n.d.
3ᵃ	Ph	L₄	n.d.
4ᵃ	Ph	L₅	n.d.
8ᵇ	CO₂Et	L₁	42
9ᵇ	CO₂Et	L₂	35
10ᵇ	CO₂Et	L₃	n.d.
11ᵇ	CO₂Et	L₄	trace
12ᵇ	CO₂Et	L₅	n.d.
13ᵇ	CO₂Et	L₆	n.d.
14ᵇ	CO₂Et	L₇	trace
15ᵇ	CO₂Et	L₈	trace
16ᵇ	CO₂Et	L₉	trace

Table 3. Evaluation of ligands

a) Conditions: 0.2 mmol of styrene, 0.3 mmol vinyl Bpin, 2 mol% [Rh(COD)OMe]2, 4 mol% xantphos, solvent (200 μL, 1 M), 90 °C, 16 h. Yields were determined by analysis of 1H NMR spectra using 1,3,5-trimethoxybenzene as an internal standard. b) Conditions: 0.2 mmol of ethyl acrylate, 0.6 mmol vinyl Bpin, 4 mol% [Rh(COD)OMe]2, 8 mol% xantphos, dioxane (200 μL, 1 M), 90 °C, 24 h. Yields were determined by analysis of 1H NMR spectra using 1,3,5-trimethoxybenzene as an internal standard. n.d.: not detected.

3.5.2.3 Evaluation of vinyl Bpin loading
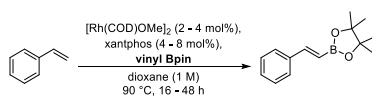
Entry	Vinyl Bpin loading	Yield %
1ᵃ	5.0 equiv	93
2ᵃ	4.0 equiv	95
3ᵃ	3.0 equiv	93
5ᵇ	2.5 equiv	94
6ᵇ	2.0 equiv	94
7ᵃ	2.0 equiv	88
8ᵇ	1.5 equiv	92

Table 4. Evaluation of vinyl Bpin loading

a) Conditions: 0.2 mmol of styrene, vinyl Bpin, [Rh(COD)OMe]2 (4 mol%), xantphos (8 mol%), dioxane (200 μL, 1 M), 90 °C, 48 h. Yields were determined by analysis of 1H NMR spectra using 1,3,5-trimethoxybenzene as an internal standard. b) Conditions: 0.2 mmol of styrene, vinyl Bpin, [Rh(COD)OMe]2 (2 mol%), xantphos (4 mol%), dioxane (200 μL, 1 M), 90 °C, 16 h. Yields were determined by analysis of 1H NMR spectra using 1,3,5-trimethoxybenzene as an internal standard.

3.5.3   Mechanistic investigations

Experiments with isotope-labeled starting materials or potential products

The experiments described below are shown in **Figure 4b** in the main text.

(1)
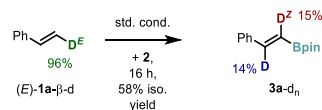
The experiment was performed according to general procedure 1 by reaction of *trans*-styrene-(b)-*d* (21.0 mg, 200 μmol) with vinyl Bpin (46.2 mg, 300 μmol) and the product was isolated by column chromatography (silica gel, 0 – 4.6% MTBE in petroleum ether) to give a colorless oil (26.7 mg,

116 µmol, 58%).

(2)
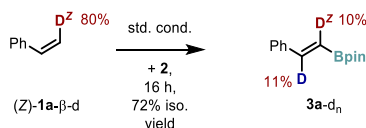
The experiment was performed according to general procedure 1 by reaction of *cis*-styrene-(b)-*d* (21.0 mg, 200 µmol) with vinyl Bpin (46.2 mg, 300 µmol) and the product was isolated by column chromatography (silica gel, 0 – 5.2% MTBE in petroleum ether) to give a colorless oil (33.1 mg, 144 µmol, 72%).

(3)
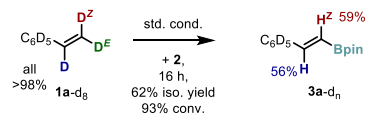
The experiment was performed according to general procedure 1 by reaction of styrene-d_8 (22.4 mg, 200 µmol) and vinyl Bpin (46.2 mg, 300 µmol) and the product was isolated by column chromatography (silica gel, 0 – 6% MTBE in petroleum ether) to give a red oil (30.1 mg, 124 µmol, 62%).

A second reaction was performed with mesitylene (6.9 µL, 6.0 mg, 50 µmol, 0.25 equiv) as an internal standard and a GC-FID analysis of the crude reaction mixture was performed.

(4)

In a nitrogen-filled glove box, a 10 mL screw-cap vial equipped with a Teflon-coated magnetic stirring bar was charged with [Rh(COD)OMe]$_2$ (3.9 mg, 8 µmol, 2 mol%), xantphos (9.3 mg, 16 µmol, 4 mol%), dioxane (400 µL), benzene-d_6 (40 µL), vinyl Bpin (92.4 mg, 600 µmol, 1.5 equiv), styrene-d_8 (44.9 mg, 400 µmol, 1.0 equiv) and mesityl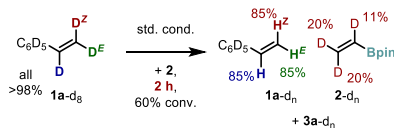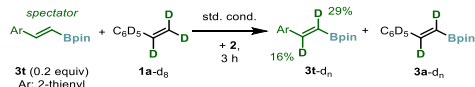ene (13.8 µL, 12.0 mg, 100 µmol, 0.25 equiv). The vial was sealed with a cap, removed from the glove box, placed in a pre-heated aluminum block, and allowed to stir (800 rpm) at 90 °C for 2 h. Upon cooling to room temperature, the reaction mixture was subjected to GC-FID and NMR analysis.

In a nitrogen-filled glove box, styrene-d_8 (22.4 mg, 200 µmol, 1.0 equiv) was added to a mixture of **(E)**-4,4,5,5-tetramethyl-2-(2-(thiophen-2-yl)vinyl)-1,3,2-dioxaborolane (**3t**, 9.2 mg, 40.0 µmol, 0.20 equiv) xantphos (4.6 mg, 8.00 µmol, 0.04 equiv), [Rh(COD)OMe]$_2$ (1.9 mg, 4.00 µmol, 0.02 equiv), and vinyl Bpin (46.2 mg, 300 µmol, 1.5 equiv) in dioxane (200 µL) in a 10 mL screw-cap vial equipped with a Teflon-coated magnetic stirring. The vial was sealed with a cap, removed from the glove box, placed in a pre-heated aluminum block and allowed to stir (800 rpm) at 90 °C for 3 h. Upon cooling to room temperature, a standard solution (100 µL of 0.5 M mesitylene in chloroform) and CDCl$_3$ (400 µL) were added to the reaction mixture. An aliquot was taken and submitted to GC-FID revealing the conversion of styrene-d_8 to be 70%. The solvent of the crude product was removed, and the residue was subjected to column chromatography (silica, 0 – 10% MTBE in petroleum ether) to yield a mixture of the partially deuterated spectator **3t**-d_n and partially deuterated product **3a**-d_n (28.1 mg, pale yellow oil).
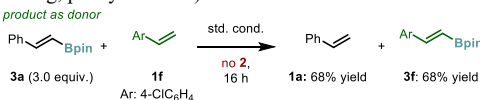
The experiment was performed according to general procedure 2 by reaction of *p*-chlorostyrene (**1f**, 27.7 mg, 200 µmol) and *trans*-2-phenylvinyl Bpin (**3a**, 138.1 mg, 600 µmol). Upon cooling to room temperature, a standard solution (100 µL of 0.5 M 1,3,5-trimethoxybenzene in chloroform) and CDCl$_3$ (400 µL) were added to the reaction mixture. The yield was determined by the ratio the integrals of the internal standard's aromatic signal and an isolated product's signal in a ^{1}H NMR experiment.

In a nitrogen-filled glove box, 4-*tert*-butylstyrene (32.1 mg, 200 µmol, 1.0 equiv) was added to a mixture of (*Z*)-4,4,5,5-tetramethyl-2-styryl-1,3,2-dioxaborolane ((*Z*)-**3a**, 9.2 mg, 40.0 µmol, 0.20 equiv), xantphos (4.6 mg, 8.00 µmol, 0.04 equiv), [Rh(COD)OMe]$_2$ (1.9 mg, 4.00 µmol, 0.02 equiv), and vinyl Bpin (46.2 mg, 300 µmol, 1.5 equiv) in dioxane (200 µL) in a 10 mL screw-cap vial equipped with a Teflon-coated magnetic stirring. The vial was sealed with a cap, removed from the glove box, placed in a pre-heated aluminum block and allowed to stir (800 rpm) at 90 °C for 3 or 16 h. Upon cooling to room temperature, a standard solution (100 µL of 0.5 M 1,3,5-trimethoxybenzene in chloroform) and CDCl$_3$ (400 µL) were added to the reaction mixture. The yield was determined by the ratio the integrals of the internal standard's aromatic signal and a product's signal in a ^{1}H NMR experiment.

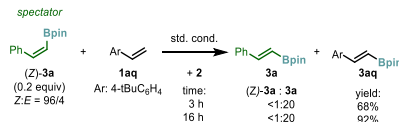In a nitrogen-filled glove box, a 10 mL screw-cap vial equipped with a Teflon-coated magnetic stirring bar was charged with [Rh(COD)OMe]₂ (1.9 mg, 4 µmol, 2 mol%), xantphos (4.6 mg, 8 µmol, 4 mol%), 1,4-dioxane (200 µL), vinyl Bpin (46.2 mg, 300 µmol, 1.5 equiv), *p*-methoxystyrene (26.8 mg, 200 µmol, 1.0 equiv) and 1-phenylvinyl Bpin (9.2 mg, 40 µmol, 0.2 equiv). The vial was sealed with a cap, removed from the glove box, placed in a pre-heated aluminum block and allowed to stir (800 rpm) at 90 °C for 3 or 16 h. Upon cooling to room temperature, a standard solution (100 µL of 0.5 M 1,3,5-trimethoxybenzene in chloroform) and CDCl₃ (400 µL) were added to the reaction mixture. The yield was determined by the ratio the integrals of the internal standard's aromatic signal and a product's signal in a ¹H NMR experiment

3.6   General procedures for Rh-catalyzed C-H borylation of alkenes

General procedure 1
In a nitrogen-filled glove box, a 10 mL screw-cap vial equipped with a Teflon-coated magnetic stirring bar was charged with [Rh(COD)OMe]₂ (1.9 mg, 4 µmol, 2 mol%), xantphos (4.6 mg, 8 µmol, 4 mol%), dioxane (200 µL), boryl group donor reagent (300 µmol, 1.5 equiv), and alkene (200 µmol). The vial was sealed with a cap, removed from the glove box, placed in a pre-heated aluminum block and allowed to stir (800 rpm) at 90 °C for 16 h. Upon cooling to room temperature, the reaction mixture was filtered through a plug of celite (eluent: ethyl acetate). The volatiles of the filtrate were removed under reduced pressure and the residue was subjected to column chromatography to isolate the corresponding product.

General procedure 2
In a nitrogen-filled glove box, a 10 mL screw-cap vial equipped with a Teflon-coated magnetic stirring bar was charged with [Rh(COD)OMe]₂ (3.9 mg, 8 µmol, 4 mol%), xantphos (9.3 mg, 16 µmol, 8 mol%), dioxane (200 µL), boryl group donor reagent (600 µmol, 3.0 equiv), and alkene (200 µmol). The vial was sealed with a cap, removed from the glove box, placed in a pre-heated aluminum block and allowed to stir (800 rpm) at 90 °C for 16 h. Upon cooling to room temperature, the reaction mixture was filtered through a plug of celite (eluent: ethyl acetate). The volatiles of the filtrate were removed under reduced pressure and the residue was subjected to column chromatography to isolate the corresponding product.

General procedure 3
In a nitrogen-filled glove box, a 10 mL screw-cap vial equipped with a Teflon-coated magnetic stirring bar was charged with [Rh(COD)OMe]₂ (3.9 mg, 8 µmol, 4 mol%), xantphos (9.3 mg, 16 µmol, 8 mol%), dioxane (200 µL), boryl group donor reagent (600 µmol, 3.0 equiv), and alkene (200 µmol). The vial was sealed with a cap, removed from the glove box, placed in a pre-heated aluminum block and allowed to stir (800 rpm) at 90 °C for 48 h. Upon cooling to room temperature, the reaction mixture was filtered through a plug of celite (eluent: ethyl acetate). The volatiles of the filtrate were removed under reduced pressure and the residue was subjected to column chromatography to isolate the corresponding product.

General procedure for the determination of the crude yield by ¹H NMR spectroscopy
For the determination of the analytical yields of the reaction, the same general procedure was used as for the determination of the isolated yields (scale: 200 µmol). Upon cooling to room temperature, a solution of the standard (100 µL of 0.5 M 1,3,5-trimethoxybenzene in chloroform) and CDCl₃ (400 µL) were added to the reaction mixture. The yield was determined based on the integrals of the signals of the aromatic protons of the internal standard and the signals of the product that did not overlap with any other signals, typically vinylic protons, in a ¹H NMR experiment.

3.7 Overview of Synthetic Capacity

Substrate	Catalyst loading [mol%]	B2pin2 loading [mol%]	Boron donor [donor, equiv.]	Tempera-ture [°C]	Time [h]	NMR yield [%][a]	Isolated yield [%][a]
1a	2	-	**2**, 1.5	90	16	92	81
1b	4	-	**2**, 2.0	90	16	80	25
1c	4	-	**2**, 3.0	90	16	69	65
1d	4	-	**2**, 3.0	90	16	80	73
1e	4	-	**2**, 3.0	90	16	58	45
1f	4	-	**2**, 3.0	90	16	87	55
1g	2	-	**2**, 1.5	90	16	82	65
1h	4	-	**2**, 3.0	90	16	83	51
1i	2	-	**2**, 1.5	90	16	n.d.	76
1j	4	-	**2**, 3.0	90	16	74	53
1k	4	-	**2**, 3.0	90	16	70	47
1l	4	-	**2**, 3.0	90	16	92	89
1m	2	-	**2**, 1.5	90	16	n.d.	66
1n	2	-	**2**, 1.5	90	16	90	75
1o	4	-	**2**, 3.0	90	16	86	79
1p	4	-	**4**, 1.0	90	48	53	22
1q	4	-	**4**, 1.0	90	48	42	17
1r	4	-	**2**, 3.0	90	16	76	43
1s	2	-	**2**, 1.5	90	16	80	n.d.
1t	4	-	**2**, 3.0	90	16	88	75
1u	4	-	**2**, 3.0	90	16	98	63
1v	2	-	**2**, 1.5	90	16	55	52
1w	4	-	**2**, 3.0	90	16	54	n.d.
1x	4	-	**2**, 3.0	90	16	80	80
1y	2	5	**2**, 1.5	90	16	97	n.d.
1z	2	5	**2**, 1.5	90	16	93	n.d.
1aa	2	5	**2**, 1.5	90	16	85	n.d.
1ab	4	10	**2**, 2.0	90	16	52	23
1ac	4	10	**2**, 3.0	150	16	81	27
1ad	4	10	**2**, 3.0	150	48	77	53
1ae	4	10	**2**, 3.0	150	16	50	29
1af	4	10	**3z**, 2.0	150	16	94	68
1af	4	10	**2**, 2.0	150	16	88	n.d.

Table 5. Concise overview for conditions of reactions of all substrates [a] Because vinylboronic esters tend to partially decompose during chromatography on silica gel[89–91], depending on the relative stability of the products, the yields of isolated material in some cases are substantially lower than the analytical yields determined by ^{1}H NMR analysis.
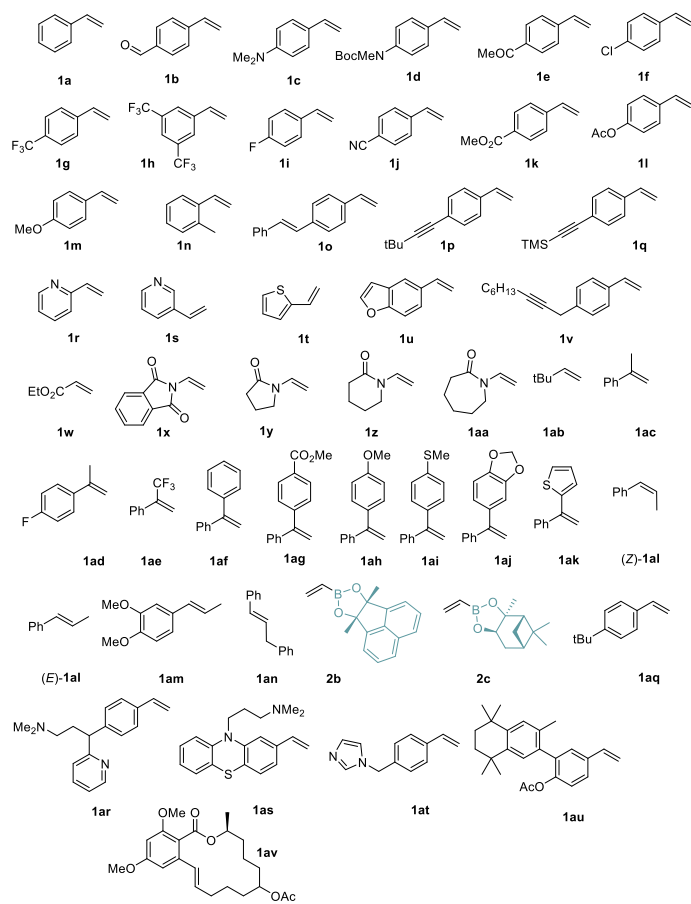
Figure 13: Overview of successful substrates
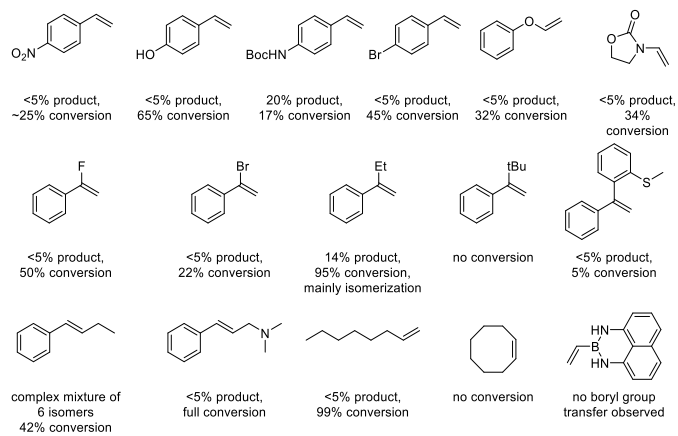
Figure 14: Overview of unsuccessful substrates.

3.8 Density Functional Theory Calculations

3.8.1 Computational details

All DFT calculations[92] were performed with the Gaussian09 suite of programs.[93] Geometries were optimized with the M06−L[94] functional and the def2-SVP basis set[95,96] together with the corresponding Coulomb fitting basis set to speed up calculations.[97] In all cases, the default numerical integration grid was modified for the denser and more accurate 'SuperFineGrid'. Stationary points were probed through vibrational analysis. Gibbs free energy corrections were performed under standard conditions (298.15 K, 1.0 atm). Transition states were verified through Intrinsic Reaction Coordinate calculations (IRC) or optimization to minima at both sides of the frequency. Single point energy calculations including the effect of 1,4-dioxane as a solvent were performed with the M06−L functional[94], the SMD solvation model[98], and the larger def2-TZVP basis set[95,96].

3.8.2 Additional computed structures

Figure 15 depicts the additional computed structures not shown in the main text.
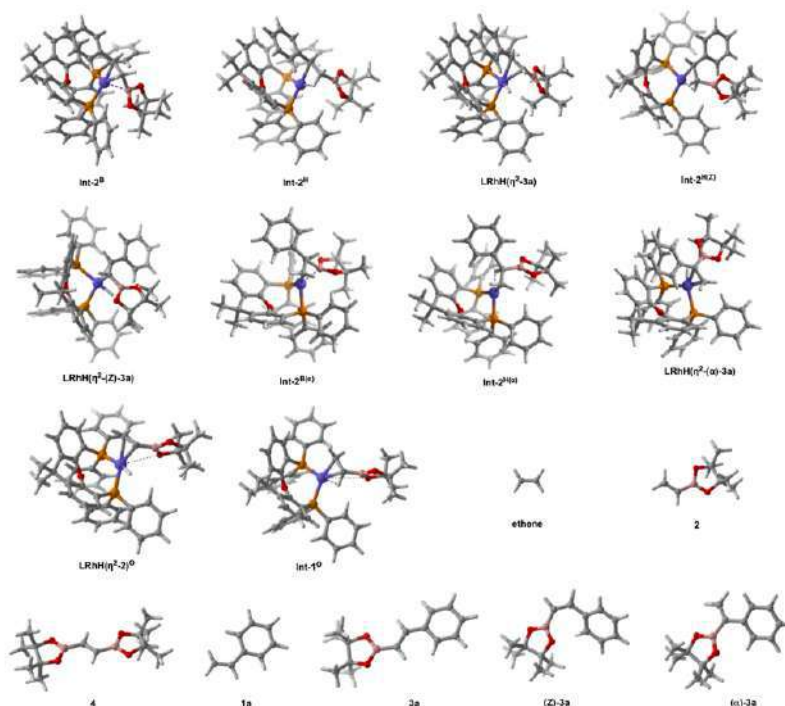
Figure 15: Additional computed structures. Calculations have been performed at the M06-L/def2-TZVP(SMD)//M06-L/def2-SVP level of theory in 1,4-dioxane as solvent (SMD solvation model); SMD, solvation model based on density; Int, intermediate.

3.9 References

(1)   Hall, D. G. *Boronic Acids: Preparation and Applications in Organic Synthesis and Medicine*; Wiley-VCH Verlag: Weinheim, 2010.

(2)   Ban, H. S.; Nakamura, H. Boron-Based Drug Design: Boron-Based Drug Design. *Chem. Rec.* **2015**, *15* (3), 616–635.

(3)   Diaz, D. B.; Yudin, A. K. The Versatility of Boron in Biological Target Engagement. *Nat. Chem.* **2017**, *9* (8), 731–742.

(4)   Miyaura, Norio.; Suzuki, Akira. Palladium-Catalyzed Cross-Coupling Reactions of Organoboron Compounds. *Chem. Rev.* **1995**, *95* (7), 2457–2483.

(5)   Nicolaou, K. C.; Bulger, P. G.; Sarlah, D. Palladium-Catalyzed Cross-Coupling Reactions in Total Synthesis. *Angew. Chem. Int. Ed.* **2005**, *44* (29), 4442–4489.

(6)   Lennox, A. J. J.; Lloyd-Jones, G. C. Selection of Boron Reagents for Suzuki–Miyaura Coupling. *Chem Soc Rev* **2014**, *43* (1), 412–443.

(7)   Xu, L.; Zhang, S.; Li, P. Boron-Selective Reactions as Powerful Tools for Modular Synthesis of Diverse Complex Molecules. *Chem. Soc. Rev.* **2015**, *44* (24), 8848–8858.

(8)   Hartwig, J. F.; Larsen, M. A. Undirected, Homogeneous C–H Bond Functionalization: Challenges and Opportunities. *ACS Cent. Sci.* **2016**, *2* (5), 281–292.

(9)   Mkhalid, I. A. I.; Barnard, J. H.; Marder, T. B.; Murphy, J. M.; Hartwig, J. F. C−H Activation for the Construction of C−B Bonds. *Chem. Rev.* **2010**, *110* (2), 890–931.

(10)   Hartwig, J. F. Regioselectivity of the Borylation of Alkanes and Arenes. *Chem. Soc. Rev.* **2011**, *40* (4), 1992.

(11)   Xu, L.; Wang, G.; Zhang, S.; Wang, H.; Wang, L.; Liu, L.; Jiao, J.; Li, P. Recent Advances in Catalytic C−H Borylation Reactions. *Tetrahedron* **2017**, *73* (51), 7123–7157.

(12)   Wright, J. S.; Scott, P. J. H.; Steel, P. G. Iridium-Catalysed C−H Borylation of Heteroarenes: Balancing Steric and Electronic Regiocontrol. *Angew. Chem. Int. Ed.* **2021**, *60* (6), 2796–2821.

(13)   Reyes, R.; Sawamura, M. An Introductory Overview of C–H Bond Activation/ Functionalization Chemistry with Focus on Catalytic C(Sp3)–H Bond Borylation. *KIMIKA* **2021**, *32* (1), 70–109.

(14)   Veth, L.; Grab, H.; Dydio, P. Recent Trends in Group 9–Catalyzed C−H Borylation Reactions: Different Strategies to Control Site-, Regio-, and Stereoselectivity. *Synthesis* **2021**, a-1711-5889.

(15)   Carreras, J.; Caballero, A.; Pérez, P. J. Alkenyl Boronates: Synthesis and Applications. *Chem. – Asian J.* **2019**, *14* (3), 329–343.

(16)   Wang, X.; Wang, Y.; Huang, W.; Xia, C.; Wu, L. Direct Synthesis of Multi(Boronate) Esters from Alkenes and Alkynes via Hydroboration and Boration Reactions. *ACS Catal.* **2021**, *11* (1), 1–18.

(17)   Flynn, A. B.; Ogilvie, W. W. Stereocontrolled Synthesis of Tetrasubstituted Olefins. *Chem. Rev.* **2007**, *107* (11), 4698–4745.

(18)   Blackwell, H. E.; O'Leary, D. J.; Chatterjee, A. K.; Washenfelder, R. A.; Bussmann, D. A.; Grubbs, R. H. New Approaches to Olefin Cross-Metathesis. *J. Am. Chem. Soc.* **2000**, *122* (1), 58–71.

(19)   Morrill, C.; Grubbs, R. H. Synthesis of Functionalized Vinyl Boronates via Ruthenium-Catalyzed Olefin Cross-Metathesis and Subsequent Conversion to Vinyl Halides. *J. Org. Chem.* **2003**, *68* (15), 6031–6034.

(20)   Morrill, C.; Funk, T. W.; Grubbs, R. H. Synthesis of Tri-Substituted Vinyl Boronates via Ruthenium-Catalyzed Olefin Cross-Metathesis. *Tetrahedron Lett.* **2004**, *45* (41), 7733–7736.

(21)   Kiesewetter, E. T.; O'Brien, R. V.; Yu, E. C.; Meek, S. J.; Schrock, R. R.; Hoveyda, A. H. Synthesis of Z-(Pinacolato)Allylboron and Z-(Pinacolato)Alkenylboron Compounds through Stereoselective Catalytic Cross-Metathesis. *J. Am. Chem. Soc.* **2013**, *135* (16), 6026–6029.

(22)   Hemelaere, R.; Carreaux, F.; Carboni, B. Cross-Metathesis/Isomerization/Allylboration Sequence for a Diastereoselective Synthesis of *Anti* -Homoallylic Alcohols from Allylbenzene Derivatives and Aldehydes. *Chem. - Eur. J.* **2014**, *20* (44), 14518–14523.

(23)   Njardarson, J. T.; Biswas, K.; Danishefsky, S. J. Application of Hitherto Unexplored Macrocyclization Strategies in the Epothilone Series: Novel Epothilone Analogs by Total SynthesisElectronic Supplementary Information (ESI) Available: Experimental Details for the Synthesis of 14 and 32. See Http://Www.Rsc.Org/Suppdata/Cc/B2/B209941a/. *Chem. Commun.* **2002**, No. 23, 2759–2761.

(24)   Nicolaou, K. C.; Tria, G. S.; Edmonds, D. J.; Kar, M. Total Syntheses of (±)-Platencin and (−)-Platencin. *J. Am. Chem. Soc.* **2009**, *131* (43), 15909–15917.

(25)   Speed, A. W. H.; Mann, T. J.; O'Brien, R. V.; Schrock, R. R.; Hoveyda, A. H. Catalytic Z-Selective Cross-Metathesis in Complex Molecule Synthesis: A Convergent Stereoselective Route to Disorazole C1. *J. Am. Chem. Soc.* **2014**, *136* (46), 16136–16139.

(26)   Williams, D. R.; Shah, A. A. Total Synthesis of (+)-Ileabethoxazole via an Iron-Mediated Pauson–Khand [2 + 2 + 1] Carbocyclization. *J. Am. Chem. Soc.* **2014**, *136* (24), 8829–8836.

(27)   Liao, L.; Zhou, J.; Xu, Z.; Ye, T. Concise Total Synthesis of Nannocystin A. *Angew. Chem. Int. Ed.* **2016**, *55* (42), 13263–13266.

(28)   Reid, W. B.; Spillane, J. J.; Krause, S. B.; Watson, D. A. Direct Synthesis of Alkenyl Boronic Esters from Unfunctionalized Alkenes: A Boryl-Heck Reaction. *J. Am. Chem. Soc.* **2016**, *138* (17), 5539–5542.

(29)   Reid, W. B.; Watson, D. A. Synthesis of Trisubstituted Alkenyl Boronic Esters from Alkenes Using the Boryl-Heck Reaction. *Org. Lett.* **2018**, *20* (21), 6832–6835.

(30)   Idowu, O. O.; Hayes, J. C.; Reid, W. B.; Watson, D. A. Synthesis of 1,1-Diboryl Alkenes Using the Boryl-Heck Reaction. *Org. Lett.* **2021**, acs.orglett.1c01567.

(31)   Coapes, R. B.; Souza, F. E. S.; Thomas, R. Ll.; Hall, J. J.; Marder, T. B. Rhodium Catalysed Dehydrogenative Borylation of Vinylarenes and 1,1-Disubstituted Alkenes without Sacrificial Hydrogenation—a Route to 1,1-Disubstituted Vinylboronates. *Chem. Commun.* **2003**, No. 5, 614–615.

(32)   Brown, J. M.; Lloyd-Jones, G. C. Vinylborane Formation in Rhodium-Catalyzed Hydroboration of Vinylarenes. Mechanism versus Borane Structure and Relationship to Silation. *J. Am. Chem. Soc.* **1994**, *116* (3), 866–878.

(33)   Mkhalid, I. A. I.; Coapes, R. B.; Edes, S. N.; Coventry, D. N.; Souza, F. E. S.; Thomas, R. Ll.; Hall, J. J.; Bi, S.-W.; Lin, Z.; Marder, T. B. Rhodium Catalysed Dehydrogenative Borylation of Alkenes: Vinylboronates via C–H Activation. *Dalton Trans* **2008**, No. 8, 1055–1064.

(34)   Kondoh, A.; Jamison, T. F. Rhodium-Catalyzed Dehydrogenative Borylation of Cyclic Alkenes. *Chem. Commun.* **2010**, *46* (6), 907.

(35)   Morimoto, M.; Miura, T.; Murakami, M. Rhodium-Catalyzed Dehydrogenative Borylation of Aliphatic Terminal Alkenes with Pinacolborane. *Angew. Chem. Int. Ed.* **2015**, *54* (43), 12659–12663.

(36)   Selander, N.; Willy, B.; Szabó, K. J. Selective C H Borylation of Alkenes by Palladium Pincer Complex Catalyzed Oxidative Functionalization. *Angew. Chem. Int. Ed.* **2010**, *49* (24), 4051–4053.

(37)   Kirai, N.; Iguchi, S.; Ito, T.; Takaya, J.; Iwasawa, N. PSiP-Pincer Type Palladium-Catalyzed Dehydrogenative Borylation of Alkenes and 1,3-Dienes. *Bull. Chem. Soc. Jpn.* **2013**, *86* (7), 784–799.

(38)   Takaya, J.; Kirai, N.; Iwasawa, N. Efficient Synthesis of Diborylalkenes from Alkenes and Diboron by a New PSiP-Pincer Palladium-

Catalyzed Dehydrogenative Borylation. *J. Am. Chem. Soc.* **2011**, *133* (33), 12980–12983.

(39)   Sasaki, I.; Doi, H.; Hashimoto, T.; Kikuchi, T.; Ito, H.; Ishiyama, T. Iridium(i)-Catalyzed Vinylic C–H Borylation of 1-Cycloalkenecarboxylates with Bis(Pinacolato)Diboron. *Chem. Commun.* **2013**, *49* (68), 7546.

(40)   Ohmura, T.; Takasaki, Y.; Furukawa, H.; Suginome, M. Stereoselective Synthesis of Cis-β-Methyl- and Phenyl-Substituted Alkenylboronates by Platinum-Catalyzed Dehydrogenative Borylation. *Angew. Chem. Int. Ed.* **2009**, *48* (13), 2372–2375.

(41)   Wang, C.; Wu, C.; Ge, S. Iron-Catalyzed *E* -Selective Dehydrogenative Borylation of Vinylarenes with Pinacolborane. *ACS Catal.* **2016**, *6* (11), 7585–7589.

(42)   Mazzacano, T. J.; Mankad, N. P. Dehydrogenative Borylation and Silylation of Styrenes Catalyzed by Copper-Carbenes. *ACS Catal.* **2017**, *7* (1), 146–149.

(43)   Lu, W.; Shen, Z. Direct Synthesis of Alkenylboronates from Alkenes and Pinacol Diboron via Copper Catalysis. *Org. Lett.* **2019**, *21* (1), 142–146.

(44)   Shi, X.; Li, S.; Wu, L. H ₂ -Acceptorless Dehydrogenative Boration and Transfer Boration of Alkenes Enabled by Zirconium Catalyst. *Angew. Chem. Int. Ed.* **2019**, *58* (45), 16167–16171.

(45)   Bhawal, B. N.; Morandi, B. Catalytic Isofunctional Reactions—Expanding the Repertoire of Shuttle and Metathesis Reactions. *Angew. Chem. Int. Ed.* **2019**, *58* (30), 10074–10103.

(46)   Rochette, É.; Desrosiers, V.; Soltani, Y.; Fontaine, F.-G. Isodesmic C–H Borylation: Perspectives and Proof of Concept of Transfer Borylation Catalysis. *J. Am. Chem. Soc.* **2019**, *141* (31), 12305–12311.

(47)   Marciniec, B.; Jankowska, M.; Pietraszuk, C. New Catalytic Route to Functionalized Vinylboronates. *Chem. Commun.* **2005**, No. 5, 663.

(48)   Marciniec, B.; Dudziec, B.; Kownacki, I. A New Catalytic Route for the Activation of Sp-Hybridized Carbon–Hydrogen Bonds. *Angew. Chem. Int. Ed.* **2006**, *45* (48), 8180–8184.

(49)   Szyling, J.; Franczyk, A.; Pawluć, P.; Marciniec, B.; Walkowiak, J. A Stereoselective Synthesis of (*E*)- or (*Z*)-β-Arylvinyl Halides *via* a Borylative Coupling/Halodeborylation Protocol. *Org. Biomol. Chem.* **2017**, *15* (15), 3207–3215.

(50)   Szyling, J.; Walkowiak, J.; Sokolnicki, T.; Franczyk, A.; Stefanowska, K.; Klarek, M. PEG-Mediated Recyclable Borylative Coupling of Vinyl Boronates with Olefins. *J. Catal.* **2019**, *376*, 219–227.

(51)   Szyling, J.; Sokolnicki, T.; Franczyk, A.; Walkowiak, J. Ru-Catalyzed Repetitive Batch Borylative Coupling of Olefins in Ionic Liquids or Ionic Liquids/ScCO2 Systems. *Catalysts* **2020**, *10* (7), 762.

(52)   Lam, K. C.; Lin, Z.; Marder, T. B. DFT Studies of β-Boryl Elimination Processes: Potential Role in Catalyzed Borylation Reactions of Alkenes. *Organometallics* **2007**, *26* (13), 3149–3156.

(53)   Kalläne, S. I.; Braun, T.; Braun, B.; Mebs, S. Versatile Reactivity of a Rhodium(i) Boryl Complex towards Ketones and Imines. *Dalton Trans.* **2014**, *43* (18), 6786.

(54)   Franke, R.; Selent, D.; Börner, A. Applied Hydroformylation. *Chem. Rev.* **2012**, *112* (11), 5675–5732.

(55)   Murphy, S. K.; Park, J.-W.; Cruz, F. A.; Dong, V. M. Rh-Catalyzed C–C Bond Cleavage by Transfer Hydroformylation. *Science* **2015**, *347* (6217), 56–60.

(56)   Wu, X.; Cruz, F. A.; Lu, A.; Dong, V. M. Tandem Catalysis: Transforming Alcohols to Alkenes by Oxidative Dehydroxymethylation. *J. Am. Chem. Soc.* **2018**, *140* (32), 10126–10130.

(57)   Tan, G.; Wu, Y.; Shi, Y.; You, J. Syngas-Free Highly Regioselective Rhodium-Catalyzed Transfer Hydroformylation of Alkynes to α,β-Unsaturated Aldehydes. *Angew. Chem. Int. Ed.* **2019**, *58* (22), 7440–7444.

(58)   Baker, R. T.; Calabrese, J. C.; Westcott, S. A.; Nguyen, P.; Marder, T. B. Insertion of Alkenes into Rhodium-Boron Bonds. *J. Am. Chem. Soc.* **1993**, *115* (10), 4367–4368.

(59)   *For Precedences of B-Boryl Elimination for Other Transition Metal Complexes, Implicated by the Results of Their Catalytic Activities, Including Zr, Ru, and Pd-Catalyzed Reactions, See Ref. 43, 46, 56, and 57.*

(60)   Miyaura, N.; Suzuki, A. The Palladium-Catalyzed "Head-to-Tail" Cross-Coupling Reaction of 1-Alkenylboranes with Phenyl or 1-Alkenyl Iodides. A Novel Synthesis of 2-Phenyl-1-Alkenes or 2-Alkyl-1,3-Alkadienes via Organoboranes. *J. Organomet. Chem.* **1981**, *213* (2), C53–C56.

(61)   Ohmura, T.; Oshima, K.; Taniguchi, H.; Suginome, M. Switch of Regioselectivity in Palladium-Catalyzed Silaboration of Terminal Alkynes by Ligand-Dependent Control of Reductive Elimination. *J. Am. Chem. Soc.* **2010**, *132* (35), 12194–12196.

(62)   Teltewskoi, M.; Panetier, J. A.; Macgregor, S. A.; Braun, T. A Highly Reactive Rhodium(I)-Boryl Complex as a Useful Tool for C   H Bond Activation and Catalytic C   F Bond Borylation. *Angew. Chem. Int. Ed.* **2010**, *49* (23), 3947–3951.

(63)   Dai, C.; Stringer, G.; Marder, T. B.; Scott, A. J.; Clegg, W.; Norman, N. C. Synthesis and Characterization of Rhodium(I) Boryl and Rhodium(III) Tris(Boryl) Compounds: Molecular Structures of [(PMe ₃) ₄ Rh(B(Cat))] and *Fac* -[(PMe ₃) ₃ Rh(B(Cat)) ₃] (Cat = 1,2-O ₂ C ₆ H ₄). *Inorg. Chem.* **1997**, *36* (3), 272–273.

(64)   Masuda, Y.; Hasegawa, M.; Yamashita, M.; Nozaki, K.; Ishida, N.; Murakami, M. Oxidative Addition of a Strained C–C Bond onto Electron-Rich Rhodium(I) at Room Temperature. *J. Am. Chem. Soc.* **2013**, *135* (19), 7142–7145.

(65)   Irvine, G. J.; Lesley, M. J. G.; Marder, T. B.; Norman, N. C.; Rice, C. R.; Robins, E. G.; Roper, W. R.; Whittell, G. R.; Wright, L. J. Transition Metal−Boryl Compounds: Synthesis, Reactivity, and Structure. *Chem. Rev.* **1998**, *98* (8), 2685–2722.

(66)   Braunschweig, H.; Colling, M. Transition Metal Complexes of Boron — Synthesis, Structure and Reactivity. *Coord. Chem. Rev.* **2001**, *223* (1), 1–51.

(67)   Esteruelas, M. A.; Oliván, M.; Vélez, A. POP–Rhodium-Promoted C–H and B–H Bond Activation and C–B Bond Formation. *Organometallics* **2015**, *34* (10), 1911–1924.

(68)   Zhao, P.; Incarvito, C. D.; Hartwig, J. F. Carbon−Oxygen Bond Formation between a Terminal Alkoxo Ligand and a Coordinated Olefin. Evidence for Olefin Insertion into a Rhodium Alkoxide. *J. Am. Chem. Soc.* **2006**, *128* (30), 9642–9643.

(69)   Richers, C. P.; Roediger, S.; Laserna, V.; Hartwig, J. F. Effects of Ligands on the Migratory Insertion of Alkenes into Rhodium–Oxygen Bonds. *Chem. Sci.* **2020**, *11* (38), 10449–10456.

(70)   *For Details, See the Supporting Information.*

(71)   Uetake, Y.; Niwa, T.; Hosoya, T. Rhodium-Catalyzed *Ipso* -Borylation of Alkylthioarenes via C–S Bond Cleavage. *Org. Lett.* **2016**, *18* (11), 2758–2761.

(72)   Lindhardt (neé Hansen), A. T.; Mantel, M. L. H.; Skrydstrup, T. Palladium-Catalyzed Intermolecular Ene–Yne Coupling: Development of an Atom-Efficient Mizoroki–Heck-Type Reaction. *Angew. Chem. Int. Ed.* **2008**, *47* (14), 2668–2672.

(73)   Kaminsky, L.; Wilson, R. J.; Clark, D. A. Stereo- and Regioselective Formation of Silyl-Dienyl Boronates. *Org. Lett.* **2015**, *17* (12), 3126–3129.

(74)   Shintani, R.; Duan, W.-L.; Park, S.; Hayashi, T. Rhodium-Catalyzed Isomerization of Unactivated Alkynes to 1,3-Dienes. *Chem.*

Commun. **2006**, No. 34, 3646.

(75)   Geier, M. J.; Vogels, C. M.; Decken, A.; Westcott, S. A. The Transition Metal Catalyzed Hydroboration of Enamines. *J. Organomet. Chem.* **2009**, *694* (19), 3154–3159.

(76)   Myhill, J. A.; Wilhelmsen, C. A.; Zhang, L.; Morken, J. P. Diastereoselective and Enantioselective Conjunctive Cross-Coupling Enabled by Boron Ligand Design. *J. Am. Chem. Soc.* **2018**, *140* (45), 15181–15185.

(77)   Hecker, S. J.; Reddy, K. R.; Lomovskaya, O.; Griffith, D. C.; Rubio-Aparicio, D.; Nelson, K.; Tsivkovski, R.; Sun, D.; Sabet, M.; Tarazi, Z.; Parkinson, J.; Totrov, M.; Boyer, S. H.; Glinka, T. W.; Pemberton, O. A.; Chen, Y.; Dudley, M. N. Discovery of Cyclic Boronic Acid QPX7728, an Ultrabroad-Spectrum Inhibitor of Serine and Metallo-β-Lactamases. *J. Med. Chem.* **2020**, *63* (14), 7491–7507.

(78)   Matteson, D. S. Boronic Esters in Asymmetric Synthesis. *J. Org. Chem.* **2013**, *78* (20), 10009–10023.

(79)   Andrés, P.; Ballano, G.; Calaza, M. I.; Cativiela, C. Synthesis of α-Aminoboronic Acids. *Chem. Soc. Rev.* **2016**, *45* (8), 2291–2307.

(80)   Du, R.; Liu, L.; Xu, S. Iridium-Catalyzed Regio- and Enantioselective Borylation of Unbiased Methylene C(Sp^3)−H Bonds at the Position β to a Nitrogen Center. *Angew. Chem. Int. Ed.* **2021**, *60* (11), 5843–5847.

(81)   Hitosugi, S.; Tanimoto, D.; Nakanishi, W.; Isobe, H. A Facile Chromatographic Method for Purification of Pinacol Boronic Esters. *Chem. Lett.* **2012**, *41* (9), 972–973.

(82)   Kloek, S. M.; Heinekey, D. M.; Goldberg, K. I. C   H Bond Activation by Rhodium(I) Hydroxide and Phenoxide Complexes. *Angew. Chem. Int. Ed.* **2007**, *46* (25), 4736–4738.

(83)   Kegley, S. E.; Schaverien, C. J.; Freudenberger, J. H.; Bergman, R. G.; Nolan, S. P.; Hoff, C. D. Rhodium Alkoxide Complexes. Formation of an Unusually Strong Intermolecular Hydrogen Bond in (PMe3)3Rh-Otol(HOtol). *J. Am. Chem. Soc.* **1987**, *109* (21), 6563–6565.

(84)   Qi, X.; Li, Y.; Bai, R.; Lan, Y. Mechanism of Rhodium-Catalyzed C–H Functionalization: Advances in Theoretical Investigation. *Acc. Chem. Res.* **2017**, *50* (11), 2799–2808.

(85)   Bhawal, B. N.; Reisenbauer, J. C.; Ehinger, C.; Morandi, B. Overcoming Selectivity Issues in Reversible Catalysis: A Transfer Hydrocyanation Exhibiting High Kinetic Control. *J. Am. Chem. Soc.* **2020**, *142* (25), 10914–10920.

(86)   Adams, G. M.; Weller, A. S. POP-Type Ligands: Variable Coordination and Hemilabile Behaviour. *Coord. Chem. Rev.* **2018**, *355*, 150–172.

(87)   Crabtree, R. H. *The Organometallic Chemistry of the Transition Metals: Sixth Edition*; John Wiley & Sons, Inc.: Hoboken, 2014.

(88)   de Oliveira Dias, A.; Gutiérrez, M. G. P.; Villarreal, J. A. A.; Carmo, R. L. L.; Oliveira, K. C. B.; Santos, A. G.; dos Santos, E. N.; Gusevskaya, E. V. Sustainable Route to Biomass-Based Amines: Rhodium Catalyzed Hydroaminomethylation in Green Solvents. *Appl. Catal. Gen.* **2019**, *574* (November 2018), 97–104.

(89)   Reid, W. B.; Spillane, J. J.; Krause, S. B.; Watson, D. A. Direct Synthesis of Alkenyl Boronic Esters from Unfunctionalized Alkenes: A Boryl-Heck Reaction. *J. Am. Chem. Soc.* **2016**, *138* (17), 5539–5542.

(90)   Du, R.; Liu, L.; Xu, S. Iridium-Catalyzed Regio- and Enantioselective Borylation of Unbiased Methylene C(Sp3)−H Bonds at the Position β to a Nitrogen Center. *Angew. Chem. - Int. Ed.* **2021**, *60* (11), 5843–5847.

(91)   Hitosugi, S.; Tanimoto, D.; Nakanishi, W.; Isobe, H. A Facile Chromatographic Method for Purification of Pinacol Boronic Esters. *Chem. Lett.* **2012**, *41* (9), 972–973.

(92)   Cramer, C. J.; Truhlar, D. G. Density Functional Theory for Transition Metals and Transition Metal Chemistry. *Phys. Chem. Chem. Phys.* **2009**, *11* (46), 10757–10816.

(93)   Frisch, M. J.; Trucks, G. W.; Schlegel, H. B.; Scuseria, G. E.; Robb, M. A.; Cheeseman, J. R.; Scalmani, G.; Barone, V.; Mennucci, B.; Petersson, G. A.; Nakatsuji, H.; Caricato, M.; Li, X.; Hratchian, H. P.; Izmaylov, A. F.; Bloino, J.; Zheng, G.; Sonnenb, D. J. *Gaussian 09*; Gaussian, Inc: Wallingford CT, 2009.

(94)   Zhao, Y.; Truhlar, D. G. Density Functionals with Broad Applicability in Chemistry. *Acc. Chem. Res.* **2008**, *41* (2), 157–167.

(95)   Weigend, F.; Ahlrichs, R. Balanced Basis Sets of Split Valence, Triple Zeta Valence and Quadruple Zeta Valence Quality for H to Rn: Design and Assessment of Accuracy. *Phys. Chem. Chem. Phys.* **2005**, *7* (18), 3297–3305.

(96)   Andrae, D.; Häußermann, U.; Dolg, M.; Stoll, H.; Preuß, H. Energy-Adjustedab Initio Pseudopotentials for the Second and Third Row Transition Elements. *Theor. Chim. Acta* **1990**, *77* (2), 123–141.

(97)   Weigend, F. Accurate Coulomb-Fitting Basis Sets for H to Rn. *Phys. Chem. Chem. Phys.* **2006**, *8* (9), 1057–1065.

(98)   Marenich, A. V.; Cramer, C. J.; Truhlar, D. G. Universal Solvation Model Based on Solute Electron Density and on a Continuum Model of the Solvent Defined by the Bulk Dielectric Constant and Atomic Surface Tensions. *J. Phys. Chem. B* **2009**, *113* (18), 6378–6396.

CHAPTER 4

DFT Studies of the Catalyst Structure – Activity & Selectivity Relationships in Rh(I)-catalyzed Transfer C–H Borylation of Alkenes
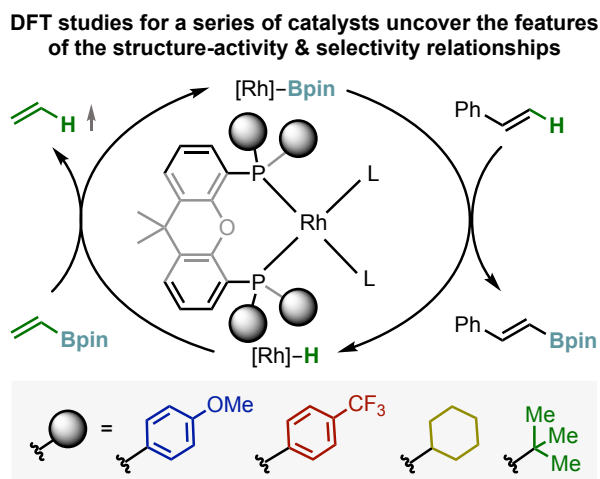
This work has been done entirely by myself under the supervision of Paweł Dydio.

.

4.1 Introduction

Methods enabling the borylation of C–H bonds are attractive for the preparation of synthetically valuable intermediates as well as for the diversity-oriented late-stage modification of complex molecules,[1–6] which can utilize a broad range of C–B bond post-functionalization reactions.[7–10] Strategies of C–H functionalization by functional group transfer, often referred to as shuttle catalysis, are particularly appealing, because they typically avoid using highly reactive reagents, thereby improving the scope and utility of the methods.[11,12] Inspired by prior works of Marciniec[13,14], Wu[15] and Marder[16], our group recently developed a potent method for the transfer C–H borylation of alkenes using a Rh(I)-xantphos catalytic system, which offers high functional group tolerance and excellent β-regio- and (Z)-stereoselectivity (Figure 1a).[17] However, some challenges remain to be addressed, such as the limited activity of the catalyst especially in the case of reactions for internal alkenes or the control of selectivity to promote formation of other regio- and stereoisomers of the product. For instance, synthesis of (α)-regioisomer of the product remains inaccessible with either transfer catalysis or any other methods of C-H borylation of alkenes.[18,19]

During our previous studies of the transfer C–H borylation reaction under Rh(I) catalysis, we unraveled the detailed mechanism of the reaction and its key features.[17] Specifically, we found that the catalytic cycle consists of a sequence of four reversible steps: (i) alkene insertion into Rh–H bond, (ii) β-boryl elimination, which was unprecedented for Rh complexes, (iii) alkene insertion into Rh–B bond, and (iv) β-hydride elimination releasing the product and closing the cycle (Figure 1b). Investigation of the free energy surface of the model reaction gave insight into the key catalytic intermediates and transition states. The DFT data revealed that alkene insertion into Rh–B bond determines the rate and regioselectivity, while β-hydride elimination determines the stereoselectivity of the reaction (Figure 1c). Furthermore, our studies showed that the oxygen atom of the xanthene motif is not involved in the coordination to the Rh center, indicating that a rigid structure of xantphos and its bite angle is more important than an additional potential coordination site. However, the importance and influence that electronic and steric properties of the coordinating phosphine moieties have on the reaction profile was not elucidated. Such features of ligands often have a dramatic effect on the activity and selectivity of catalysts.[20,21]

Using DFT studies as a tool, the effects that certain modifications to the catalyst structure have on the reaction profile can be easily explored and understood.[22] Such studies are particularly attractive prior to tedious experimentation required for the synthesis of new putative catalysts.[23] The computational insights can facilitate a rational design and selection of new candidates, thereby saving significant resources and time[24], as shown for instance in works dedicated to the design and development of (Z)-selective catalysts for the cross-metathesis reaction.[21,25,26]

With the overall goal of addressing the remaining challenges in the transfer C–H borylation of alkenes, we aim to gain further insights into the reaction and understand the catalyst structure – activity and selectivity relationships. Here we present our studies to reveal how the electronic and steric features of the phosphine ligand of the Rh catalyst influences the activity and selectivity of the transfer C–H borylation reaction. A computational investigation of four Rh catalysts bearing analogues of xantphos ligand with either electron-donating, electron-withdrawing, or sterically demanding motifs was performed (Figure 1d). The study revealed the effects that these modifications have on the free energy surfaces of the reaction. Insights into the effects on each elementary step of the catalytic cycle are also discussed.
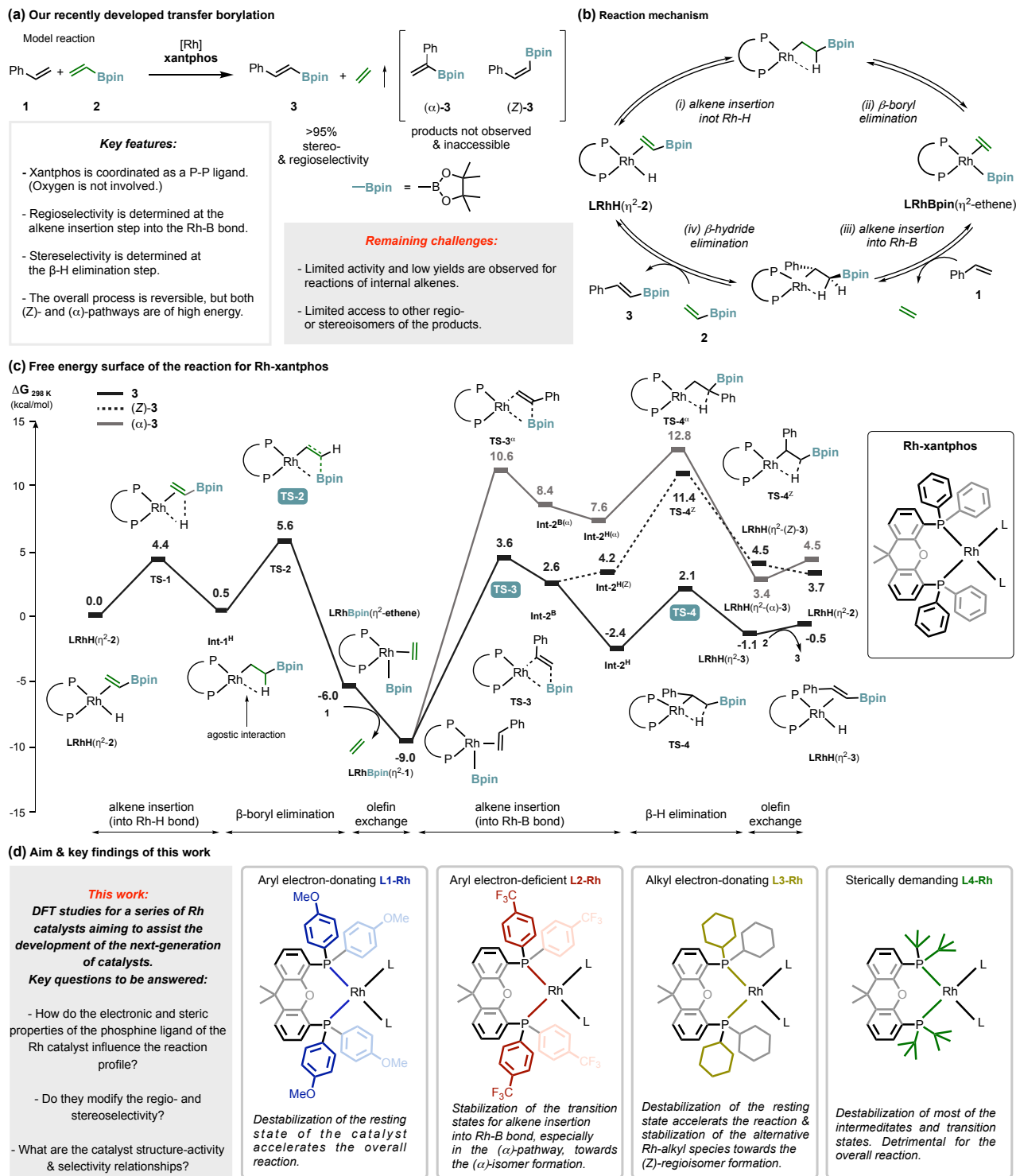
Figure 1. (a) Previously reported transfer C-H borylation under Rh(I)-catalysis and its key features, (b) reaction mechanism, and (c) its free energy surfaces with the Rh-xantphos catalyst leading to products **3**, (Z)-**3**, or (α)-**3**. Int, intermediate, TS, transition state. (d) Catalysts studied in this work bearing different electronic and steric properties, and the key findings.

4.2 Results and Discussion

4.2.1 Influence of the electronic properties

We commenced our studies by analyzing the influence that electronic features of the ligand of the catalyst have on the reaction profile, by installing either electron-donating or electron-withdrawing motifs in the *para*-positions of all four phenyl groups of the Rh-xantphos system. Specifically, we studied **L1-Rh** catalyst bearing phenyls with electron-donating methoxy functions and **L2-Rh** catalyst bearing phenyls with electron-withdrawing trifluoromethyl functions (Figure 1d). Considering the relatively small size of the substituents and their positions, these modifications have minor influence on the steric requirements, thereby allowing to dissect the electronic effects irrespectively of the steric demand.

The free energy surfaces for the reactions with **L1-Rh** and **L2-Rh** (Figure 2) closely resemble that with the original Rh-xantphos catalyst (Figure 1c; for the overlays of energy surfaces, see Figures 3-4). In this context, the resting state of the catalyst (Rh(I)-boryl intermediate coordinating to an alkene starting material), as well as the rate-limiting and regioselectivity determining step (alkene insertion into Rh–B bond), and the stereoselectivity determining step (β-hydride elimination) remain the same for all three catalysts. Although the data indicate a rather limited impact of the electronic properties of the ligand on the overall reaction profile, the detail analysis reveals distinct influences on the reaction intermediates and the elementary reactions, which will be discussed below.

L1-Rh catalyst bearing electron-rich aryl groups

Resting state. The formation of the lowest energy intermediate **L1RhBpin**(η^2-**1**) from the initial Rh(I)-hydride complex **L1RhH**(η^2-**2**) through alkene insertion into Rh-H bond, β-boryl elimination to generate Rh(I)-boryl intermediate, **L1RhBpin**(η^2-ethene), followed by olefin exchange (and ethene extrusion) occurs with slightly higher free energy barriers in comparison to those with Rh-xantphos catalyst (Figures 4a-b and 3). Most notably, the relative free energy of **L1RhBpin**(η^2-**1**) is higher than that of **xantphos-RhBpin**(η^2-**1**), (-7.0 kcal/mol vs. -9.0 kcal/mol, respectively), indicating that electron rich ligands can destabilize the lowest energy intermediate without affecting the subsequent transition state. Importantly, such a resting state destabilization might be used as a strategy to increase the activity of catalytic reactions, as previously observed for processes catalyzed by enzymes or transition metal complexes.[27,28]

Rate & regioselectivity. Analogous to the Rh-xantphos catalyst, alkene insertion into Rh(I)−B bond, occurring through **TS-3(L1)** with a free energy barrier of +11.0 kcal/mol, is predicted to be the rate and regioselectivity determining step of the reaction, favoring the formation of product **3.** The other pathway leading to the formation of (α)-**3** through alkene insertion through **TS-3$^\alpha$(L1)** presents a substantially higher free energy barrier of +16.1 kcal/mol. Additionally, the subsequent b-hydride elimination step, occurring through high energy **TS-4$^\alpha$(L1)**, leads to an overall free energy barrier of +20.4 (Figure 9). Most notably, in the productive pathway for the formation of **3**, the barrier for the rate determining step is 1.6 kcal/mol lower with **L1-Rh** than with Rh-xantphos. This difference is mainly due to a destabilization of the **L1RhBpin**(η^2-**1**) intermediate rather than a stabilization of the corresponding transition state. Specifically, a comparison with the Rh-xantphos system showed that complex **L1RhBpin**(η^2-**1**) is 2.0 kcal/mol less stable in respect to the initial hydride complex, whereas the transition state **TS-3(L1)** is only 0.4 kcal/mol less stable in respect to the hydride complex (Figure 3).

Figure 2. Free energy surfaces for the transfer borylation reaction leading to products **3**, (Z)-**3**, or (α)-**3** for: (a) catalyst **Rh-L1** bearing aryl electron-donating groups; (b) catalyst **Rh-L2** bearing aryl electron-deficient groups. Int, intermediate, TS, transition state.

Stereoselectivity. Subsequently, **Int-2^B(L1)**, the formed Rh-alkyl intermediate engaged in a C–B-Rh agostic-like interaction, is predicted to easily interconvert to **Int-2^H(L1)**, Rh-alkyl intermediate engaged in a C–H-Rh agostic interaction. The latter undergoes readily (*E*)-selective *β*-hydride elimination, through **TS-4(L1)** with a relative free energy barrier of +3.0 kcal/mol for the formation of product **3**. The alternative (*Z*)-selective pathway is predicted to occur through less stable intermediate and transition state, **Int-2^(H(Z))(L1)** and **TS-4^Z(L1)**, accounting for a higher relative free energy barrier of +7.1 kcal/mol and overall free energy barrier of +19.2. kcal/mol for the formation of (*Z*)-**3**.
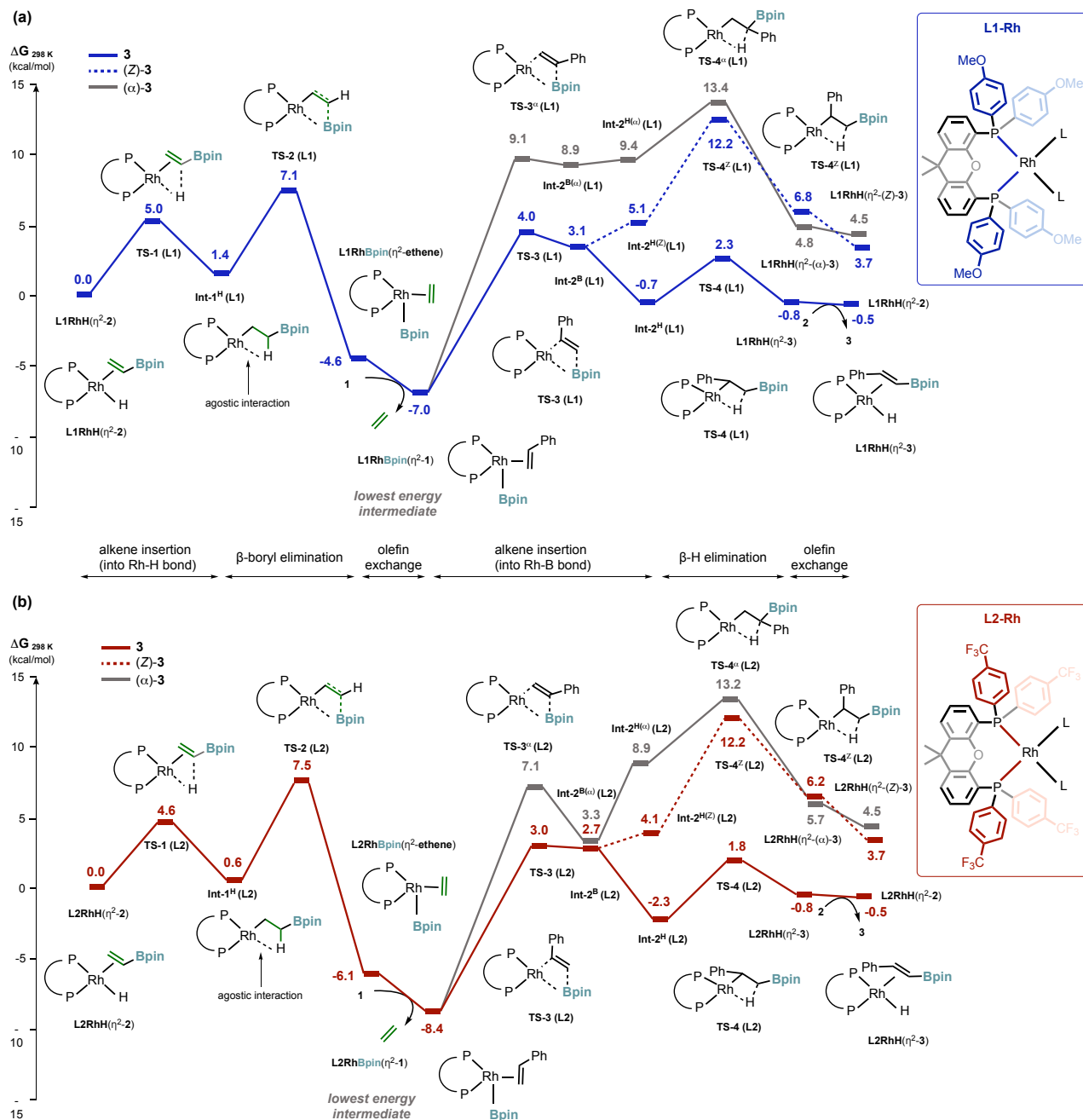

Figure 3. Overlay of free energy surfaces for the transfer borylation reaction leading to products **3**, (*Z*)-**3**, or (α)-**3** for catalyst **Rh-L1** bearing aryl electron donating groups and **Rh-xantphos**. Int, intermediate, TS, transition state.

L2-Rh catalyst bearing electron-deficient aryl groups

Resting state. The profile for the formation of the intermediate **L2RhBpin**(η^2-**1**) closely resembles that of the Rh-xantphos system, presenting a similar barrier for the alkene insertion step occurring through **TS-1(L2)** (+4.6 kcal/mol) and a slightly higher free energy barrier for the β-boryl elimination step occurring through **TS-2(L2)** (+7.5 kcal/mol, Figure 9a-9b). When compared to the profile of the Rh-xantphos catalyst, the higher free energy barrier is imposed mostly by the transition state destabilization, while the relative stability of **L2RhBpin**(η^2-**ethene**) and **L2RhBpin**(η^2-**1**) complexes remained nearly unmodified (Figure 4).
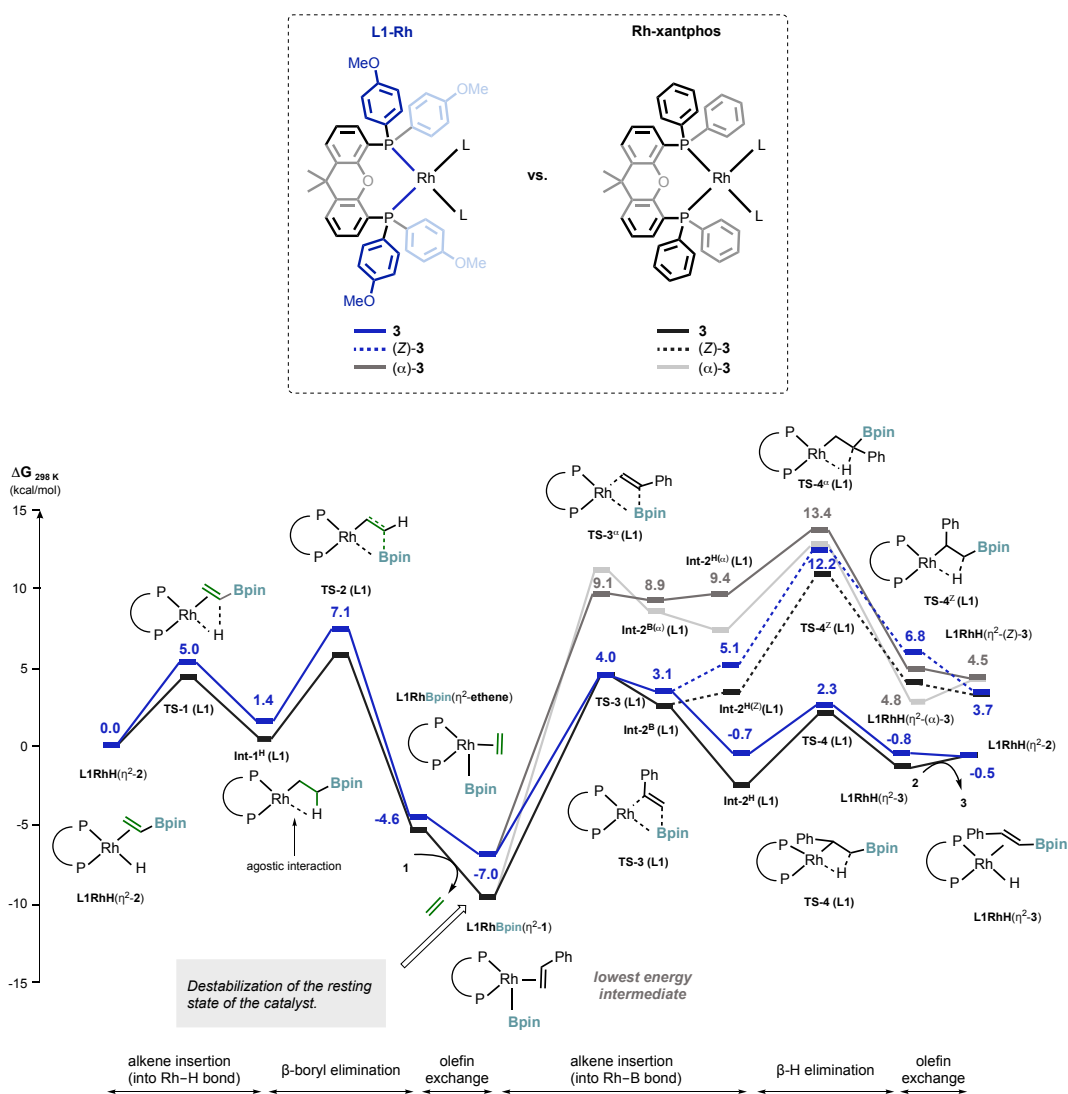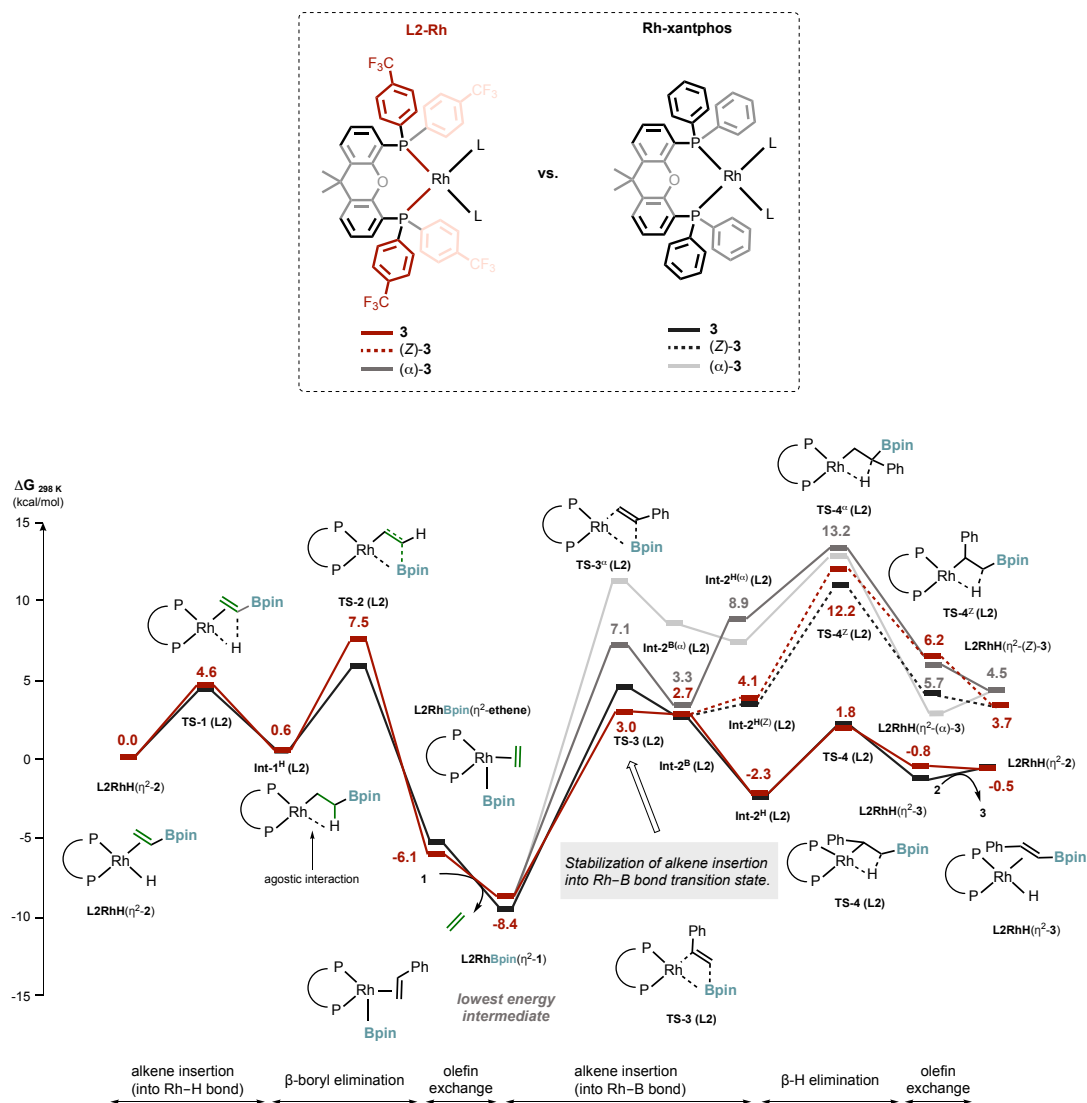

Figure 4. Overlay of free energy surfaces for the transfer borylation reaction leading to products **3**, (Z)-**3**, or (α)-**3** for catalyst **Rh-L2** bearing aryl electron-deficient groups and **Rh-xantphos**. Int, intermediate, TS, transition state.

Rate & regioselectivity. The rate determining step for the reaction with **L2-Rh** catalyst is also predicted to be alkene insertion into Rh(I)−B bond occurring through **TS-3(L2)**, which accounts for a free energy barrier of +11.4 kcal/mol for the formation of product **3**. When compared with that of the Rh-xantphos catalyst, the slightly lower barrier with **L2-Rh** results from the stabilization of the corresponding transition state, in contrast to the resting destabilization observed for **L1-Rh** (compare Figure 3 vs. 4). The alternative alkene insertion occurring at the α-position through **TS-3$^\alpha$(L2)** accounts for a higher free energy barrier (+15.5 kcal/mol). However, it is worth noting that **L2-Rh** catalyst causes a significant decrease in the free energy difference between the insertion at α-position *vs.* β-position. In this context, the original difference of 7.0 kcal/mol observed for the Rh-xantphos catalyst is lowered to 4.1 kcal/mol for **L2-Rh** (Figure 4). Assuming a consistent trend, this result suggests that the regioselectivity of the reaction could be modified by means of catalysts bearing ligands with even stronger electron withdrawing groups.

Stereoselectivity. The following steps of the profile leading to products **3** and (*Z*)-**3** are closely related to those observed in the original Rh-xantphos system (Figure 4). The β-hydride elimination step leading to the (*E*)-product **3** occurs through the more stable **Int-2^H(L2)** and **TS-4(L2)**, with a relative free energy barrier of +4.1 kcal/mol, while the alternative β-hydride elimination leading to (*Z*)-product requires to adapt to a significantly less stable **Int-2$^{H(Z)}$(L2)**, overcoming **TS-4^Z(L2)** with a significantly higher energy barrier of +8.1 kcal/mol, accounting for an overall barrier of +20.6 kcal/mol for the formation of (*Z*)-**3** (Figure 9d-e).

L3-Rh catalyst bearing electron-rich cyclohexyl groups

Bolstered by the results obtained for **L1-Rh** catalyst bearing the electron rich aryl ligand, we investigated **L3-Rh** catalyst bearing a ligand with cyclohexyl groups in place of the phenyl groups, the catalyst with a strongly increased electron donating character on the phosphine moieties. Noteworthy, besides the electronic effects, the replacement of the phenyl rings by cyclohexyl groups leads to a moderate increase of the steric demand,[29] thus caution should be taken when comparing the data. The obtained free energy surface for the **L3-Rh** catalyst resembles the profile for the original Rh-xantphos catalyst (Figures 5a vs. 1c; for the overlay of the profiles, see Figure 6). However, notable changes are observed regarding the alkene insertion into Rh(I)−H bond and β-hydride elimination steps (Figure 9a-d), which hint toward the abovementioned electronic changes being beneficial for the design of prospective (*Z*)-selective catalysts.

Resting state. A notable change in the profile is observed for the alkene insertion into Rh(I)−H bond occurring through **TS-1(L3)** with a small free energy barrier of +0.8 kcal/mol (vs. +4.4 kcal/mol for the Rh-xantphos system, Figure 9a). Additionally, the energy barrier for the β-boryl elimination step occurring through **TS-2(L3)** is increased (+7.0 kcal/mol, Figure 9b), while both **L3RhBpin**(η^2-ethene) and **L3RhBpin**(η^2-**1**) complexes are destabilized in respect to their counterparts in the Rh-xantphos system (Figure 6). In general, these changes to the reaction profile resemble those observed for electron-rich **L1-Rh**, indicating consistent trends imposed by increasing the electron donating properties of the ligands.

Figure 5. Free energy surfaces for the transfer borylation reaction leading to products **3**, (Z)-**3**, or (α)-**3** for: (a) catalyst **Rh-L3** bearing alkyl electron donating groups; (b) catalyst **Rh-L4** bearing alkyl electron rich and sterically demanding tert-butyl groups. Int, intermediate, TS, transition state.

Rate & regioselectivity. The alkene insertion into Rh(I)−B bond, occurring through **TS-3(L3)** with a free energy barrier of +11.1 kcal/mol, remains the rate limiting and regioselectivity determining step of the reaction (Figure 9c). Alike for **L1-Rh**, the observed lower free energy barrier originates from the destabilization of the resting state rather than from the stabilization of the corresponding transition state (Figure 6). Notably, the difference in free energy for insertion at the α-position through **TS-3$^{\alpha}$(L3)** *vs.* insertion at the β-position through **TS-3(L3)** is increased to +7.8 kcal/mol. These findings are consistent with the predicted stabilization of the corresponding α-transition state when the catalyst bearing an electron-deficient ligand **L2-Rh** was employed (Figure 9c).
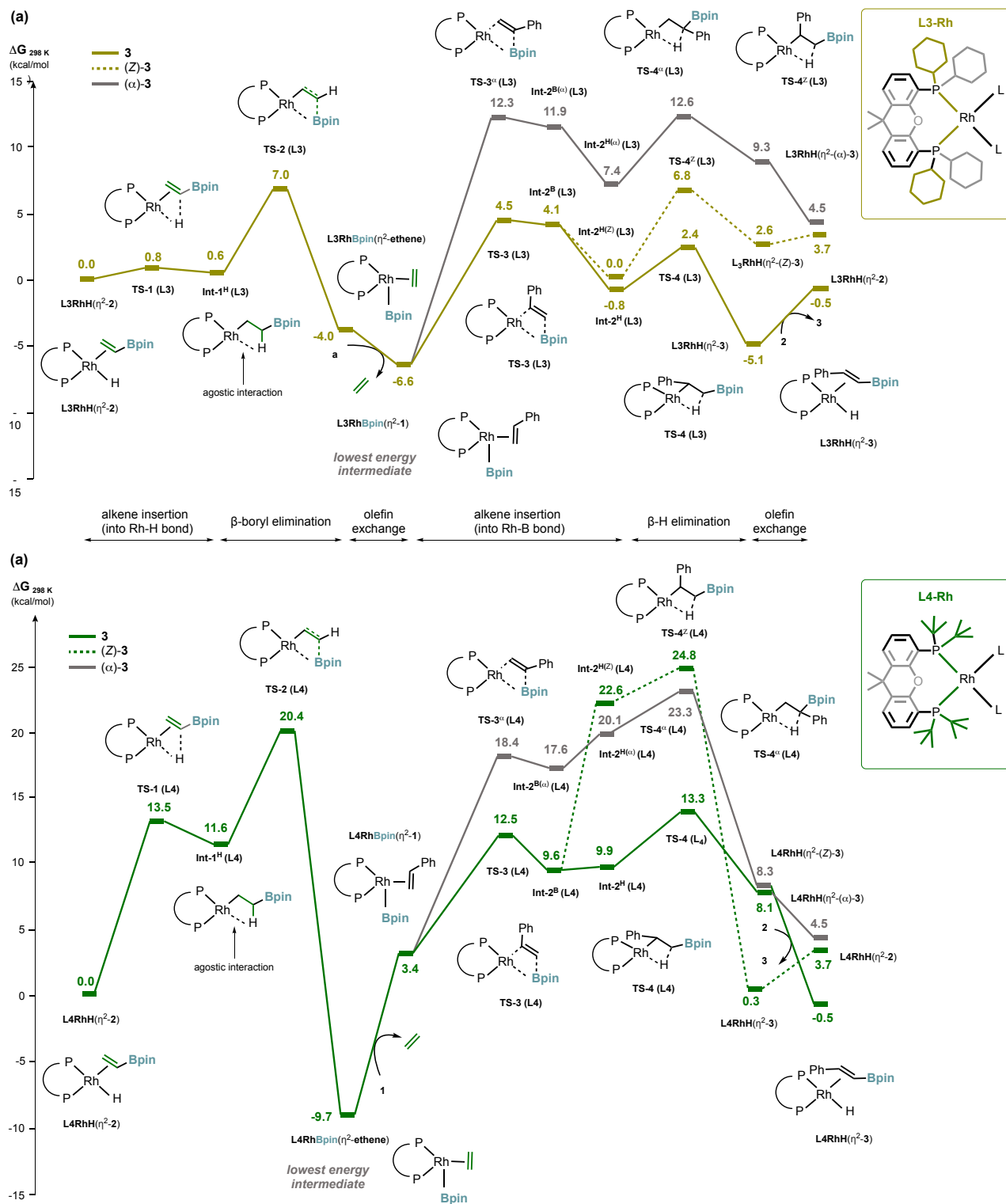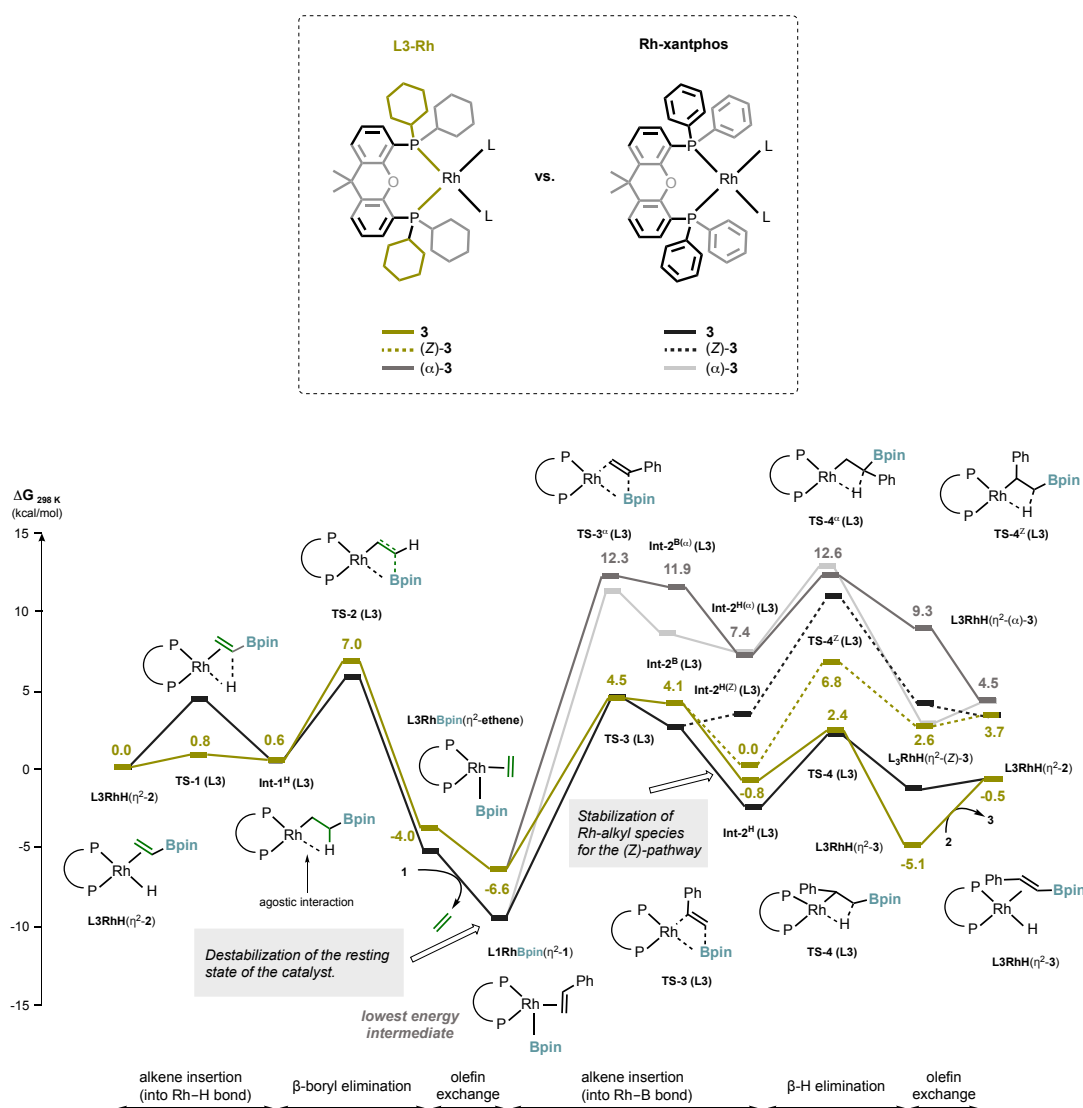

Figure 6. Overlay of free energy surfaces for the transfer borylation reaction leading to products **3**, (Z)-**3**, or (α)-**3** for catalyst **Rh-L3** bearing alkyl electron donating groups and **Rh-xantphos**. Int, intermediate, TS, transition state.

.

Stereoselectivity. The β-hydride elimination proceeds readily from **Int-2^H(L3)**, through **TS-4(L3)** with an energy barrier of +3.3 kcal/mol, towards the formation of product **3**. Once more, this reveals the selectivity toward the *E*-selective pathway over the *Z*-selective pathway occurring through an alternative **Int-2$^{H(Z)}$(L3)** and **TS-4^Z(L3)**, which accounts for a higher barrier of +6.7 kcal/mol for the formation of the (*Z*)-**3** product (Figure 9d). However, the free energy difference between the competing transition states, that is, the difference that determines the stereoselectivity is significantly decreased for **L3-Rh** in comparison to the other systems studied; $\Delta\Delta G^\ddagger_{TS-4(Z-E)}$ is +4.4 kcal/mol for **L3-Rh** vs. +9.3 kcal/mol for **Rh-xantphos**, +9.9 kcal/mol for **L1-Rh**, +10.4 kcal/mol for **L2-Rh** (Figure 9d). This decreased difference originates from the substantial stabilization of the alternative alkyl intermediate presenting an agostic interaction, **Int-2$^{H(Z)}$(L3)**, respect to **Int-2^H(L3)**, which differ in energy only +0.8 kcal/mol (Figure 5a). This result suggests that catalysts bearing strong electron-donating alkyl phosphines could be a good starting point towards the development of (Z)-selective catalyst candidates, which would capitalize on electronic stabilization of the intermediates of the (Z)-selective pathway.

4.2.2 Influence of the steric demand on the reaction profile

<u>**L4-Rh** catalyst bearing electron-rich, sterically demanding *tert*-butyl groups</u>

Because the increased steric demand of phosphine ligands might accelerate the transition metal catalyzed reactions,[30–34] we next evaluated the reaction profile for **L4-Rh** catalyst bearing a xantphos analogue with sterically demanding *tert*-butyl groups in place of the phenyl rings. Noteworthy, the electronic influence of *tert*-butyl group at the phosphine center is similar to that of a cyclohexyl ring,[35] hence **L3-Rh** and **L4-Rh** are electronically similar, but the latter carries a substantially increased steric demand.[29] The obtained reaction profile is presented in Figure 5b (for the overlays with profiles for the Rh-xantphos catalyst or **L3-Rh**, see Figure 7-8). Overall, the increased steric demand leads to the destabilization of transition states and intermediates bearing sizeable alkene or alkyl ligands, thereby resulting in high free energy barriers for most of the steps of the catalytic cycle.

Resting state. Both alkene insertion into Rh(I)−H bond through **TS-1(L4)** and β-boryl elimination steps through **TS-2(L4)** occur with significantly higher free energy barriers, +13.5 kcal/mol and +20.4 kcal/mol, respectively, than the counterparts with any other ligands (Figure 9a-b). In addition, **L4RhBpin**(η^2-ethene) is found to be the lowest energy intermediate, instead of the commonly found **LRhBpin**(η^2-**1**), reflecting the remarkable steric repulsion even for coordination of substrate **1** (vs. ethene), leading to a change of the prospective resting state of the catalyst.

Rate & selectivity. In addition to the change of the resting state, the β-hydride elimination step is predicted to be the rate, regio- and stereoselectivity determining step. The formation of **3** requires endergonic alkene exchange for **1** (+13.1 kcal/mol), endergonic alkene insertion into Rh(I)−B bond (+6.2 kcal/mol) through **TS-3(L4)**, followed by rate-limiting and selectivity determining β-hydride elimination through **TS-4(L4)**, accounting for an overall free energy barrier of +23.0 kcal/mol. The formation of (α)-**3** and (Z)-**3**, through rate limiting **TS-4$^\alpha$(L4)** and **TS-4^Z(L4)**, respectively, is predicted to involve substantially higher overall free energy barriers, +33.0 kcal/mol and +34.5 kcal/mol respectively.

Overall, the computed profile for **L4-Rh** indicate that a significant increase in the catalyst steric demand is rather detrimental for the title reaction.

Figure 7. Overlay of free energy surfaces for the transfer borylation reaction leading to products **3**, (Z)-**3**, or (α)-**3** for catalyst **Rh-L4** bearing alkyl electron donating and sterically demanding *tert*-butyl groups and **Rh-xantphos**. Int, intermediate, TS, transition state.
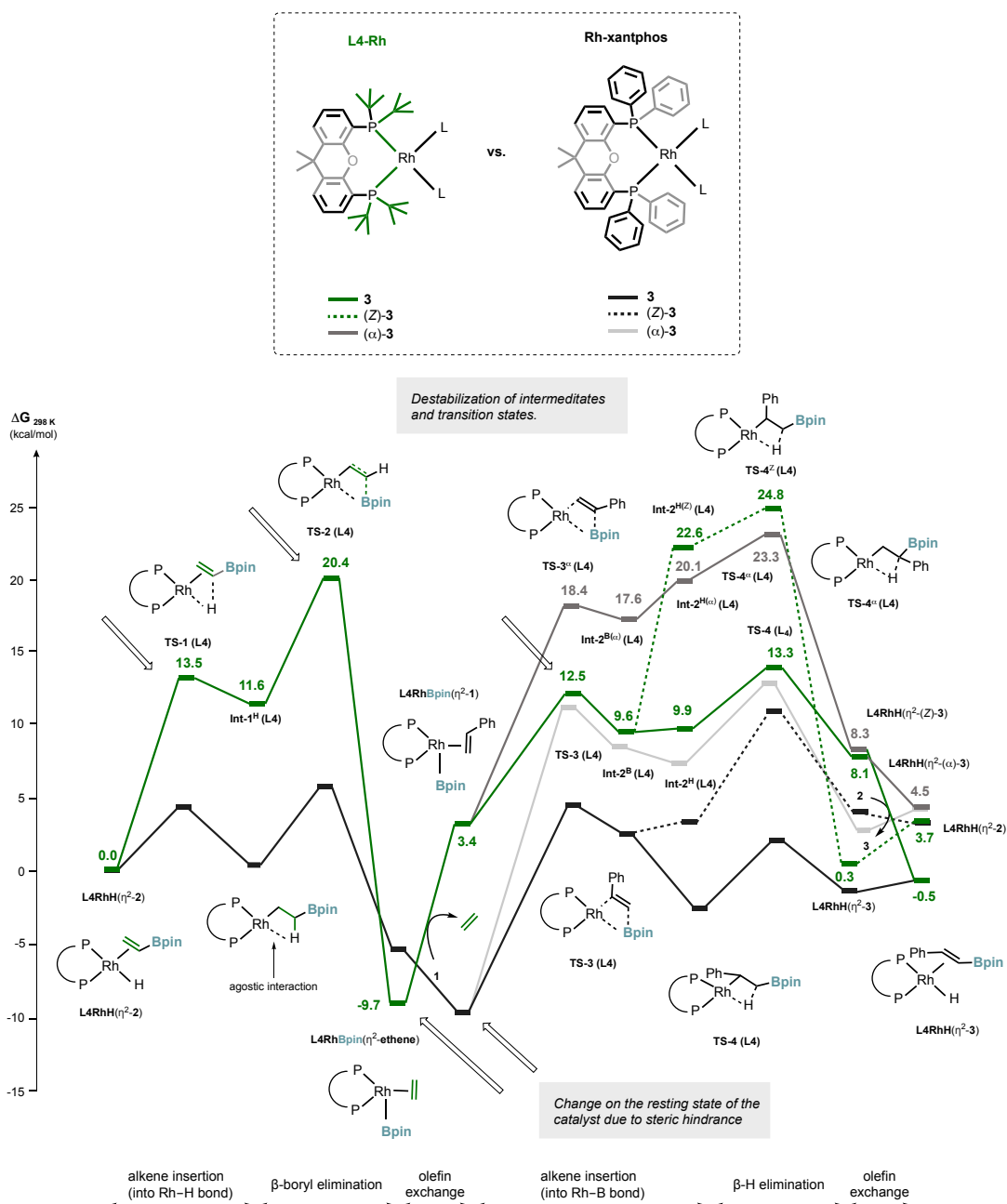
Figure 8. Overlay of free energy surfaces for the transfer borylation reaction leading to products **3**, (Z)-**3**, or (α)-**3** for catalyst **Rh-L3** bearing alkyl electron donating groups and **Rh-L4** bearing alkyl electron donating and sterically demanding *tert*-butyl groups. Int, intermediate, TS, transition state.

4.3 Conclusions

In summary, the study provides an insight into the influence that electronic and steric properties of the Rh catalysts' ligands have on the free energy surface of the transfer C−H borylation of alkenes. In general, modifications to the electron-donating ability of the phosphine moiety led to similar reaction profiles, maintaining the original regio- and stereoselectivity determining steps, and presenting the highest energetic barrier for the alkene insertion into Rh−B bond step. In contrast, an increase to the steric demand of the phosphine moiety modified the reaction profile substantially. The analysis of the changes to the relative stabilities of the intermediates and the free energy barriers for the elementary steps indicated the following trends:

I)   Increasing the electron donating ability of the phosphine moieties may accelerate the reaction through the destabilization of the resting state of the catalyst, **LRhBpin(η^2-1)** intermediate (as observed for **L1-Rh** and **L3-Rh**).

II)   Decreasing the electron donating ability of the phosphine moieties may accelerate the reaction through the stabilization of the transition state of the alkene insertion into Rh−B bond, especially toward the formation of α-regioisomer (as observed for **L2-Rh**), thereby assisting the development of prospective α-selective catalysts.

III)   Increasing the electron donating ability of the phosphine moieties may stabilize the alternative Rh-alkyl species, promoting the pathway toward the formation of the (*Z*)-regioisomer (as observed for **L3-Rh**), thereby assisting the development of prospective Z-selective catalysts.

IV)   Increasing the steric demand of the phosphine moieties leads to a destabilization of reaction intermediates and transition states, leading to higher free energy barriers, thereby being rather detrimental for the development of new Rh-based catalysts.

Although the set of catalysts interrogated in this study is predicted to carry out the title reaction with overall similar activities and selectivities (except for unproductive **L4-R**h; Figure 9e), the understanding of the difference between their profiles provides the suggestions for the design of future catalysts. Understanding of the importance of the backbone core of the ligand, i.e., its size, rigidity, and imposed bite-angle, would be also instrumental for further reaction development.[36] Based on the studies just described, we foresee that catalysts bearing electron-rich bisalkyl phosphines or unsymmetric electron-rich electron-deficient bisphosphines, plausibly with modifications to the backbone core of the ligand, would be attractive candidates to develop Z-selective or a-selective methodologies respectively. Overall, this work sets the stage for the rational design of new catalysts to address the remaining challenges of the transfer C−H borylation reaction.
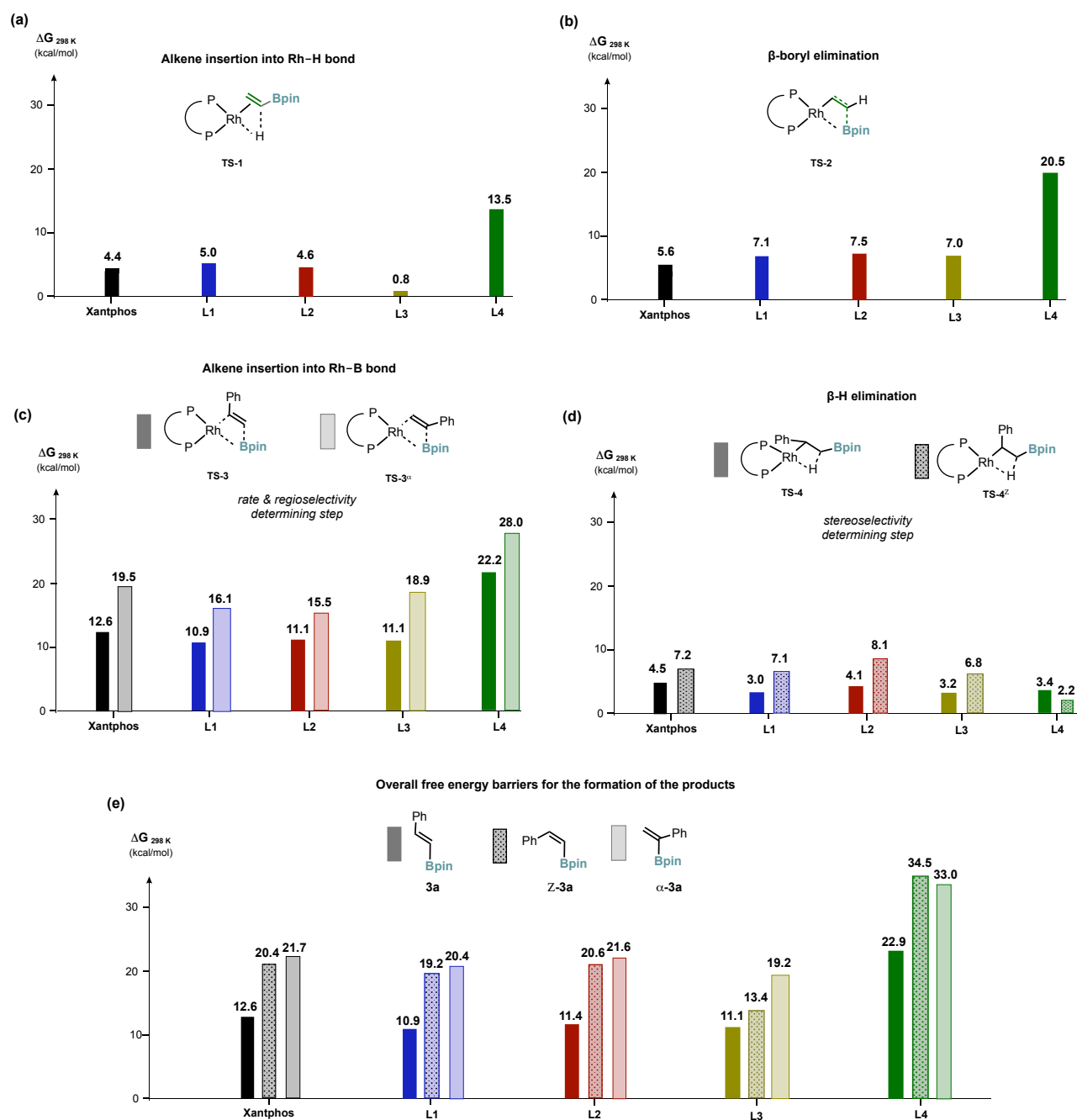
Figure 9. Influence of the electronic and steric variations on the free energy barriers of the elementary steps of the reaction: (a) alkene insertion, (b) β-boryl elimination, (c) alkene insertion into Rh–B bond, and (d) β–H elimination, as well as (e) Overall barriers for the formation of the products **3**, (*Z*)-**3**, or (a)-**3**.

4.4 Computational details

All DFT calculations[37] were performed with the Gaussian09 suite of programs.[38] Geometries were optimized with the M06−L[39] functional and the def2-SVP basis set[40,41] together with the corresponding Coulomb fitting basis set to speed up calculations.[42] In all cases, the default numerical integration grid was modified for the denser and more accurate 'SuperFineGrid'. Stationary points were probed through vibrational analysis. Gibbs free energy corrections were performed under standard conditions (298.15 K, 1.0 atm). Transition states were verified through Intrinsic Reaction Coordinate calculations (IRC) or optimization to minima at both sides of the frequency. Single point energy calculations including the effect of 1,4-dioxane as a solvent were performed with the M06−L functional[39], the SMD solvation model[43], and the larger def2-TZVP basis set[40,41].

4.5 References

(1)   Hartwig, J. F.; Larsen, M. A. Undirected, Homogeneous C–H Bond Functionalization: Challenges and Opportunities. *ACS Cent. Sci.* **2016**, *2* (5), 281–292.

(2)   Mkhalid, I. A. I.; Barnard, J. H.; Marder, T. B.; Murphy, J. M.; Hartwig, J. F. C−H Activation for the Construction of C−B Bonds. *Chem. Rev.* **2010**, *110* (2), 890–931.

(3)   Hartwig, J. F. Regioselectivity of the Borylation of Alkanes and Arenes. *Chem. Soc. Rev.* **2011**, *40* (4), 1992.

(4)   Xu, L.; Wang, G.; Zhang, S.; Wang, H.; Wang, L.; Liu, L.; Jiao, J.; Li, P. Recent Advances in Catalytic C−H Borylation Reactions. *Tetrahedron* **2017**, *73* (51), 7123–7157.

(5)   Reyes, R.; Sawamura, M. An Introductory Overview of C−H Bond Activation/ Functionalization Chemistry with Focus on Catalytic C(Sp3)−H Bond Borylation. *KIMIKA* **2021**, *32* (1), 70–109.

(6)   Veth, L.; Grab, H.; Dydio, P. Recent Trends in Group 9–Catalyzed C−H Borylation Reactions: Different Strategies to Control Site-, Regio-, and Stereoselectivity. *Synthesis* **2021**, a-1711-5889.

(7)   Miyaura, Norio.; Suzuki, Akira. Palladium-Catalyzed Cross-Coupling Reactions of Organoboron Compounds. *Chem. Rev.* **1995**, *95* (7), 2457–2483.

(8)   Nicolaou, K. C.; Bulger, P. G.; Sarlah, D. Palladium-Catalyzed Cross-Coupling Reactions in Total Synthesis. *Angew. Chem. Int. Ed.* **2005**, *44* (29), 4442–4489.

(9)   Lennox, A. J. J.; Lloyd-Jones, G. C. Selection of Boron Reagents for Suzuki–Miyaura Coupling. *Chem Soc Rev* **2014**, *43* (1), 412–443.

(10)   Xu, L.; Zhang, S.; Li, P. Boron-Selective Reactions as Powerful Tools for Modular Synthesis of Diverse Complex Molecules. *Chem. Soc. Rev.* **2015**, *44* (24), 8848–8858.

(11)   Bhawal, B. N.; Morandi, B. Catalytic Isofunctional Reactions—Expanding the Repertoire of Shuttle and Metathesis Reactions. *Angew. Chem. Int. Ed.* **2019**, *58* (30), 10074–10103.

(12)   Rochette, É.; Desrosiers, V.; Soltani, Y.; Fontaine, F.-G. Isodesmic C–H Borylation: Perspectives and Proof of Concept of Transfer Borylation Catalysis. *J. Am. Chem. Soc.* **2019**, *141* (31), 12305–12311.

(13)   Marciniec, B.; Jankowska, M.; Pietraszuk, C. New Catalytic Route to Functionalized Vinylboronates. *Chem. Commun.* **2005**, No. 5, 663–665.

(14)   Marciniec, B.; Dudziec, B.; Kownacki, I. A New Catalytic Route for the Activation of Sp-Hybridized Carbon-Hydrogen Bonds. *Angew. Chem. Int. Ed Engl.* **2006**, *45* (48), 8180–8184.

(15)   Shi, X.; Li, S.; Wu, L. H2-Acceptorless Dehydrogenative Boration and Transfer Boration of Alkenes Enabled by Zirconium Catalyst. *Angew. Chem. Int. Ed.* **2019**, *58* (45), 16167–16171.

(16)   Lam, K. C.; Lin, Z.; Marder, T. B. DFT Studies of β-Boryl Elimination Processes: Potential Role in Catalyzed Borylation Reactions of Alkenes. *Organometallics* **2007**, *26* (13), 3149–3156.

(17)   Veth, L.; Grab, H.; Martínez, S.; Antheaume, C.; Dydio, P. Transfer C-H Borylation of Alkenes under Rh(I)-Catalysis: Insight into the Synthetic Capacity, Mechanism & Selectivity-Control. *Chem. Catalysis X*, XX.

(18)   Carreras, J.; Caballero, A.; Pérez, P. J. Alkenyl Boronates: Synthesis and Applications. *Chem. – Asian J.* **2019**, *14* (3), 329–343.

(19)   Wang, X.; Wang, Y.; Huang, W.; Xia, C.; Wu, L. Direct Synthesis of Multi(Boronate) Esters from Alkenes and Alkynes via Hydroboration and Boration Reactions. *ACS Catal.* **2021**, *11* (1), 1–18.

(20)   Torker, S.; Müller, A.; Sigrist, R.; Chen, P. Tuning the Steric Properties of a Metathesis Catalyst for Copolymerization of Norbornene and Cyclooctene toward Complete Alternation. *Organometallics* **2010**, *29* (12), 2735–2751.

(21)   Khan, R. K. M.; Torker, S.; Hoveyda, A. H. Reactivity and Selectivity Differences between Catecholate and Catechothiolate Ru Complexes. Implications Regarding Design of Stereoselective Olefin Metathesis Catalysts. *J. Am. Chem. Soc.* **2014**, *136* (41), 14337–14340.

(22)   Funes-Ardoiz, I.; Schoenebeck, F. Established and Emerging Computational Tools to Study Homogeneous Catalysis—From Quantum Mechanics to Machine Learning. *Chem* **2020**, *6* (8), 1904–1913.

(23)   Holy Grails for Computational Organic Chemistry and Biochemistry | Accounts of Chemical Research https://pubs.acs.org/doi/abs/10.1021/acs.accounts.6b00532 (accessed 2022 -03 -21).

(24)   Ahn, S.; Hong, M.; Sundararajan, M.; Ess, D. H.; Baik, M.-H. Design and Optimization of Catalysts Based on Mechanistic Insights Derived from Quantum Chemical Reaction Modeling. *Chem. Rev.* **2019**, *119* (11), 6509–6560.

(25)   Reim, I.; Occhipinti, G.; Törnroos, K. W.; Fogg, D. E.; Jensen, V. R. Toward E-Selective Olefin Metathesis: Computational Design and Experimental Realization of Ruthenium Thio-Indolate Catalysts. *Top. Catal.* **2022**, *65* (1), 448–461.

(26)   Smit, W.; Koudriavtsev, V.; Occhipinti, G.; Törnroos, K. W.; Jensen, V. R. Phosphine-Based Z-Selective Ruthenium Olefin Metathesis Catalysts. *Organometallics* **2016**, *35* (11), 1825–1837.

(27)   Phillips, R. S.; Vita, A.; Spivey, J. B.; Rudloff, A. P.; Driscoll, M. D.; Hay, S. Ground-State Destabilization by Phe-448 and Phe-449 Contributes to Tyrosine Phenol-Lyase Catalysis. *ACS Catal.* **2016**, *6* (10), 6770–6779.

(28)   Aldrich, K. E.; Kansal, D.; Odom, A. L. Catalyst Design Insights from Modelling a Titanium-Catalyzed Multicomponent Reaction.

Faraday Discuss. **2019**, *220* (0), 208–230.

(29) Tolman, C. A. Steric Effects of Phosphorus Ligands in Organometallic Chemistry and Homogeneous Catalysis. *Chem. Rev.* **1977**, *77* (3), 313–348.

(30) Hamann, B. C.; Hartwig, J. F. Sterically Hindered Chelating Alkyl Phosphines Provide Large Rate Accelerations in Palladium-Catalyzed Amination of Aryl Iodides, Bromides, and Chlorides, and the First Amination of Aryl Tosylates. *J. Am. Chem. Soc.* **1998**, *120* (29), 7369–7370.

(31) Old, D. W.; Wolfe, J. P.; Buchwald, S. L. A Highly Active Catalyst for Palladium-Catalyzed Cross-Coupling Reactions: Room-Temperature Suzuki Couplings and Amination of Unactivated Aryl Chlorides. *J. Am. Chem. Soc.* **1998**, *120* (37), 9722–9723.

(32) Dai, C.; Fu, G. C. The First General Method for Palladium-Catalyzed Negishi Cross-Coupling of Aryl and Vinyl Chlorides: Use of Commercially Available Pd(P(*t* -Bu) $_3$) $_2$ as a Catalyst. *J. Am. Chem. Soc.* **2001**, *123* (12), 2719–2724.

(33) Ma, D.; Zhang, Y.; Yao, J.; Wu, S.; Tao, F. Accelerating Effect Induced by the Structure of α-Amino Acid in the Copper-Catalyzed Coupling Reaction of Aryl Halides with α-Amino Acids. Synthesis of Benzolactam-V8. *J. Am. Chem. Soc.* **1998**, *120* (48), 12459–12467.

(34) Surry, D. S.; Buchwald, S. L. Dialkylbiaryl Phosphines in Pd-Catalyzed Amination: A User's Guide. *Chem Sci* **2011**, *2* (1), 27–50.

(35) Tolman, C. A. Electron Donor-Acceptor Properties of Phosphorus Ligands. Substituent Additivity. *J. Am. Chem. Soc.* **1970**, *92* (10), 2953–2956.

(36) van Leeuwen, P. W. N. M.; Kamer, P. C. J.; Reek, J. N. H.; Dierkes, P. Ligand Bite Angle Effects in Metal-Catalyzed C−C Bond Formation. *Chem. Rev.* **2000**, *100* (8), 2741–2770.

(37) Cramer, C. J.; Truhlar, D. G. Density Functional Theory for Transition Metals and Transition Metal Chemistry. *Phys. Chem. Chem. Phys.* **2009**, *11* (46), 10757–10816.

(38) Frisch, M. J.; Trucks, G. W.; Schlegel, H. B.; Scuseria, G. E.; Robb, M. A.; Cheeseman, J. R.; Scalmani, G.; Barone, V.; Mennucci, B.; Petersson, G. A.; Nakatsuji, H.; Caricato, M.; Li, X.; Hratchian, H. P.; Izmaylov, A. F.; Bloino, J.; Zheng, G.; Sonnenb, D. J. *Gaussian 09*; Gaussian, Inc: Wallingford CT, 2009.

(39) Zhao, Y.; Truhlar, D. G. Density Functionals with Broad Applicability in Chemistry. *Acc. Chem. Res.* **2008**, *41* (2), 157–167.

(40) Weigend, F.; Ahlrichs, R. Balanced Basis Sets of Split Valence, Triple Zeta Valence and Quadruple Zeta Valence Quality for H to Rn: Design and Assessment of Accuracy. *Phys. Chem. Chem. Phys.* **2005**, *7* (18), 3297–3305.

(41) Andrae, D.; Häußermann, U.; Dolg, M.; Stoll, H.; Preuß, H. Energy-Adjustedab Initio Pseudopotentials for the Second and Third Row Transition Elements. *Theor. Chim. Acta* **1990**, *77* (2), 123–141.

(42) Weigend, F. Accurate Coulomb-Fitting Basis Sets for H to Rn. *Phys. Chem. Chem. Phys.* **2006**, *8* (9), 1057–1065.

(43) Marenich, A. V.; Cramer, C. J.; Truhlar, D. G. Universal Solvation Model Based on Solute Electron Density and on a Continuum Model of the Solvent Defined by the Bulk Dielectric Constant and Atomic Surface Tensions. *J. Phys. Chem. B* **2009**, *113* (18), 6378–6396.

CHAPTER 5

Mechanism of the Isoselective Hydroformylation of Propylene by Iodide-Assisted Palladium Catalysis

Reaction mechanism, origins of *iso*-selectivity & role of iodide

propylene

CO

H₂

isobutanal
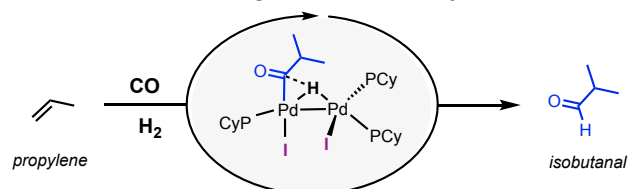
Insights by DFT studies

neutral binuclear reductive elimination

iodide is key for intermediates & transition states stabilization
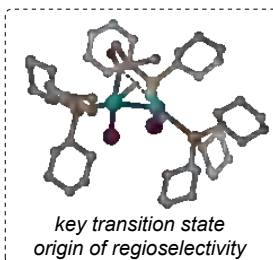
*key transition state origin of regioselectivity*

5.1 Introduction

The synthesis of n-butanal and iso-butanal via hydroformylation reaction of propylene and syngas is an industrially important process, with a global production of over 7 million tons per year.[1] One of the challenges of this process represents the selective formation of *iso*-butanal, which is a material of increasing demand, over *n*-butanal. Recently, our group reported a novel protocol for the title reaction that yields outstanding selectivity for *iso*- over *n*-product, by using a catalytic system based on PdI$_2$ and PCy$_3$ (Figure 1a).[2] However, the mechanism of the reaction, origins of the unprecedented selectivity, and role of the iodide anion, all of which are crucial for understanding and further rational improvement of the system, remain unclear. Among the different possibilities from which the reaction may occur, there are mononuclear and binuclear pathways (Figure 1b).[3–5]
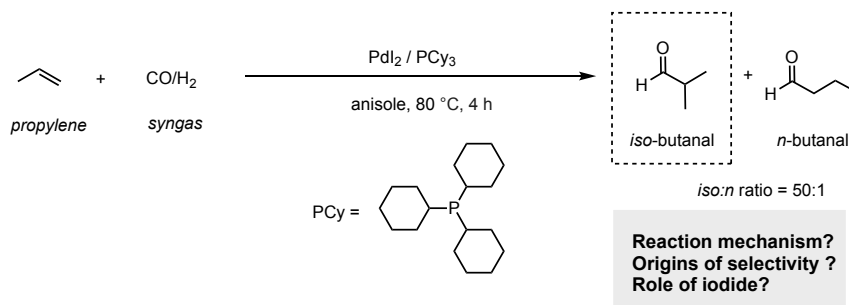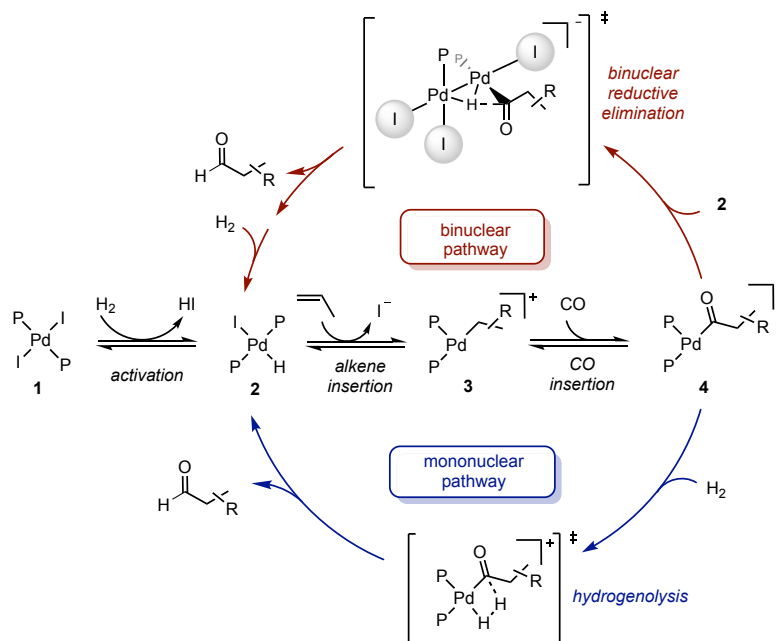

Figure 1. (a) Reported *iso*-selective hydroformylation of propylene and key questions to be answered. (b) Mechanistic proposals for the hydroformylation reaction involving mononuclear and binuclear pathways.

The typically invoked mononuclear mechanism as proposed by Drent and coworkers[3], involves the direct hydrogenolysis of a mononuclear Pd–acyl complex to form the aldehyde product. In particular, the pre-catalyst PdI_2 **1** is proposed to from Pd–hydride complex **2** upon heterolytic splitting of dihydrogen at the electrophilic palladium center. Then, coordination of the olefin to Pd-hydride **2** follow by migratory insertion into the Pd–H bond generates Pd–alkyl species **3**. Subsequent coordination of carbon monoxide and its migratory insertion yields the key intermediate Pd–acyl **4**, which undergoes direct hydrogenolysis to form the product (blue line, Figure 1b).

The binuclear mechanism,[4] which was reported recently by our group for related Pd-catalyzed hydroformylation reactions, involves the reaction between Pd–acyl and Pd–hydride complexes to form a binuclear intermediate, that undergoes an unusual iodide-assisted binuclear reductive elimination to form the product (red line, Figure 1b). In addition to the above stated, the iodide anion is proposed to have a crucial role on the hydroformylation reaction, by affecting significantly the rate, chemo- and regioselectivity, as proposed and shown in the literature.[2,4,6]

In this chapter, I present my mechanistic investigation based on DFT calculations to unravel the reaction pathway that is most likely to occur by studying a variety of different pathways including commonly invoked proposals, with the overall goal to provide computational insights and further support to the mechanistic experimental evidence.[2,7]

5.2 Results and Discussion

I commenced the mechanistic study taking into account the existing mechanistic experimental data, that provided clear evidence that **L₂−Pd$^{(II)}$(H)I** and **L₂−Pd$^{(II)}$(acyl)I** are key intermediates formed during the reaction.[2,7] From that evidence, I raised the following questions that serve as a guideline to this studies:

1) What is the mechanism by which **L₂−Pd$^{(II)}$(acyl)I** complex is formed from coordinatively saturated **L₂−Pd$^{(II)}$(H)I**? Is it formed via a cationic or a neutral pathway, i.e., is the iodide ligand or one of the phosphine ligands temporarily decoordinated during the process?
2) What is the mechanism by which the aldehyde product is formed starting from the **L₂−Pd$^{(II)}$(acyl)I** complex? Is it via classical hydrogenolysis or via binuclear mechanism? Is it occurring via a neutral or a cationic pathway?
3) How does the iodide anion influence the mechanism of the reaction?
4) What is the origin of the regioselectivity?

In the following sections I provide answers and computational support to these key questions.

5.2.1 Summary of the mechanistic study

The main results of the computational study are discussed below and presented in Figure 2.

Formation of L₂−Pd$^{(II)}$(acyl)I complex

The most feasible pathway leading to the formation of **L₂−Pd$^{(II)}$(acyl)I** complex from **L₂−Pd$^{(II)}$(H)I** is a neutral pathway, in which the iodide anion stays always coordinated to the Pd center. Via this pathway, the formation of Pd-acyl species overcomes a free energy barrier of 16.3 (iso) and 16.8 (n) kcal/mol, indicating that iso species are formed faster than n species. Moreover, the presence of HI in the system promotes the decoordination of PCy₃ ligand by the formation of $[PCy_3]^+[I]^-$ salt, leading to free energy surfaces that are 13.1 kcal/mol lower in energy than these in which the ligand decoordinates as free PCy₃. Moreover, n-acyl species are predicted to be lower in energy than iso-acyl species, in agreement with experiments.[7]

Formation of **L₂−Pd$^{(II)}$(acyl)I** species via a cationic pathway would involve a significantly high free energy barrier of 36.7 kcal/mol, resulting from the highest free energy penalty (24.9 kcal/mol) for the iodide anion decoordination. Additionally, this pathway predicts that n-intermediates are formed faster than iso species.

Formation of the aldehyde product

The most favorable pathway for the formation of the aldehyde product was found to occur via a neutral binuclear reductive elimination step involving the reaction of **L₂−Pd$^{(II)}$(acyl)I** and **L₂−Pd$^{(II)}$(H)I**. This reaction requires decoordination of one PCy₃ ligand, which is promoted by HI. The barrier for such reductive elimination is 17.9 kcal/mol. A cationic binuclear reductive elimination pathway is unlikely, as the barrier for such process was found to be 72.7 kcal/mol. Additionally, transmetalation reaction between **L₂−Pd$^{(II)}$(acyl)I** and **L₂−Pd$^{(II)}$(H)I** species was considered and found to be thermodynamically unfavorable ($\Delta G = +29.0$ kcal/mol). Hydrogenolysis of Pd-acyl complex via neutral or cationic pathways is rather unlikely to occur, as the computed free energy barriers account for 30.1 kcal/mol and 49.3 kcal/mol, respectively.

Insights into the regioselectivity

The experimentally observed regioselectivity iso over n product, is predicted to be a consequence of a faster binuclear reductive elimination iso over n. It should be noted that, although the iso **L₂−Pd^(II)(acyl)I** species are formed faster than **L₂−Pd^(II)(n-acyl)I** species, their formation is predicted to be reversible. The **L₂−Pd^(II)(n-acyl)I** intermediate is thermodynamically more stable and predicted to be present in higher concentration than the more readily reacting **L₂−Pd^(II)(iso-acyl)I** intermediate, in line with experimental studies.

Insights into the influence of iodide

The presence of stochiometric amounts of iodide (vs. Pd) lead to a neutral reaction pathway, with the lower energy barriers than those found in the commonly invoked cationic pathway, in which the cationic Pd remains coordinated by two phosphine ligands. In contrast, in the neutral pathway, the iodide anion remains bound to the Pd center and hence plays key roles in the formation of the Pd-acyl intermediate and in the release of the aldehyde product.
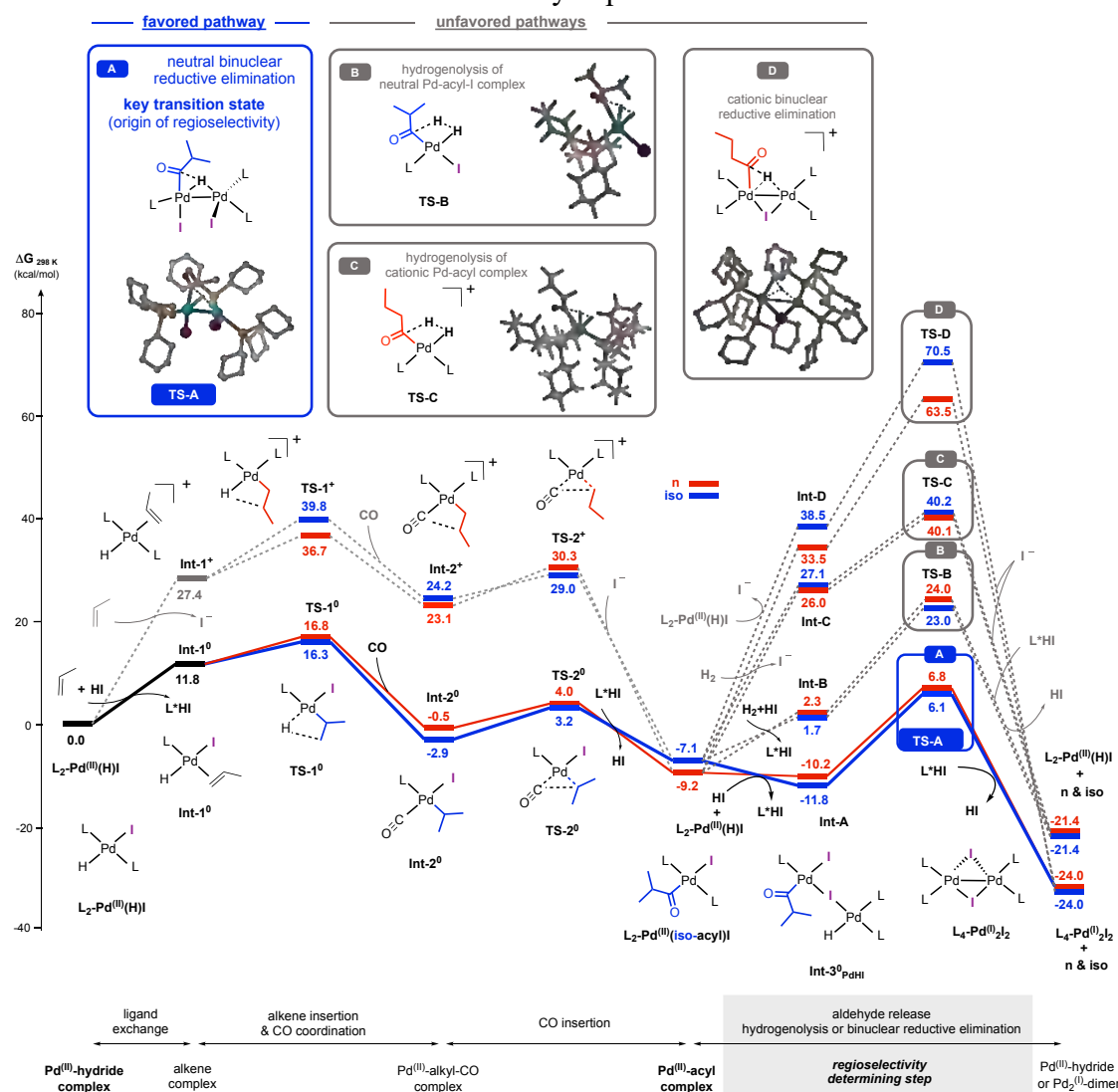

Figure 2. Mechanistic computational studies on the *iso*-selective Pd-catalyzed hydroformylation of propylene assisted by iodide. For computational details, see Section 5.4.

5.2.2 Formation of L$_2$−Pd$^{(II)}$(acyl)I complex.

I calculated the free energy surfaces for the formation of **L$_2$−Pd$^{(II)}$(acyl)I** complex, the formation of which has been observed experimentally in experiments starting from the activated **L$_2$−Pd$^{(II)}$(H)I** complex.[7] The ground state structure of **L$_2$−Pd$^{(II)}$(H)I** is supported by the crystal structure data.[2] Two possible pathways for the title process were considered: a commonly invoked cationic pathway, in which iodide is initially decoordinated to form the cationic hydride complex (bearing two phosphine ligands) and later coordinated back to the Pd center upon formation of Pd−acyl species, and a neutral pathway in which the iodide ligand (along with one phosphine ligand) remains coordinated to the Pd center throughout the process, but one of the ligands is decoordinated instead (Figure 3). I considered that phosphine decoordination might be promoted by the presence of HI (formed upon activation of the precatalyst)[2] which leads to the formation of phosphine*HI salt, in line with observation of PCy$_3$*HI in catalytic experiments.[7] I found that free energy surfaces corresponding to the neutral pathway are significantly lower in energy, whether phosphine decoordination is promoted by HI (overall free energy barrier 16.3 kcal/mol) or free phosphine decoordination is considered (overall free energy barrier 29.4 kcal/mol), than the one corresponding to the cationic pathway (overall free energy barrier 36.7 kcal/mol). Moreover, the experimentally observed regioselectivity during the formation of Pd−acyl species n over iso, is in agreement with the computed relative stability of these Pd-acyl species. Finally, I performed control computations to note that in the absence of the iodide anions, that is, the strongly coordinating anions, the cationic pathway is feasible.

5.2.2.1 Formation of L$_2$−Pd$^{(II)}$(acyl)I complex via neutral pathway in the presence of HI.

Reaction of the **L$_2$−Pd$^{(II)}$(H)I** complex with HI and propene leads to formation of the neutral **Int-1^0** complex, while one molecule of PCy$_3$ (L) ligand is decoordinated from the initial complex and protonated by HI to form [PCy$_3$H$^+$][I$^-$], with a free energy penalty of 11.8 kcal/mol (Figure 3). Subsequent alkene coordination and insertion via **TS-1^0** generates alkyl complex **L−Pd$^{(II)}$(alkyl)I**. The relative free energy barrier for this step is 4.5 kcal/mol (for iso) and 5.0 kcal/mol (for n). Upon CO coordination, alkyl complex is transformed to **Int-1^0** complex, which undergoes CO insertion via **TS-2^0** to form monophosphine complex **L−Pd$^{(II)}$(acyl)I**, overcoming a free energy barrier of 6.1 kcal/mol (for iso) and 4.5 kcal/mol (for n). Subsequent deprotonation of phosphine [PCy$_3$H$^+$][I$^-$] and coordination of free PCy$_3$ to the monophosphine acyl complex leads to the formation of experimentally observed **L$_2$−Pd$^{(II)}$(acyl)I**, while regenerating HI (Figure 3). The overall free energy barrier for the formation of the title acyl complex was found to be 16.3 kcal/mol (for *iso*) and 16.8 kcal/mol (for *n*), indicating that *iso* acyl complex are formed faster than *n* acyl complex. Moreover, **L$_2$−Pd$^{(II)}$(*n*-acyl)I** complex was found to be more stable than the **L$_2$−Pd$^{(II)}$(*iso*-acyl)I** complex by 2.1 kcal/mol, which is in agreement with our experimental findings. Additionally, the formation of the acyl complexes was found to be a thermodynamically favored process, accounting for a relative free energy variation of -7.1 kcal/mol (for *iso*) and -9.2 kcal/mol (for *n*) at ambient temperature (298 K). However, the energies of the formation of the Pd-acyl species are strongly dependent on the reaction temperature (vie infra, section 5.2.1.2). For computed structures that are not displayed in Figure 3, see Chart 1.

5.2.2.2 Formation of $L_2-Pd^{(II)}$(acyl)I complex via neutral pathway in the absence of HI.

In the absence of HI, reaction of $\mathbf{L_2-Pd^{(II)}(H)I}$ complex with propene, releasing a molecule of PCy_3 (L) ligand, leads to formation of neutral $\mathbf{Int\text{-}1^0}$ complex with a free energy penalty of 24.9 kcal/mol, which is 13.1 kcal/mol higher than the corresponding penalty found when HI promote the decoordination of the ligand generating $[PCy_3H^+][I^-]$ (Figure 3, grey line). The following steps are analogous to those discussed in the section above, when HI is present. Alkene insertion via $\mathbf{TS\text{-}1^0}$ generates alkyl complex $\mathbf{L-Pd^{(II)}(alkyl)I}$, with a free energy barrier of 29.4 kcal/mol (for iso). Upon CO coordination, alkyl complex is transformed to $\mathbf{Int\text{-}1^0_{iso}}$ complex, which undergo CO insertion via $\mathbf{TS\text{-}2^0}$ to form monophosphine complex $\mathbf{L-Pd^{(II)}(acyl)I}$, overcoming a free energy barrier of 16.3 kcal/mol (for iso) relative to the initial Pd−hydride complex. Finally, re-coordination of the phosphine ligand to the monophosphine acyl complex leads to the formation of $\mathbf{L_2-Pd^{(II)}(acyl)I}$.

5.2.2.3 Formation of $L_2-Pd^{(II)}$(acyl)I complex via cationic pathway.

Reaction of the $\mathbf{L_2-Pd^{(II)}(H)I}$ complex with propene leads to formation of the cationic $\mathbf{Int\text{-}1^+}$ complex, while I^- ligand is decoordinated from the initial complex (Figure 3). This step has a remarkable high free energy penalty of 27.4 kcal/mol. Subsequent alkene insertion via $\mathbf{TS\text{-}1^+}$ generates alkyl complex $\mathbf{L_2-Pd^{(II)}(alkyl)^+}$, overcoming a relative free energy barrier of 11.3 kcal/mol (for *iso*) and 8.2 kcal/mol (for *n*). Upon CO coordination, alkyl complex is transformed to $\mathbf{Int\text{-}1^+}$ complex, which undergo CO insertion via $\mathbf{TS\text{-}2^+}$ to form acyl complex $\mathbf{L_2-Pd^{(II)}(acyl)^+}$. The relative free energy barrier for this step is 4.8 kcal/mol (for *iso*) and 7.2 kcal/mol (for *n*). Subsequent I^- coordination to the cationic acyl complexes leads to the formation of $\mathbf{L_2-Pd^{(II)}(\mathit{n}\text{-acyl})I}$ and $\mathbf{L_2-Pd^{(II)}(\mathit{iso}\text{-acyl})I}$. For computed structures that are not displayed in Figure 3, see Chart 1.
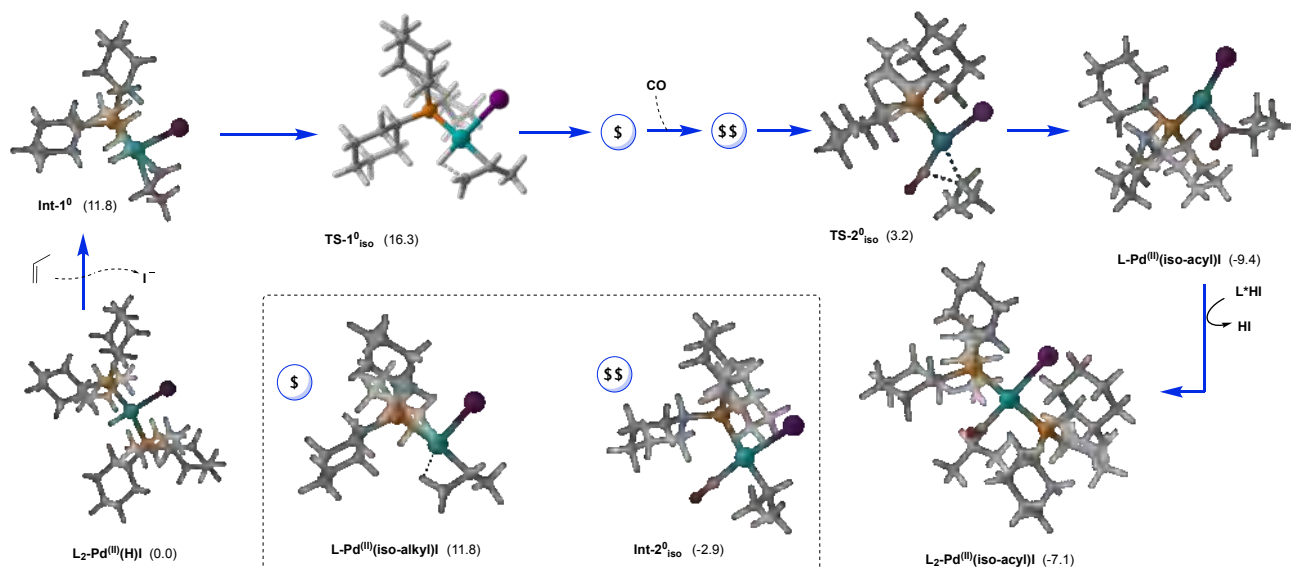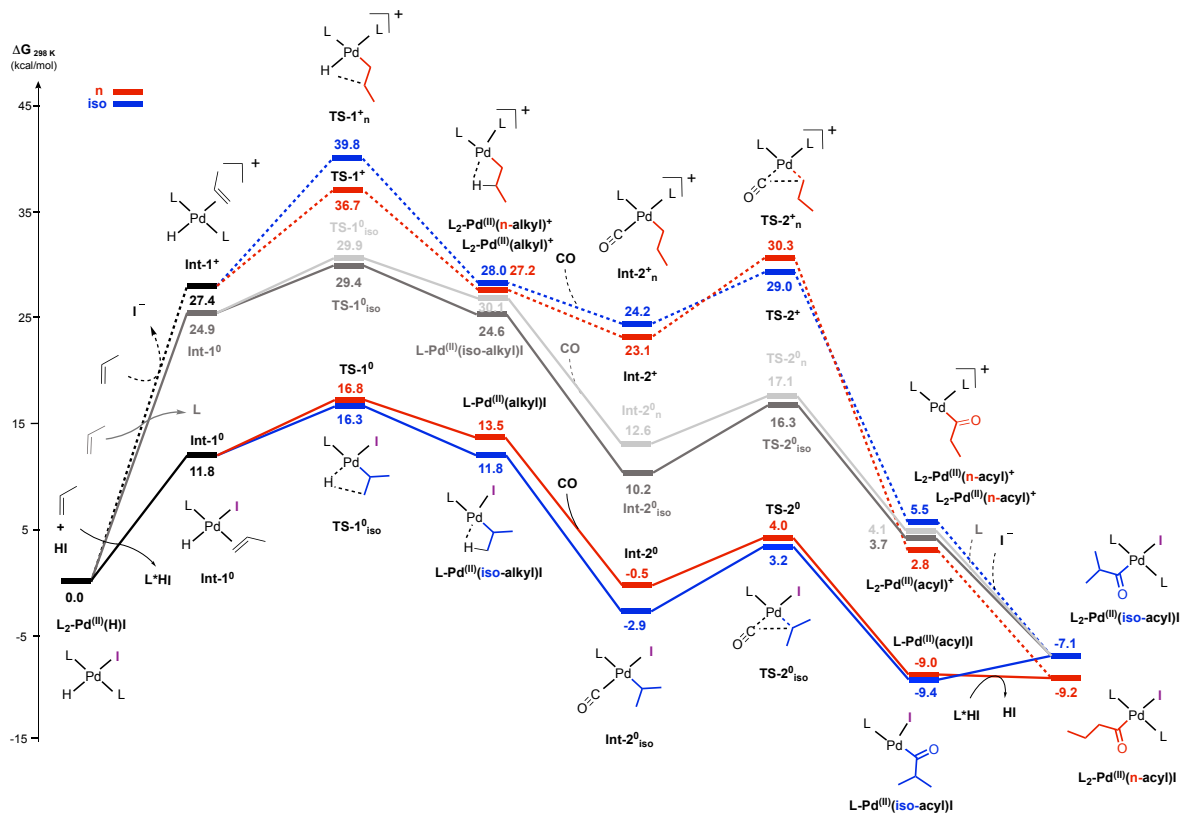
Figure 3. Free energy surface for the formation of **L₂-Pd⁽ᴵᴵ⁾(acyl)I** complex via neutral (plain lines) and cationic pathways (dashed lines). Grey lines correspond to the neutral pathway in the absence of HI. **Int**, intermediate, **TS**, transition state. For computational details, see Section 5.4.

TS-1$^+_{iso}$

L$_2$-Pd$^{(II)}$(iso-alkyl)$^+$

Int-2$^+_{iso}$

TS-2$^+_{iso}$

L$_2$-Pd$^{(II)}$(iso-acyl)$^+$

[Pcy-H]$^+$ I$^-$

Pcy

[Pcy-H]$^+$

TS-1^0_n

L-Pd$^{(II)}$(n-alkyl)I

Int-2^0_n

TS-2^0_n

L$_2$-Pd$^{(II)}$(HI)I-cis

L-Pd$^{(II)}$(n-acyl)I

propene

CO

anisole

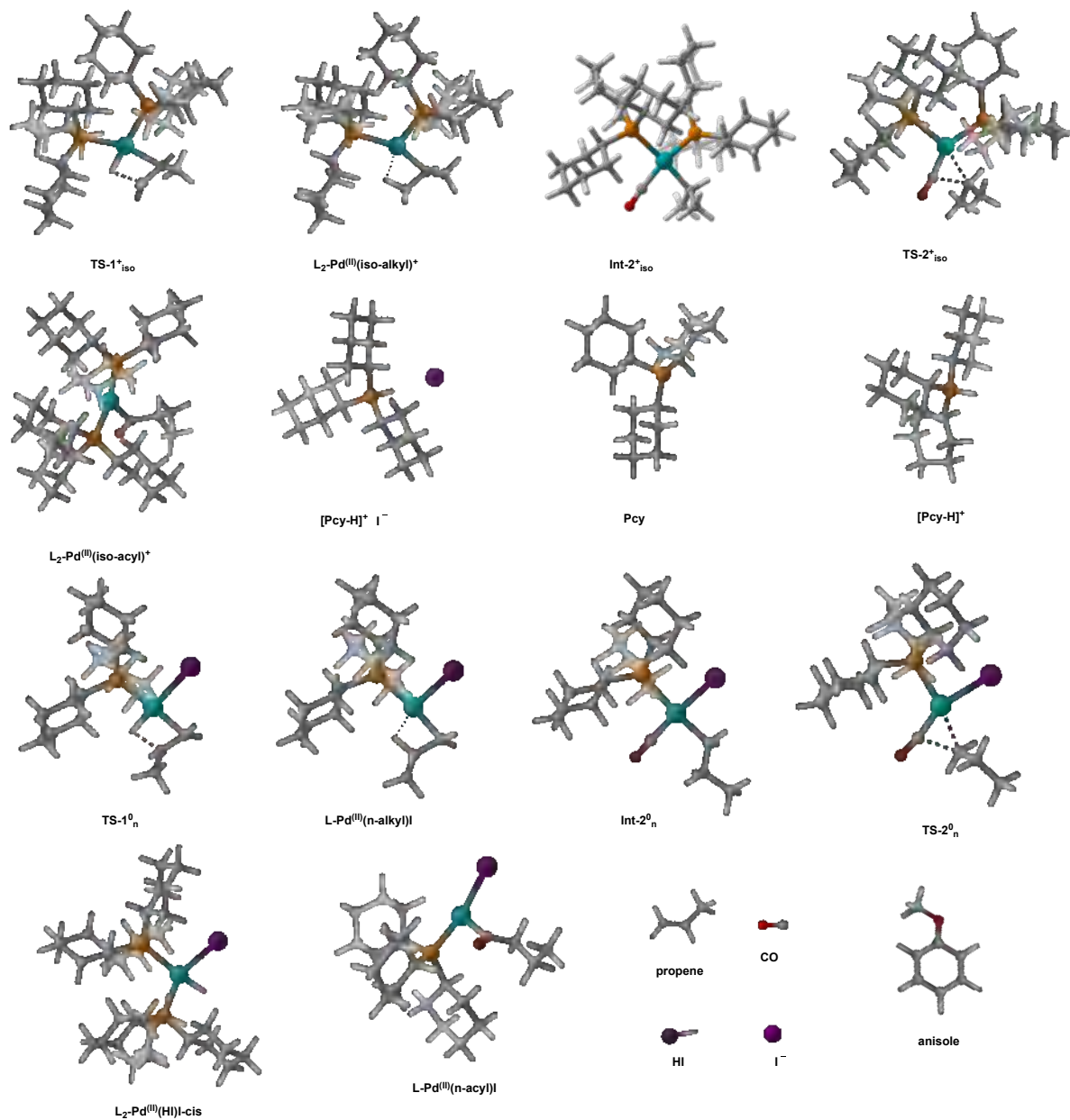**HI**

I$^-$

Chart 1. Additional computed structures for the formation of **L$_2$-Pd$^{(II)}$(acyl)I** complex via neutral and cationic pathways. **Int**, intermediate, **TS**, transition state. For computational details, see Section 5.4.

5.2.2.4 Formation of $L_2-Pd^{(II)}(acyl)^+$ species in the absence of strongly coordinating anions.

I performed control computations to show that in the absence of strongly coordinating anions such as iodide, the formation of **$L_2-Pd^{(II)}(acyl)^+$** via a cationic pathway is feasible, as often referred in the literature[8–10]. I evaluated the reaction profile starting from cationic Pd−hydride species bearing two phosphine ligands. The fourth coordination position was considered to be occupied by a molecule of CO or anisole, as both are present in excess in the system. I found that the formation of **$L_2-Pd^{(II)}(H)(CO)^+$** from **$L_2-Pd^{(II)}(H)^+$** species is thermodynamically favored ($\Delta G = -22.4$ kcal/mol) while the formation of **$L_2-Pd^{(II)}(H)(anisole)^+$** is non-favored thermodynamically ($\Delta G = +16.2$ kcal/mol), and therefore I consider the first one as a starting point in the reaction profile (Figure 4a). Reaction of **$L_2-Pd^{(II)}(H)(CO)^+$** complex with propene leads to formation of the cationic **Int-1$^+$** complex, while CO ligand is decoordinated from the initial complex (Figure 4b), accounting for a free energy penalty of 17.3 kcal/mol. Subsequent alkene insertion via **TS-1$^+$** generates alkyl complex **$L_2-Pd^{(II)}(alkyl)^+$**, overcoming an overall free energy barrier of 29.8 kcal/mol (for *iso*) and 26.8 kcal/mol (for *n*). Upon CO coordination, alkyl complex is transformed to **Int-1$^+$** complex, which undergo CO insertion via **TS-2$^+$**, overcoming a relative free energy barrier (respect to the initial hydride complex) of 20.4 kcal/mol (for *iso*) and 19.0 kcal/mol (for *n*), leading to the formation of acyl complex **$L_2-Pd^{(II)}(acyl)^+$**. Computed structures are displayed in Figure 3 and Chart 1.

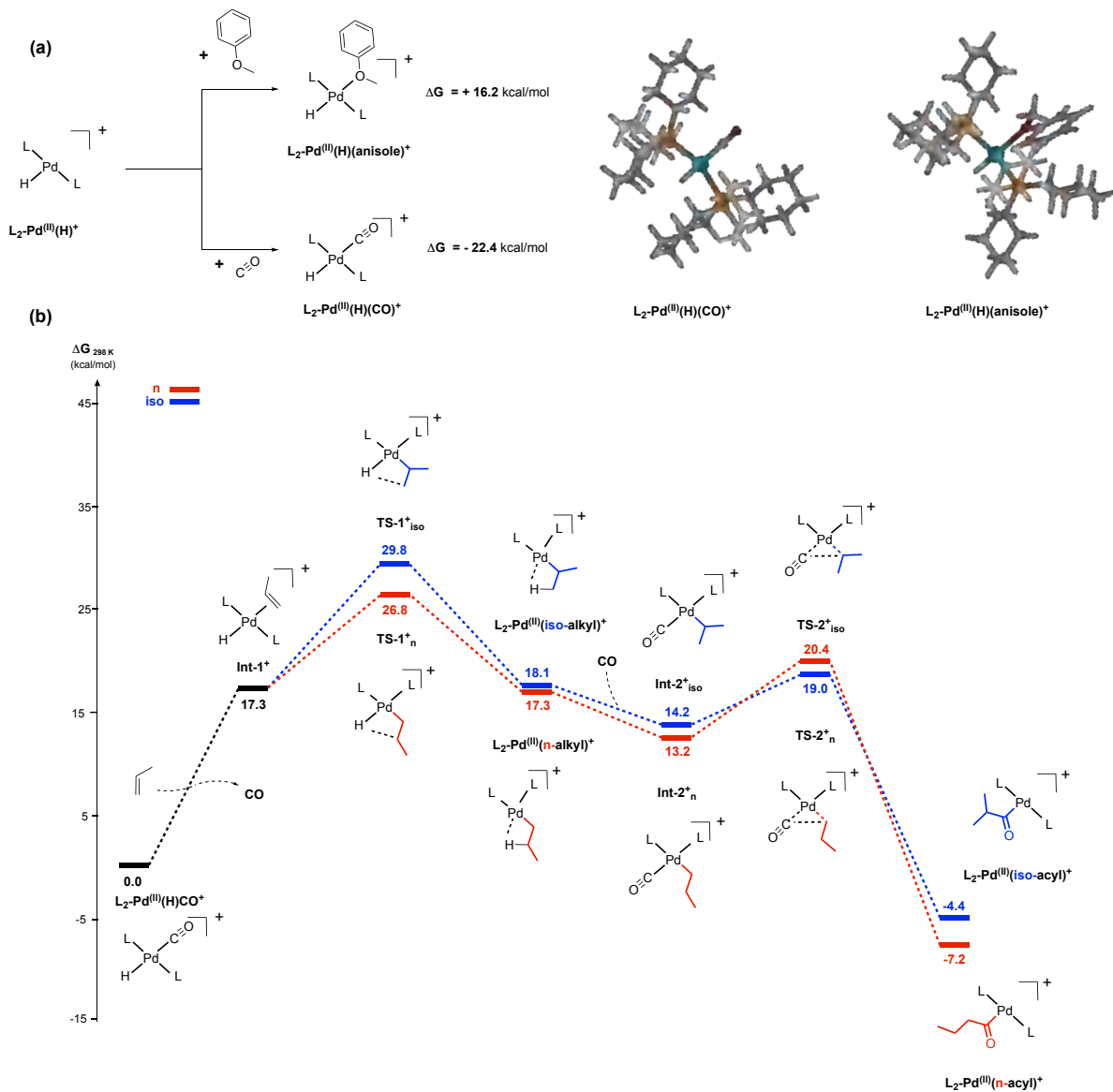**Figure 4.** (a) Variation of Gibbs free energy for the formation of **L₂-Pd$^{(II)}$(H)(CO)$^+$** and **L₂-Pd$^{(II)}$(H)(anisole)$^+$** from L₂-Pd-H$^+$ species. (b) Free energy surface for the formation of **L₂-Pd$^{(II)}$(acyl)$^+$** complex via cationic pathway in the absence of strongly coordinating anions. **Int**, intermediate, **TS**, transition state. For computational details, see Section 5.4.

5.2.3 Formation of the aldehyde from $L_2-Pd^{(II)}(acyl)I$ species.

In this section I discussed the free energy surfaces leading to the product formation from $L_2-Pd^{(II)}(acyl)I$ species. In particular, 1) formation of the product by reductive elimination of binuclear species formed by reaction of $L_2-Pd^{(II)}(acyl)I$ and $L_2-Pd^{(II)}(H)I$, considering cationic and neutral pathways. For the later, the effect of HI in the surfaces is also discussed. 2) formation of the product by hydrogenolysis, this is, reaction of $L_2-Pd^{(II)}(acyl)I$ and molecular H_2, considering as well, cationic and neutral pathways.

5.2.3.1 Reactions of $L_2-Pd^{(II)}(acyl)I$ complex with $L_2-Pd^{(II)}(H)I$ complex.

I calculated the free energy surfaces for the reaction of $L_2-Pd^{(II)}(acyl)I$ complexes with $L_2-Pd^{(II)}(H)I$ complex to form neutral or cationic binuclear species, $L_3-(Pd^{(II)})_2(H)(acyl)I_2$ or $L_4-(Pd^{(II)})_2(H)(acyl)I^+$, that undergo reductive elimination to form the product (Figure 5). I found that free energy surfaces corresponding to the neutral pathway are significantly lower in energy, whether phosphine decoordination is promoted by HI (overall free energy barrier 17.9 kcal/mol) or free phosphine decoordination is considered (overall free energy barrier 26.2 kcal/mol), than the one corresponding to the cationic pathway (overall free energy barrier 72.7 kcal/mol).
I conclude therefore that a binuclear reductive elimination scenario would most likely occur via a neutral pathway. Moreover, the neutral pathway provides a likely explanation for the regioselectivity of the overall reaction.

5.2.3.1.1 Reaction of $L_2-Pd^{(II)}(acyl)I$ complex with $L_2-Pd^{(II)}(H)I$ complex via neutral pathway, in the presence of HI.

Reaction of $L_2-Pd^{(II)}(acyl)I$ complex with $L_2-Pd^{(II)}(H)I$ leads to formation neutral binuclear species **Int-A**, while a phosphine ligand is decoordinated and protonated with HI generating $[PCy_3H^+][I^-]$(Figure S5). **Int-A** undergoes binuclear reductive elimination via **TS-A** to form the aldehyde product and binuclear $Pd^{(I)}$-$Pd^{(I)}$ species **Int-A2**, overcoming a relative free energy barrier of 17.9 kcal/mol (for *iso*) and 17.0 kcal/mol (for *n*). Subsequent aldehyde release and reaction with $[PCy_3H^+][I^-]$ forms (presumably) $L_4-Pd^{(I)}_2I_2$, and HI. For computed structures that are not displayed in Figure 5, see Chart 2.

5.2.3.1.2 Reaction of $L_2-Pd^{(II)}(acyl)I$ complex with $L_2-Pd^{(II)}(H)I$ complex via neutral pathway, in the absence of HI.

In the absence of HI, reaction of $L_2-Pd^{(II)}(acyl)I$ complex with $L_2-Pd^{(II)}(H)I$, releasing a molecule of PCy_3 (L) ligand, leads to formation neutral binuclear species **Int-A** (Figure 5, grey line). The following steps are analogous to those discussed in the section above, when HI is present, but the corresponding energy barriers are higher. **Int-A** undergoes binuclear reductive elimination via **TS-A** to form the aldehyde product and binuclear $Pd^{(I)}$ species **Int-A2**, overcoming a relative free energy barrier of 26.2 kcal/mol (for *iso*). Subsequent aldehyde release and recoordination of PCy_3 ligand forms $L_4-Pd^{(I)}_2I_2$. For computed structures that are not displayed in Figure 5, see Chart 2.

5.2.3.1.3 Reaction of $L_2-Pd^{(II)}$(acyl)I complexes with $L_2-Pd^{(II)}$(H)I complex via cationic pathway.

In the absence of HI, reaction of **$L_2-Pd^{(II)}$(acyl)I** complex with **$L_2-Pd^{(II)}$(H)I** leads to the formation cationic binuclear species **Int-D**, upon decoordination of I^- ligand from the initial acyl complex (Figure 5). Then, **Int-D** undergoes binuclear reductive elimination via **TS-D** to form the aldehyde product and binuclear $Pd^{(I)}-Pd^{(I)}$ species **Int-2D**, overcoming a notably high overall free energy barrier of 47.3 kcal/mol (for *iso*) and 49.3 kcal/mol (for *n*). Subsequent aldehyde release and I^- coordination forms dimeric species **$L_4-Pd^{(I)}_2I_2$**. For computed structures that are not displayed in Figure 5, see Chart 2.

5.2.3.1.4 Reaction of $L_2-Pd^{(II)}$(acyl)I complex with $L_2-Pd^{(II)}$(H)I complex via transmetalation.

The reaction of $L_2-Pd^{(II)}$(acyl)I complex with $L_2-Pd^{(II)}$(H)I complex via transmetalation, leading to the formation of $L_2-Pd^{(II)}$(H)(acyl)I is rather unlikely, as the formation of the intermediate prior to the transmetalation step, accounts for a high free energy penalty of +29 kcal/mol. (Scheme 1)
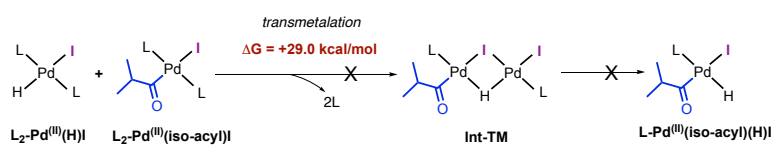
Scheme 1. Free energy penalty of the reaction of $L_2-Pd^{(II)}$(acyl)I complex with $L_2-Pd^{(II)}$(H)I complex via transmetalation.
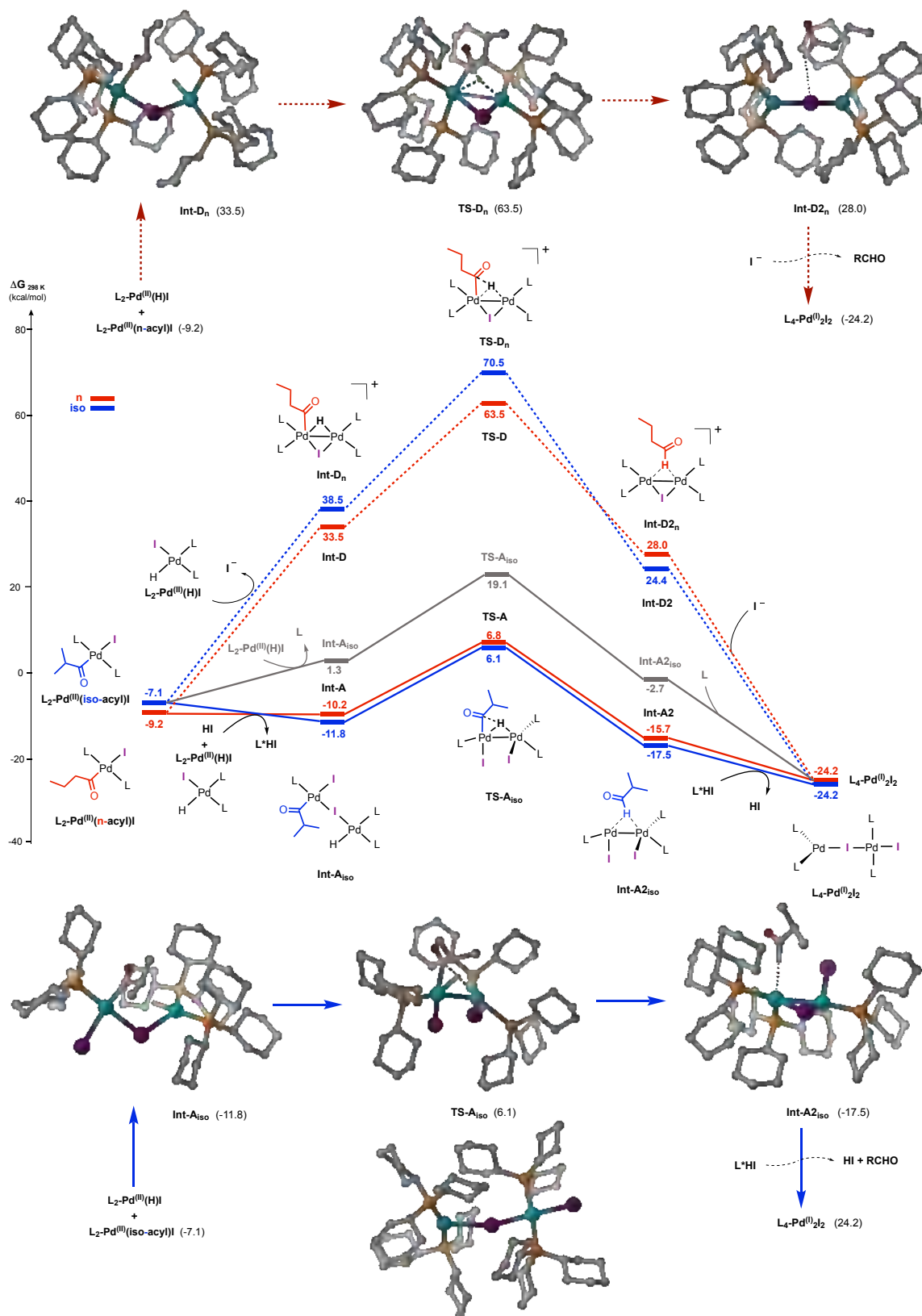
Figure 5. Free energy surface for the reaction of **L₂−Pd(II)(acyl)I** complex with **L₂−Pd(II)(H)I** via neutral (plain lines) and cationic pathways (dashed lines). **Int**, intermediate, **TS**, transition state. C−H hydrogen atoms were omitted for clarity. For computational details, see Section 5.4.

Int-D$_{iso}$

TS-D$_{iso}$

Int-D2$_{iso}$

Int-A$_n$

TS-A$_n$

Int-A2$_n$

n product

iso product

Chart 2. Additional computed structures for the reaction of **L$_2$−Pd$^{(II)}$(acyl)I** complex with **L$_2$-Pd$^{(II)}$(H)I** via neutral and cationic pathways. **Int**, intermediate, **TS**, transition state. C−H hydrogen atoms were omitted for clarity. For computational details, see Section 5.4.
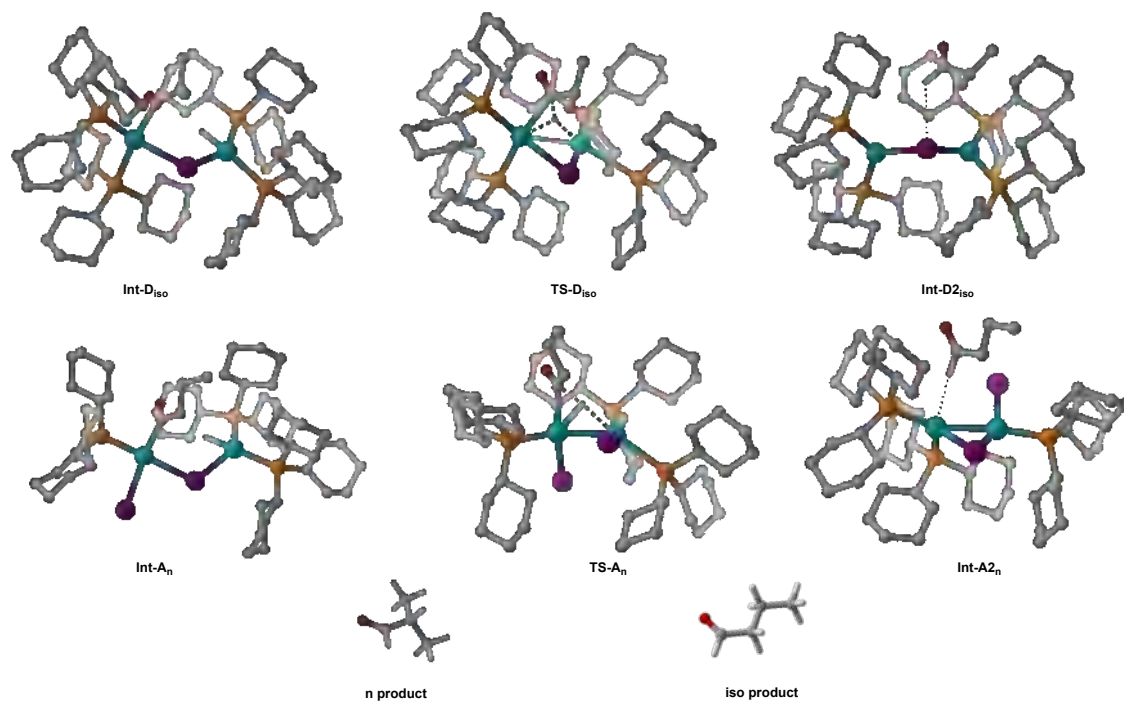
5.2.3.2 Free energy surfaces for the reaction of $L_2-Pd^{(II)}$(acyl)I complex with H_2.

I calculated the free energy surfaces for the reaction of $L_2-Pd^{(II)}$(acyl)I complexes with H_2 through neutral or cationic intermediates, $L-Pd^{(II)}(H_2)$(acyl)I or $L_2-Pd^{(II)}(H_2)$(acyl)$^+$, that undergo hydrogenolysis to form the aldehydes (Figure 6). I found that free energy surfaces corresponding to a neutral pathway are significantly lower in energy than those ones corresponding to a cationic pathway. The computed overall free energy barrier for the neutral vs cationic pathways were found to be 30.1 kcal/mol vs 49.3 kcal/mol, values which correspond to iso and n pathways, respectively.

5.2.3.2.1 Reaction of $L_2-Pd^{(II)}$(acyl)I complex with H_2 complex via neutral pathway.

Reaction of $L_2-Pd^{(II)}$(acyl)I complex with H_2, leads to formation of neutral species **Int-B**, while a phosphine ligand is decoordinated and protonated by HI generating $[PCy_3H^+][I^-]$ (Figure 6). **Int-B** undergoes hydrogenolysis via **TS-B** to form the aldehyde product and species **Int-B2**, overcoming a free energy barrier of 30.1 kcal/mol (for *iso*) and 33.2 kcal/mol (for *n*). Subsequent aldehyde release leads to the formation of $L-Pd^{(II)}$(H)I, which reacts with $[PCy_3H^+][I^-]$ to form $L_2-Pd^{(II)}$(H)I and HI. For computed structures that are not displayed in Figure 6, see Chart 3.

5.2.3.2.2 Reaction of $L_2-Pd^{(II)}$(acyl)I complex with H_2 complex via cationic pathway.

Reaction of $L_2-Pd^{(II)}$(acyl)I complex with H_2 and decoordination of I^- leads to formation of cationic species **Int-C** (Figure 6). The later undergoes hydrogenolysis via **TS-C** to form the aldehyde product and species **Int-C2**, overcoming a free energy barrier of 47.3 kcal/mol (for *iso*) and 49.3 kcal/mol (for *n*). Subsequent aldehyde release leads to the formation of $L_2-Pd^{(II)}$(H)$^+$, which reacts with I^- to form $L_2-Pd^{(II)}$(H)I. For computed structures that are not displayed in Figure 6, see Chart 3.
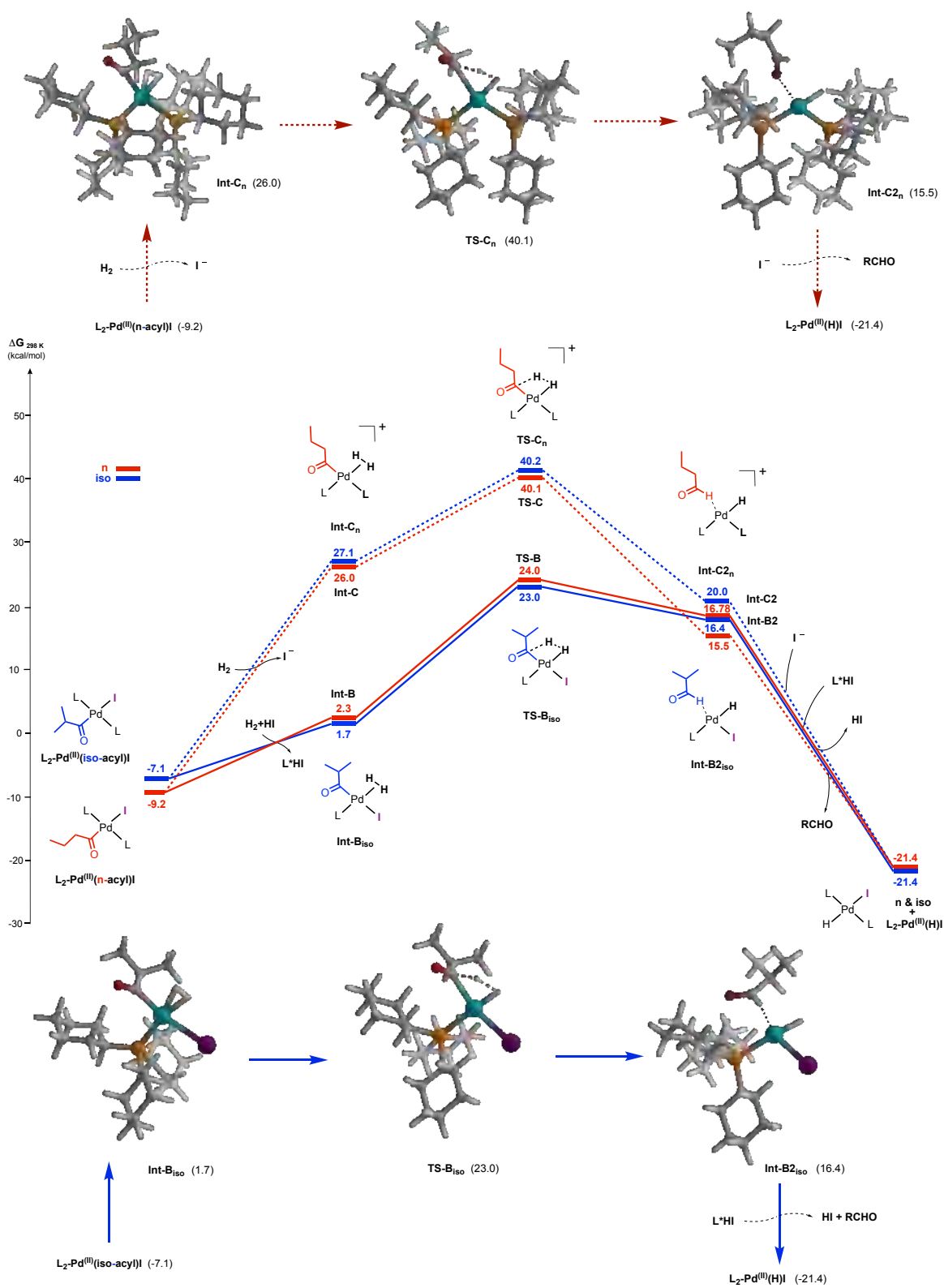
Figure 6. Free energy surface for the reaction of $L_2-Pd^{(II)}(acyl)I$ complex with H_2 via neutral (plain lines) and cationic pathways (dashed lines). **Int**, intermediate, **TS**, transition state. For computational details, see Section 5.4.

Chart 3. Additional computed structures for the reaction of **L₂−Pd^(II)(acyl)I** complex with **H₂** via neutral and cationic pathways. **Int**, intermediate, **TS**, transition state. For computational details, see Section 5.4.

5.2.4 Formation of the aldehyde through hydrogenolysis of $L_2-Pd^{(II)}(acyl)^+$ species (in the absence of any strongly coordinating anions)

I computed the classical hydrogenolysis of $L_2-Pd^{(II)}(acyl)^+$ as a control free energy surface for our calculations (Figure 7). Initial coordination of H_2 to the $L_2-Pd^{(II)}(acyl)^+$ complex leads to intermediate **Int-C**, accounting for a free energy penalty of 23.3 kcal/mol. It is worth noting that CO or anisole may also coordinate $L_2-Pd^{(II)}(acyl)^+$ species stabilizing these intermediates. In such a scenario, CO or aniosol need to decooridnate from the Pd center prior to coordination of H_2 to the $L_2-Pd^{(II)}(acyl)^+$ complex, resulting in the increase of the energy barrier of the overall process.. Subsequent hydrogenolysis of **Int-C** via **TS-C** overcoming an overall barrier of 37.4 kcal/mol, leads to the formation of product and **Int-C2**. The later undergoes hydrogenolysis via **TS-C** to form the aldehyde product and species **Int-C2**. Finally, aldehyde release and CO coordination leads to the formation of $L_2-Pd^{(II)}(H)(CO)^+$.

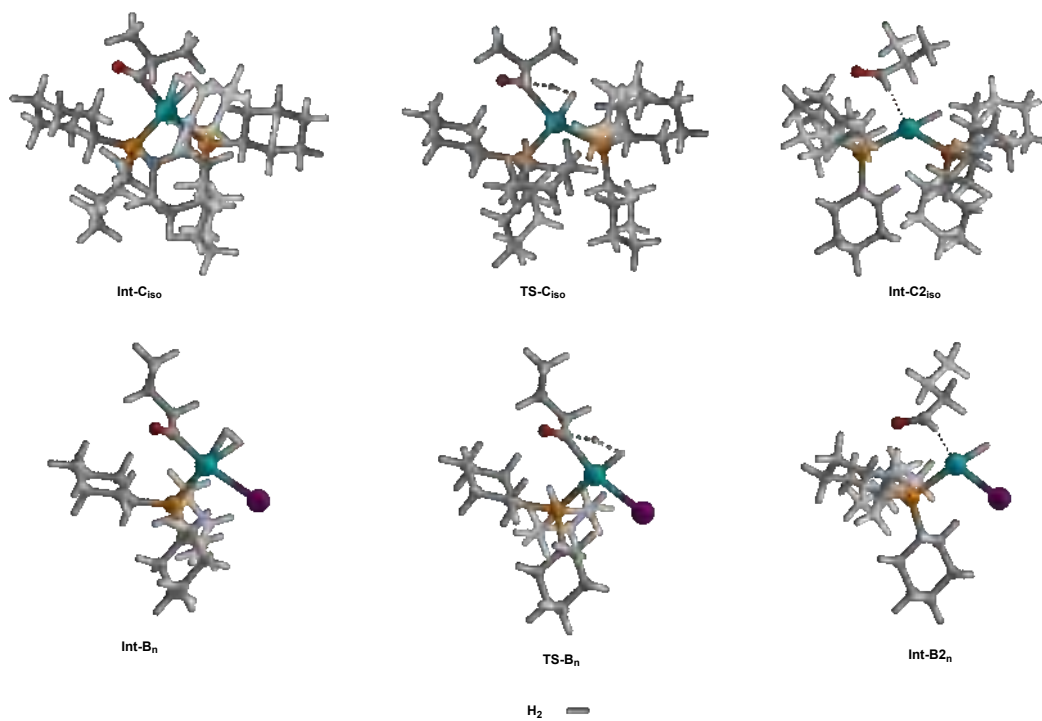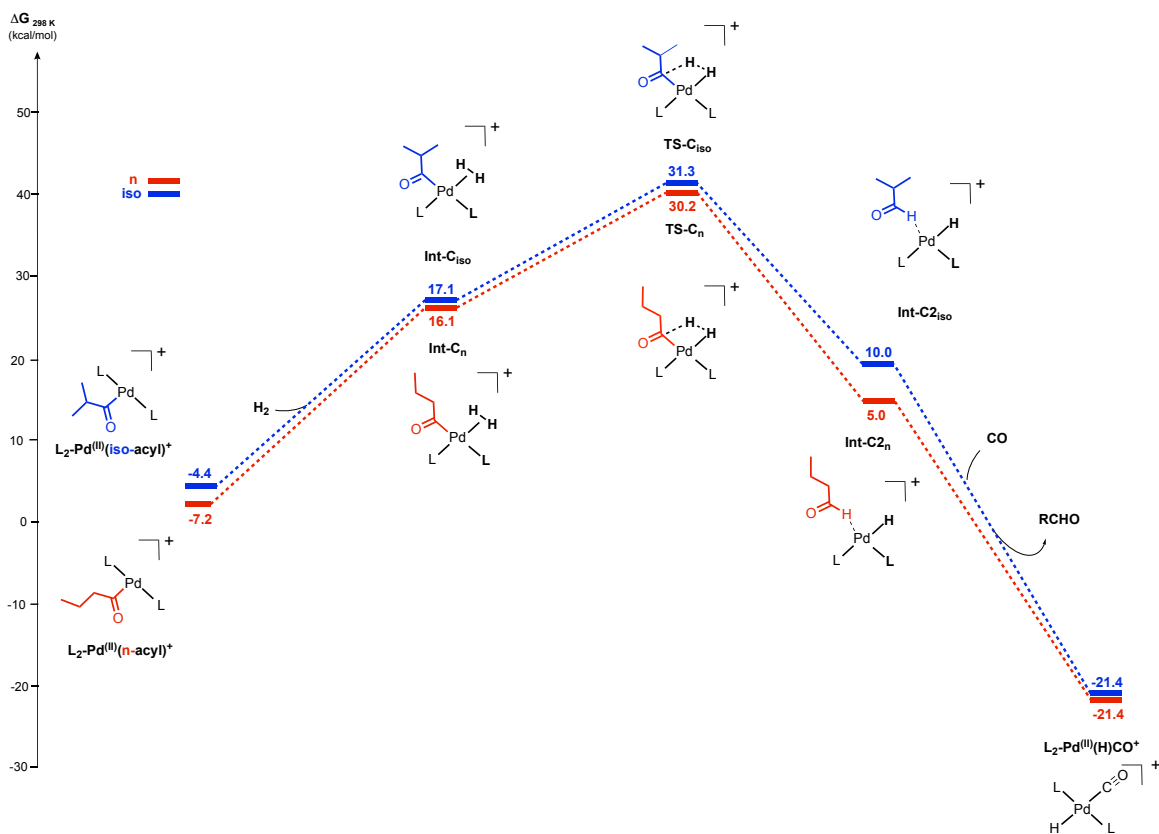**Figure 7.** Free energy surface for the reaction of $L_2-Pd^{(II)}(acyl)^+$ complex with H_2 via classical cationic pathway. **Int**, intermediate, **TS**, transition state. For computational details, see Section 5.4.

5.2.5 Effect of temperature on free energy surfaces

5.2.5.1 Equilibria between $L_2-Pd^{(II)}(H)I$ and $L_2Pd^{(II)}(acyl)I$

I evaluated the effect of temperature on the equilibria position for the reaction between to potential resting states of the catalyst, that is:

$L_2-Pd^{(II)}(H)I$ + *CO* + *propene* → $L_2Pd^{(II)}(acyl)I$, by evaluating the variations of the thermodynamic equilibrium constant (K) at 25 °C, 50 °C, 80 °C, 100 °C, 120 °C and 150 °C. I found that the values of K become lower as temperature increase, as shown in Figure 8 (values of Ln (K) *vs*. T), due to a negative entropic variation. Therefore, it is predicted that at room temperature the reaction will lead to nearly complete formation of $L_2Pd^{(II)}(acyl)I$ species, and as temperature increases, the equilibrium will favor the $L_2Pd^{(II)}(acyl)I$ species to react backwards to form $L_2-Pd^{(II)}(H)I$ species. It is worth noting that in all cases, $L_2Pd^{(II)}(n\text{-}acyl)$ is more stable than the $L_2Pd^{(II)}(iso\text{-}acyl)$ complex. These findings are in agreement with the experiments.[7]
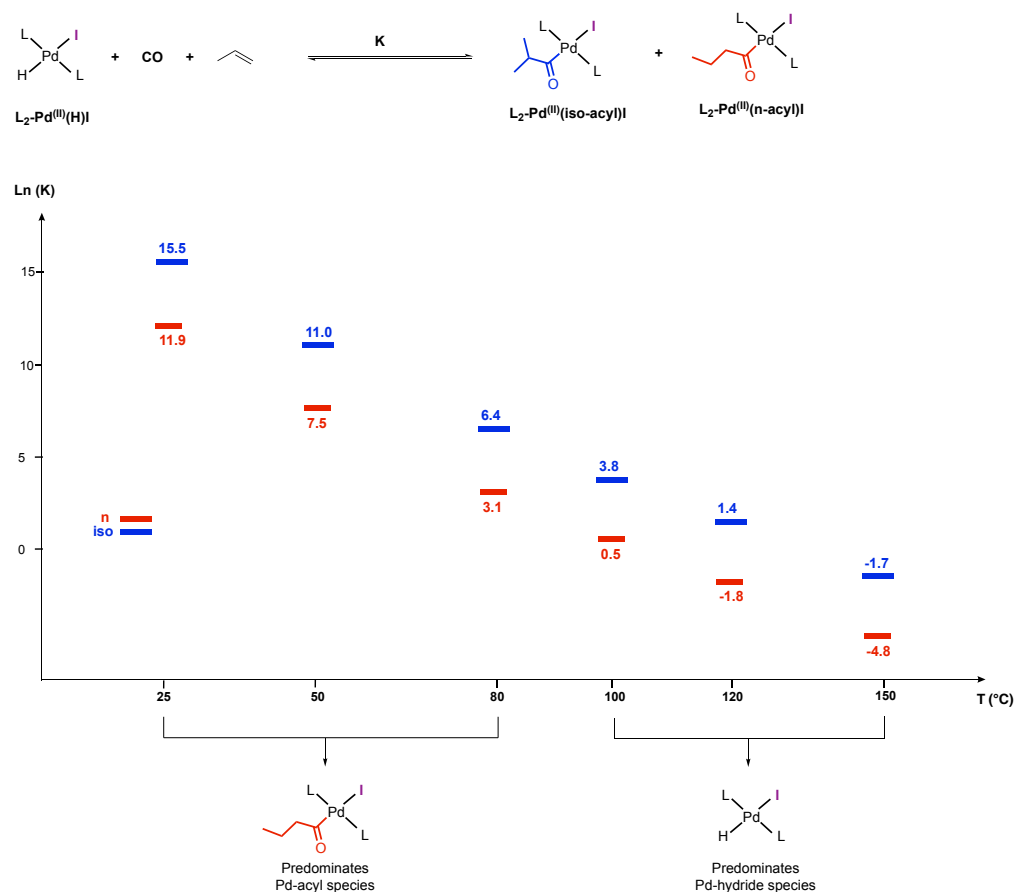

Figure 8. Effect of temperature on the equilibria between $L_2-Pd^{(II)}(H)I$ and $L_2-Pd^{(II)}(acyl)I$.

5.2.6 Formation of the aldehyde via the lowest energy pathway

Because the reactions with gaseous reactants tend to be temperature sensitive, as also observed experimentally in the title reaction, I evaluated the effect of temperature on the free energy surfaces leading to the formation of the aldehyde product via a neutral binuclear reductive elimination pathway, which is the lowest energy pathway. At 373 K, the free energy surface of the reaction is at least 2 kcal/mol higher in energy than the corresponding surface at 298 K (Figure 9). The formation of $L_2Pd^{(II)}(acyl)I$ species at 373 K accounts for a minimal change in Gibbs free energy, suggesting that at that temperature both $L_2-Pd^{(II)}(H)I$ and $L_2Pd^{(II)}(acyl)I$ species are in a dynamic equilibrium, preferentially leading to the formation of the $L_2Pd^{(II)}(n\text{-}acyl)I$ complex. Notably, at 373 K the binuclear reductive elimination step for the formation of the *iso* product is predicted to be faster than for the *n* product, which is in line with experimental regioselectivity observed at that temperature.
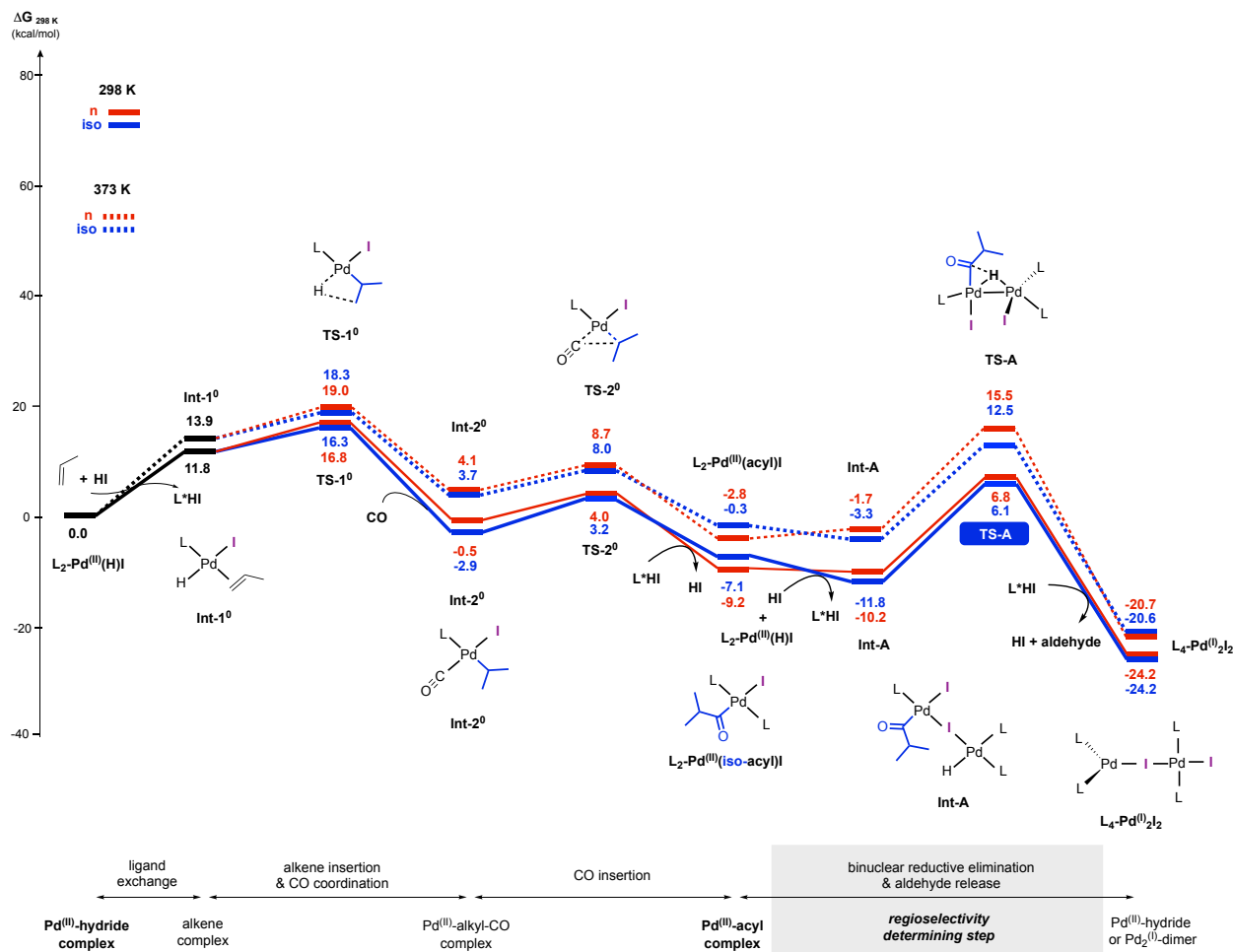

Figure 9. Free energy surfaces at 298 K and 373 K for the formation of the aldehyde product via neutral binuclear reductive elimination. **Int**, intermediate, **TS**, transition state. For computational details, see Section 5.4.

148

5.3 Conclusions

My computational studies show that the lowest energy pathway leading to the formation of the aldehyde product involves an i*so*-selective binuclear reductive elimination step from neutral species. The iodide anion present in the system is a key ligand to ensure lower free energies on the formation of the reacting neutral species in respect to the cationic ones, of which its formation account for higher free energy penalties and barriers. Other pathways commonly proposed, such as hydrogenolysis of the Pd-acyl complexes, have significantly higher free energy barriers and therefore are unlikely as possible competing pathways. Moreover, the effect of HI generated during the reaction is predicted to favor the reaction, by promoting decoordination of the PCy_3 ligand during critical elementary steps of the catalytic cycle. Overall, this work contributes to gain insights into the sequence of catalytic events that is most likely to occur, providing valuable knowledge for further improvement on the performance of the catalyst and the development of its new generations.

5.4 Computational details

All DFT calculations[11] were performed with the Gaussian09 suite of programs.[12] Geometries were optimized with the M06−L[13] functional and the def2-SVP basis set[14,15] together with the corresponding Coulomb fitting basis set to speed up calculations.[16] In all cases, the default numerical integration grid was modified for the denser and more accurate 'SuperFineGrid'. Stationary points were probed through vibrational analysis. Gibbs free energy corrections were performed under standard conditions (298.15 K, 1.0 atm). Transition states were verified through Intrinsic Reaction Coordinate calculations (IRC) or optimization to minima at both sides of the frequency. Single point energy calculations including the effect of anisole as a solvent were performed with the M06−L functional[13], the SMD solvation model[17], Grimme's dispersion correction GD3[18] and the larger def2-TZVP basis set[14,15].

5.5 References

(1)   Cornils, B.; Börner, A.; Franke, R.; Zhang, B.; Wiebus, E.; Schmid, K. Hydroformylation. In *Applied Homogeneous Catalysis with Organometallic Compounds*; John Wiley & Sons, Ltd, 2017; pp 23–90.

(2)   Sigrist, M.; Zhang, Y.; Antheaume, C.; Dydio, P. Isoselective Hydroformylation of Propylene by Iodide-Assisted Palladium Catalysis. *Angew. Chem. Int. Ed. n/a* (n/a), e202116406.

(3)   Drent, E.; Van Broekhoven, J. A. M.; Doyle, M. J. Efficient Palladium Catalysts for the Copolymerization of Carbon Monoxide with Olefins to Produce Perfectly Alternating Polyketones. *J. Organomet. Chem.* 1991, *417* (1), 235–251.

(4)   Zhang, Y.; Torker, S.; Sigrist, M.; Bregović, N.; Dydio, P. Binuclear Pd(I)–Pd(I) Catalysis Assisted by Iodide Ligands for Selective Hydroformylation of Alkenes and Alkynes. *J. Am. Chem. Soc.* 2020, *142* (42), 18251–18265.

(5)   Zhang, Y.; Sigrist, M.; Dydio, P. Palladium-Catalyzed Hydroformylation of Alkenes and Alkynes. *Eur. J. Org. Chem.* 2021, *2021* (44), 5985–5997.

(6)   Konya, D.; Almeida Leñero, K. Q.; Drent, E. Highly Selective Halide Anion-Promoted Palladium-Catalyzed Hydroformylation of Internal Alkenes to Linear Alcohols. *Organometallics* 2006, *25* (13), 3166–3174.

(7)   Zhang, Y.; Dydio, P. Unpublished Mechanistic Experimental Results.

(8)   Drent, E.; Budzelaar, P. H. M. The Oxo-Synthesis Catalyzed by Cationic Palladium Complexes, Selectivity Control by Neutral Ligand and Anion. *J. Organomet. Chem.* 2000, *593–594*, 211–225.

(9)   Konya, D.; Almeida Leñero, K. Q.; Drent, E. Highly Selective Halide Anion-Promoted Palladium-Catalyzed Hydroformylation of Internal Alkenes to Linear Alcohols. *Organometallics* 2006, *25* (13), 3166–3174.

(10)   Pospech, J.; Fleischer, I.; Franke, R.; Buchholz, S.; Beller, M. Alternative Metals for Homogeneous Catalyzed Hydroformylation Reactions. *Angew. Chem. Int. Ed.* 2013, *52* (10), 2852–2872.

(11)   Cramer, C. J.; Truhlar, D. G. Density Functional Theory for Transition Metals and Transition Metal Chemistry. *Phys. Chem. Chem. Phys.* 2009, *11* (46), 10757–10816.

(12)   Frisch, M. J.; Trucks, G. W.; Schlegel, H. B.; Scuseria, G. E.; Robb, M. A.; Cheeseman, J. R.; Scalmani, G.; Barone, V.; Mennucci, B.; Petersson, G. A.; Nakatsuji, H.; Caricato, M.; Li, X.; Hratchian, H. P.; Izmaylov, A. F.; Bloino, J.; Zheng, G.; Sonnenb, D. J. *Gaussian 09*; Gaussian, Inc: Wallingford CT, 2009.

(13)   Zhao, Y.; Truhlar, D. G. Density Functionals with Broad Applicability in Chemistry. *Acc. Chem. Res.* 2008, *41* (2), 157–167.

(14)   Weigend, F.; Ahlrichs, R. Balanced Basis Sets of Split Valence, Triple Zeta Valence and Quadruple Zeta Valence Quality for H to Rn: Design and Assessment of Accuracy. *Phys. Chem. Chem. Phys.* 2005, *7* (18), 3297–3305.

(15)   Andrae, D.; Häußermann, U.; Dolg, M.; Stoll, H.; Preuß, H. Energy-Adjustedab Initio Pseudopotentials for the Second and Third Row Transition Elements. *Theor. Chim. Acta* 1990, *77* (2), 123–141.

(16)   Weigend, F. Accurate Coulomb-Fitting Basis Sets for H to Rn. *Phys. Chem. Chem. Phys.* 2006, *8* (9), 1057–1065.

(17)   Marenich, A. V.; Cramer, C. J.; Truhlar, D. G. Universal Solvation Model Based on Solute Electron Density and on a Continuum Model of the Solvent Defined by the Bulk Dielectric Constant and Atomic Surface Tensions. *J. Phys. Chem. B* 2009, *113* (18), 6378–6396.

(18)   Grimme, S.; Ehrlich, S.; Goerigk, L. Effect of the Damping Function in Dispersion Corrected Density Functional Theory. *J. Comput. Chem.* 2011, *32* (7), 1456–1465.

List of abbreviations

ACS	american chemical society
3-OmeBz	3-methyoxybenzoic acid
4CzIPN	1,2,3,5-Tetrakis(carbazol-9-yl)-4,6-dicyanobenzene, 2,4,5,6-Tetrakis(9H-carbazol-9-yl) isophthalonitrile
Ac	acetate
acac	acetylacetonate
Alk	alkyl
APCI	atmospheric pressure chemical ionization
binol	1,1′-Bi-2-naphthol
boc	tert-butoxycarbonyl
Bpin	bis(pinacolato)diboron
Bu	butyl
Cat	catalyst
Cbz	benzyloxycarbonyl
cod	cyclooctadiene
Cp	cyclopentadienyl
cym	para-Cymene or 4-Isopropyltoluene
D	deuterium
dba	dibenzylideneacetone
DCM	dichloromethane
DFT	density functional theory
DIAD	diisopropyl azodicarboxylate
DMSO	dimethyl sulfoxide
DPEPhos	bis[(2-diphenylphosphino)phenyl] ether
dppf	1,1′-Bis(diphenylphosphino)ferrocene
EDG	electron donatig group
ELSD	evaporative light scattering detector
ESI	electrospray ionization
Et	ethyl
Et2O	diethyl ether
EtOAc	ethyl acetate
EWG	electron withdrawing group
FG	functional group
GC	gas chromatography
GC-MS	gas chromatography coupled with mass spectrometry
HAT	hydrogen atom transfer
HRMS	high-resolution mass spectrometry
Int	intermediate

KHDMS	potassium bis(trimethylsilyl)amide
LDA	lithium diisopropylamide
Me	methyl
Mes	mesitylene or 1,3,5-trimethylbenzene
NADP+	oxidized form of nicotinamide adenine dinucleotide phosphate
NADPH	reduced form of nicotinamide adenine dinucleotide phosphate
NBS	N-Bromosuccinimide
NMR	nuclear magnetic resonance
OTf	trifluoromethanesulfonate
p-TsOH	paratoluenesulfonic acid
PC	photo catalyst
PCy3	tricyclohexylphosphine
PET	photoinduced electron-transfer
Ph	phenyl
PMHS	poly(methylhydrosiloxane)
Pr	propyl
Py	pyridine
rac	racemic
RT	room temperature
SET	single electronyTransfer
TBDPS	tert-Butyldiphenylsilyl
TBS	tert-butyl(dimethyl)silyl
TFA	trifluoroacetic acid
THF	tetrahydrofuran
TMS	trimethylsilyl
Ts	toluenesulfonyl group
TS	transition state

UNIVERSITÉ DE STRASBOURG

Sebastián MARTÍNEZ

EDSC
École Doctorale des
Sciences Chimiques

Développement de procédés chimiques exploitant des réactions catalytiques réversibles, à partir d'une approche mécanistique.

Résumé

Dans ma thèse de doctorat, j'ai cherché à souligner l'importance de la multicatalyse en tant que domaine émergent pour renforcer la synthèse organique. J'ai développé un système bi-catalytique qui exploite des réactions d'hydrofonctionnalisation catalytique réversible orthogonale à la réaction de Diels-Alder pour accéder à une réactivité non-inhérente sans précédent des matériaux de départ, montrant que l'augmentation de la coopérativité et de la complexité en catalyse ouvre l'accès à des raccourcis précieux en synthèse organique. Par la suite, je me suis concentré sur nouvelles réactions catalytiques réversibles. Dans une projet collaboratif, nous avons conçu et développé une nouvelle réaction de borylation. Une étude DFT nous a permis de comprendre l'importance des propriétés électroniques et stériques du ligand du catalyseur sur le profil réactionnel. Au final, je présente une étude DFT pour décomposer le mécanisme d'un nouveau protocole pour l'hydroformylation isosélective du propylène.

Mots clés: multicatalyse, réactions d'hydrofonctionnalisation catalytique réversible, réaction de borylation, réaction de hydroformylation.

Résumé en anglais

In my doctoral thesis, I sought to highlight the importance of multicatalysis as an emerging field to enhance organic synthesis. I developed a bi-catalytic system that exploits reversible catalytic hydrofunctionalization reactions orthogonal to the Diels-Alder reaction to access unprecedented non-inherent reactivity of starting materials, showing that increasing cooperativity and complexity in catalysis opens access to valuable shortcuts in organic synthesis. Subsequently, I focused on new reversible catalytic reactions. In a collaborative project, we designed and developed a new borylation reaction. A DFT study allowed us to understand the importance of the electronic and steric properties of the catalyst ligand on the reaction profile. In the end, I present a DFT study to understand and unravel the mechanism of a new protocol for the isoselective hydroformylation of propylene.

Keywords: multicatalysis, reversible catalytic hydrofunctionalization reactions, borylation reaction, hydroformylation reaction.